DE GRUYTER

Alfredo Aguilera,
J. Paulo Davim (Eds.)

WOOD COMPOSITES

MATERIALS, MANUFACTURING AND ENGINEERING

ADVANCED COMPOSITES

Alfredo Aguilera, J. Paulo Davim (Eds.)
Wood Composites
Advanced Composites

Also of Interest

Series: Advanced Composites.
J. Paulo Davim (Ed.)
ISSN 2192-8983
Published titles in this series:
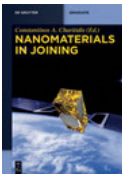Vol. 5: Ceramic Matrix Composites (2016) Ed. by Davim, J. Paulo
Vol. 4: Machinability of Fibre-Reinforced Plastics (2015)
Ed. by Davim, J. Paulo
Vol. 3: Metal Matrix Composites (2014) Ed. by Davim, J. Paulo
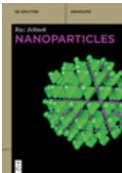Vol. 2: Biomedical Composites (2013) Ed. by Davim, J. Paulo
Vol. 1: Nanocomposites (2013) Ed. by Davim, J. Paulo/
Charitidis, Constantinos A.

Nanomaterials in Joining.
Constantinos A. Charitidis (Ed.), 2015
ISBN 978-3-11-033960-4, e-ISBN 978-3-11-033972-7

Nanoparticles.
Raz Jelinek, 2015
ISBN 978-3-11-033002-1, e-ISBN 978-3-11-033003-8
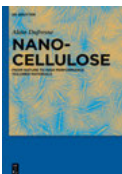
Nanocellulose.
From Nature to High Performance Tailored Materials
Dufresne, 2012
ISBN 978-3-11-025456-3, e-ISBN 978-3-11-025460-0

Holzforschung.
International Journal of the Biology, Chemistry, Physics,
and Technology of Wood
Faix, Oskar (Editor-in-Chief)
ISSN 0018-3830, e-ISSN 1437-434X

Wood Composites

——

Materials, Manufacturing and Engineering

Edited by
Alfredo Aguilera and J. Paulo Davim

DE GRUYTER

Editors
Prof. Alfredo Aguilera
Universidad Austral de Chile
Facultad de Ciencias Forestales y Recursos Naturales
Valdivia 5090000, Chile
aguilera@uach.cl

Prof. Dr. J. Paulo Davim
University of Aveiro
Department of Mechanical Engineering
Campus Santiago
3810-193 Aveiro, Portugal
pdavim@ua.pt

Contents

Ana Henriques, Cristina Coelho, João M. Ferra, Jorge Manuel Martins,
Fernão D. Magalhães, and Luísa Carvalho

Stephane Molina

A. Pizzi

José Reinaldo Moreira da Silva, Anna Carolina de Almeida Andrade,
and Jordão Cabral Moulin

Jorge Manuel Martins, Cristina Coelho, João Pereira, João Macias Ferra,
and Luísa Carvalho

List of contributing authors

Anna Carolina de Almeida Andrade
Universidade Federal de Lavras
Laboratório de Ciência e Tecnologia da
Madeira – DCF/UFLA
Caixa Postal 3037 – Lavras/MG
Brasil
Chapter 7

Frank C. Beall
University of California, Berkeley
130 Mulford Hall #3114
Berkeley CA, 94720
USA
Chapter 4

Luísa Carvalho
LEPABE – Departamento de Engenharia Química
Faculdade de Engenharia
Universidade do Porto
Rua Dr. Roberto Frias
Porto, Portugal
and
Departamento de Engenharia de Madeiras
Escola Superior de Tecnologia e Gestão de Viseu
Instituto Politécnico de Viseu
Campus Politécnico de Repeses
Viseu, Portugal
Chapters 1 and 8

Cristina Coelho
LEPABE – Departamento de Engenharia Química
Faculdade de Engenharia
Universidade do Porto
Rua Dr. Roberto Frias
Porto, Portugal
and
Departamento de Engenharia de Madeiras
Escola Superior de Tecnologia e Gestão de Viseu
Instituto Politécnico de Viseu
Campus Politécnico de Repeses
Viseu, Portugal
Chapters 1 and 8

João Macias Ferra
Euroresinas – Indústrias Químicas S.A.
Plataforma I Lote Industrial I Monte Feio
Sines 7520-064
Portugal
Chapters 1 and 8

Ana Henriques
LEPABE – Departamento de Engenharia Química
Faculdade de Engenharia
Universidade do Porto
Rua Dr. Roberto Frias
Porto, Portugal
Chapter 1

Fernão D. Magalhães
LEPABE – Departamento de Engenharia Química
Faculdade de Engenharia
Universidade do Porto
Rua Dr. Roberto Frias
Porto, Portugal
Chapter 1

Jorge Manuel Martins
LEPABE – Departamento de Engenharia Química
Faculdade de Engenharia
Universidade do Porto
Rua Dr. Roberto Frias
Porto, Portugal
and
Departamento de Engenharia de Madeiras
Escola Superior de Tecnologia e Gestão de Viseu
Instituto Politécnico de Viseu
Campus Politécnico de Repeses
Viseu, Portugal
Chapters 1 and 8

Stephane Molina
LERMAB-CETELOR
Université de Lorraine
Campus Fibres
27, rue Philippe SEGUIN
88051 EPINAL cedex
France
Chapter 2

Jordão Cabral Moulin
Universidade Federal de Lavras
Departamento de Ciências Florestais
Caixa Postal 3037 – Lavras/MG
Brasil
Chapter 7

João Pereira
LEPABE - Departamento de Engenharia Química
Faculdade de Engenharia
Universidade do Porto
Rua Dr. Roberto Frias
Porto, Portugal
and
ARCP - Associação Rede de Competência em Polímeros
Porto, Portugal
Chapter 8

A. Pizzi
LERMAB
University of Lorraine
Nancy and Epinal, France
and
Dept. of Physics
King Abdulaziz University
Jeddah, Saudi Arabia
Chapters 3 and 6

Henrique Reis
University of Illinois at Urbana-Champaign
Department of Industrial and Enterprise
Systems Engineering
217 Transportation Building, 104 S. Mathews
Urbana IL, 61801
USA
Chapter 4

José Reinaldo Moreira da Silva
Universidade Federal de Lavras
Laboratório de Ciência e Tecnologia da Madeira – DCF/UFLA
Caixa Postal 3037 – Lavras/MG
Brasil
Chapter 7

Xiaozhou Song
Northwest A&F University
No. 3 Taicheng Road, Yangling
Shan Xi, 712100
China
Chapter 5

Yafang Lei
Northwest A&F University
No. 3 Taicheng Road, Yangling
Shan Xi, 712100
China
Chapter 5

Zhangjing Chen
Northwest A&F University
No. 3 Taicheng Road, Yangling
Shan Xi, 712100
China
Chapter 5

Ana Henriques, Cristina Coelho, João M. Ferra,
Jorge Manuel Martins, Fernão D. Magalhães, and Luísa Carvalho

1 Introduction of advanced functionalities in laminates for wood-based panels: surface quality evaluation

Abstract: High-pressure laminates (HPL), manufactured with paper and thermosetting resins, are a value-added product that has been increasingly used for home and commercial surfaces and a practical solution for horizontal or vertical surfaces that require high physical, mechanical, and chemical performances, with a high versatility and excellent decoration ability. Intensive applications as scholar furniture with mar resistance, abrasion resistance, and dirt repellent; laboratory countertops with chemical resistance and dirt repellent; exterior flooring with UV resistance, mar resistance, and abrasion resistance; technical flooring with phosphorescent properties, abrasion and mar resistance for public buildings; hospital furniture with dirt repellence and antimicrobial properties; whiteboards with mar and abrasion resistance demands the introduction of advanced functionalities in high-pressure laminates not existent in the market. The development of innovative impregnation resins with new functionalities could result in multifunctional laminates as the result of the combination of new and better properties. In this chapter, the focus is on the production and characterization of decorative laminates, as well as the modification of this material in order to provide advanced functionalities.

Keywords: high-pressure laminates, advanced functionalities

1.1 The HPL and its manufacture

1.1.1 Introduction

According to the European Standard EN 438-2 [1] a high pressure laminate (Fig. 1.1) consists of layers of cellulosic fibrous material. These layers consisting of an assembly of kraft paper sheets impregnated with thermosetting resins (the number of such sheets is dependent on the intended thickness), a printed or patterned layer designated as the decorative paper impregnated with a melamine resin, and in some cases an overlay paper sheet on the surface [2]. The decorative paper represents a cost between 2.1 and 18.4 % of HPL total price, the kraft paper a cost between 17.3 and 32.2 %, the phenolic resin between 11.5 and 28.2 %, the overlay between 0.5 and 3.4 %, the melamine resin between 1.2 and 10.4 %, and the energy between 6.9 and 8.2 % to the manufacturer [3].

Fig. 1.1: High-pressure laminates (courtesy of Sonae Indústria de Revestimentos).

Decorative HPL are available in a wide range of colors, patterns, and abstracts combined with different textures and gloss levels. Excellent reproductions of natural materials such as textiles, fabrics, exotic wood veneers, and stone can be achieved. Different printing technologies, e.g. digital, screen, and offset printing, can be used to produce customized designs. Because of their impervious surfaces, HPL are easy to clean and maintain. Offered in various sizes, they allow large areas to be covered without seams.

The manufacture of such laminates commonly starts with impregnation of decorative and kraft papers (Fig. 1.2 (a)). After a drying process, the impregnated paper sheets are bonded together by high-pressure pressing (Fig. 1.2 (b)). The high pressure is defined as the simultaneous application of heat (temperature ≥ 120 °C) and high pressure (5 MPa), to provide flowing and subsequent curing of the melamine and the phenolic resins. Curing the melamine resin makes the surface hard, providing scratch and damage resistance, while curing the phenolic resin bonds the kraft layers together and developing water resistance. The press cycle time is designed to cure the lami-
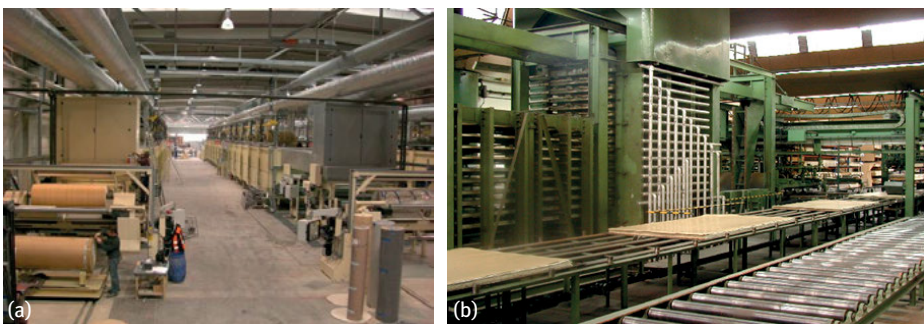
Fig. 1.2: (a) Impregnation and (b) pressing process (courtesy of Sonae Indústria de Revestimentos).

nates within the pack as uniformly as possible, so that they all perform the same. The longer they are pressed, the more extensively cured and less flexible is the laminate.

The market share of laminates has been growing over the years. Global demand for decorative laminates is expected to rise 5.6 % per year to 10.7 billion m^2 in 2018, valued at US\$ 40.8 billion [4]. Due to its durability and versatility, HPL is a common choice for horizontal and vertical applications in the construction and furnishing industries for high traffic settings such as hospitality, office furniture, healthcare, retail casework, commercial interiors, and education facilities [5]. Furniture and cabinets were the largest market for decorative laminates in 2013, accounting for nearly 70 % of the total demand. However, the expected increase of ready-to-assemble (RTA) furniture and flooring, which are made from engineered wood and laminates, will benefit from the demand of these products [4].

Nowadays, Pacific Asia represents the largest and fastest growing market for decorative laminates, followed by North America and Europe. The Chinese market alone accounted for 31 % of the global demand in 2013. India is expected to post the most rapid gains in laminate demands worldwide through 2018 [4]. Increasing available income, constant economic growth, rising standards of living, and increased demand for housing in urban areas are some of the key growth drivers in the Pacific Asian region. Increasing available income allow the customer to spend more on furniture, home accessories, and furnishings, among which decorative laminates play a key role. Additionally, a wide range of colors, designs, textures, and styles led to increased consumer interest and is expected to provide ample growth opportunities for the decorative laminates market [5]. Germany, France, and Sweden, where wood and paper industries are highly developed, are regional leaders in RTA furniture. The US also has a significant production capacity for RTA furniture, cabinets, and laminate flooring. Laminate counter tops and laminated doors will benefit from an acceleration of building construction in 2018. Laminate countertops face competition of other products as natural stone, engineered quartz, and solid surface, while in doors vinyl films are also gaining a market share [4].

The major companies operating in the decorative laminates market include Formica Group, FunderMax, Kingboard Laminates Holdings Ltd., ABET Laminati, ARPA, Sonae Indústria de Revestimentos, Ronotex GmbH & Co., Kronospan Holdings Limited, Advanced Technology Inc., Armstrong World Industries Inc., Roseburg Forest Products Company, Sekisui Chemical Company Limited, Sierra Pine Ltd., Tarkett SA, Timber Products Company, Woodcraft Industries Incorporated, OMNOVA Solutions Inc., Wilsonart International and Trespa [5].

1.1.2 The raw materials

1.1.2.1 Paper

Three types of paper are used in the manufacture of HPL: kraft, decorative and overlay paper (Fig. 1.3). The kraft is used in the bottom layers. This type of paper, impregnated with phenolic resin, provides mechanical resistance, moisture and chemical resistance to HPL. The mechanical resistance depends on fibre orientation. The weight of kraft paper is around 43 to 300 g/m^2. Decorative foils are alpha-cellulose papers with weights ranging between 40 and 200 g/m^2. The decorative paper should have good mechanical properties, quick resin absorption combined with sufficient mechanical resistance when humid, high opacity, and homogeneous fiber orientation. Furthermore, it should comply with general requirements related to capillary absorption, porosity, air permeability, durability in dry or humid conditions, surface pH, and specific requirements related to appearance characteristics as light resistance, smoothness, color, and pattern. The overlay paper, mainly composed of alpha-cellulose, is placed over the decorative paper and is generally impregnated with melamine resin. When pressed over the decorative paper, it becomes transparent or translucent and allows a clear view of the decorative layer. It contributes to an increase of the resistance to staining, scratching and abrasion, which allows use in flooring applications. For that purpose mineral particles such as silica, alumina, corundum, or tungsten carbide are added. This kind of paper has an initial weight between 24 and 32 g/m^2.

Overlay paper
(melamine resin)

Decorative paper
(melamine resin)

Kraft paper
(phenolic resin)
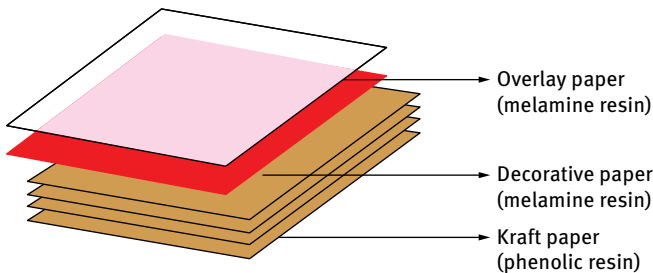
Fig. 1.3: Paper used in the manufacture of HPL.

1.1.2.2 Melamine formaldehyde resin

The most common resins used in the impregnation of decorative paper are melamine formaldehyde resins (MF resins). These are used because of their unique surface properties in terms of hardness, chemical stability, and transparency, which allow brilliant visual appearance of the surface decors and good performance in use at reasonable prizes [6].

However, these resins also present some disadvantages, such as poor long-term oxidation resistance and susceptibility to attack by strong acids and bases [7].

Melamine formaldehyde (MF) resins are a prominent type of aminoplastics. In the first step (methylolation), depending on the reaction conditions (mainly the melamine-to-formaldehyde molar ratio), up to six molecules of formaldehyde may react with melamine to form water-soluble methylolated melamine compounds, also known as methylols. These methylols may further condense under liberation of water to form MF prepolymers, which consist of either methylene- or methylene ether-bridged melamine rings. Typically, MF resin prepolymers intended for paper impregnation are of low molecular weight and consist of a statistical mixture of oligomers with about three to five melamine units, in oder to keep the viscosity low and allow for good paper penetration [8].

The main properties of melamine-formaldehyde resins are described in Tab. 1.1.

During MF synthesis, the most important parameters are:
– molar ratio of the different monomers:
    – molar ratio formaldehyde/melamine (F/M);
    – molar ratio formaldehyde/amine groups (F/N$_2$);
    – solid content;
– raw materials purity;
– synthesis process:
    – pH;
    – Temperature;
    – Sequence and addition of different raw materials;
    – Length of the different stages of synthesis.

The effective curing temperature range of MF resins starts at about 100 °C and reaches the optimum at approximately 150 °C [9].

Tab. 1.1: Main properties of melamine-formaldehyde resins.

Attribute	Melamine formaldehyde resins
Appearance	Colorless
Solid content (%)	50 ± 10
pH	9.5 ± 0.5
Density (g/cm^3)	1.250 ± 0.010
Viscosity (s)	16 ± 2
Hardening temperature	Starting at 100 °C

1.1.3 HPL manufacturing process

1.1.3.1 Paper impregnation

Impregnated décor papers must perform an external function and therefore it is important that precision and uniformity in impregnation/coating be achieved [10].

As a first step, the décor paper is impregnated with resin, where the paper is soaked in the impregnated resin and then dried. In a second step, the impregnated paper is coated with the impregnated resin and then dried to final moisture content of 6–7 % and generally a weight between 60 to 130 g/m^2 [10, 11].

An important quality estimate used by the industry to characterize dried semifinished paper sheets is the amount of volatiles in the impregnated film, which is dominated mainly by the moisture content. The determination of the residual moisture content (volatile content) occurred by differential weighing after a 5 min drying at 160 °C. If the moisture content is too high the stacked or rolled sheets are often found to stick together (block formation). On the other hand, if the content is too low the resin often has lost too much reactivity during impregnation and drying already, so that it will not show sufficient adhesion when finally laminated onto the carrier board. In both cases, the resin does not allow for forming surfaces that fulfil the customer's requirements [6].

Another important feature is the flow that represents the amount of excess resin in the sample. Flow is determined from weight differences after pressing a 3 inch diameter piece, partially cured, submitted to pressing and temperature for 5 min. After the pressing process, the disk laminate is cooled and weighed (initial weight). After removing the resin, which has flowed out of the disk (the amount of resin located at the side of the blank), the laminate is weighed again (final weight). The difference between the initial and final weight, related to the weight of the original disk laminate, gives the flow of the impregnate [12].

The wettability of paper by impregnation resins is a very important to ensure a correct impregnation of paper with the resin. The penetration of resin in paper is a complex process, which involves a series of physicochemical process (wetting phenomena, viscous drag, etc.). In paper, the lower the contact angle of the fluid with the sheet is, the higher the penetration into paper, due to higher capillary pressure according the Young–Laplace–Gauss theory (equation (1.1)):

$$P = 2\Upsilon \cos \Theta_\Upsilon. \tag{1.1}$$

Contact angles can be measured in a surface energy evaluation system (Fig. 1.4) using the sessile drop method. The probe liquids can be the impregnation resins as melamine, polyurethane, or phenolic resin. The drop image is acquired using a CCD camera, and the corresponding contact angle is calculated after fitting the drop contour line to an ellipse. Contact angles of resins in different papers used in the laminate could be evaluated, e.g, the contact angle between melamine and polyurethane resins

Fig. 1.4: Contact Angle System Dataphysics OCA 20.

with decorative paper, phenolic resin with kraft paper, and water with a high-pressure laminate.

Normally the static mode is used, and the data acquisition should be performed at a frequency of one sample per second. The droplet volume is usually 4 µl. For each sample, an average of the contact angles of three drops of each liquid should be considering by measuring at different sites of the substrate. Contact angles should be measured over time during approximately 60 s allowing the drop to reach the equilibrium.

The determination of surface energy-free energy of papers is also important to evaluate the affinity of paper towards layers to phenolic resins, thus predetermining the variable penetration/withdrawal of resin upon industrial impregnation and providing a homogeneous distribution of resin in depth of impregnated papers. The measurements of contact angles are also important to assess the quality of the final surface, namely dirt repellence.

The equipment ABES (automated bonded evaluation system) designed by Philip Humphrey [13] can be used to study the degree of cure of the resin in impregnated papers. It provides a quantitative means for evaluating the dynamics of bond strength development under highly controlled conditions, including those that may occur during manufacture of HPL or melamine-faced boards [14]. To test different impregnated papers (e.g. kraft, decorative, and overlay), they are cut into (117 × 20 mm) strips using a pneumatically driven cutting device used for standardized ABES sample preparation. Due to the different mechanical properties of the impregnated papers (kraft, decorative, and overlay) and their different thickness, several sample configurations

can be selected, always with a standard overlap area of 100 mm^2 (20 × 5 mm). It is possible to test several different types of bonds that occur on HPL (e.g. overlay paper over decorative paper, decorative paper over kraft paper, and kraft paper over kraft paper). After the configuration is established, the specimen is put in the device and pressed in a miniature hotpress. Immediately after curing to a preselected extension (pressing time), the press opens and the lap-shear specimen is tested in shear mode (Fig. 1.5). Tensile load and pulling head movement are monitored until failure occurs.
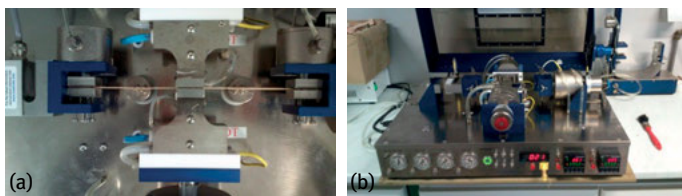
Fig. 1.5: ABES equipment.

1.1.3.2 The pressing process
After the impregnation process, the paper is cut to size and stacked. The number of kraft sheets placed in the stack depends on the intended thickness of the HPL. The stack is then loaded onto the laminating press.

It is important to notice that the layer structures, paper used, resins properties and pressing operating conditions (time, temperature) influence the HPL characteristics. A pressing time too long can cause excessive resin curing, and the paper becomes too brittle. If the time is too short, curing is insufficient, the laminate tends to stick to the press plate, and the physical and chemical performances of the product surface are negatively affected.

1.2 HPL properties

1.2.1 Test methods for HPL characterization

EN 438 standard specifies the methods of test for determination of the properties of high-pressure laminates, namely: determination of thickness, determination of length and width, determination of edge straightness, determination of edge squareness, determination of flatness, resistance to surface wear, resistance to abrasion, resistance to immersion in boiling water, resistance to water vapor, resistance to wet conditions, resistance to dry heat, dimensional stability at elevated temperature, dimensional stability at ambient temperature, resistance to climatic shock, resistance to impact by a small-diameter ball, resistance to impact by a large-diameter ball, resistance to crack-

ing under stress, resistance to crazing, resistance to scratching, resistance to staining, lightfastness, resistance to UV light, resistance to artificial weathering, resistance to cigarette burns, and resistance to blistering.

1.2.1.1 Assessment of appearance

The laminates are inspected for surface appearance under standardized conditions of lighting and viewing. A horizontal inspection table, with a height of approximately 700 mm and large enough to accommodate the largest sheets to be inspected, is used. The light source provides a diffused illumination of (1200 ± 400) lx over the whole area of the largest sheets to be inspected. This may be either diffused daylight or diffused artificial daylight. The laminates are observed at a convenient distance, approximately 1.5 m, of the lights from the inspection table.

1.2.1.2 Resistance to surface wear

According to EN 438-2, this test measures the ability of the decorative surface of the laminate being tested to resist abrasive wear through to the sublayer. Abrasion is achieved by rotating a specimen in contact with a pair of loaded cylindrical wheels covered with abrasive paper. As the wheels are turned by the rotating specimen, they abrade an annular track on the specimen's surface. The numbers of revolutions of the specimen required to cause defined degrees of abrasion are used as measures of resistance to surface wear. This test is not applicable to flooring grade laminates.

An apparatus Taber model 5135 is generally used (Fig. 1.6).

Two wheels are prepared with preconditioned unused abrasive paper. Then the wheels are fitted to the machine, and the specimen is clamped in the holder. The wheels are lowered onto the specimen starting the abrading step. At the beginning of the test, the specimen should be observed after each 25 revolutions. The test con-

Fig. 1.6: The TABER® rotary platform abrasion tester – Model 5135 – taber abraser.
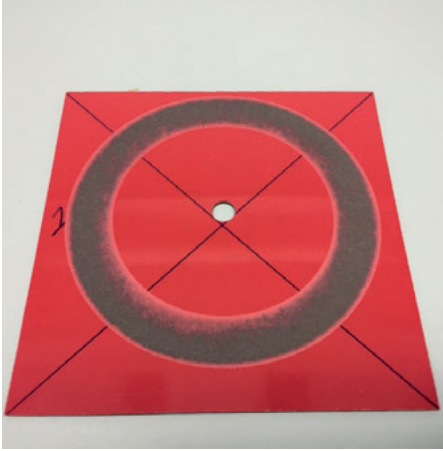
Fig. 1.7: Exceeded IWP in surface wear test.

tinues until the initial wear point (IP) is reached, which is defined as the point at which the first clearly recognisable wear-through of the print, pattern, or plain color appears and the sublayer becomes visible in three quadrants (Fig. 1.7).

The IP is recorded as the number of revolutions. The resistance to surface wear of the laminate under test is the IP rounded to the nearest 50 revolutions or, in case of complaints, the average of the three specimen IP, rounded to the nearest 50 revolutions.

1.2.1.3 Resistance to abrasion (flooring-grade laminates)

This test measures the ability of the decorative surface of the laminate being tested to resist abrasive wear-through to the sublayer (EN 438-2). The test is similar to the former one. The specimen rotates in contact with a pair of loaded cylindrical wheels covered with abrasive paper. As the wheels are turned by the rotating specimen, they scratch an annular track on the specimen's surface. The number of revolutions of the specimen required to cause a defined degree of abrasion is used as measures of resistance to abrasion. This test is applicable only to flooring-grade laminates.

The same apparatus of the previous test method is used (see Fig. 1.6). The initial procedure is similar. The specimen is observed after each 100 revolutions, and the abrasive papers should be renewed after every 200 revolutions, until the initial wear point (IP) is reached, as described in the previous test.

The initial wear point (IP) is the point at which the first clearly recognizable wear-through on the print, pattern or plain color appears and the sublayer becomes exposed in three quadrants. The initial wear point is reached when there are areas of at least 0.60 mm^2 wear-through in two quadrants and an area of 0.60 mm^2 wear-through becomes visible in a third quadrant. The sublayer for printed patterns is the background on which the pattern is printed; for plain colors it is the first sublayer of different color.
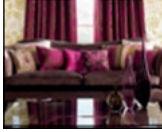
AC1	AC2	AC3	AC4	AC5
•Light residential use •Infrequent traffic (i.e.bedroom)	•Most residential spaces •Moderate foot traffic (i.e. living room or dining room)	•High-traffic rooms •Commercial space with light traffic (i.e. small officers)	•All residential uses •Heavily traffic commercial areas	Commercial use in high–traffic spaces (i.e. department stores and public bulding)

Fig. 1.8: AC rating for abrasion resistance [15].

The number of revolutions is recorded as the IP-value. The resistance to abrasion of the laminate being tested is the average of the initial wear-point (IP) values obtained on three specimens, rounded to the nearest 100 revolutions.

Taber Industries [15] suggests an AC rating for abrasion resistance (Fig. 1.8).

1.2.1.4 Resistance to immersion in boiling water

The effect of immersion in boiling water for 2 h is determined by the increase in mass and thickness of test specimens and by noting any change in appearance, according to EN 438-2. Four specimens are taken from the same laminate with 50 ± 1 mm square, and of the thickness of the laminate being tested, and cut in such a way that no appreciable heat is generated and the edges are free from cracks. Cut edges should be smooth.

Each specimen is weighed to the nearest 1 mg, and the thickness is measured at the middle of each of the four cut edges. The specimens are placed in a vessel containing boiling distilled water. After 120 ± 5 min, the specimens are removed from the boiling water and allowed to cool for 15 ± 5 min in the vessel of distilled water maintained at 23 ± 2 °C (Fig. 1.9). The specimens are dried with a clean dry cloth and then weighed again to the nearest 1 mg.

The percentage by mass of boiling water absorbed by the laminate under test and the percentage increase in thickness are the average of the values obtained on the three specimens.

Resistance to water vapor

According to EN 438-2, this test determines the ability of the laminate surface to resist water vapor.

A specimen of 100 × 100 mm, cut from the laminate being tested, is held in place over the neck of a flask containing boiling water, so that the decorative surface of the

Fig. 1.9: Resistance to immersion in boiling water.

Fig. 1.10: Resistance to water vapor.

Tab. 1.2: Rating scale for surface appearance in resistance to immersion in boiling water test.

Rating scale	Surface appearance
5	No visible change
4	Slight change of gloss and/or color, only visible at certain viewing angles
3	Moderate change of gloss and/or color
2	Marked change of gloss and/or color
1	Blistering and/or delamination

specimen is exposed to the water vapor (Fig. 1.10). After 1 h the specimen is removed and allowed to recover for 24 h in normal ambient conditions before examination.

The result of the examination, in terms of change in appearance, is expressed in accordance with the following rating scale specified in Tab. 1.2.

1.2.1.5 Resistance to dry heat

This test determines the suitability of decorative laminates for use in kitchens, where contact with moderately hot cooking utensils can occur (EN 438-2).

The laminate specimen bonded to chipboard is put in contact with a standard aluminium alloy block (Fig. 1.11) with a given specific heat, initially at a specified test temperature of 160 °C, and is cooled down for 20 min. After this time has elapsed, the block is removed.

Resistance to the test conditions is assessed by visual examination in accordance with the rating scale specified in Tab. 1.3.

Fig. 1.11: Apparatus for the dry heat test.

Tab. 1.3: Rating scale for surface appearance in dry heat resistance test.

Rating scale	Surface appearance
5	No visible change
4	Slight change of gloss and/or color, only visible at certain viewing angles
3	Moderate change of gloss and/or color
2	Marked change of gloss and/or color
1	Surface damage and/or blistering

1.2.1.6 Resistance to climatic shock

Specimens taken from the laminate being tested are subjected to a 5-day test cycle of rapid changes in temperature and relative humidity, after which they are visually inspected and tested to determine any changes in mechanical properties (EN 438-2).

On the first day, four specimens are placed in a hot wet conditioning chamber for 8 h, and then the procedure described in Tab. 1.4 is followed.

After 4 cycles, the specimens are assessed in accordance with the rating scale specified in Tab. 1.5.

All the specimens and control specimens are tested for flexural strength and modulus of elasticity in flexure in accordance with EN ISO 178 [16].

Tab. 1.4: The 5-day test cycle.

	Climate conditions			
	Duration (h)	Temperature (ºC)	Relative humidity (%)	Condition
First day	8	+80	90	Hot wet
	16	+80		Hot dry
Second day	8	+80	90	Hot wet
	16*	−20		Cold dry
Third day	8	+80	90	Hot wet
	16	+80		Hot dry
Fourth day	8*	−20		Cold dry
	16	+80		Hot dry
Fifth day	8	+80	90	Hot wet
	16*	−20		Cold dry

* Longer durations in cold dry conditions are permitted to accommodate nonworking day.

Tab. 1.5: . Rating scale for surface appearance in resistance to climatic shock test.

Rating scale	Surface appearance
5	No visible change
4	Change of gloss only
3	Hairline surface cracks and/or erosion of surface
2	Surface cracks
1	Blistering and/or delamination

1.2.1.7 Resistance to impact by small-diameter ball

In this test, a specimen from the laminate is bonded to a particle-board panel, and its surface is subjected to the impact of a 5 mm steel ball mounted at one end of a spring-loaded bolt (EN 438-2). The resistance to impact is measured as the spring force for which no visible damage occurs (Fig. 1.12).

The impact resistance of the laminate being tested is the maximum value of the spring force, in Newtons, for which no damage occurs in a series of five strikes.

1.2.1.8 Resistance to scratching

The resistance to scratching of the decorative laminate sheet being tested is expressed as a numerical rating which defines the maximum applied load which does not produce a continuous surface scratch (EN 438-2). A test specimen square measuring 100 ± 1 mm is cut from the sheet being tested, and a scratch testing apparatus with a diamond scratching point is used (Fig. 1.13).
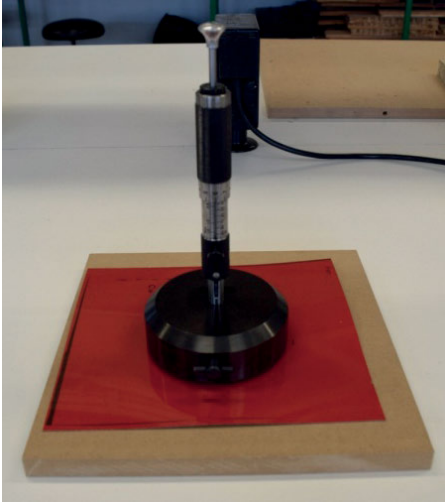
Fig. 1.12: Impact tester with support fixture for impact tester.
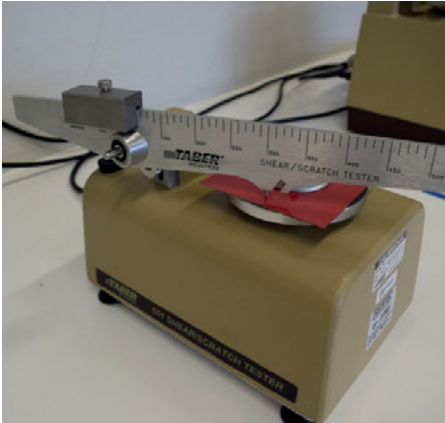
Fig. 1.13: Type of apparatus for measuring resistance to scratching.

This equipment permits to apply a load with an accuracy of ±0.1 N to the scratching point, since it has a moveable weight that according its position permits fixation of the load. The diamond scratching point is hemispherical, with a point radius of 0.090 ± 0.003 mm and an included angle of 90 ± 1°. The height of the arm is adjusted so that it is horizontal when the diamond point rests on the test specimen.

The test starts by making two scratches at 1.0 N load with a spacing of 1 to 2 mm between the scratch marks. This procedure is repeated on the same specimen with loads of 2.0 N, 4.0 N, and 6.0 N, leaving a space of 3–5 mm between each pair of scratches. The specimen is removed from the apparatus, and the scratched area of the surface is rubbed with a suitable contrast medium to help the observation of the scratches using a viewing enclosure.

Fig. 1.14: Type of apparatus to observe surface damage after testing.

Tab. 1.6: Rating scale for scratch resistance.

Rating scale	Discontinuous scratches, or faint superficial marks, or no visible marks	≥ 90 % continuous double circle of scratch marks clearly visible
5	6 N	> 6 N
4	4 N	6 N
3	2 N	4 N
2	1 N	2 N
1	—	1 N

The surface is observed (Fig. 1.14) to determine the lowest load for which an almost continuous (i.e. > 90 %) double circle of scratch marks can be observed.

The scratch resistance of the laminate being tested is expressed in accordance with the rating scale shown in Tab. 1.6.

1.2.1.9 Resistance to staining

The staining resistance method (EN 438-2) determines the chemical resistance of HPL when in contact with a series of agents. The time and conditions of contact are specified for each agent. At the end of the specified contact period, the specimens are washed and examined for residual surface marks. In Tab. 1.7, the list of staining agents of EN 438-2, organized in three groups, is presented. The reference agents of each group are marked with an asterisk; if the laminate under test meets specification requirements when tested with each of the five staining agents marked with an asterisk and underlined, then it is considered to comply with the specification for stain resistance. In the case of a specific complaint, the staining agent in question (selected from Group 1, 2, or 3) is used to verify the quality of the laminate (Tab. 1.7). This test method may also be applied using other staining agents to cover specific requirements, e.g. other chemicals.

A disc is immersed into the staining agent for between 30 and 60 s, quickly placed on the test surface. and immediately covered with an inverted glass Petri dish. After the test period (Tab. 1.8), the glass Petri dish is removed and lifted off the disc with the tweezers. Any remaining test liquid is removed with the absorbent paper without rubbing. Then, for each liquid the test surfaces are observed. and the test area is compared with the area surrounding it, according to Tab. 1.8.

Tab. 1.7: Staining agents and test conditions.

Staining agent		Test conditions
Group 1	*Acetone* Other organic solvents Toothpaste Hand cream Urine Alcoholic beverages Natural fruit and vegetable juices Lemonade and fruit drinks Meats and sausages Animal and vegetable fats and oils Water Yeast suspension in water Salt (NaCl) solutions Mustard Lyes, soap solutions Cleaning solution consisting of: 23 % dodecylbenzene sulfonate, 10 % alkyl aryl polyglycol ether, 67 % water Commercial disinfectants Stain or paint removers based on organic solvents Citric acid (10 % solution)	Apply staining agent at ambient temperature – 16 h
Group 2	*Coffee* (120 g of coffee per liter of water) Black tea (9 g of tea per liter of water) Milk (all types)	Apply staining agent at approximately 80 °C – 16 h
	Wine vinegar Alkaline-based cleaning agents (to 10 % concentration with water) Hydrogen peroxide (3 % solution) Ammonia (10 % solution of commercial concentrate) Nail polish Nail polish remover Lipstick Water colors Laundry marking inks Ballpoint inks	Apply staining agent at ambient temperature – 16 h

Tab. 1.7: (continued)

Staining agent		Test conditions
*Group 3[a]	*Sodium hydroxide* (25 % solution) *Hydrogen peroxide* (30 % solution) Concentrated vinegar (30 % acetic acid) Bleaching agents and sanitary cleaners containing them Hydrochloric acid-based cleaning agents (≤ 3 % HCl) Acid-based metal cleaners Mercurochrome (2,7-dibromo-4-hydroxymercuri- fluoresein, disodium salt) *Shoe polish* Hair coloring and bleaching agents Iodine Boric acid Lacquers and adhesives (except fast curing materials) Amidosulfonic acid descaling agents (< 10 % solution)	Apply staining agent at ambient temperature – 10 min

a Some commercial cleaning agents contain acids and alkalines in concentrations stronger than those shown in Group 3, and can cause surface marking or damage. Any spillage of such materials must be washed off immediately.

Tab. 1.8: Rating scale for staining test.

Rating scale	Surface appearance
5	No visible change
4	Slight change of gloss and/or color, only visible at certain viewing angles
3	Moderate change of gloss and/or color
2	Marked change of gloss and/or color
1	Surface damage and/or blistering

1.2.1.10 Resistance to UV light (exterior-grade laminates)

This test simulates the degradation of the polymer matrix on laminate surface by exposure to high levels of UV radiation. The apparatus is specified in EN ISO 4892-3 [17]: a test chamber with eight fluorescent UV-Iamps, a heated water pan, test specimen rack, and provisions for controlling and indicating operation times and temperature (Fig. 1.15). The lamps are UV-B lamps of 40 W with a peak emission at 313 nm and a spectral energy distribution as specified in EN ISO 4892-3. Usually two specimens are cut from the laminate. One specimen is exposed, and the other (the control specimen) is kept in dark conditions. According to EN ISO 4892-3, the specimens are cycled through periods of exposure to UV radiation, followed by periods of no radiation, where the samples are turned to the inside lamps.

Fig. 1.15: UV chamber.

Tab. 1.9: Rating scale for staining resistance test.

Rating scale	Surface appearance
5	No visible change
4	Change of gloss only
3	Hairline surface cracks and/or erosion of surface
2	Surface cracks
1	Blistering and/or delamination

The cycle consists of 4 h of dry UV exposure at a black-standard temperature of 60 ± 3 °C, followed by 4 h of condensation exposure, without radiation, at a black-standard temperature of 50 ± 3 °C. After a specified light dosage, the effect on the test specimen is assessed by comparing with the control specimen in accordance with the rating scale as specified in Tab. 1.9.

1.2.1.11 Resistance to artificial weathering (exterior-grade laminates)

This test simulates the degradation due to the combined effect of artificial daylight, simulated by the filtered light of one or more xenon arc lamp(s), and rain. The test is carried out in a chamber in accordance with EN ISO 4892-2 with the following operating conditions (Fig. 1.16):
- irradiance at the test specimen surface in the wavelength range 300 nm to 400 nm: 60 ± 3 W/m^2; or at wavelength 340 nm: (0.5 ± 0.03) W/m^2;
- continuous exposure of radiation from the source;
- black-standard temperature: 65 ± 3 °C;
- Relative humidity: 65 ± 10 %;
- Spray cycle: duration of spraying 18 ± 0.5 min interval between spraying 102 ± 0.5 min.
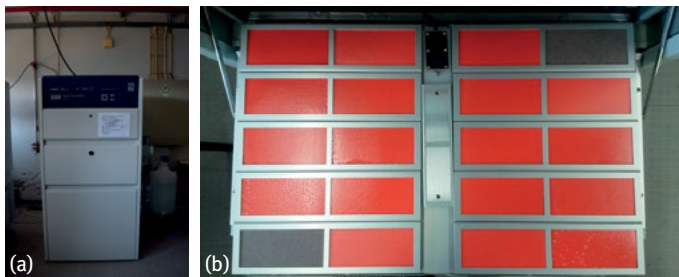
Fig. 1.16: Xénon test chamber for artificial weathering.

The specimen cut from the laminate is examined in a viewing enclosure with the naked eye and the appearance compared with the control specimen (unexposed). Any change of appearance of the test specimen is assessed using the same rating scale as the previous test (Tab. 1.9). Quantitative assessment can be carried out using a color meter and a gloss meter.

1.2.1.12 Resistance to cigarette burns

This test is intended to determine the ability of decorative laminates to resist heat from a burning cigarette placed on the surface. Three test pieces (each 100 × 100 mm) are cut out of the laminates. For this test, pale tobacco filter cigarettes from each of three well-known brands are used. The cigarette is ignited and allowed to burn approximately 10 mm. Then the burning cigarette is placed for full-length contact with the horizontal surface of the specimen in a draught-free area. The glued seam of the cigarette should not be in contact with the specimen. The cigarette continues burning until an additional 20 mm length is consumed. If the cigarette goes out before this occurs, the test must be repeated (Fig. 1.17).

The surface is cleaned with a soft cloth moistened with ethanol to remove any combustion residues. The surface is examined, and the assessment is done in accordance to the rating scale specified in Tab. 1.10.

Fig. 1.17: Cigarette test in high-pressure laminates.

Tab. 1.10: Rating scale for cigarette burn resistance.

Rating scale	Surface appearance
5	No visible change
4	Slight change of gloss and/or color, only visible at certain viewing angles
3	Moderate change of gloss and/or color
2	Marked change of gloss and/or color
1	Surface damage and/or blistering

1.2.1.13 Gloss level

The determination of gloss level is very important for the evaluation of the surface quality of HPL. Using either a specular gloss meter or a reflectometer (Fig. 1.18) the aim of this test is to assess the specular gloss of the test piece as a numerical value or to compare the specular gloss of the test piece against a master sample.

Fig. 1.18: Specular gloss meter/reflectometer.

A 200×200 mm test piece is cut from the laminate being tested. When different designs and surface finishes are used the surface for comparison should be stated. The gloss meter is placed on the surface of the test piece. Measurements are carried out using a gloss meter with the specified geometries and according to the following procedure: measure the gloss using the 60° geometry method. If the result is > 70 units (high specular gloss), additional measurements shall be carried out using the 20° geometry method.

At least 2 measurements are carried out in each of the four directions of the board (longitudinal and transverse) at the determined angle. The mean value for each direction is calculated.

1.2.1.14 Determination of color of HPL

The aim of this test is to measure the surface color level of laminates when there are doubts about the intensity of color, yellowing, mate surfaces, etc. The equipment used – a color meter (Fig. 1.19) – has a light source and three filters that simulate the behavior of human vision and measure the amount of light reflected by the sample. Colors can be described by means of a qualitative or quantitative system.

Fig. 1.19: Color meter.

The qualitative system CIELAB is a color space specified by the CIE (Commission internationale de l'éclairage) and indicates if the sample is lighter, darker, redder, greener, more or less yellow, or blue compared with a standard piece. According to this system, the color is described by 3 coordinates: L^* represents the lightness, a^* represents the content from red to green and b^* represents the content from yellow to blue. ΔL^*, Δa^*, Δb^* represent the differences between the tested sample and the standard piece, and can be calculated by the difference between the coordinate value of the sample and the coordinate value of control. The color difference ΔE^* can be calculated using equation (1.2):

$$\begin{aligned}
\Delta L^* &= L^*_{\text{sample}} - L^*_{\text{control}}, \\
\Delta a^* &= a^*_{\text{sample}} - a^*_{\text{control}}, \\
\Delta b^* &= b^*_{\text{sample}} - b^*_{\text{control}}, \\
\Delta E^* &= \sqrt{(\Delta L^*)^2 + (\Delta a^*)^2 + (\Delta b^*)^2}.
\end{aligned} \tag{1.2}$$

1.2.2 HPL specifications

The type of final applications could change the main properties and specifications desired in a high-pressure laminate. However, there are several requirements for a standard HPL, as reported in Tab. 1.11.

Tab. 1.11: HPL specification.

Properties	Test method	Property requirements
Thickness	EN 438-2	0.8 ± 0.1 mm
Abrasion behavior	EN 438-2	> 400 revolutions
Scratch resistance	EN 438-2	2 N
Resistance to staining	EN 438-2	Grade 5 for group 1–2; Grade 4 for group 3
Resistance to impact	EN 438-2	≥ 20 N
Resistance to dry heat	EN 438-2	Grade 3 for bright finishes/Grade 4 for other finishes
Resistance to boiling water	EN 438-2	Grade 4; weight increase max. 6 %; thickness increase in max. 6 %
Resistance to cigarette burn	EN 438-2	Grade 3
Resistance to accelerated weathering	8 h QUV and 4 h condensation	No loss of gloss, no cracking or delamination

1.3 Upgrading HPL characteristics

Given the worldwide interest in this type of material, the industry has been focusing on developing new products with improved characteristics, such as mar resistance, abrasion resistance, resistance against strong chemicals, weathering resistance, dirt-repellent features, self-healing properties, antibacterial and antifungal properties, and special properties like fluorescent properties and heat sink features.

1.3.1 Mar resistance

Mar resistance is the ability to withstand scratching, scuffing, and/or denting actions which lead to disfiguring or marring of the surface. Mar resistance is the resistance of the coating surface to permanent superficial damage, as a consequent of the application of dynamic mechanical forces [18].

In order to introduce this property in HPL, there are some strategies that report the incorporation of additives in the decorative paper impregnation resin. U.S. Patent No. US 4532170 A (1985) [19] proposes the production of a high-pressure laminate with scuff resistance by incorporating finely divided polyethylene wax having a particle size of about 1–25 microns and a melting point of 220–230 °F. The wax is incorporated as part of a coating mixture applied to the face of a nonimpregnated décor paper sheet in an ultra-thin layer, and then impregnated with conventional melamine formaldehyde resin. The use of an ultra-thin facing layer comprising abrasion-resistant particles and sufficient binder material has also been reported [20]. Another proposed solu-

tion consists of the use of a combination of a thermosetting resin, substantially fully hydrolyzed polyvinyl alcohol, fumed amorphous silica, and particulate abrasive material with a hardness higher than that of silica [21]. However, incorporation of abrasive materials in paper often results in severe damage to the delicate, highly polished, or intricately etched surfaces of the press plates when the abrasive particles deposited in the papers come into contact with them [22] . The damage in the press plates requires replacement or reconditioning, which implies an extremely high cost. Therefore, new studies were done in with the aim of protecting the plate finish, namely the use of mixture of melamine formaldehyde resin, alumina particles, a silane coupling agent, and a thickening agent, that suspends the alumina and protects the plates in the impregnation and coating process [23]. Another approach was to treat the surface of the finishing plates in order to make them more resistant [24].

Wilsonart® HD® High Definiton® Laminates and AR Plus® are high-pressure laminates with mar resistance.

1.3.2 Abrasion resistance

When a product has abrasion resistance, it will resist to the erosion caused by scraping, rubbing, or other types of mechanical wear. This allows the material to retain its integrity and keep its form. This feature is particularly important in horizontal applications where wear is accentuated, in particular in products for flooring applications.

Nowadays, in HPL, abrasion resistance is provided by adding aluminum trioxide (corundum) particles to the melamine resin used to impregnate the decorative or overlay papers. The finer the particle size of the corundum, the greater must be the amount applied to the decorative paper in order to achieve sufficient wear resistance [25].

Another approach involves addition of organosilica particles, produced by sol-gel method, to the impregnation resin of the decorative and/or the overlay papers [26].

Commercially there is the MONOCHROM from Polyrey with this feature.

1.3.3 Resistance against strong chemicals

Taking into account the exceptional mechanical strength properties of HPL, it is important to improve its resistance to strong chemical agents, making them a solution for use in different types of laboratories such as research, photographic, and cosmetic.

In order to develop HPL with higher chemical resistance, many solutions have been described in patents. It is suggested that a chemical-resistant decorative laminate made with a bottom portion impregnated with phenolic resin, a top portion impregnated and coated with vinyl ester terminated bisphenol A epoxy resin, and a middle portion impregnated with aminotriazine-aldehyde resin which acts as a barrier to phenolic resin contact with the vinyl ester terminated bisphenol A epoxy resin.

These resins present a viscosity between 400 and 800 cP. In order to control the viscosity some thixotropic agents were added [27]. It was also proposed to coat the decorative paper with vinyl ester terminated bisphenol A epoxy resin matrix containing hollow plastic microspheres through its thickness [28]. When these laminates were put into contact with sodium hydroxide 10 % and 50 %, sulphuric acid 70 %, concentrated hydrochloric acid, concentrated phosphoric acid, glacial acetic acid, formic acid 90 %, concentrated ammonium hydroxide, potassium permanganate and acetone, they were not affected. However, concentrated nitric acid destroyed the laminate. Dion (1992) suggested a coating with a mixture comprising an unsatured acrylated urethane, a diluting monomer, and a photo initiator [29].

To improve acid resistance, in particular, it has been proposed to combine melamine chemistry with other amino aldehyde compounds with reduced basicity. This approach could reduce not only the basicity of the film, but would also permit the buildup of an amino self-condensed network with better resistance properties. Imidazolidinone derivatives are one of the prime candidates for such modification [30].

Nowadays, some solutions of HPL with high chemical resistance are available on the. CHEMARMOR®, by Nevamar, has been tested and proven to have superior chemical resistance and significantly higher NEMA wear value than competitive laminates. It provides resistance to acids/bases, solvents, stains, indicators, and general reagents. Pionite ChemGuard incorporates the decorative features of high pressure laminate into a durable chemical resistant surfacing material. In order to test the chemical resistance of laminates, two methods were applied. In method A, volatile chemicals are tested by placing a cotton ball saturated with the reagent in the mouth of a 1-ounce bottle and inverting the bottle on the surface of the laminate. In method B, nonvolatile chemicals are tested by placing five drops of the reagent onto the surface of the laminate and covering with 24 mm watch glass. For both methods, the reagents are left on the laminate for a period of 24 h. The laminate is then washed with water, cleaned with detergent and naphtha, rinsed with deionized water and dried with a towel. The effect of the different reagents is then evaluated.

Formica has a commercial solution called Chemtop2™. In the HPL Chemtop2™, chemicals and reagents were placed in contact with the surface of the Chemtop2 laminate sheet in a covered method (watch glass cover) for a period of 16 h prior to visual examination and evaluation. This evaluation encompassed acids, alkalis, dental supplies, photo lab supplies, solvents, general reagents, hospital and health care, mortician supplies, harsh household products, ANSI/NEMA reagents. Only the dichromate cleaning solution, formic acid 90 %, sulfuric acid 96 %, potassium permanganate 25 %, silver nitrate 10 %, wrights blood stain may cause a slight change in gloss or color, depending upon the duration or exposure, while the nitric acid 70 % cause slight damage, depending upon the duration or exposure.

Manufactured with Trespa's unique Electron Beam Curing (EBC) technology, Trespa® Toplab® PLUS surface is easy to clean and shows a high resistance to a large number of aggressive chemicals.

1.3.4 Weathering resistance

Exposure to climatic conditions affects various aspects of the coatings properties such as physical and mechanical properties. Sunlight and humidity are the most important weathering factors [31]. To have weathering resistance is essential in laminates used in facades of buildings, outdoor furniture and partitions and bulkheads balconies.

Coatings formulated for exterior durability should exclude or minimize resins components that are readily oxidized and that absorb UV radiation at wavelengths longer than 290 nm.

To improve the UV resistance of decorative laminates the application of UV-resistant top layers of polyacrylates or butyl rubber to aminoplast layers is prescribed. However, these top layers present low scratch resistance.

Ratzch [32] showed that it is possible to obtain an UV-resistant decorative laminate if the paper is impregnated with an aminoplastic resin that contains UV stabilizers (HALS alone or combinations of HALS with UV absorbers).

Kamoun and coworkers [33] reported that in MF resins water and weather resistance can be enhanced by the addition of hexamine under alkaline conditions.

Synthetic transparent iron oxides could be also an excellent choice for UV resistance in decorative laminates. Nowadays, they are readily available in powder form and as predispersed dispersions for solvent- or waterborne applications. Available in a range of natural color shades from yellow through red to brown, transparent iron oxides offer the wood-finish formulator the combination of the following properties:
– excellent transparency;
– permanence to light;
– durability;
– chemical resistance;
– UV screening;
– economy;
– nontoxicity.

This type of pigment finds application on a wide variety of wood-care systems, including those for fencing, decks, lawn furniture, siding, cabinetry, and flooring [34].

There are several commercial solutions presently available. Trespa® Meteon® panels are reported to have good performance outdoors. The panels are described to be practically impervious to acid rain as well. The Formica group offers an innovative solution, the VIVIX® solid phenolic, engineered exterior façade panels, having a decorative surface on both sides. This lightweight rainscreen cladding solution combines excellent weather and UV resistance properties for enhanced durability and ease of maintenance. Prodema and Durian use a PVDF layer on the upper surface that shows UV resistance. This PVDF film is also antigraffiti and non-stick, preventing organic matter from developing on the panel's surface and reducing the buildup of dust and dirt cause by pollution.

1.3.5 Self-healing properties

One major problem in polymeric layers is the propensity to damage when exposed to critical conditions or long-term use The surfaces may develop microcracks with negative visual impact, which are impossible to remove in thermosetting materials [35]. One solution would be HPL with self-healing properties.

Self-healing materials have the ability to repair microcracks independently of their location, restoring the structure and performance of the material, and, to some degree, minimizing negative visual impact of the damaged surface [35]. This approach allows obtaining more durable materials, with reduced maintenance costs and with a broader range of application in aggressive environments [35]. The concept of self-healing mimics the healing of biological injured tissue. It may be classified according to two aspects [35, 36]:

- autonomic (without any external intervention) or nonautonomic (with external intervention);
- extrinsic (requiring an additional regeneration agent) or intrinsic (without any additional regeneration agent).

An autonomic extrinsic self-healing system for incorporation as an additive in the impregnation resin of the HPL decorative paper has been proposed by Antunes [37] (2013). This approach can be described as follows:

(i)   the healing agent (a drying oil) and an appropriate drying catalyst are encapsulated within the polymeric matrix;
(ii) when the laminate surface is damaged, capsules rupture, releasing the healing and drying agents by capillary action;
(iii) upon contact with atmospheric oxygen, the healing agent undergoes crosslinking, promoting the repair of the cracked areas [36].

So far, all the large HPL producers do not have any solutions in this area. Only the furniture company Haworth is testing a polyurethane resin in order to confer self-healing properties to its products. Arpa also has a product called FENIX NTM TM, which possesses thermal recovery to microcracking.

FENIX NTM™ is an innovative material created for interior design by Arpa Industriale. It is produced by the simultaneous application of heat (approx. 150 °C) and high specific pressure (> 7 MPa) in order to have a homogeneous nonporous high density product. The core structure of FENIX NTM is composed of paper impregnated with thermosetting resins. Its external surface involves the use of nanotechnology, and its decor is obtained through next generation resins developed by Arpa Industriale's research.

1.3.6 Postformable laminates

Especially for the production of kitchen tops, laminates are curved around the edges of a wooden substrate in a postforming line. For this purpose the laminate is exposed to heat for a short period of time provided by hot air or infrared radiation and then bent around the edges [38].

In order to add postformability to a laminate, many solutions have been described in patents.

The approaches reported are related to the modification of the melamine resin that is used to impregnate the decorative layer with caprolactams [39], glucosides [40], carbamates [41], mannatin [42], epoxies [43], and polyethylenoglycol [44]. Also several patents describe modifications to the phenolic resins to improve postforming characteristics [45, 46].

1.3.7 Dirt repellence

For a liquid to spread on a material it must have a surface energy lower than the surface free energy of that material. To achieve a hydrophobic surface the surface free energy must therefore be lower than 72 mN/m, which is the surface tension of water. To achieve an oleophobic surface, the surface free energy must be even lower since most oils have a surface tension around 20–30 mN/m.

In decorative laminates the dirt repellency could be achieved applying a surface treatment to the dried overlay to form a treated overlay, wherein the surface treatment consists of a fluorourethane reaction product of at least one diisocyanate, polyisocyanate, or a mixture of polyisocyanates [47].

1.3.8 Antibacterial action

In use, high-pressure laminates are a breeding ground for bacteria, fungi, and other microorganisms. Therefore, attempts have been made to develop high-pressure laminates exhibiting antimicrobial action [48].

Growth-retarding or microbicidal additives can be incorporated into melamine coatings to produce so-called "active" coatings. The additives can be incorporated onto melamine surfaces in an additional coating step by applying them as a solution or dispersion, or during the production together with the coating resin.

Antimicrobial additives fall into two groups: organic and inorganic. The organic compounds described in the literature include phosphonium salts, protoporphyrine-based sulfonium salts, antibiotics, chlorophenyl derivatives, biomimetic polyamides, arylsulfonyl alkenenitrile, aminobenzylsulfonyl acrylamide, quaternary ammonium salts, and 2,4,4′-trichloro-2′-hydroxydiphenolether (triclosan), and 2,3,5,6-tetrachloro-

4-methylsulfonylpyridine, and the inorganic compounds. Inorganic additives are typically heavy metals such as silver, copper, and zinc in different forms (metallic–salt; colloidal–nano-sized), light-activated singlet oxygen sources such as titanium dioxide, or other salts such as barium metaborate.

Besides the addition of antimicrobial additives, also nanoparticles have been associated with improved antimicrobial properties, although their mode of action in this regard has not yet been thoroughly investigated.

HPL with this property are already seen on the market. A collaboration of Formica® and BioCote® presents Protec+™, a high-performance premium laminate product. Protec+™ introduces an additional layer of hygienic protection through the utilization of the antimicrobial properties of silver.

Also Trespa® Virtuon® has inherent antibacterial properties, without the addition of antimicrobial additive, with a surface manufactured using Trespa's unique in-house technology, electron beam curing (EBC).

1.3.9 Thermal comfort

Phase change materials (PCM) are "latent" heat storage materials. The thermal energy transfer occurs when the material changes from solid to liquid, or liquid to solid. Unlike conventional materials, PCM can absorb and release heat at a nearly constant temperature. They store 5–14 times more heat per unit volume than conventional storage materials such as water, masonry, or rock. A large number of phase change materials (organic, inorganic, and eutectic) are available in any required temperature range [49].

1.3.10 Phosphorescence

Phosphorescence is a specific type of photoluminescence related to fluorescence.

Photoluminescence is light emission from any form of matter after the absorption of photons. It is one of many forms of luminescence (light emission) and is initiated by photoexcitation (excitation by photons); hence the prefix "photo".

The introduction of this feature in HPL has great potential, since it can not only focus on usual applications (furniture and decoration) but also open up new markets (signage, security, entertainment, and homes). It can already be made for its use in vertical and horizontal signage (emergency exit signs and emergency plans) and also in commercial and leisure areas (shops, bars, and clubs) and home environments (child room).

The afterglow could be achieved by incorporating the phosphorescent pigment in the melamine resin impregnated overlay paper. The laminate produced with this special overlay should maintain good surface appearance to natural and artificial light and have the fluorescent effect in the dark.

References

[1]   High-pressure decorative laminates (HPL). Sheets based on thermosetting resins (usually called laminates). Determination of properties; 2005. BSI. p. 74.

[2]   Figueiredo AB, et al. Structure-Surface Property Relationships of Kraft Papers: Implication on Impregnation with Phenol-Formaldehyde Resin. Industrial & Engineering Chemistry Research. 2011; 50(5): 2883–2890.

[3]   Fletcher Building Laminates & Panels Division Analysts; 2012 [cited 2015, Jul]. Available from: www.fbu.com/media/18773/190911-formicagroupanalystspresentation19sept.pdf.

[4]   The significant global rise of decorative laminates. In: Wood based panels international; 2015 [cited 2015, Jul]. Available from: www.wbpionline.com/features/the-significant-global-rise-of-decorative-laminates-4637936/.

[5]   Decorative laminates market: global industry analysis and forecast to 2020. [cited 2015, Jul]; Available from: www.persistencemarketresearch.com/market-research/decorative-laminates-market.asp.

[6]   Kohlmayr M, Zuckerstätter G, Kandelbauer A. Modification of melamine-formaldehyde resins by substances from renewable resources. Journal of Applied Polymer Science. 2012; 124(6): 4416–4423.

[7]   Lokensard E. Industrial Plastics: Theory and Applications. Boston: Cengage Learning; 2010.

[8]   Merline DJ, Vukusic S, Abdala AA. Melamine formaldehyde: curing studies and reaction mechanism. Polym J. 2013; 45(4): 413–419.

[9]   Kloeser L, et al. Panels boards and conventional adhesives. In: Kües U, editor. Wood production, wood technology and biotechnology impacts. Göttingen: Universitätsverlag Göttingen; 2007.

[10] Nemli G, Usta M. Influences of some manufacturing factors on the important quality properties of melamine-impregnated papers. Building and Environment. 2004; 39(5): 567–570.

[11] Kandelbauer A, et al. On the performance of a melamine–urea–formaldehyde resin for decorative paper coatings. European Journal of Wood and Wood Products. 2010; 68(1): 63–75.

[12] Zwan R, Strunk S. Compressible decorative paper impregnating agent which can be printed by the inkjet method. United States patent US 8,460,767 B2. 2010.

[13] Humprey PE. Outline Standard for Adhesion DYnamics Evaluation Employing the ABES (Automated Bonding Evaluation System) Technique. International Conference on Wood Adhesive, Lake Tahoe; 2009.

[14] Martins JM, et al. A New Methodology to Evaluate the Cure of Resin-Impregnated Paper for HPL. The Journal of Adhesion. 2015; 91(10/11): 792–800.

[15] [cited 2015, Sep]. Available from: www.abrasiontesting.com/case-studies/laminate-flooring/.

[16] Plastics. Determination of flexural properties; 2011. ISO 178:2010.

[17] Plastics. Methods of exposure to laboratory light sources. Fluorescent UV lamps; 2013. BSI. p. 24. ISO 4892-3:2013.

[18] Guevin P. Hardness, in Paint and Coating testing. In: Koleske J, editor. Manual. American Society for Testing and Materials; 1995.

[19] O'Dell R, Ungar I, Scher H. Scuff-resistant laminates. United States patent US 4,532,170 A. 1985.

[20] O' Dell R, Ungar I, Scher H. Scuff-resistant in abrasion-resistant laminates. United States patent US 4,741,946 A. 1986.

[21] Park J, White P, Richardson C. Damage resistant decorative laminates. United States patent US 4,880,689 A. 1989.

[22] Fuerst P. Abrasive-resistant decorative laminates and method for making same. United States patent US 3,445,327 A. 1969.

[23] Albrinck DJ, Mascavage JJ. Wear-resistant decorative laminates and methods of producing same. United States patent US 5,558,906 A. 1996.

[24] Ma M, Oliver J. Coated pressing surfaces for abrasion resistant laminate and making laminates therefrom. United States patent US 6,656,329 B1. 2003.

[25] Gaa P, et al. Method of impregnating decorative paper with melamine resin. Patent EP0819794 A3. 2002.

[26] Magina SP, et al. Organic-inorganic sol-gel coating of paper surfaces of High-pressure laminates. in 12th International Chemical and Biological Engineering Conference. 2014. Porto, Portugal: FEUP Edições.

[27] Brooker L, Jarrell D. Chemical Resistant Decorative Laminates. Westinghouse Electric Corp., United States; 1984. p. 12.

[28] Cannady D, Brooker L. Decorative laminates having a thick chemical resistant outer layer. United States patent US 4,726,986 A. 1986.

[29] Dion A. Urethane acrylate surfaced laminate. Patent EP0474470 A2. 1992.

[30] Blank WJ, et al. Melamine Formaldehyde Networks with Improved Chemical Resistance. Polymer Materials Science and Engineering. 1997; 77: 391–392.

[31] Mohseni M, Ramezanzadeh B, Yari H. Effects of Environmental Conditions on Degradation of Automotive Coatings, In: Chiaberge PM, editor. New Trends and Developments in Automotive Industry. Rijeka: InTech; 2011.

[32] Ratzsch M, et al. UV-Resistant, thermocurable aminoplast composite, the production thereof and the use of the same. United States; 2005. p. 5.

[33] Kamoun C, Pizzi A, Zanetti M. Upgrading melamine–urea–formaldehyde polycondensation resins with buffering additives. I. The effect of hexamine sulfate and its limits. Journal of Applied Polymer Science. 2003; 90(1): 203–214.

[34] Wright P, McKenna, M. Using transparent iron oxide pigments in wood finish applications Paint & Coating Industry. 2000; 16(11): p. 44.

[35] Ghosh K. Self-Healing Materials: Fundamentals, Design Strategies, and Applications in Self-Healing Materials. Wiley-VCH Verlag GmbH & Co. KGaA; 2009. p. 1–28.

[36] Suryanarayana C, Rao K, Kumar D. Preparation and characterization of microcapsules containing linseed oil and its use in self-healing coatings. Progress in Organic Coatings. 2008; 63: 72–78.

[37] Antunes A, et al. Self-healing laminates for surfacing wood-based panels. In: Cost Action FP1006 "Bringing new functions to wood through surface modification", Ghent, Belgium; 2013.

[38] Lepedat K, Wagner R, Lang J. Laminates. In: Pilato L, editor. Phenolic Resins: A century of progress. New York: Springer; 2010.

[39] Kropa EL, Thomas WM, Wohnsiedler HP. Modified aminoplast and products prepared therefrom. United States patent US 2,584,177 A. 1952.

[40] Magrane JK, Sloatman W. Laminate and resinous composition. United States patent US 2,773,788 A. 1956.

[41] Coutras A, Updergaff I. Alkyl carbamate plasticized melaminealdehyde resin composition. United States patent US 2,937,966 A. 1960.

[42] Grudus GM, Larkin JD. Melamine laminating resin modified with mannitan; 1965.

[43] McCaskey HO, Brooker L. Melamine-aldehyde resin and postformable laminate made therefrom; 1977.

[44] Brooker L, Mungin H. Polyethylene glycol modified melamine aldehyde resin and postformable laminate made therewith. United States patent US 4,405,690 A. 1983.

[45] Hawthorn J. Laminated sheet materials. United States patent US 3,322,613 A. 1968.

[46] Grosheim G, Fay C. High pressure decorative laminate suitable for use as postforming and standard laminate. United States patent US 3,131,116 A. 1972.

[47] Wu D, Yen J. Paper laminates having improved easy clean and abrasion resistance properties. United States patent US 8,486,219 B2. 2013.

[48] Trogolo J, Barry J. Antibiotic high-pressure laminates. United States patent US 6,248,342 B1. 2001.

[49] Sharma A, et al. Review on thermal energy storage with phase change materials and applications. Renewable and Sustainable Energy Reviews. 2009; 13(2): 318–345.

Stephane Molina

2 Activation of natural fibers using physical routes: Applications for composites materials

Abstract: Natural fibers as reinforcing elements in composites have attracted much attention as emphasized by the numerous reviews on the topic. In recent decades, driven by increasing environmental requirements, manufacturers made significant advancements in development and production of natural fiber-based materials. With respect to matrices, because of their poor recyclability, thermosets are nowadays supplanted by thermoplastics polymers. Nonetheless, the development of thermoplastic–natural fiber materials is especially constrained by significant differences in the surface energies of components. Improvement of interface quality by chemical means is not detailed in this chapter, which is merely devoted to physical routes for fiber activation. Of these we focused here on wave and radiation activations, physico-chemical treatments, and thermomechanical technologies. In general, the effects on fibers are detailed: the chemical, physical and mechanical modifications.

2.1 Introduction

What is really a composite material? No universal literal definition can be found, but only a compromise. Indeed, any strict definition is at best imprecise and could or could not include systems considered by some to be composite. According to Lee, the following description has been chosen after deliberation [1]:

> A multiphase material formed from a combination of materials which differ in composition or form, remain bonded together, and retain their identities and properties. Composites maintain an interface between components and act in concert to provide improved specific or synergistic characteristics not obtainable by any of the original components acting alone.

From this description, a composite can be considered to be a combination of two or more materials: reinforcing elements, fillers, and matrix binder. Polymer composites can be described as plastics within which fibers or particles are embedded. The plastic is called the matrix, and the fibers or particles dispersed within it are the reinforcements. The latter is usually stiffer than the matrix, giving a stiffening effect to the overall material. Examples of products manufactured using composite systems include automobile and aircraft parts, bathtubs, vanities, truck hoods, recreational boats, small appliances, and storage tanks. Composite use has continuously grown since its introduction in the 1960s.

2.1.1 Reinforcements

With respect to fillers, natural fibers as reinforcing elements have attracted much attention, as emphasized by the numerous reviews on the topic. In recent decades, driven by increasing environmental requirements, manufacturers made significant advancements in the development and production of natural fiber-based composites. The automotive market sector is an example of an area that has an important increase in cellulose fiber usage. In this case, biosourced fiber materials are commonly used for dashboards, door panels, seat backs, and interior parts. Due to their good mechanical properties, glass and mineral fillers or reinforcements are able to fit the structural and durability demands of automobile exterior and interior parts. Nevertheless, mineral fiber-reinforced polymers exhibit several disadvantages. These are known to be abrasive, difficult to condition, and frequently lead to important tool wear. They are obtained from nonrenewable resources and present potential health hazards caused by particles released during machining. Cellulose-based fibers are identified as good reinforcing fillers. This is one of the two major factors of the very existence of natural fiber plastic composites: (i) to produce a less expensive composite, (ii) to obtain a material with better properties overall compared to those of both raw polymer and fibers.

As an example, the effect of the nature of fillers on the mechanical properties of polypropylene-based composites is reported in Tab. 2.1.

Tab. 2.1: Mechanical properties of filled polypropylene composites (according to Williams [2]).

Filler	Flexural		Tensile	
	Strength (MPa)	Modulus (GPa)	Strength	Modulus
None (neat PP)	28.7	1.38	27.6	1.40
33 % hemp	45.0	3.01	40.0	4.20
33 % hemp woody core	69.6	3.21	57.2	4.32
30 % glass fiber	115.1	4.07	53.1	4.89

In addition, an ecobalance applied to cellulosic fiber composites shows that these materials are very valuable [3, 4]. For instance, the energy required to manufacture a flax fiber material (including activation, harvesting, and fiber preparation) is only 9.55 MJ kg^{-1} versus 54.7 MJ kg^{-1} for a glass fiber compound, i.e. six times lower. Besides, breaking mineral filled composites results in sharp splinters that can be involved in injuries of workers and/or users. Glass fiber-based materials have poor recycling properties and high density: approximately 40 % higher than those made of natural fibers [5]. Moreover, using biosourced reinforcements in composites also presents several advantages: the bio-based resource is widely available, environment friendly, sus-

tainable, not abrasive and low in cost. Natural fibers also have lower densities, high specific properties, and allow high filling levels [6, 7]. At this time, researchers as well as automakers are evaluating the environmental impact of a vehicle's entire life cycle and developing natural fiberr composites. However, regarding markets, the automotive industry has no monopoly: the use of biofibers is current in several other sectors, such as leisure, medical, and building, with an increase of 13 % over the last 10 years and an annual use of nearly 275 million kg.

But there is also a disadvantage related to the use of natural fibers as a reinforcement of matrices. The presence of hydroxyl and other polar groups involves high moisture adsorption properties. During the processing of hot melt under high pressure, water present in fibers does not boil at normal processing temperatures. As an example, at 800 psi (55 bar) in the extruder, water boils at 270 °C (518 °F). Furthermore, when the blend passes through zones where pressure is lowered, water suddenly and violently boils. Thus, it is recognized that adsorbed water in cellulosic fibers can lead to steam formation during processing. As a result, the porosity of the obtained material is increased and its density lowered. The water also accelerates the oxidation of the hot melt during processing leading to a composite weaker and less durable. In the 1980s attention was paid to reduce moisture from cellulosic fibers: treatment of biofibers with glyoxal [8] or thermal coupled chemical treatment with alcohols [9].

Regarding the final material, the higher the fibrous filler content in a composite material is, the higher the water adsorption, unless each cellulose particle is fully encapsulated in the matrix and thus inaccessible to water. Actually, moisture adsorption typically shows a linear increase with the increase in cellulose ratio in the composite.

2.1.2 Polymer matrix

The matrix is the other component of a composite. Because of their poor recyclability, thermosets are nowadays supplanted by thermoplastics in natural fiber-based composites. The development of thermoplastics–natural fibers materials is constrained by two main physical limits [10]:
–   the upper temperature at which the fiber can be processed,
–   the significant difference in the surface energies of compound.

Dealing with the first point, plant materials generally contain a third to three quarters cellulose, a third or less of lignin, a third or less of hemicellulosics and minerals, by weight (Tab. 2.2). Typically, natural fibers begin to undergo some dehydratation at temperatures belong the thermoplastic melting point (110 °C). This phenomenon is followed by a decrease of the degree of polymerization of the three main constituents, which is enhanced in the presence of moisture. Lignin and hemicelluloses begin to degrade at about 150 °C and 160 °C, respectively. Because of their limited thermal stability, natural fibers can be formally deteriorated between 130 and 230 °C, depend-

Tab. 2.2: Composition of commonly used fibers.

Component	Hemp	Flax	Softwoods	Rice hulls
Cellulose	76 ± 3	75 ± 4	42 ± 2	38 ± 8
Hemicellulose	17 ± 3	20 ± 2	26 ± 3	25 ± 3
Lignin	4.5 ± 1	4.5 ± 1	29 ± 4	14 ± 2
Minerals	< 1	< 1	< 1	19

ing on the processing duration. As a consequence, matrices generally used in natural fiber-based composites are polypropylene and polyethylene. These polymers have processable melt viscosities at or below the higher temperature permitted for fibers.

Concerning the second point, since natural fibers are highly polar and hydrophilic, it makes them subject to both loss of mechanical properties upon atmospheric moisture absorption and poorly compatibility with nonpolar matrices. As a consequence, the potential of biosourced fillers in composites is reduced, because the interfacial adhesion is often insufficient to lead to good macroscopic mechanical properties.

In order to avoid these drawbacks, natural fibers can be submitted to specific surface modifications so as to provide an efficient hydrophobic barrier and/or minimize their interfacial energy and thus involve optimum interactions. Modification of natural cellulosic fibers can be done by chemical or physico-chemical routes.

By the chemical route, improvement in interfacial strength is generally achieved by grafting onto fibers molecules playing the role of a "bridge" or a "crossbeam" between fillers and matrix, or by establishing a continuity of covalent bonds at the interface of both components. Hydroxyl functions are the cellulose chemical groups involved in this route. The chemistry of alcohols is very well known and they are used to prepare a wide range of cellulose derivatives, e.g. esters, ethers, halides, etc. Such surface modification of fiber would not only decrease moisture adsorption, but would also concomitantly increase wettability of fibers with resin and thus improve interfacial bond strength, which are critical factors for obtaining better mechanical properties of a composite. The coupling reagents used in this context are expected to block the hydroxy groups of natural fillers, thus making the fibers more hydrophobic. The improvement of interface quality by the chemical route will not be detailed in this chapter.

Physical or physico-chemical treatments applied to composite fields are carried out on fibers for two main reasons: activation or modification and separation of fiber networks into individual filaments. This chapter is not a comprehensive description of these processes, because these are abundant in the literature. It aims at a brief description of (i) techniques which are either used or can be used readily to activate fiber surfaces, (ii) the main effects obtained, and (iii) the consequence on final composite properties.

2.2 Surface activation of cellulosic fibers: Wave and radiation technologies

2.2.1 Ultraviolet (UV) technology

2.2.1.1 Basic principles

The origin of the term is from the Latin "ultra", meaning beyond, and violet, the color of the shortest wavelengths of visible light. Accordingly, UV light has shorter wavelengths than visible light, between 100 and 400 nm. This band is divided into number of ranges as described by the draft ISO standard on determining solar irradiances [11]. The regions are distinguished by wavelengths and thus by how energetic the ultraviolet radiation is.

In plant materials, lignin is claimed to be a photosensitive component, and its degradation under UV light is known to be largely responsible for the fading of wood and wood plastic composites (WPC). However, ultraviolet radiation has also been used to modify natural fibers, and a number of studies have been devoted to this subect.

2.2.1.2 Treatment effects on fibers

Merlin [12] extracted cellulose from an Egyptian commercial cotton with the method developed by Corey [13] and bleached it in sodium hypochlorite. Cellulose was submitted to a steam lamp of high-pressure mercury emitting predominately 313 and 365 nm wavelengths in the presence of benzophenone. The irradiation (90 minutes) of this cellulose was directly driven in the cavity of a ESR spectrometer device (Thomsom, THN 250) used for analyses. Merlin observed signals resulting from radicals developed on cellulose. By examining the radicals likely to form by bond breaking, dehydrogenation, and dehydroxylation, the recorded ESR pattern can be successfully interpreted. The radicals identified are of several types.

The glugosidic bond break led to the generation of alcoxy radicals as shown in Fig. 2.1 (a). Hydrogen breakout on what is usually referred to as C1 to C6 carbons can lead to the radical formation shown in Fig. 2.1 (b). Cellulose dehydroxylation on C2, C5, and C6 location can lead to the species shown in Fig. 2.1 (c). Other authors have confirmed these observations [14, 15].

Koichi et al. [16] worked on three types of methanol extracted cellulose fibers such as nonwoven fabrics of cuprammonium rayon, nonwoven fabrics of natural cellulose and absorbent cotton. The above materials were submitted to vacuum ultraviolet irradiation (VUV) in a bid to establish the efficiency of such a technique in terms of oxidation capacity. The authors compared their results with other common oxidation techniques, e.g. ozone, peroxide, chromic, and nitric acids treatments. The evolution of the surface chemical composition was investigated by FTIR spectroscopy analysis. Following the intensity variation of the band pointed at 1720 cm^{-1}, the authors con-
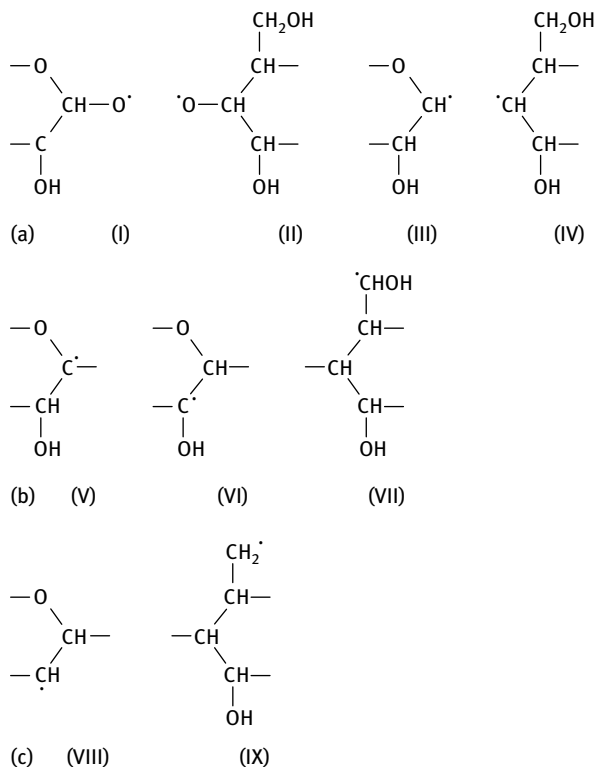
Fig. 2.1: (a) Radical production on cellulose under UV radiation. (b) Radical production on cellulose under UV radiation. (c) Radical production on cellulose under UV radiation.

cluded that vacuum ultraviolet irradiation induced surface oxidation as efficiently as chromic and nitric acids.

Commercially available tossa jute fibers were UV treated at atmospheric pressure by Gassan et al. [17] in order to improve the mechanical properties of natural fiber/epoxy composites made of them. In the case of UV treated fibers and yarn, the results obtained reveal significant enhancement of the polar component of free surface energy and that of polarity with the treatment time increase. These trends were explained by a surface oxidation induced by an increase of concentration of carboxyl groups on fiber surfaces. As a consequence, the wettability towards epoxy resin is improved.

On one hand, the authors gave evidence that at constant treatment time, the distance between substrate and UV source has a significant influence on the degree of oxidation of the sample surface. Under the conditions of the experiments, the atomic oxygen is supposed to recombine or to react with other gas molecule before it reaches the surface. As a result, the concentration of oxygenated species (hydroxyl or carboxylic groups) decreases with increasing the distance between fibers and the bulb.

On the other hand, drastic treatment conditions such as a long treatment time or a short distance lead to a reduction of the fiber tenacity.

All these studies gave evidence that UV irradiation can be successfully used to enhance the reactivity of natural fibers and to generate radicals or oxidation onto the fiber surface. The final result clearly depends on substrate and wavelengths (energy) used, on the distance the samples are placed away from the source, and the atmosphere conditions under which the experiments are carried out. Time treatment is also important, and usually UV requires long time treatment to penetrate deepest into the bulk material. Natural fibers is not the unique field of application of such a treatment: UV irradiation has been used on other substrates, for instance in order to improve the adhesion performance of polymers [18, 19].

2.2.1.3 Applications for composite materials

Gassan and Gutowski [20] prepared jute fibers/epoxy resin composites and examined the influence of UV treatment on the physical properties of the fibers and the composites made of them. The dynamic contact angle measurements reveal a significant increase in the polar component of free surface energy and that of fiber polarity when treatment time increases. According to the authors, these trends are related to a production of carboxyl groups on the fiber surface. Consequently, the wettability of fibers and thus the composite strength were improved. In appropriate radiation conditions (distance between sample and source and treatment time), a growth of 30 % in composite strength is possible. Once the optimum distance is exceeded, the increase in the polarity is too small to enhance the composite properties. Drastic treatment conditions, such as short distances or long treatment times, result in the degradation of fiber tenacity and thus poor mechanical properties. As a consequence, a balance between an increase in polarity of the fiber surface and a decrease of the fiber mechanical properties is needed to successfully improve the composite strength. Under optimum treatment conditions, the composite flexural strength raised by about 30 %.

In a recent work, Rahman [21] measured the physico-mechanical properties of UV-cured henequen (Agave fourcroydes) fiber/HEMA (2-hydroxyethylmethacrylate) and EA (ethylacrylate) material at different UV intensities and monomer concentrations. Grafting ratio passes through a maximum versus radiation dose. Mechanical properties were investigated by measuring the tensile strength factor (T_f), elongation factor (E_f), and modulus factor (M_f). Achieving the maximum tensile strength depends both on the impregnation solution and the UV radiation dose. Some authors attribute the decrease of T_f at higher grafting value to the formation of excess three-dimensional cross-linked structure in the fiber grafting zone. This excess forms insubstantial polymer that impacts the tensile strength of the treated fibers.

2.2.2 Plasma technologies

2.2.2.1 Basic principles

Plasma is a separate phase of matter, distinct from the traditional solid, liquid, and gas phases. At a macroscopic scale in a plasma medium, a balance between the densities of negative and positive particles is established. Since the particles in plasma are electrically charged, it is frequently described as an "ionized gas". Plasma components include electrons (0–10 eV), ions (10–30 eV), and photons (mainly UV and vacuum UV). Electrical discharge is the common and simplest way to produce plasma for a long time [22]. Plasma is usually associated with thermal phenomena. As a consequence, cold plasma is typically a plasma in which the ionization degree is low. In this medium, electrons do not have sufficient energy to escape from the influence of their corresponding ions. Although the electron temperature is 10–100 times higher than the temperature as a gas, due to very low density and the very low electron heat capacity the plasma is not hot. This is the main reason why cold plasma can be used in surface treatment of polymers and natural fibers [23].

Low-temperature plasma chemistry has received much attention in the last decades in the fields of fiber surface modification and its applications [24]. From a technical point of view, there are two kinds of available treatments: atmospheric or vacuum. In a vacuum treatment, the sample is treated in a chamber under low vacuum pressure. In contrast, the atmospheric plasma technique allows the samples to be treated in situ rather than in a chamber. In one case as in another, through the use of specific molecule in the gas phase, cold plasma appears to be an original method of functionalization.

2.2.2.2 Treatment effects on fibers

The application of plasma techniques to fibers began with studies related to the textile industry.

In 1962, glow-discharge treatment was first applied on cotton yarn by Stone and Barrett [25]. They showed that in the presence of air, plasma treatment increased the cotton strength by 31–76 %, as well as its water absorbency.

In the 1970s, Coleman [26] related the initiation of chemical reactions on a polymer surface by means of discharge at atmospheric pressure. The author grafted acrylic acid to polymeric substrates by initiating free radical site formation on the surface of materials such as cotton-polyester blends, textile fabrics made of cotton, and polyethylene films.

Pavlath et al. designed a small reactor suitable for a continuous glow discharge treatment of a wool yarn [24]. The authors found that the exposure of wool to low-temperature plasmas increased its strength and abrasion resistance while reducing felting shrinkage.

A number of later studies devoted to cellulosic fibers confirm that plasma treatment improves wettability, dyeability, and also adhesion properties [27, 28] and that it induces surface oxidation, a fiber erosion also referred to as the etching effect [29]. This phenomenon leads to a weight loss due to degradation linked to free-radical formation. This etching effect implies the collision between the fiber surface and reactive particles from the plasma medium. The fiber surface can undergo a large series of modifications: creation of microcavities, or of simple vacancy.

It is well known that plasma activation produces free radicals on cellulose or natural materials having anhydroglucose units linked by a glucosidic bond [30]. These transient species decay rapidly in oxygen but slowly in nitrogen, and the decay results in chemiluminescence. According to this study, it seems that free radicals are formed by the breakage of glycosidic bonds as well as by either dehydrogenation or dehydroxilation of the C2 and C3 carbons in glucose rings.

The results of Sabharwal et al. [31] are helpful in understanding the mechanism involved in the generation of free radicals on the surface of argon plasma treated jute fibers. The study of modified surface by XPS analysis and the results related to the build up and decay of radical species showed that although the polysaccharides had a significant contribution, lignin was their primary source. Free radical intensity is dramatically reduced under atmospheric conditions. In a vacuum, raising the temperature also decreases free-radical concentration. The whole experimental data of this study suggest new routes for grafting lignocellulosics fibers in the field of potential application to obtain new composites materials.

Ward et al [32, 33] investigated the effect of a cold plasma treatment on water absorption of cotton under argon, air, nitrogen, and ammonia [34]. These authors gave evidence that the chosen cotton treated with argon, nitrogen, or air plasma was found to adsorb water and oils at a faster rate than an untreated one. Besides XPS, infrared absorption spectroscopy (IR) characterizations revealed that carbonyl groups and hydroxyperoxide groups were generated on cotton. The authors noticed that the concentration of carbonyl groups is greater on the surface than in the bulk. In addition, as detected by electron spin resonance (ESR) analyses, carbon-free radicals could be formed. In contrast, ammonia plasma treatment resulted in the addition of nitrogen in cotton, while ESCA and MIR (multiple internal-reflectance spectroscopy) suggested an amide structure. XRD patterns gave no indication of changes in the crystalline lattice of cellulose, unlike liquid ammonia treatment. From their results, the authors developed a process [35] for producing a polymeric film in the surface of cotton fabrics. After ammonia molecules have been activated to plasma, polymer is generated upon the surface of the cellulosic fibers. This coating is shown to be alkali resistant, water-repellent, and improves the wrinkle recovery of the fabrics. This seems to be the first evidence that the generation of a surface composite or grafting with plasma technology is achievable.

Active centers created within the cellulose chain by plasma treatment were also used to initiate copolymerization reactions with vinyl monomers to allow hydropho-

bic character to lightweight cotton fabrics [36]. The efficiency of the grafting process and the monomer presence over cotton surfaces were confirmed using the UATR-FTIR technique.

Plasma generated from CF_4 can induce intense surface fluorination of paper substrates [37]. Treatment times as low as 30 s can generate relative surface fluorine atomic concentrations as high as 30 %. As evidenced by high resolution C_{1s} ESCA diagrams, the CF_4 plasma treatment induces CF_3C-O-O, $CFCF_2O$ and CF_x moieties formation giving rise to high hydrophobic properties. In addition, surface fluorination reaction mechanisms can be controlled by treatment time, CF_4-pressure in the reaction chamber, and power dissipated to the electrodes. It is noticeable that the bulk characteristics of the treated materials are not altered significantly, confirming that plasma is a surface treatment. Thin layers on pulp sisal paper can also be functionalized using fluorotrimethylsilane $(CH_3)_3SiF$ by the implantation over the surface of fluorine and $-Si(CH_3)_x$ species [38]. These functionalities work on a hydrophobic character when involving optimal plasma treating times. The chemical linkage seems to be mainly due to the lignin component over the paper surface by means of mainly $C-O-Si-F$ sequences, and with some $C-Si-F$ groups.

2.2.2.3 Applications for composite materials

Carlsson et al. [39] prepared composite materials by lamination of filter paper and greaseproof paper with polyethylene. They measured the adhesive strength between both components for untreated papers or hydrogen or oxygen plasma treated ones. ESCA analysis was used to get information on surface composition. Hydrogen plasma treatment reduces cellulose surface and forms low-molecular-weight degradation products. The authors showed that the cellulose surface reduction has no influence on adhesion, but the degradation products strongly decrease the adhesive strength. Oxygen plasma treatment increases adhesion, and the authors suggest that it is probably by removing low-molecular-weight wood resin from the surface and by forming covalent bonds across the interface.

Felix et al. [40] discussed the effect of plasma treatment on a mixture containing cellulose (86 %), hemicelluloses (13 %) and small amounts of residual lignin. In this contribution, plasma treatment consisted in submitting fibers to a 200 W discharge under a 50 ml/min gas flow for both ammonia and nitrogen and 15 ml/min in the case of methacrylic acid. Concerning NH_3 and N_2 plasma, XPS patterns revealed the presence of $C-N$ and $C=N$ bonds over the surface, whereas in MMA plasma condition, carboxylic groups were evidenced. The effectiveness of treatment in terms of acid/base modification of the material was also confirmed by inverse gas chromatography analysis. Surface modified fibers were used in manufacturing composites with polystyrene, chlorinated polyethylene, and polypropylene as basic, acidic, and neutral matrices, respectively. When the preparation is conducted under favorable acid/base interactions, the mechanical properties are enhanced, and glass transition temperatures of

composites are increased. In the design of composites using cellulose fibers as reinforcing agents, acid/base interaction appears to be an important, but not only, consideration.

In order to improve compatibility between radiata pine wood fibers and polypropylene (PP) Yuan et al. [41] used argon and air cold plasma treatments. Various mass ratios were chosen for filler in the final composites. Wood fibers were mixed with polypropylene fibers in a blender, and the consolidation process was carried out using heat, pressure, and vacuum. Final materials were characterized using tensile tests, scanning electron micrographs (SEM), and XPS. According to this study, whenever the plasma treatment tensile strengths and moduli are increased, and air-plasma improves these values more than Ar-plasma system (Fig. 2.2). SEM analysis of the composites fracture surfaces evidenced that in the case of plasma-treated fillers, blend morphology shows less fiber pull-out for Ar-plasma than for air-plasma systems whereas the most fiber pull-out is observed in the untreated materials case. Moreover, fewer pores in the air-plasma-treated sample were observed. This indicates that the interfacial bonding between matrix and wood fiber is generally improved after plasma treatment. Furthermore, the surface roughness in wood fibers increases after both Ar- and air-plasma treatments, leading to higher interfacial contact and thus possibly better mechanical interlocking. As a result, the overall mechanical properties are improved.

Nowadays, nonwovens are commonly used in composite preparation. In a recent study [42], flax fiber nonwovens were manufactured and submitted to a helium plasma treatment. Composite materials were prepared by pouring a liquid unsaturated polymer resin onto both treated and untreated nonwovens. The resulting system was then
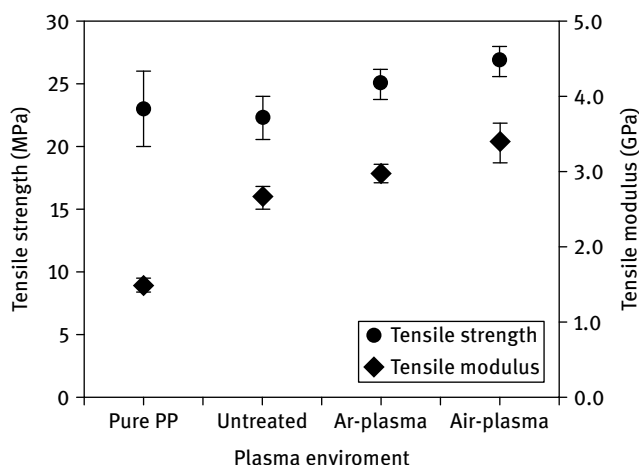

Fig. 2.2: Tensile strengths and moduli of different composites: 20 % of fiber by weight (results from Yuan et al. [41]).

placed under a press in order to obtain a calibrated thickness. The final materials were characterized by water permeation measurements, mechanical tests, and SEM micrographs. The applied treatment reduces the water permeability of flax in fibers reinforced composites. Mechanical tests gave evidence that:

(i) matrix/fiber adhesion is improved by plasma treatment and the stiffness of composite material increases,
(ii) fibers are weakened by plasma treatment and thus breaking strength of composite materials decreases.

As an explanation, the author believes that plasma treatment brings reactive free-radicals onto the surface, and these species lead to cross-linking reactions giving functionalities by forming peroxides with oxygen from the ambient air. These peroxides react with the polymer resin unsaturations during the radical polymerization process. Moreover, He plasma is well known for its etching effect, which can increase the surface area thus allows better wetting. All these phenomena contribute to create strong interactions and reduce void volume between the components leading to the obtained results.

Plasma is thought to bring a physical modification upon the surface through roughening fiber having etching effect, resulting in an increased specific area. Various gases can be used, including helium, argon, oxygen, nitrogen, and air. In the plasma phase, formed ions bombard the surface causing numerous chemical and physical surface changes. Plasma creates reactive species able to activate and/or attack the substrate. Chemical changes are complex but involve removing moieties or breaking bonds which leads to free radical evolution and cross linking. Plasma modification of the surface results in the following events in various degrees, which strongly affect interfacial properties:

(i) ablation or etching of fibers, which leads to a rougher surface, improving mechanical anchorage;
(ii) cross linking or branching of materials upon surface which may strengthen the surface layer;
(iii) modification of the surface chemical structure and free radicals generation.

2.2.3 Corona technologies

2.2.3.1 Basic principles
Corona is defined as a luminous and audible discharge generated by applying high voltage to electrodes separated by only a weak distance. Corona discharges are a relatively low power electrical phenomenon which occurs at or near atmospheric pressure but sufficient to cause gas ionization. It is characterized by a light purple emission that can be seen in a darkened environment. The audible part of the corona effect is usually a subtle crackling sound increasing with the potential difference set between

electrodes. These can be of different geometries or polarity. Electrons, radicals (depending on the gas), ozone, and UV light with high energy are generated within the area of the corona discharge. All of these species are available for chemical and physical reactions with introduced fibrous substrate, as mentioned below.

2.2.3.2 Treatment effects on fibers

As already mentioned above, the reinforcing efficiency of fibers in a natural fiber/synthetic matrix is related to the physical and chemical nature of the interactions between both components. As a consequence, approaching mechanical properties as surface ones i.e. acid-base characteristics, specific area, free energy of each material, is of the highest interest.

There is no consensus about who first used corona discharge on natural fibers but the first results are linked to textile industry. W.J. Thorsen [43] adapted a pilot-scale corona reactor to process cotton slivers. Corona treatment improved cotton spinnability and increased yarn and fabric strength, as well as abrasion resistance. In a further work, using transmission electron microscope analysis, Thorsen studied the modification induced by corona treatment [44] on cuticle and primary wall of cotton. According to the author, surface analysis of air-corona and air-chlorine corona treated cotton fibers revealed essentially no topographical changes. Wax is affected by air-chlorine corona causing increased wettability. Furthermore, chlorination occurs: chlorine that reacts with cotton seems to be covalently bonded to carbon in the wax. Chlorine is also bonded to nonextractable components of both cuticle and primary wall, while the secondary wall remains essentially unchanged. Increased accessibility of the fiber interior or secondary wall component to swelling reagents such as caustic and yarn setting reagents indicates that corona treatment strongly modify the surface layer or primary wall in such a way as to weaken it and possibly to increase its permeability.

Uehara and Sakata [45] prepared cellulose from beech wood via alcohol/benzene extraction, delignification by the chlorite method and alkali treatment. The resulting cellulose was treated in a corona discharge under air or nitrogen flow at ambient temperature. Chemical changes produced on fibers were investigated using infrared spectrum, Schiff's reaction, adsorption of methylene blue and orange II, and intrinsic viscosity. Both the FTIR patterns and the color reaction obtained with the Schiff reagent revealed the presence of aldehyde groups. The decoloration of orange II solution suggested that some basic functions had been formed during long treatment times under nitrogen. Intrinsic viscosity was decreased by the air corona treatment, but was not affected by the nitrogen corona treatment. A low molecular weight fraction was removed by washing, and the intrinsic viscosity of the remaining cellulose showed the occurrence of chain scission in the case of air plasma treatment.

In another work devoted to surface characterization, Belgacem et al. [46] used XPS and IGC techniques to investigate the consequence of a corona treatment on α-cellulose fibers. In order to compare the validity of the various methods for the assess-

ment of corona discharge efficiencies, IGC data were correlated with surface chemical composition. The latter property was deduced from XPS analyses and from measuring pH and electrical conductance of water suspensions of untreated and corona treated fibers. As surface oxidation occurs, corona treatment significantly changed the cellulose surface chemical composition as shown in Tab. 2.3. The effect of corona current observed were ascribed to a competition between oxidative degradation that predominates at lowest current and removal of resulting low molecular weight products evidenced for higher corona intensities values.

Tab. 2.3: Characteristics of the cellulose surface determined by different methods (from Belgacem et al. [46]).

Corona current (mA)	O : C ratio	Dispersive component of surface tension (mJ m^{-2})	pH of water suspension of cellulose fibers
0	0.66	31.9	6.1
15	0.74	40.2	3.9
32	0.93	42.2	4.6
40	0.90	46.3	5.0

Applications for composite materials

The following examples show how a corona treatment applied on components can noticeably increase the resulting composite properties.

Dong et al. [47] prepared four kinds of polyethylene based composites using untreated or air corona treated wood fibers as well as matrices. Mechanical properties of final materials were investigated as a function of fiber volume content (from 6 up to 40 %). The authors found that at a fiber content of 28 % by volume, corona discharge was effective in enhancing the ductility of composites and in increasing yield strength. Effects are particularly highlighted in composites where (i) fiber only and (ii) both constituents were corona treated. Comprehensively and in the experimental conditions practiced, corona treatment has varying effects on mechanical properties of final material. On one hand, ultimate strength and Young moduli are related to the fiber volume fraction but are mostly independent of the treatment, this giving evidence that these characteristics are insensitive to interfacial properties in the materials. On the other hand, the author found that elongation at rupture, yield strengths, and strains are strongly affected by corona discharge treatment, revealing that these intrinsic properties were highly sensitive to interfacial interactions.

In the same point of view, Belgacem et al. [48] were interested in mechanical properties of compounds (30 % w/w fibers content) obtained by various combinations of untreated or air corona treated cellulose fibers and polypropylene. Mechanical properties of composites were found to be improved when either one or both constituents underwent a corona discharge treatment as shown in Fig. 2.3.
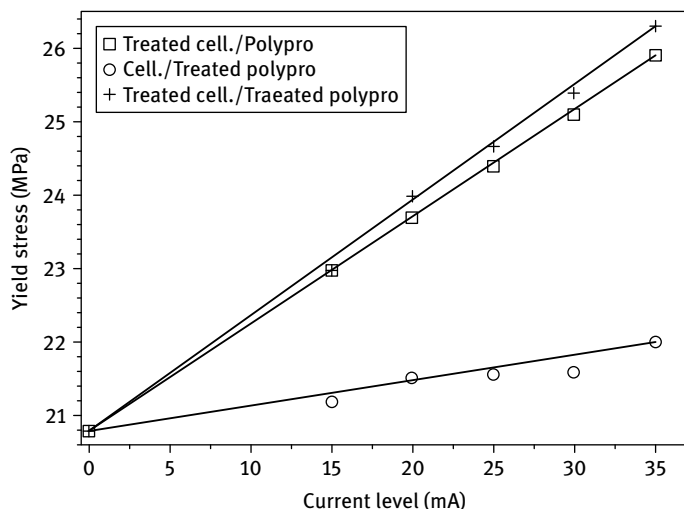
Fig. 2.3: Influence of current level on composite properties for a 30 % fiber system
(from Belgacem et al. [48]).

As evidenced, cellulose rather than polypropylene modification yields a greater improvement in composite properties. The authors related this phenomenon to a smaller specific area of propylene particles, due to a larger relative size. Corona remains a surface treatment and induced surface oxidation. When the surface area is too low, and after polypropylene melting, oxidized species concentration is not sufficient to come in full contact with fibers and thus to improve interaction.

At a constant corona current, mechanical properties of the obtained materials also depend on treatment time.

Interfacial adhesion between a couple of different constituents results from polar, acid-base, or dispersive interactions. Under the experimental conditions used in this study, and concerning cellulose/polypropylene or treated cellulose/polypropylene composites, adhesion seems to come mostly from dispersive adhesion. For dispersive interactions, the work of adhesion is given by the following relation [49]:

$$W_{adh} = 2[\gamma_c^d \gamma_{pp}^d]^{1/2},$$

γ_c^d and γ_{pp}^d being the dispersive components of cellulose fibers and polypropylene, respectively. As reported by the authors, the work of adhesion increases with treatment level (treatment time or current level). Moreover, yield stress linearly increases with work adhesion. It confirms that dispersive interactions play an important role in improving mechanical properties of final materials.

Numerous research groups have exploited the reinforcement potential of flax, hemp, or jute for developing thermoplastic composites [50, 51]. These materials have been successful in semistructural as well as structural applications. Hemp-based ther-

moplastic composites are promising candidates in applications where high specific stiffness is required.

The effect of corona discharge treatment on hemp fibers or polypropylene and the influence of fiber content have been studied by Ragoubi et al. on hemp/PP systems [52]. Materials were prepared by the extrusion moulding procedure and characterized by mechanical tests and SEM analysis. When fibers are treated, the strength at the break is shown to be significantly increased, whereas the deformation is nearly unchanged. PP treatment does not significantly affect the mechanical properties, compared to composite based on raw constituents. The low specific area of PP granules used (3 mm diameter) leads to a proportion of oxidized species too small to develop sufficient interactions. Confirming tensile test results, discharge corona treatment improves the compressive strength of prepared materials. Composites made of treated fibers are always stiffer. SEM analysis, performed to observe the fracture surface of composites, gives evidence that good interfacial adhesion between reinforcement and matrix is only obtained for composites based on treated fibers. This mechanical enhancement is explained by a mechanical anchorage improved by the etching effect. This phenomenon permits a large surface contact with PP matrix and favours its insertion in the bulk of fibers.
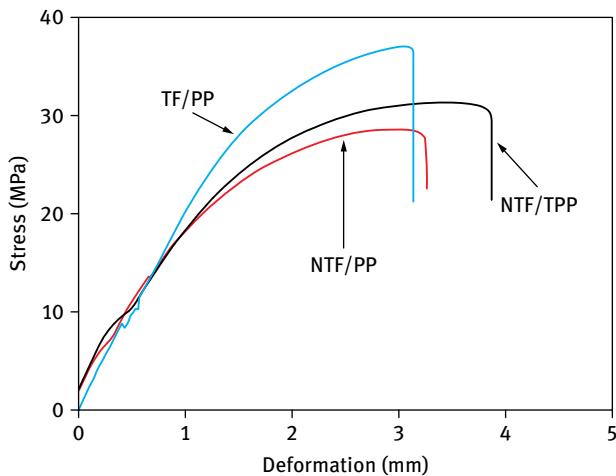
Fig. 2.4: Tensile curve for composites materials with 20 wt% fibers, results from Ragoubi et al. [52]. TF: treated fibers, NTF: nontreated fibers, same marking for polypropylene PP.

In a recent work, Pizzi et al. [53] attempt at producing natural fibers/natural matrices composites of good performance by using tannin resins, lignin resins, and soy resins as matrices, impregnated within nonwoven flax mats. In Tab. 2.4 we see the results of the effect that corona pretreatment of nonwoven fiber mat has on final composite performance. According to this work, corona treatment leads to a rougher fiber surface by

Tab. 2.4: Corona treatment effect. Mechanical test average results of thicker lower density composites of corona-treated nonwoven flax fiber mats impregnated with a mimosa tannin–hexamine matrix (results from Pizzi et al. [53]).

Corona treatment (min)	Resin load (%)	MOE binding (MPa)	MOE tensile (MPa)	Tensile break force (MPa)
0	40.8	1284	780 ± 41	10.4 ± 1.1
5	43.1	1376	651 ± 32	30.4 ± 1.9
10	41.2	1872	1301 ± 72	6.4 ± 1.4
15	41.8	1909	1175 ± 68	9.4 ± 1.4
30	41.0	1847	1038 ± 71	5.2 ± 1.6

raising its surface layers. A rougher surface would improve both mechanical gripping of the substrate by the resin as well as increase the surface area of the substrate. As a consequence, secondary forces of adhesion between resin and substrate are improved.

2.2.4 High energy radiations technologies

2.2.4.1 Basic principles

Gamma radiation, also known as gamma rays, is an electromagnetic radiation of very short wavelength, i.e. of high frequency. They are commonly produced by radioactive decay, fusion, fission, or subatomic particle interactions. γ-rays typically have frequencies above 1019 Hz, and therefore have energies above 100 keV and wavelength less than 10 picometers. Gamma radioactive decay photons commonly have a few hundred keV energies, almost always less than 10 MeV. Many units of measure or exposure can be found in the literature. The gray (Gy) is the SI unit (J/kg) of absorbed dose, and thus is the amount of radiation required to deposit 1 joule of energy in 1 kilogram of any kind of matter. Based on this last definition, the rad is the traditional unit and is equal to 0.01 J deposited per kg, 100 rad = 1 Gy. Gamma-rays are more penetrating than alpha and the beta radiations, but are less ionizing. They are the same nature that x-rays but are of different origin: x-rays are produced by electronic transitions generally generated by the collision of an electron with an atom.

2.2.4.2 Treatment effects on fibers

Research on the exposure of fibrous materials to high energy radiations (accelerated electrons, ion beams, γ-rays, x-rays) has mostly been carried out on radiation-initiated polymerization. Thus, many studies deal with coatings or grafting on fiber using a monomer [54], but less attention has been paid to simple fiber exposure. Nevertheless, exposure to high energy radiations, such as electron or γ-rays, is claimed to be a valuable route for cellulosic substrates activation.

These treatments considerably change the structure, reactivity, and physicochemical properties of cellulose polymer. They induce reactions in cellulose core generating highly reactive intermediates such as long and short lived free radicals, ions, and excited states [55]. The formation of radical species is followed by dehydration, leading to an allyl type radical [56]. At lower irradiation doses crosslinking can be observed, increasing molecular weight, while at higher doses degradation via chain scission predominates, lowering both molecular weight [57, 58] and degree of polymerization (Fig. 2.5).
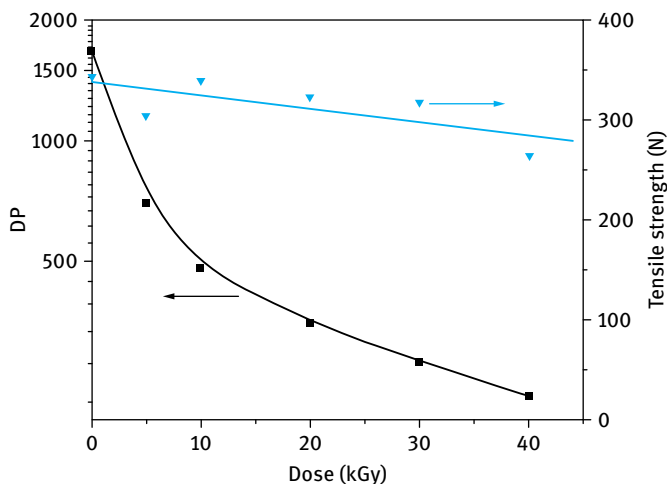

Fig. 2.5: Degree of polymerization (DP) and tensile strength (TS) of cotton cellulose as a function of absorbed dose (data from Takács et al. [59]).

When cellulose is irradiated in the presence of air, radicals generated on the polymer backbone react with oxygen forming peroxy and alkoxy radicals [60]. The higher the absorbed dose is, the higher is the carboxyl and carbonyl content. However, only a slight modification on mechanical properties is observed [57, 59]. The crystalline structure of cellulose does not seem to be affected by irradiation up to several hundred kGy absorbed doses, and furthermore there is no change in the crystalline and amorphous region ratios. Treatment by ionizing radiation due to carbonyl group formation increases the accessibility of cellulose [61], i.e. reactivity of cellulose towards various reagents [62].

Concerning other substrates than cellulose or wood, the interaction of high-energy radiation with starch, lignocelluloses, and pectin finally results in dehydration, oxidative degradation by cleavage of glycosidic bonds, and destruction of the basic monomer unit [57].

As oil palm fibers have been found to be an excellent reinforcement in phenolic matrices, Sreekala and Thomas [63] investigated the water sorption characteristics of these reinforcements after various surface modifications such as gamma irradiation, latex coating and chemical treatments. Gamma-ray irradiation partially eliminates the porous structure and causes microlevel disintegration of fibers. Consequently, diffusion and permeability coefficients are increased. Regarding mechanical properties, the various treatments reduce fibers strength except for silane treatment (Tab. 2.5). The authors concluded that treatments lead to bound structure breakage and disintegration of the noncellulosic materials, while reducing fiber strength.

Tab. 2.5: Tensile properties of treated oil palm fibers, from Sreekala and Thomas [63].

Treatment	Tensile strength (MPa)	Elongation at break (%)	Young's modulus (MPa)
Untreated	248 (12)	14 (0.8)	6700 (25)
Mercerization	224 (11)	16 (0.9)	5000 (48)
Latex	98 (3)	23 (1)	1850 (14)
γ irradiation	88 (4)	25 (0.9)	1600 (14)
Silane	273 (10)	16 (0.7)	5250 (60)

The standard deviations are in parentheses.

In another contribution, γ-radiation was applied to jute, and the physical and chemical properties were investigated [64]. It has been shown that this radiation affected all anhydroglucose, hemicellulose, and lignin units, resulting in molecules fragmentation. This chemical degradation increases with the increase in the radiation dose. The high degradation of lignocellulose observed for a relatively small irradiation dose is attributed to the chemical link weakness between hemicelluloses, lignin, and cellulose units. The irradiation of jute by γ-radiation reduces elongation, tensile strength, and the work done at the break. At a higher dose, the reduction in these parameters is not more significant, because concurrent chain scission and cross-linking reactions occur.

In the case of wood, high energy radiation leads to similar results. The mechanical properties (tensile and compression strength) decrease significantly as the irradiation dose increases, as a consequence of cellulose fiber degradation [65]. At low doses (< 120 kGy), the cellulose content seems to remain constant. Increasing irradiation doses goes towards cellulose decomposition induced by chain scission, the highest irradiation dose (9000 kGy) leading to the total destruction of wood as evidenced in Tab. 2.6 [66].

Tab. 2.6: Cellulose content of wood as a function of radiation dose (data from Borysiak [66]).

Wood sample (Pinus sylvestris)	Radiation dose (kGy)	Cellulose content (%)
0	0	44.7
1	20	44.1
2	60	45.2
3	120	43.0
4	300	40.1
5	500	34.2
6	1500	14.4
7	4500	traces
8	9000	0

2.2.4.3 Applications for composite materials

Borysiak [66] studied polypropylene film crystallinity in the presence of γ-ray treated wood. Sandwich composites were prepared by heating a material made of wood placed between two PP films. The resulting materials were characterized by differential scanning calorimetry and polarizing optical microscopy. The main results showed that wood acts as a nucleating agent for polypropylene. The nucleation onto wood surface is selective, as the chemical composition of the wood plays an important role in the polymer nucleation process. When wood is devoid of cellulose (as a consequence of an important gamma dose), the nucleation ability of PP is significantly decreased, resulting in a lack of transcrystalline structure formation. Thus cellulose presence in wood is likely to be essential to the transcrystallinity formation.

In another work [67], the influence of γ-ray treatment on both components of jute/polypropylene composites was studied with respect to the mechanical properties of final composites made of it. Composites were prepared by heating "sandwiches" of four layers of jute fabrics between five layers of PP sheets. The jute fibers were characterized by scanning electron microscopic analysis and final materials by electrical tests (dielectric properties), mechanical tests (tensile strength TS and bending strength BS), water uptake and accelerated weather ageing. As showed by Fig. 2.6, γ-ray radiation improves the tensile strength of all studied materials, and a maximum is obtained for a 500 krad dose. The same behavior has been seen for bending strength. The authors suggest two main explanations of the observed phenomena. On one hand, SEM analysis reveals a rough surface with lot of fractures over the γ-treated sample, compared to the smooth appearance of an untreated one. Thus, γ-radiation on jute results in a significant change of morphology and specific area of fiber, and this is effective for better mechanical bonding between fiber and a polymer matrix. As a consequence of this mechanical anchorage, mechanical properties are improved significantly. On the other hand, free radicals produced by radiation exposure may react to change the polymer structure and thus physical properties of the corresponding macroscopic ma-
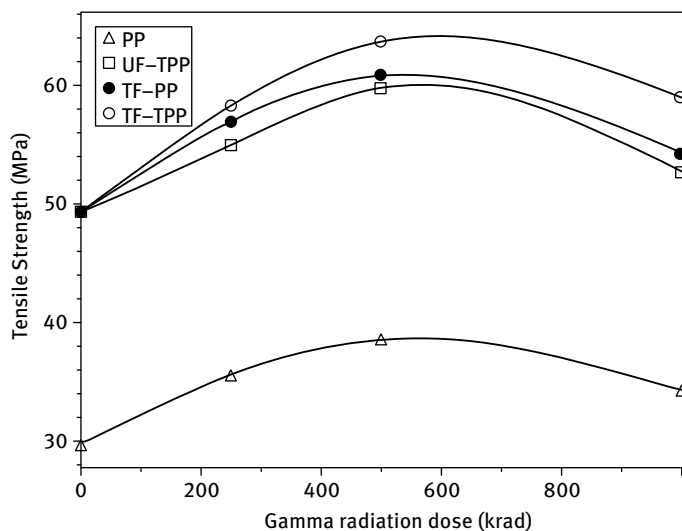
Fig. 2.6: Tensile strength (TS) of composites made of irradiated components vs radiation dose. PP: polypropylene, F: fibers, U: untreated, T: treated. From Haydaruzzama et al. [67].

terials. It also may undergo cross-linking, and molecules may be linked together into larger ones.

Gamma-ray irradiation can also be performed directly on a composite, i.e. on a blend of untreated components. In the case of polypropylene compounds with sisal fiber and wood flour [68], ESR analysis shows that peroxide radicals formation (in situ) strongly increases with the irradiation dose. The main degradation mechanism is chain scission, which highly influences the behavior of thermal, mechanical, and morphological samples. For tensile strength and elongation at break, a slight increase at 10 kGy doses is observed, followed by a slight decrease at lower doses. The gain can be explained by both cross-linking and improvement of filler/matrix interactions due to slight oxidation of PP, while degradation in the amorphous regions appears to be the primary cause of physical property loss.

2.3 Surface activation of cellulosic fibers: Physico-chemical technologies

2.3.1 Ultrasound technologies

2.3.1.1 Basic Principles

The term ultrasound defines sound waves of frequencies above the detection threshold of human hearing in the range of 20 kHz–10 MHz. Ultrasound offers a wide range of both medical and industrial applications, as it can be directed as a beam and reflected

by objects of small size. This treatment applied in liquid media results in "cavitation", a physical phenomenon that includes the formation, expansion, and implosion of a microscopic gas bubble. Bubble collapse in liquids produces an enormous density of energy. The high local temperatures and pressures, combined with extraordinarily rapid cooling, provide a unique means for driving chemical reactions under extreme conditions [69]. With liquids containing solids, similar phenomena may occur with exposure to ultrasound. Once cavitation phenomenon occurs near a solid surface, cavity collapse is nonspherical and drives high-speed jets of liquid to the surface.

2.3.1.2 Treatment effects on fibers

Treatment of natural fibers with ultrasound has been widely studied. As an example, it has been shown that the morphology and reactivity of cellulose fibers dispersed in water are changed after ultrasound treatment: microfibrills appear, accessibility and oxidation reactivity of cellulose towards sodium periodate are enhanced, as is the accessibility of cellulose in terms of water retention [70].

Laine et al. [71] studied the influence of ultrasonic irradiation on the physical and chemical properties of pulp fibers. The authors reported a gain in fiber-wall porosity and a slight increase in carbonyl group content essentially asigned to carbohydrate hydroxyls oxidation.

Ultrasound can also be used as a "reaction assistant" with respect to natural fibers. In the case of wood, alkali treatment removes both hemicellulose and lignin from the structure and increases hydroxyl moieties number over cellulose surface. Chang et al. [72] Produced evidence that this reaction is promoted by ultrasound treatment. Moreover, in the same contribution, the authors showed that further investigation revealed that alkali treatment slightly reduced particle size, phenomenon enhanced by ultrasound assistance. In the same way, Pappas et al. [73] conducted a comparative study of classical and ultrasound-assisted extraction and purification of cellulose from kenaf and eucalyptus. The authors showed that the use of ultrasound reduces the total treatment time and increases crystallinity. As a consequence, the purity of the obtained cellulose was very high.

Ultrasound treatment is also responsible for a radical species creation in liquid media. In this field of experiments, Seino et al. [74] used both electron spin resonance (ESR) and a trapping reagent to characterize unstable radicals generated during ultrasound treatment of lignin solutions in DMSO. They found that the alkyl-phenyl-ether bonds, known as lignin linkage bonds, were homolytically scissioned. They also deduced that the major scission is the β-0-4 bond even if α-O-4 rupture also occurs to some extent (Fig. 2.7).
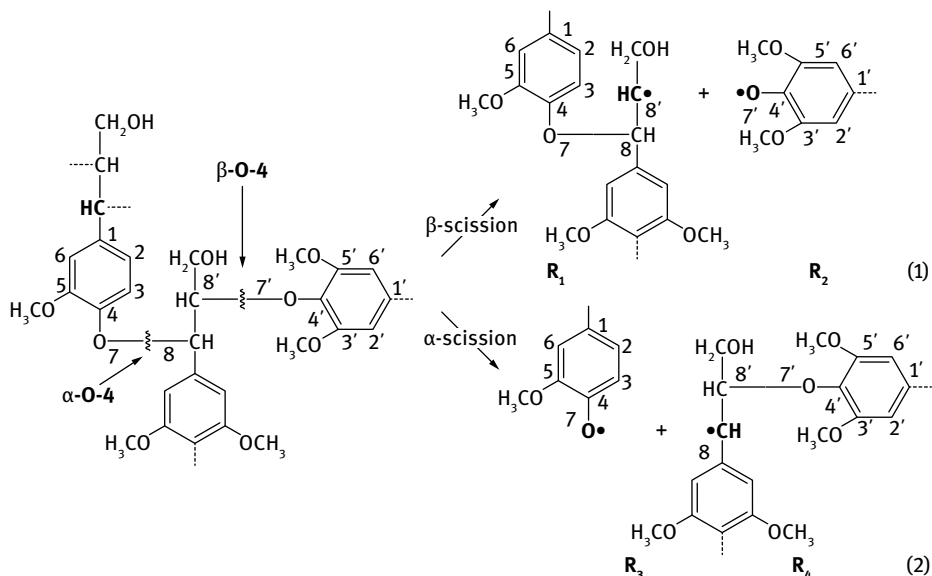
Fig. 2.7: Reaction pathway in lignin scission induced by ultrasound treatment [74].

2.3.1.3 Applications for composite materials

In the literature, there are only a few works which deal with the application of ultrasound on composite material fields.

Chang et al. [72] examined the combined effects of alkali and ultrasound treatment of wood flour on the moisture absorption behavior of polypropylene-based wood/plastic composites. Mechanical testing of samples of injection-molded materials gave evidence that alkali treatment improved both composite strength and modulus when polypropylene grafted with maleic acid was used as a coupling agent. Strength variation is attributed to improved adhesion between the fiber and the matrix, while improved modulus is related to the removal of lignin and hemicellulose that are not as stiff as cellulose. Polarized optical microscopy revealed the presence of well-defined polymer crystals over the modified wood particle surfaces, and this is also responsible for mechanical properties enhancement. It has been conclusively shown that a combination of chemical treatment of wood fibers and ultrasound assistance is more effective in improving mechanical properties of composites than the simple use of a chemical treatment.

Ultrasonic energy has been employed to fibrillate decorticated fibers of flax, which are well-known to be suitable as reinforcements of polymer-based composites [75, 76]. The treatment, based on ultrasound, involves the implosion of tiny bubbles or other particles that abrade hemicellulose and pectin sheaths of raw cellulose fiber. It operates in aqueous media temperature/pH range suitable to leave the cellulose

mostly undisturbed, while attacking hemicelluloses, lignin, and pectins. A significant increase in stiffness and strength of the end composites was observed.

As cavitation can only occur in liquids, chemical reactions are not possible in solids or solid-gas systems, and this is one of the drawbacks of such a process when dealing with composites manufacture.

2.3.2 Solvent technologies

In liquid-solid extraction, a solvent (hydrophobic or hydrophilic, acidic, basic, or neutral) is added to a solid. Insoluble material can be separated by gravity or vacuum filtration, and soluble material is "extracted" into the solvent. Many investigations [77–79] have been devoted to a simple solvent treatment of plant materials and to the study of the nature of the resulting surface. The materials and fibers concerned are also numerous: eucalyptus kreft pulps, white pine and birch meal, recycled and hardwood cellulose, chemical and thermochemical pulps, extracted with cold or hot water, acetone, ethanol/toluene mixtures or diethyl ether. As mentioned above, the three main components of the plant materials are cellulose, lignin, and hemicellulosics. Cellulose and hemicellulosics are polysaccharides. Lignin is a phenol propane-based amorphous solidified resin filling the space between the polysaccharide fibers. Besides these three principal components, lignocellulosic materials contain nonstructural components: water, inorganic ash, and extractives. Data analysis from raw and solvent extracted fibers gives evidence that at least part of the extractives and lignin fragments (aromatic and aliphatic impurities) initially present over the surface are removed by this treatment. As an example, for three materials: stone ground-wood pulp, commercial newsprint paper, and hardwood cellulose fibers, acetone and diethyl ether are the best solvents for removing impurities with practically 50 % of the decontamination extracted. The presence of unextracted residues was related to the following suppositions: extractives could have been sterically bound into the structure wood/cellulose/lignin matrix, making their percolation onto the surface relatively slow and/or they were chemically bound substances through well-documented lignin-carbohydrates links.

2.4 Surface activation of cellulosic fibers: Thermomechanical technologies

2.4.1 Steam explosion (SE) technology

2.4.1.1 Basic principles
The steam explosion (SE) process is a physical treatment applied to a wooden or lignocellulosic structure. The technique as it has been developed and practiced is better

defined as "flash hydrolysis". In a first step, natural fibers or finely divided wood particles are rapidly brought to pressure and temperature in the vicinity of 500 psi and 230 °C. At such pressures, water present in fibers remains liquid and does not boil. During a second step, when the material is ejected from the reactor, pressure drops sharply; water suddenly and violently boils, producing steam. This instantaneous decompression and violent production of steam in lignocellulosic particles causes the so-called steam explosion. Many types of steam treatments have been developed in the last decades. All of them consist in vapor treatment under pressure, but they differ from one to another mainly in the way pressure is released at the end of the procedure: quickly or slowly. Treatment time is currently 60 s or less. The reactor design has been described in Canadian patents [80, 81]. It constitutes the heart of the explosion process, allows the use of high pressure during heating, and can be of either a batch or a continuous type. An example of a classical explosion pulping (SEP) equipment is given is Scheme 2.1 [82].
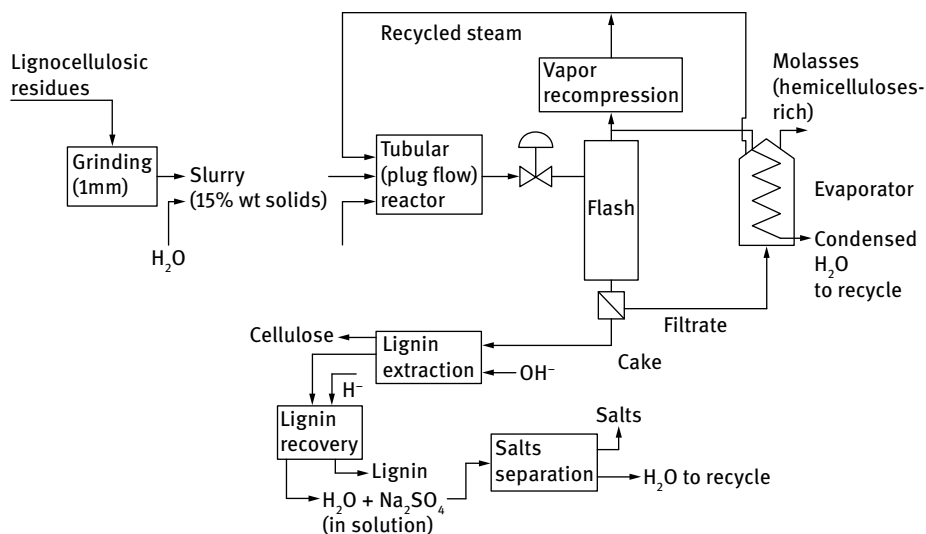
Scheme 2.1: Classical steam explosion pulping process [82].

The steam explosion process separates lignocellulosic material into its main components: cellulose fibers, amorphous lignin, and hemicellulose [83] (in a molasses form). For wood, explosion technology appears to be a potentially inexpensive means of destructuring lignocellulosics. Indeed, the cost of fiber production are relatively low: $ 0.077/kg plus raw materials [84].

2.4.1.2 Treatment effects on fibers

Steam explosion process affects all the constitutive components of wood and lignocellulosic resources [85, 86]. Hemicelluloses are hydrolyzed to monosaccharides and oligosaccharides, which become extractable with water. The molecular weight of lignin is reduced, and amorphous cellulose is partially depolymerized and highly enzyme accessible. Many small molecules, such as acetic acid, xylose, vanillin, etc., are readily obtainable. Thus, the potential seems to be enormous in many industrial fields: the paper and textile industry, fine chemical and biodegradable polymer synthesis, extraction biotechnology.

SE treatment also causes ultrastructural changes [87], such as fibers softening, lignin aggregation, and increase in porosity. SEM micrographs of wood fibers [88] or flax [89] after SE clearly show the surface irregularities resulting from the process [90] (Fig. 2.8). The surface appears very heterogeneous: various phenomenon are observed: microfibrils, fibrillation of the fiber surface layers, ridges and folds along the fiber.

Moreover, lignin seems to be brought to a state which is best described as liquid [91]. Because chemical linkage has been broken, lignin is able to readjust its external surface area and flows to form larger domains; thus it coalesces and exudes at the fiber edges (Fig. 2.8).

One consequence of SE treatment is that the remaining wood fibers have a reduced hygroscopicity and a higher content of crystalline cellulose [92, 93]. Treatment severity, combining steam temperature and residence time, increases surface energy and apparent specific surface; it also results in a loss of entirety, in a thinning down and in a shortening of softwood sawdust fiber.

Steam explosions of sodium hydroxide preimpregnated semiretted hemp bundles was evidenced to be an effective method to degrade pectins from the middle lamella, which allows the production of elementary bast fibers [94]. During SE treatment, fiber bundles are separated into single fibers, and polysaccharides are then arranged at the surface and between fibers. Pectins, hemicelluloses, and lignin are partially degraded and soluble in NaOH solution, which allows the fibers to degum. Furthermore, according to this study, SE treatment can effectively be employed to open the structure of hemp chènevotte and, carried out under chosen experimental conditions, the processs can lead to different yields in terms of homogeneity, delignification, cellulose quality, and degradation. As an example the cellulose degree of polymerization can vary from 250 to 1400 [94] as a function of temperature and pretreatment (Fig. 2.9).

In another study using flax [95], the steam explosion process was divided into four main steps: penetration, degumming, fibrillation, and cellulose decomposition. The process, followed by retting, leads to good fiber quality with minimum loss in fiber yield. Flax fibers still have a sufficient tenacity to endure all spinning systems even after steam explosion. As a consequence of higher purity and homogeneity, blended yarns containing SE fibers show a better spinnability compared to mechanically cottonized flax.
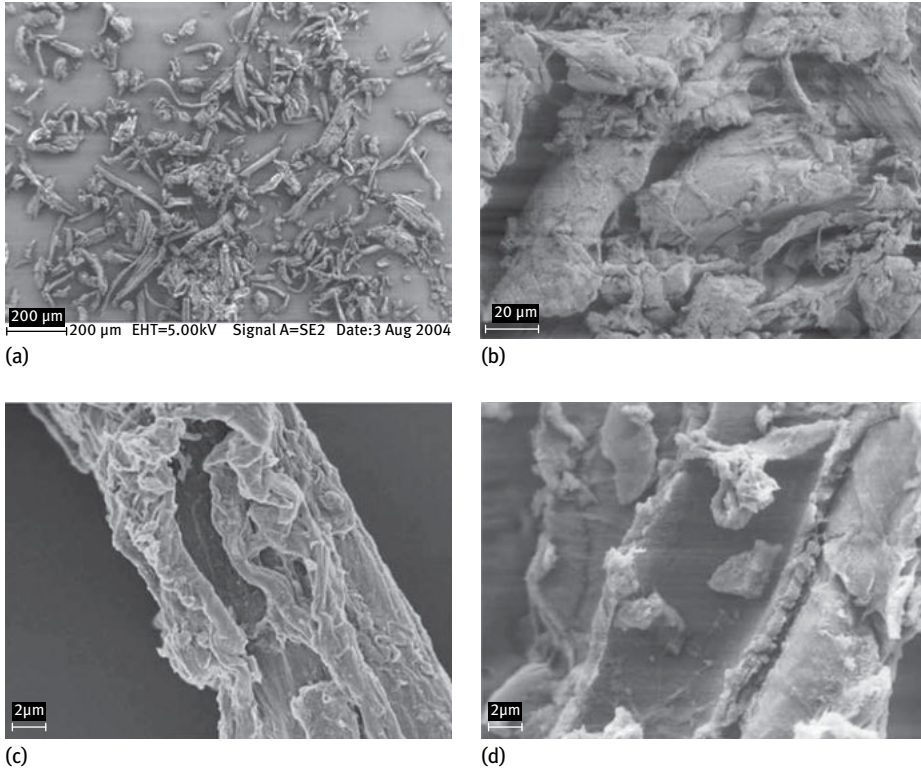
(a)

(b)

(c)

(d)

Fig. 2.8: SEM micrographs of steam exploded fibers. (a) Overview; (b) an aggregate of fiber fragments glued by lignin; (c) outside surface of a fiber fragment covered by lignin; (d) inside surface of a fiber fragment with lignin droplets. From Yin et al. [90].

Steam explosion has been applied to oil palm empty fruit bunches in the presence of a 2 % NaOH solution [96]. It involves many changes in fibers:
(i)   increase in specific area,
(ii) rougher surface,
(iii) and increase in fiber porosity due to lignin redistribution, hydrolysis, and removal of hemicellulose.

The nonexhaustive examples of SE effects given above highlight a number of advantages to the steam exploded fibers and especially as reinforcing potential filler for improving strength, dimensional stability, and durability of polymer-based composites.
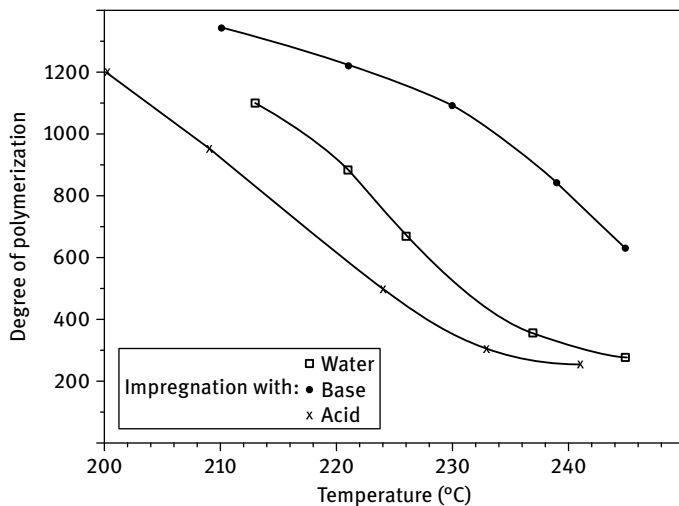
Fig. 2.9: Evolution of the degree of polymerization of steam-exploded hemp chènevotte cellulose samples as a function of temperature and pre-treatment. Figure from Vignon et al. [94].

2.4.1.3 Applications for composite materials

Several research teams have studied the influence of fiber surface treatment by SE on composites properties.

Different weight percentage of steam-exploded hemp bast fibers were compounded with polypropylene (PP), either directly or after surface treatment with maleate-modified polypropylene (PPMA). Obviously, fibers increased the tensile modulus of whole composites. The percent for elongation and strength at yield is low for untreated fiber composites films that did not contain PPMA. Decrease in strength in untreated fiber systems was mainly attributed to poor adhesion between the matrix and fillers, and thus having a bad interface quality.

In a similar manner, broom fibers have been used as fillers for polypropylene and polypropylene-maleic anhydride copolymer (PPMA) [97]. A conventional alkaline procedure or a steam explosion treatment was applied to obtain cellulosic reinforcements. Although water adsorption tests and SEM analysis evidence that fillers extracted by alkaline treatment seem to produce poorer fiber/matrix adhesion compared with steam-exploded broom fibers, the chemically treated fiber-based composites show superior mechanical properties. This result is attributed to the minor structure damage produced by soda treatment that allows obtaining fibers with a greater aspect ratio. Using steam-exploded materials as a reinforcement for PPMA/broom composites contributes to reduce water penetration into the structure with respect to chemically extracted fibers: this effect is related both to the higher crystallinity of steam-exploded fibers and to better interfacial adhesion.

Residual softwood sawdust treated by the steam-explosion technique has been used as a natural filler in polypropylene to manufacture composites [98]. From this study, under specific experimental conditions, steam-exploded softwood was evidenced to be ineffective, giving similar Young's modulus and lower strengths compared with both pure polypropylene and composites made of raw softwood fibers. The reinforcing effect depends on two main principles: (i) the aspect ratio of the fiber, and (ii) the intimate adhesion between components, which induces efficiency of the stress transfer from the matrix to the reinforcements. Both phenomena evolve in the opposite way with the severity of the steam-explosion process. The harder the pretreatment conditions are, the higher are the surface energy, roughness, and specific area, but the lower is the aspect ratio. Thus, according to the authors, aspect ratio plays the leading effect on the final mechanical behavior of their polypropylene-based composites.

In another contribution, Takatani and coworkers [99] investigated the effect of steam-exploded wood flour added to wood flour/plastic composites. These materials were manufactured from three different sources of steam exploded fibers and three kinds of thermoplastic polymer. It is clearly shown that the composition at which the best mechanical performance of system is obtained differs, depending on the plastic polymer and, to a lesser extent, wood SE fibers. In any case, the moduli of rupture and elasticity and the water resistance of wood-plastic composite were generally increased by substituting wood flour with SE fibers. As wood and plastic are not expected to generate a strong mutual interactive force unless some additive or process improving the compatibility is applied, it seems that steam-exploded fibers might behave as a compatibilizer with properties intermediate between both components.

Other studies were done to evaluate the benefit of the use of steam-explosion treatment in the fabrication of natural fiber-based composites: yellow poplar/cellulose acetate butyrate [100], bamboo/MAPP [101], or pine/PP [90].

2.4.1.4 Application for fiberboards

To find an eco-friendly alternative to conventional composite panels usually bonded with synthetic resins, some attempts have been made to produce composite boards without using resin binders [102]. Steam-exploded cellulosic materials can be used in this way.

Anglès et al. applied this procees at various severities to softwood residual substrate in order to determine the most suitable pretreatment for the manufacture of binderless panels [103]. High severities caused material defibrillation allowing links to form in the panels. Although lignin seemed to diminish slightly when the severity increased, analysis showed that it became more superficial and melted. Thus it covered hemicelluloses and cellulose and prevented fibers from absorbing water.

In another contribution, binderless boards were prepared from steam-exploded fibers of oil palm frond [104]. Findings suggest that boards satisfying the relevant standards requirements can be produced from these resources without using any

binders. The main bonding strength of boards is believed to be due to lignin-furfural linkages, generated during the hot-pressing process of steam-exploded fibers. It was confirmed that severe steam-explosion conditions result in better internal bonding strength among fibers, which give high stability against moisture. Nevertheless, the boards' chemical components seem to be seriously modified, including cleavage of aromatic nuclei of lignin, and thus the board mechanical strength becomes very poor.

Steam-exploded miscanthus fibers have also been chosen for manufacturing fiberboards with no synthetic binders [105, 106]. Treatment is confirmed to hydrolyze most of the hemicelluloses and plastifies the lignin: the obtained fiberboards used their own lignin as a thermoplastic adhesive. A correlation between hemicellulose content and properties related to dimensional stability (water absorption and thickness swelling) was evidenced. This confirms that hemicelluloses are responsible for dimensional instability because of their hydrophilic character. Under applied conditions, grinding has important and positive effects on density and internal bonds without affecting the moduli of rupture and of elasticity of the fibrous materials.

More recently, banana bunches was used to produce fiberboard with nonsynthetic binders [107]. Fibers were steam-exploded using various temperature and pressure conditions. The fiberboards thus obtained presented good properties and satisfied requirements, despite a lower quality than those obtained from conifers or miscanthus. The effect of the treatment severity on the lignin, cellulose, and xylan content was investigated. The decrease in xylans was clearly related to the dimensional stability increase of the fibreboards. The authors concluded that banana bunches are an alternative raw material for obtaining high particle density binderless fiberboards.

Actually, these few examples give evidence that the more severe the steam-explosion treatment is, the smaller the particles of the obtained material are [108]. Although it deteriorates a part of the mechanical properties, this decrease in particle size improves significantly internal bonds, water absorption, and thickness swelling. Besides, when a material is steam exploded at low severity, so as not to drastically reduce the particle size, and then subjected to a delicate milling process, the quality of the fiberboards can significantly be improved.

2.5 Surface activation of cellulosic fibers: Other technologies

Two additional ways are described in the following.

2.5.1 Steam technologies

In a similar way, natural fibers can be treated by steam in order to improve adhesion with the matrix and increase moisture resistance. Indeed, when natural fibers are pressed into a composite or a fiber board, they are compressed and parhaps flat-

tened. Overall, fillers are deformed even if they conserved a memory of their original configuration. When the final material is submitted to moisture, compressed fibers absorb water. Accordingly, swelling takes place, and compressive force transferred to the material during processing is relieved as a consequence of the recovery of the fiber's original configuration. This phenomenon adversely affecting adhesion is known as the spring back of fiber [109] and traduces some stress relaxation. One way to reduce this irreversible swelling is to plasticize the cell walls by steaming. Thusly treated, the fibers cannot recover their original shape [110, 111] and only undergoes the reversible swelling phenomenon of water absorption.

Marais et al. [112] investigated the interest in and the role played by flax fibers steam-treated for reinforced unsaturated polyester resine (UPR). Flax nonwovens were manufactured via a dry laying technique, steam treated in an autoclave under mild conditions and dried. Composite materials were prepared by pouring the liquid UPR onto nonwovens, and systems were pressed at ambient temperature for 24 h. Water permeation measurements gave evidence that steam treatment reduces the water permeability in the flax fiber composites. By analogy with what was previously shown in the case of the SE process, it can be suggested that during treatment pectins, hemicelluloses, and lignin are depolymerized into lower molecular chemical moieties which, after recombination and reaction, lead to a plasticizing effect [113]. However, as a result of the weakening effect of the autoclave treatment, composites reinforced by steam-treated fillers are characterized by lower mechanical performances compared with composites reinforced by native ones. In another series of characterizations, prior to mechanical testing, composite materials were immersed in water at 60 °C for 4 days. Contrary to dry composite, wet composite reinforced by steam-treated flax fibers showed an increase of tensile modulus E with respect to the material reinforced with untreated fiber. This result was explained by an increase in moisture resistance for autoclave treated fibers.

Steam treatment can also be applied in a preformed fibrous material particularly in order to implement dimensionally stable fiberboard. Vapor can be introduced via steam-injection pressing technology [114]. It can also be created in situ by adding water sprayed to the fiber prior to placing them in a pressing mold and the mat in a hydraulic heated press [115]. Whatever the process, under proper experimental conditions, (i) high-performance binderless board can be manufactured, and (ii) steam treatment imparts dimensional stability to fiber board.

2.5.2 Carding technologies

One way to obtain biosourced composite is to manufacture a nonwoven mat from natural and polymer fibers mixed in various proportions and to hot press this product. Using hybrid nonwovens as semifinished products made from a blend of natural and thermoplastic fibers provides a good basis for high product quality. During hot

pressing, polymer fibers melted and flowed out between the natural fibers, forming a continuous matrix phase. Semiproducts are generated by carding or air-laid processes and subsequent mechanical bonding [116].

Specific fiber surface area is a physical characteristic which is of great importance when dealing with interface properties. It is defined as the accessible area of solid surface per unit of mass material. Different mechanical preparation of fibers can lead to differences in surface area and thus in the reactivity of the original materials. In a study conducted by Kaewprasite et al. [117], the effect of different preparations on cellulose fiber surface area is evidenced. Fiber processing such as opening by hand, carding, or drawing was carried out to individualize fibers. Preparation clearly affects the specific area of dried cotton. as evidenced in Tab. 2.7. When drawn, fibers exhibit a lower surface area whereas carding fibers gave larger values.

Tab. 2.7: The effect of different sample preparations on the specific surface area. Data from Kaewprasit [117].

Cotton preparation	Raw	Drawn	Carded 1 time	Carded 3 times
Surface area ($m^2 g^{-1}$)	32.42	32.23	44.75	42.76

These results can be explained by the fact that the carding process separates cellulose fibers and increases dthe available surface. On the other hand, it also results in fibers more parallel and very tight to each other.

By using x-ray microtomography, Alemdar and coworkers [118] studied the size distributions of hemp fibers having undergone several separation techniques (thermo-mechanical processed, separated with enzymes, or carded). The mean length of uncarded fibers was calculated and found to be 232 µm, compared to 308 µm for
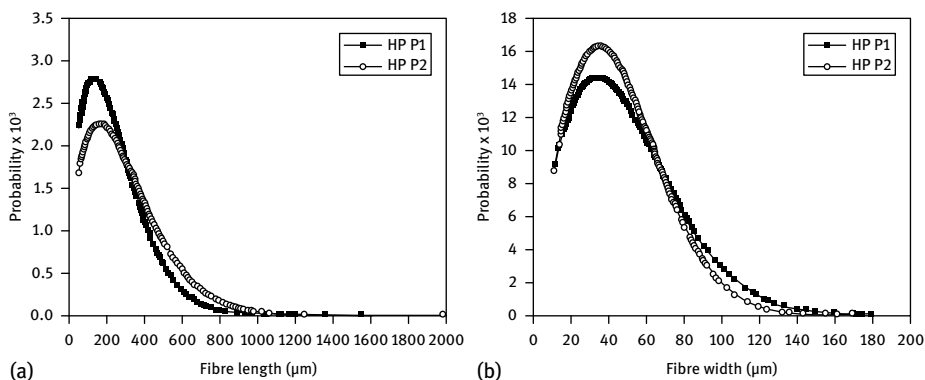

Fig. 2.10: Fiber length (a) and fiber width (b) distribution of hemp fibers in a composite. (HPP1: un-carded/HPP2: carded). Data from Alemdar et al. [118].

carded ones. Besides, the amount of short fibers is higher in the case of uncarded hemp, showing that the uncarded sample contained more impurities. Moreover, fiber width was smaller in the case of carded fibers. As a result, the mean aspect ratio was found to be 6.40 for carded fibers vs 4.85 for uncarded ones.

Thus, this separation process appears to produce more uniform fiber and is really a superior technique for upgrading fibers for composite applications.

2.6 Conclusions

"Green composites" are and have been an area of growing interest and a subject of active research for quite some time now. This is due to both environmental concerns as well as to the foreseeable future scarcity of oil and oil-derived products. Biocomposites use natural fibers and commonly oil-derived polymer matrices and are now available commercially. Moisture adsorption which ensues of poor compatibility between the hydrophilic component (matrix) and the hydrophobic one (reinforcements) remains a challenge and restriction for applications. Fiber surface modification by a physical route appears to be an eco-friendly alternative to chemical activation. The effects of such treatments on fibers are quite numerous, from radical creation to an oxidation or etching effect. The mechanical properties of resulting materials are generally improved. As a consequence, various processes can be used to perform composites of good performance.

References

[1]   Lee S. Dictionary of composite materials technology. Boca Raton (USA): CRC Press; 1995.
[2]   Williams K. Automotive industry uses of natural fiber reinforced composites. In: The Global Outlook for Natural Fiber & Wood Composites 2003, Intertech, New Orleans, LA, December 2003.
[3]   Zadorecki P, Michell AJ. Future prospects for wood cellulose as reinforcement in organic polymer composites. Polym. Compos. 1989; 10; 69–77.
[4]   Nabi Saheb D, Jog JP. Natural fiber polymer composites: a review. Adv Polym Technol. 1999; 18: 351–363.
[5]   Garkhail SK, Heijenrath RWH, Peijs T. Mechanical properties of naturalfiber-mat-reinforced thermoplastics based on flax fibers and polypropylene. Appl Compos Mater. 2000; 7: 351–372.
[6]   A.K Bledzki, S. Reihmane, J. Gassan. Thermoplastics reinforced with wood fillers: a literature review. Polym Plast Technol Eng. 1998; 37: 451–468.
[7]   Gassan J, Gutowski VS, Bledzki AK.. About the surface characteristics of natural fibers. Macromol Mater Eng. 2000; 283: 132–139.
[8]   United States patent US 4,783,493 (November 8, 1988): Motegi T, Aoki K, Kimura K. Thermoplastic resins with cellulosic fillers.
[9]   U.S. Pat. 4,833,011 (May 23, 1989). Horimoto K. Synthetic pulp and adsorbent comprising the same.

[10] Pitt WG, Lakenan JE, Strong AB. The influence of plasma gas species on the adhesion of thermoplastic to organic fibers. J Appl Polym Sci. 1993; 48: 845–856.

[11] Iso 21348: Space environment (natural and artificial)- Processes for determining solar irradiances

[12] Merlin A. PhD thesis. Université de Mulhouse; 1974.

[13] Corey A, Gray C. Notes on the preparation of standard cellulose. Ind Eng Chem. 1924; 16: 853–1130.

[14] Hon NS. Behavior of hydrogen atoms and formyl radicals formed in photoirradiated cellulose. J Polym Sci, Polym Chem Ed. 1976; 14(4): 225–229.

[15] Hon NS. formation of free radicals in photoirradiated cellulose and related compounds. J Polym Sci Polym Chem Ed. 1976; 13(12): 2653–2669.

[16] Koichi K, Victor VN, Mikhail FN, Masashi M, Yoshito I, Katsuhiko N. Surface oxidation of cellulose fibers by vacuum ultraviolet irradiation. J Polym Sci, Part A, Polym Chem. 1999; 37: 357–362.

[17] Gassan J, Gutowski VS. Effects of corona discharge and UV treatment on the properties of jute-fibre epoxy composites. Compos Sci Techn. 2000; 60: 2857–2863.

[18] Oosterom R, Ahmed TJ, Poulis JA, Bersee HEN. Adhesion Performance of UHMWPE after Different Surface Modification Techniques. Medical Engineering & Physics. 2005; 28(4): 323–330.

[19] Laroussi M, Alexeff I, Kang WL. Biological decontamination by nonthermal plasmas. IEEE Trans Plasma Sci. 2000; 28: 184–189.

[20] Gassan J, Gutowski VS. Effects of corona discharge and UV treatment on the properties of jute-fiber epoxy composites. Composites Science and Technology. 2000; 60: 2857–2863.

[21] Rahman MM. UV-cured henequen fibers as polymeric matrix reinforcement: Studies of physico-mechanical and degradable properties. Materials and Design. 2009; 30: 2191–2197.

[22] Liebermann MA, Lichtenberg AJ. Principle of plasma discharges and materials processing. New York: John Wiley; 1994. Chapter 1, Introduction; pp. 1–53.

[23] Stefecka M, Rahel J, Cernak M, Hudec I, Mikula M, Mazur M. Atmospheric-pressure plasma treatment of ultrahigh molecular polyethylene fibers. J Mat Sci Lett. 1999; 18: 2007–2008.

[24] Pavlath AE, Slater RF. Low temperature plasma chemistry, I. Shrink proofing of wool. Appl Polym Symp. 1971; 18: 1317–1324.

[25] Stone RB Jr, Barrett JR Jr. U.S.D.A. Study Reveals Interesting Effects of GasPlasma Radiations on Cotton Yarn, Textile Bull. 1962; 88: 65–68.

[26] Coleman JH. Method of Grafting Ethylenically Unsaturated Monomer to a Polymeric Substrate, United States patent US 3,600,122, August 1971.

[27] Ferrero F, Bongiovanni R. Improving the surface properties of cellophane by air plasma treatment, Surface and Coatings Technology. 2006; 200(16/17): 4770–4776.

[28] Soignet DM, Hinojosa O, Ward TL, Benerito RR. The Effects of Plasma Irradiation on Saccharides. J Macromolecular Sci A. 1982; 17(3): 403–414.

[29] Reza M, Malek A, Holme I. The effect of plasma treatment on some properties of cotton. Iranian Polymer J. 2003; 12(4): 271–280.

[30] Ward TL, Jung HZ, Hinojosa O, Benerito RR. Characterization and use of radio frequency plasma-activated natural polymers. J Appl Polymer Sci. 1979; 23: 1987–2003.

[31] Sabharwal HS, Denes F, Nielsen L, Young RA. Free-radical formation in jute from argon plasma treatment. J Agri. Food Chem. 1993; 41: 2202–2210.

[32] Jung HZ, Ward TL, Benerito RR. Effect of Cold Plasma on Water Absorption of Cotton. Textile Res J. 1977; 47: 217–222.

[33] Benerito RR, Ward TL, Soignet DM, Hinojosa O. Modifications of Cotton Cellulose Surfaces by Use of Radiofrequency Cold Plasmas and Characterization of Surface Changes by ESCA. Text Res J. 1981; 51(4): 224–232.

[34] Ward TL, Benerito RR. Modification of Cotton by Radiofrequency Plasma of Ammonia. Text Res J. 1982; 52(4): 256–263.

[35] Ward TL, Benerito RR. New surface in cellulosic fibers by use of radiofrequency plasma of ammonia, U.S. Patent 4351857.

[36] Abidi N, Hequet E. Cotton fabric graft copolymerization using microwave plasma. I. Universal attenuated total reflectance-FTIR study. J Appl Polym Sci. 2004; 93: 145–154.

[37] Sahin HT, Manolachel S, Young RA, Denes F. Surface fluorination of paper in CF4-RF plasma environments. Cellulose. 2002; 9: 171–181.

[38] Navarro F, Davalos F, Denes F, Cruz LE, Young RA, Ramos J. Highly hydrophobic sisal chemithermomechanical pulp (CTMP) paper by fluorotrimethylsilane plasma treatment. Cellulose. 2003; 10: 411–424.

[39] Gilbert Carlsson CM, Ström GR. Adhesion between plasma-treated cellulosic materials and polyethylene. Surface and Interface Analysis. 2004; 17(7): 511–515.

[40] Felix J, Gatenholm P, Schreiber HP. Plasma modification of cellulose fibers: Effects on some polymer composite properties. J Appl Polym. 1994; 51(2): 285–295.

[41] Yuan X, Jayaraman K, Bhattacharyya D. Effects of plasma treatment in enhancing the performance of woodfiber-polypropylene composites. Composites A. 2004; 35: 1363–1374.

[42] Marais S, Gouanve F, Bonnesoeur A, Grenet J, Poncin-Epaillard F, Morvanc C, Metayer M. Unsaturated Polyester Composites Reinforced with Flax Fibers: Effect of Cold Plasma and Autoclave Treatments on Mechanical and Permeation Properties. Composites A. 2005; 36: 975–986.

[43] Thorsen WJ. Improvement of Cotton Spinnability, Strength, and Abrasion Resistance by Corona Treatment. Textile Research J. 1971; 41(5): 455–458.

[44] Thorsen WJ. Modification of the Cuticle and Primary Wall of Cotton by Corona Treatment. Textile Research J. 1974; 44(6): 422–428.

[45] Uehara T, Sakata I. Effect of corona discharge treatment on cellulose prepared from beech wood. J Appl Polym Sci. 1990; 41(7/8): 1695–1706.

[46] Belgacem MN, Czeremuszkin G, Sapieha S. Surface characterization of cellulose fibers by XPS and inverse gas chromatography. Cellulose. 1995; 2: 145–157.

[47] Dong S, Sapieha S, Schreiber HP. Mechanical properties of corona-modified cellulose/polyethylene composites. Polym Engin Sci. 1993; 33(6): 343–346.

[48] Belgacem MN, Bataille P, Sapieha S. Effect of corona modification on the mechanical properties of polypropylene/cellulose composites. J Appl Polym Sci. 1994; 53(4): 379–385.

[49] Wu S. Polymer interface and adhesion. New York: M. Dekker, Inc.; 1982.

[50] O'Donnell A, Dweib MA, Wool RP. Natural fiber composites with plant-oil based resin, Composites Sci Techn. 2004; 64: 1135–1145.

[51] Panthapulakkal M, Sain MM. Injection-molded short hemp fiber/glass fiber-reinforced polypropylene hybrid composites- mechanical, water absorption and thermal properties. J Appl Polym Sci. 2007; 103: 2432–2441.

[52] Ragoubi M, Bienaimé D, Molina S, George B, Merlin A. Impact of corona treated hemp fibers onto mechanical properties of polypropylene composites made thereof. Industrial Crops and Products. 2010; 31(2): 344–349.

[53] Pizzi A, Kueny R, Lecoanet F, Massetau B, Carpentier D, Krebs A, Loiseau F, Molina S, Ragoubi M. High resin content natural matrix–natural fiber biocomposites. Industrial Crops and Products. 2009; 30(2): 235–240.

[54] Walsh WK, Oraby W. Radiation processing. In: Lewin M, Sello SB, editors. Handbook of Fiber Science and Technology: vol. II, Chemical Processing of Fibers and Fabrics, Functional Finishing. Part B. New York: Dekker; 1984, p. 44.

[55]   Takács E, Wojnárovits L, Borsa J, Papp J, Hargittai P, Korecz L. Modification of cotton-cellulose by preirradiation grafting. Nuclear Instruments and Methods in Physics Research B. 2005; 236: 259–265.

[56]   Kuzina SI, Mikhailov AI. The oxidation and thermal transformations of macroradicals in gamma irradiated cellulose. Russ J Phys Chem. 2006; 80: 1666–1670.

[57]   Pekel N, Yoshii F, Kume T, Guven O. Radiation crosslinking of biodegradable hydroxypropyl methylcellulose. Carbohyd Polym. 2004; 55: 139–147.

[58]   Charlesby A. Atomic Radiation and Polymers. London: Pergamon Press; 1960.

[59]   Takács E, Wojnárovits L, Borsa J, Földváry C, Hargittai P, Zöld O. Effect of γ-irradiation on cotton-cellulose. Radiat Phys Chem. 1999; 55: 663–666.

[60]   Takács E, Wojnárovits L, Borsa J, Hargittai P, Korecz L. Modification of cotton-cellulose by preirradiation grafting. Nucl Instr Meth Phys Res B. 2005; 236: 259–265.

[61]   Arthur JC Jr. Derivatives of cellulose: reactions induced by high-energy radiation. High Polym. 1971; 5: 937–975.

[62]   Dubey KA, Pujari PK, Ramnani SP, Kadam RM, Sabharwal S. Microstructural studies of electron beam-irradiated cellulose pulp. Radiat Phys Chem. 2004; 69: 395–400.

[63]   Sreekalal MS, Thomas S. Effect of fiber surface modification on water-sorption characteristics of oil palm fibers. Comp Sci Technol. 2003; 63: 861–869.

[64]   Khan F, Ahmad SR, Kronfli E. γ-Radiation Induced Changes in the Physical and Chemical Properties of Lignocellulose. Biomacromolecules. 2006; 7: 2303–2309.

[65]   Ajji Z, Preparation of pinewood/polymer/composites using gamma irradiation. Rad Phy Chem. 2006; 75: 1075–1079.

[66]   Borysiak S. A study of transcrystallinity in polypropylene in the presence of wood irradiated with gamma rays. J Therm Anal Calorim. DOI 10.1007/s10973-010-0780-2.

[67]   Haydaruzzaman RA, Khan MA, Khan AH, Hossain MA. Effect of gamma radiation on the performance of jute fabrics-reinforced polypropylene composites. Rad Phys Chem. 2009; 78: 986–993.

[68]   Albano C, Reyes J, Ichazo M, González J, Brito M, Moronta MD. Analysis of the mechanical, thermal and morphological behaviour of polypropylene compounds with sisal fiber and wood flour, irradiated with gamma rays. Polym Degr Stab. 2002; 76: 191–203.

[69]   Suslick KS, Didenko Y, Fang MM, Hyeon T, Kolbeck KJ, McNamara III WB, Mdleleni MM, Wong M. Acoustic cavitation and its chemical consequences. Phil Trans R Soc Lond A. 1999; 357(1751): 335–353.

[70]   Aimin T, Hongwei Z, Gang C, Guohui X, Wenzhi L. Influence of ultrasound treatment on accessibility and regioselective oxidation reactivity of cellulose. Ultrasonics Sonochemistry. 2005; 12: 467–472.

[71]   Laine JE, Goring DAI. Influence of Ultrasonic Irradiation on the Properties of Cellulosic Fibers. Cell Chem Technol. 1977; 11(5): 561–567.

[72]   Chang WP, Kim KJ, Gupta RK. Moisture Absorption Behavior of Wood/Plastic Composites Made with Ultrasound-Assisted Alkali-Treated Wood Particulates. Composite Interfaces. 2009; 16(7–9): 937–951.

[73]   Pappas C, Tarantilis PA, Daliani I, Mavromoustakos T, Polissiou M. Comparison of classical and ultrasound-assisted isolation procedures of cellulose from kenaf (Hibiscus cannabinus L.) and eucalyptus (Eucalyptus rodustrus Sm.). Ultrasonics Sonochemistry. 2002; 9(1): 19–23.

[74]   Seino T, Yoshioka A, Fujiwara M, Chen KL, Erata T, Tabata M, Takai M. ESR Studies of radicals generated by ultrasonic irradiation of lignin solution. An Application of the Spin Trapping Method. Wood Sci Technol. 2001; 35(1/2): 97–106.

[75]   Krishnaswamy P. Fibrillated bast fibers as reinforcement for polymeric composites. US Patent 6,767,634; July 27, 2004.

[76] Lennox-Kerr P. Fibers – Fibrillation makes flax better for composite reinforcement. Adv Textiles Techn. 2005; May: 1–3.

[77] Yuan TQ, Xu F, He J, Sun RC. Structural and physico-chemical characterization of hemicelluloses from ultrasound-assisted extractions of partially delignified fast-growing poplar wood through organic solvent and alkaline solutions. Biotechn Adv. 2010; 28(5): 583–593.

[78] Nielsen NPK, Gardner DJ, Felby C. Effect of extractives and storage on the pelletizing process of sawdust, Fuel. 2010; 89(1): 94–98.

[79] Amidon TE, Liu S. Water-based woody biorefinery. Biotechn Adv. 2009; 27(5): 542–550.

[80] Delong EA. Method of rendering lignin separable from cellulose and hemicellulose in lignocellulosic material and the product so produced. Canadian patent CA 1,217,765. June 13, 1978.

[81] Delong EA. Method of rendering lignin separable from cellulose and hemicellulose material and the product so produced. Canadian patent CA 1,141,376. June 13, 1978.

[82] Chorne E, Overend RP. Phenomenological kinetics and reaction engineering aspects of steam/aqueous treatments. In: Focher B, Marzetti A, Crescengi V, editors. Steam explosion techniques: fundamentals and industrial applications. Philadelphia, Gordon and Breach Science Publishers; 1991. pp. 21–58.

[83] Josefsson T, Lennholm H, Gellerstedt G. Steam explosion of aspen wood, characterisation of reaction products. Holzforschung. 2002; 56(3): 289–297.

[84] Avellar B, Glasser WG. Steam-assisted biomass fractionation. 1. Process considerations and economic evaluation. Biomass Bioenergy. 1998; 14: 205–218.

[85] Tanahashi M. Characterization and degradation mechanisms of wood components by steam explosion and utilization of exploded wood. Wood Research. 1990; 77: 49–117.

[86] Kokta BV, Ahmed A. Steam explosion pulping. In: Young RA, Akhtar M, editors. Environmentally friendly technologies for the pulp and paper industry. New York: John Wiley & Sons, Inc.; 1998. pp. 191–214.

[87] Donaldson LA, Wong KKY, Mackie KL. Ultrastructure of steam exploded wood. Wood Sci Technol. 1988; 22: 103–114.

[88] Renneckar S, Zink-Sharp A, Glasser WG. Fiber modification by steam-explosion: microscopic analysis of co-refined wood and polypropylene. IAWA J. 2007; 28(1): 13–27.

[89] Eichhorn SJ, Sirichaisit J, Young RJ. Deformation Mechanisms in Cellulose Fibers, Paper and Wood. J Mat Sci. 2001; 36: 3129–3135.

[90] Yin S, Wang S, Rials TG, Kit KM, Hansen MG. Polypropylene composites filled with steam-exploded wood fibers from beetle-killed loblolly pine by compression-molding. Wood Fiber Sci. 2007; 39(1): 95-108.

[91] Marchessault RH, St Pierre L. A new understanding of the carbohydrate system. In: St. Pierre L, Brown GR, editors. Future Source of Organic Raw Materials. Elmsford, NY: Pergamon Press; 1980. pp. 613–626.

[92] Anglès MN, Salvado J, Dufresne A. Steam-exploded residual softwood-filled polypropylene composites. J Appl Polym Sci. 1999; 74: 1962–1977.

[93] Josefsson T, Lenholm H, Gellerstedt G. Changes in cellulose supramolecular structure and molecular weight distribution during steam explosion of aspen wood. Cellulose. 2002; 8(4): 289–296.

[94] Vignon MR, Dupeyre D, Garcia-Jaldon C. Morphological characterization of steamexploded hemp fibers and their utilization in polypropylene-based composites. Bioresource Techn. 1997; 58: 203–215.

[95] Kessler RW, Becker U, Kohler R, Goth B. Steam explosion of flax – a superior technique for upgrading fiber value. Biomass and Bioenergy. 1998; 14(3): 237–249.

[96]   Shaji J, Sreekumar PA, Kenny JM, Puglia D, Thomas S, Joseph K. Dynamic Mechanical Analysis of Oil Palm Microfibril-Reinforced Acrylonitrile Butadiene Rubber Composites. Polymer Composites. 2010; 31(2): 236–244.

[97]   Avella M, Casale L, Dell'Erba R, Focher B, Martuscelli E, Marzetti. Broom Fibers as Reinforcing Materials for Polypropylene-Based Composites. J Appl Polym Sci. 1998; 68: 1077–1089.

[98]   Anglès MN, Salvadó J, Dufresne A. Steam-Exploded Residual Softwood-Filled Polypropylene Composites. J Appl Polym Sci. 1999; 74: 1962–1977.

[99]   Takatani M, Kato O, Kitayama T, Okamoto T, Tanahashi M. Effect of adding steam-exploded wood flour to thermoplastic polymer/wood composite. J Wood Sci. 2000; 46: 210–214.

[100] Glasser WG, Taib R, Jain RK, Kander R. Fiber-Reinforced Cellulosic Thermoplastic Composites. J Appl Polym Sci. 1999; 73: 1329–1340.

[101] Okubo K, Fujii T, Yamamoto Y. Development of bamboo-based polymer composites and their mechanical properties. Composites A. 2004; 35: 377–383.

[102] Shen KC. Binderless composite panel products. In: Burton RJ, Tarlton GL, Rotourua AB, editors. Proceedings of the Composite Wood Products Symposium, New Zealand; 1990. pp. 105–1077.

[103] Angles MN, Ferrando F, Farriol X, Salvado J. Suitability of steam exploded residual softwood for the production of binderless panels. Effect of the pre-treatment severity and lignin addition. Biomass and Bioenergy. 2001; 21: 211–224.

[104] Laemsak N, Okuma M. Development of boards made from oil palm frond II: properties of binderless boards from steam-exploded fibers of oil palm frond. J Wood Sci. 2000; 46: 322–326.

[105] Velasquez JA, Ferrando F, Farriol X, Salvado J. Binderless fiberboard from steam exploded Miscanthus sinensis. Wood Sci Technol. 2003; 37: 269–278.

[106] Velasquez JA, Ferrando F, Salvado J. Binderless fiberboard from steam exploded Miscanthus sinensis: The effect of a grinding process. Holz als Roh- und Werkstoff. 2002; 60: 297–302.

[107] Quintana G, Velasquez J, Betancourt S, Ga nán P. Binderless fiberboard from steam exploded banana bunch. Industrial Crops and Products. 2009; 29: 60–66.

[108] Suchsland O, Woodson GE, McMillin CW. Effect on cooking conditions on fiber bonding in dry-formed binderless hardboard. Forest Prod J. 1987; 37: 65–69.

[109] Carrano AL, Taylor JB, Lemaster RL. Machining-induced subsurface damage of wood. Forest Prod J. 2004; 54(1): 85–91.

[110] Higashihara T, Morooka T, Tanaka F, Inoue M, Norimoto M. Permanent fixation of cellulose fiber by steaming and its mechanism. Mokuzai Gakkaishi/J Jap Wood Res Soc. 2003: 49(4): 260–266.

[111] Inoue MM, Norimoto M, Tanahashi RM. Steam or heat fixation of compressed wood. Wood Fiber Sci. 1993; 25(3): 224–235.

[112] Marais S, Gouanvé F, Bonnesoeur A, Grenet J, Poncin-Epaillard F, Morvan C, Métayer M. Unsaturated polyester composites reinforced with flax fibers: effect of cold plasma and autoclave treatments on mechanical and permeation properties, Composites A Appl Sci Manu. 2005: 36(7): 975–986.

[113] Stamboulis A, Baillie CA, eijs T. Effects of environmental conditions on mechanical and physical properties of flax fibers. Composite A. 2001; 32: 1105–1115.

[114] Xu J, Han G, Wong ED, Kawai S. Development of binderless particleboard from kenaf core using steam-injection pressing. J Wood Sci. 2003; 49: 327–332.

[115] Das S, Saha AK, Choudhury PK, Basak RK, Mitra BC, Todd T, Lang S, Rowell RM. Effect of Steam Pretreatment of Jute Fiber on Dimensional Stability of Jute Composite. J Appl Polym Sci. 2000; 76: 1652–1661.

[116] Mueller DH. New Discovery in the Properties of Composites Reinforced with Natural Fibers. J Indust Textiles. 2003; 33(2): 111–130.

[117] Kaewprasit C, Hequet E, Abidi N, Gourlot JP. Quality measurements: Application to Methylene Blue Adsorption to Cotton Fiber Specific Area Measurement: Part I. Methodology. J Cotton Sci. 1998; 2: 164–173.

[118] Alemdar A, Zhang H, Sain M, Cescutti G, Müssig J. Determination of Fiber Size Distributions of Injection Moulded Polypropylene/Natural Fibers Using X-rayMicrotomography. Adv Eng Mat. 2008; 10(1/2): 126–130.

A. Pizzi

3 Natural matrix/non wood natural fibers composites

Abstract: Biobased composites composed of natural non-wood fibers such as hemp and other vegetable fibers and bonded with natural matrix resins are presented, together with their performance and their characterization. Tannin-hexamine, tannin-resorcinol-aldehyde, tannin-furfuryl alcohol, and epoxidized vegetable oils are presented as natural biobased matrix resins.

Biocomposites are and have been an area of growing interest and a subject of active research for quite sometime now. This is due to both environmental concerns as well as to the foreseen future scarcity of oil and oil-derived products. Biocomposites using natural fibers and oil-derived synthetic polymer matrices have now existed and been available commercially for quite some time. Thus, composites from natural fibers plus polypropylene and other oil-derived thermoplastic matrices for car door interiors and other applications are well known and widely used, although not as extensively as could be wished. However, for the same type of applications, composites also using natural matrices while still presenting high performance are discussed, but in reality are either still just in the beginning phase or have not been properly developed or commercialized. This is due to the difficulty in finding matrices of natural origin capable of imparting all the required performance to the resulting composites. For example, starch-bonded [1] biocomposites have poor water and moisture resistance, while others such as polylactic acid-bonded biocomposites, while showing good promise in other fields, also have some deficits.

Some composites with good performance formed from nonwoven mats of flax and hemp fibers and natural resin matrices have been developed [2, 3], and this chapter will concentrate specifically on these. The natural matrices used were based either on commercial vegetable tannin extracts with 5 % hexamine added as hardener, or on a mix of tannin and hexamine with glyoxalated organosolve lignin of low molecular weight [2, 3]. However, these composites need particular attention during preparation, because as the matrix resins are water-born, minimization of distortion, excessive resin flow, and other potential problems due to the presence of water have to be taken into account [3]. While these technical problems appear to have been overcome, matrices not based on water containing natural resins might be preferable for ease of manufacture. The his chapter will survey all the types of natural matrices that have been used for the preparation of such composites.

Both higher density thin composites as well as lower density thicker composites have been developed. Two natural matrices types were used: (i) commercial mimosa flavonoid tannin extract with 5 % hexamine added as hardener, and (ii) a mix of mimosa tannin and hexamine with glyoxalated organosolv lignin of low molec-

ular weight, these two resins being mixed 50/50 with solid content weight [2]. The composites prepared were tested for MOE in bending and in tension and for maximum breaking strength in tension. Some of the mats were corona treated and the optimum length of corona treatment is determined to improve the composite's MOEs and breaking strength. These were related to the morphology of the treated fiber. Thermomechanical analysis, Brinell surface hardness, and contact angle tests were also carried out with good results. The composites made with the mix of tannin and lignin resins as a matrix remained thermoplastic after a first pressing. The flat sheets prepared after the first pressing were then thermoformed into the desired shape.

It has been found that for making composites, natural pH tannin hexamine matrix gives better results in terms of mechanical properties than the pH corrected one with NaOH usually used for wood gluing. The pH correction with NaOH in the formulation is meant to slow down the curing time of the resin and allow the opening of a second aromatic cycle in the tannin molecule for a better cross-linking in the glue joint. In the case of composites with a high matrix percentage, the amount of NaOH in the resin (which remains unreacted after composite manufacture) causes a higher sensibility to moisture changes and direct water exposure, and in some way reduce the average strength of the composite. By removing NaOH from the resin formulation, the bonding between fibers is better and makes possible a multilayer construction which has been proven to be almost impossible with pH10 resin, while having mechanical properties much higher than the European norm EN 622-2 requirements. This is a major improvement in the process, allowing a quicker predrying phase, a better control of the overall moisture content across the composite section, and the possibility to create "sandwiches" with different kind of fabrics. First experiments with both nonwoven and unidirectional fibermats confirmed this.

– *Influence of moisture content*: As the curing reaction required water, a too small amount of it causes poor mechanical resistance values: a MOE of only 3.64 GPa for 10 % of MC (moisture content). The curing reaction is then incomplete. Going up to 15 % MC significantly improved the mechanical properties: 5.33 GPa and the best result is for 20 % MC: 5.58 GPa. Increasing MC further causes a decline of the properties: 5.26 GPa for 25 % MC. The MC has not been tested at higher values, as it is known that going any higher than 25 % makes the fibermats spread under pressure, causing a significant drop in mechanical properties [8].

– *Influence of curing pressure*: At an MC of 15 %, increasing the pressure from 15 to 20 bar and then to 25 bar decreases the mechanical properties of the composite: 5.33 GPa, 4.92 GPa, and 4.83 GPa, respectively. When the MC is at 20 % the effect is the opposite: MOE values are 5.58, 5.77, and 5.97 GPa for 15, 20, and 25 bar, respectively. However, the density of composites made at 15 bar pressure is slightly under the densities of the ones made at 20 and 25 bar. For the specific modulus the composites at 15 bar appear to be better than the others: for a density of 1 the values are 4.74, 4.38, and 4.59 for 15, 20, and 25 bar, respectively.

–   *Influence of curing time*: The best result is observed for 35 min of curing: 5.58 GPa. With only 25 min, the value is lower: 5 GPa, because the reaction is not completely finished. On the other hand, with a longer curing time of 45 min, the composite starts to deteriorate under the action of heat, explaining the lower values down to 4.54 GPa.
–   *Influence of curing temperature*: A temperature of 130 °C can be used by this and leads to a very long curing time. Two different temperatures were tested to lower this duration: 160 °C (20 min curing time) and 190 °C (8 min curing time). The mechanical resistance results were close: 5.11 GPa at 160 °C and 5.10 GPa at 190 °C, but under the 5.58 GPa obtained for a 35 min curing time. The drop is no higher than 10 %, and thus an increase of the curing temperature may be considered.

3.1 Comparison with UD fiber-reinforced composites

Additional composites were prepared using unidirectional (UD) flax mats. Woven mats may be used when a higher mechanical resistance is required in a certain direction rather than in any direction. Different combinations of fibers and orientations were tested, mainly, composites made of a single layer of nonwoven mat as a core and four layers of UD mats on each side. These UD mats were piled up either all in the same orientation (0° orientation) or perpendicularly one to each other (0°/90° orientation). Control composites were made, with only nonwoven mats or only UD mats also using the two 0° and 0°/90° fibers orientations.

For the nonwoven ones a MOE of 4.9 GPa was obtained which is an average value considering their low density of 0.981. With the UD mats, when all fibers are in the same direction the MOE goes up to 12 GPa for a density of 1.32 g/cm^3, and if half the fibers are angled perpendicularly this value drops to 6.92 GPa, at comparable density.

The composites made with both nonwoven and UD fibers show lower results than the ones using only nonwoven or only UD fibers. 3.60 GPa were obtained for the ones with UD fibers all in the same direction and 4.52 GPa for the ones with UD fibers placed perpendicularly to each other. Considering the fact that they have different densities (respectively 0.793 and 1) these composites appear to have almost the same mechanical resistance: by increasing the density of the first ones to a density of 1 g/cm^3 their modulus would most likely increase to 4.53 GPa. However, in any cases these results are still higher than the European norm requirements.

Replacing a part of the nonwoven mats by UD mats in this way does not seem to improve the properties of the composite. On the other hand, analysis showed that the UD prepregs employed with nonwoven ones had higher fiber content: nonwoven prepregs were 50 % fibers, 50 % resin, and the UD prepregs 70 % fibers, 30 % resin. Higher resin content may be required to increase the mechanical efficiency of those UD fibers.

3.2 Water resistance of the composites

In addition to the mechanical testing, tests were performed to verify the resistance of the composites to water, following the European norm EN 622-2.

All the composites made at 130 °C have very similar results except for the one with a MC of 10 %. For these, the swelling after 24 h in cold water (20 °C) is between 11.7 and 13 %. The worst value (13 %) is for the one pressed at 15 bar with a MC of 15 %, and the best (11.7 %) is for the one pressed at 25 bar with a MC of 20 %. For the 10 % MC composite, the result is much higher: 21.1 % of swelling. In this case the MC of the composite was too low to ensure a full cure of the materials, and a lot of unreacted tannins with OH groups remain, making the fixation of water much easier. The composite cured at 160 °C show slightly better results, with an average of 10.4 % of swelling.

3.3 Influence of the layers on the composite properties

– *Traction testing*: One can assemble such composites in two different manners: with multiple layers of thin fibermats, or instead of a single thick one. Yet it is important to know if this choice significantly impacts the quality of the composites. When comparing the mechanical properties of the single-layer composites to a two-layer ones of the same total thickness, there is only a small difference: for instance in the experiments reported [5] the MOE value is 5.69 GPa for a single-layer and 5.42 GPa for the two-layer composite, which is an acceptable 3 % drop. Furthermore the rupture of the two-layer samples occurs in the same way as the single-layer ones – a clear crack perpendicular to the tension direction, without delamination between the two fibermats forming the composite.
– *Internal bond strength testing*: When the first tannin-hexamine composites were made with multiple layers of fibermats, the poor adhesion between the layers gave low internal bond properties: the composites easily delaminated at the bound between layers [5, 6]. The advent of new and optimized formulations [5] resulted in an improved performance: the two-layer composites had an internal bond strength value of 1.85 MPa, which is even higher than the 1.75 MPa of the single-layer ones. Although the interface between the two layers is still a privileged area for initiating delamination, the structure of the multilayer composites achievable today is now strong enough to reach the same properties as single-layer composites.

– *Water resistance testing*: Regarding the behavior of such materials in water, the results of the two types of composites were also found to be closer, with an average swelling of 12.8 % for the two-layer composites and of 11.2 % for the single-layer one [5]. As the water swelling seems mainly sensitive to the fiber content of the material [7], this difference may be explained by a slightly higher fiber content of the two-layer composite: 51.8 %, compared to the 49.4 % of the single-layer ones. These values are both lower than the ones of composites using a resin with NaOH, which was about 16 to 22 % [7, 8], and meet the most restrictive NF EN 622-2 requirements.

Not only tannin-hexamine formulations were tested for natural fiber composites, but also natural matrices capable of cold-setting rather than needing heat to harden. Thus, tannin-resorcinol-aldehyde resins [9, 10] were prepared and optimized for such an application, the aldehyde being used being formaldehyde as well as alternative aldehydes such as glyoxal and glutaraldehyde. The matrix resin thus formed were examined by matrix assisted laser desorption ionization time of flight (MALDI-TOF) mass spectrometry.

The Maldi-TOF mass spectrometry of tannin-resorcinol glyoxal and tannin-resorcinol-glutaraldehyde resins showed that both formulations were not a simple mix of resorcinol-aldehyde species and flavonoid oligomers. A lot of different combinations coexist in those resins: tannin-aldehydes, tannin-resorcinol, aldehyde-resorcinol chains, and tannin-resorcinol-aldehydes, all with various levels of polymerization. It is interesting to note that the intermediate species, namely tannin-aldehydes, tannin-resorcinol, and aldehydes-resorcinol, are more present than the tannin-resorcinol-aldehydes ones. Eventually, this analysis shows that the better results of TRGlutaraldehyde adhesive compared to TRGlyoxal obtained in previous work [9, 10] could be explained by a better reactivity of glutaraldehyde with phenolic compounds such as resorcinol and tannins. The reaction schemes for the two aldehyde are as follows, indicating how the various chemical species present are formed.

Schemes 3.1–3.3 show the different manners in which the tannin-resorcinol-glyoxal adducts are formed. However also resorcinol-aldehyde oligomers are present as shown in Scheme 3.4.

Similar reaction schemes and pathways as for tannin-resorcinol-glyoxal also occur for the tannin-resorcinol-glutaraldehyde reactions (Schemes 3.5–3.9).
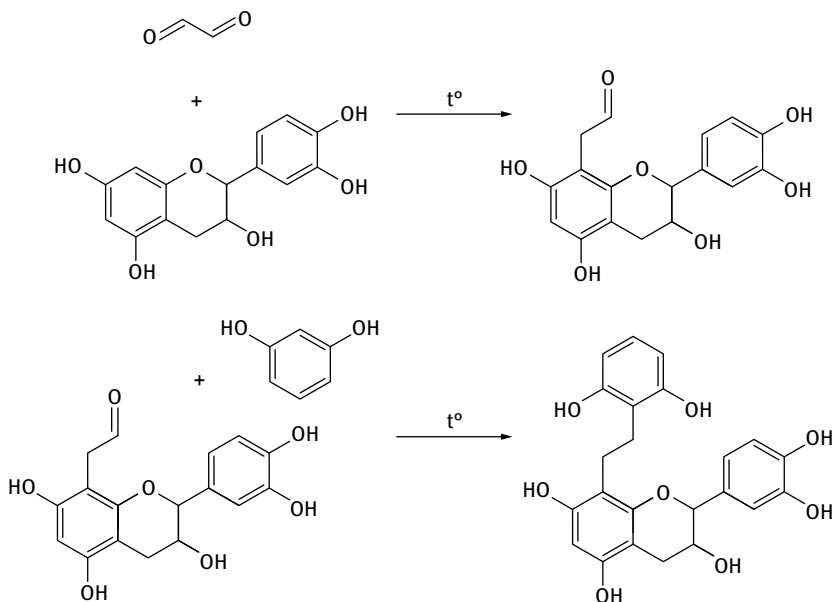
Scheme 3.1: Reaction for the formation of a tannin-resorcinol-glyoxal matrix resin by first reaction of glyoxal with the tannin.
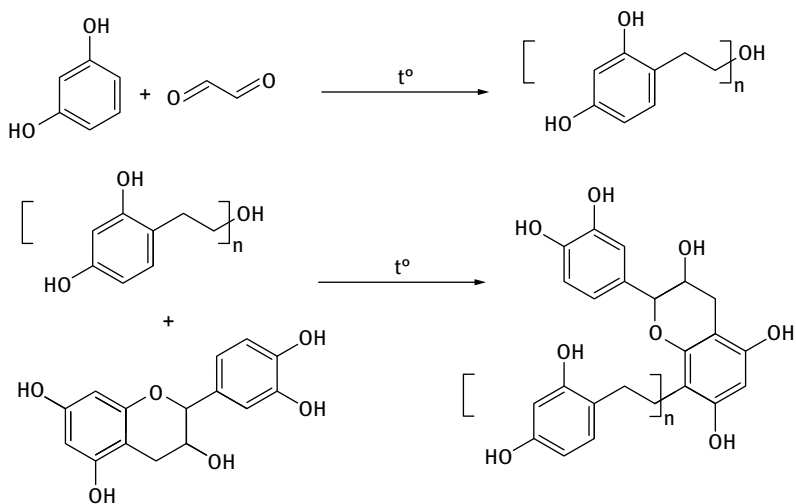

Scheme 3.2: Reaction for the formation of a tannin-resorcinol-glyoxal matrix resin by first reaction of glyoxal with the resorcinol.
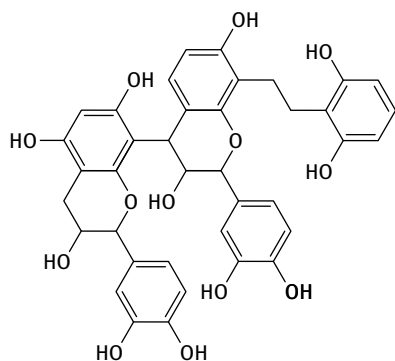
Scheme 3.3: Example of a tannin-resorcinol-glyoxal matrix resin oligomers in which a flavonoid dimer is involved.
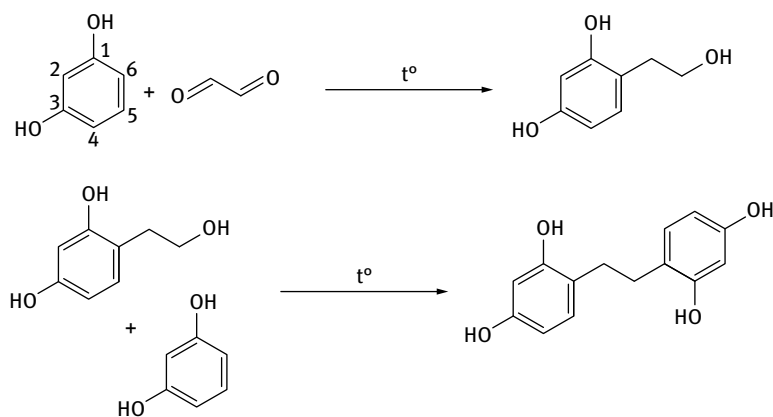

Scheme 3.4: Resorcinol glyoxal reaction in competition with the tannin-resorcinol-glyoxal reaction and leading to resorcinol-glyoxal oligomers in the reaction mixture.
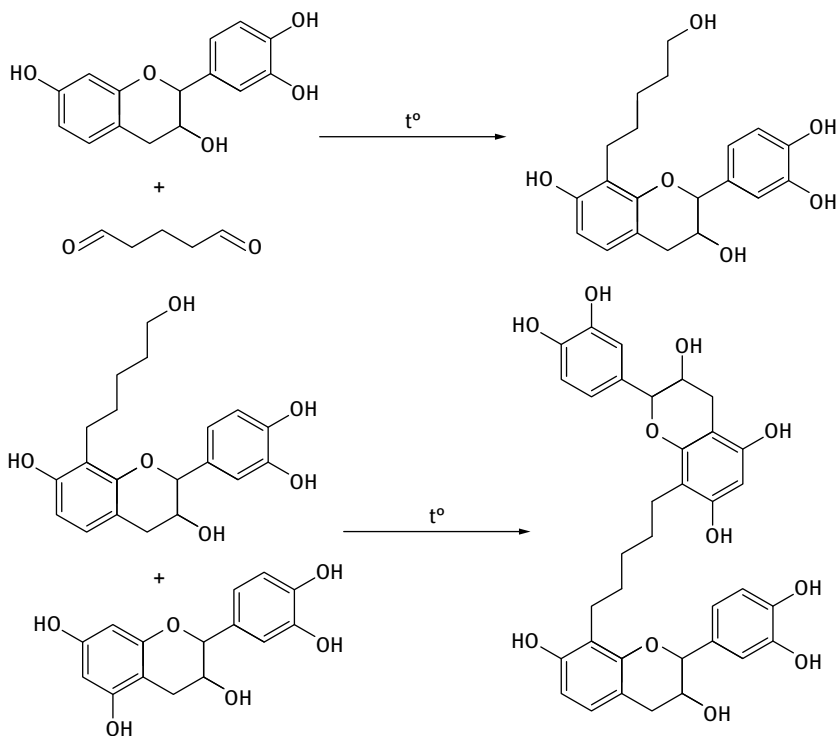
Scheme 3.5: Tannin-resorcinol-glutaraldehyde reactions leading to oligomers constituting the matrix resin when only flavonoid monomers are involved.
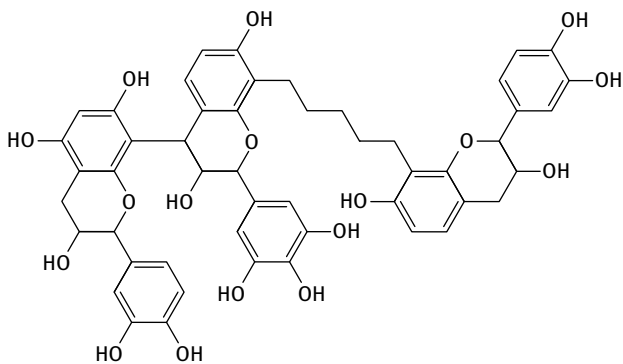
Scheme 3.6: Tannin-resorcinol-glutaraldehyde matrix resin oligomer involving higher flavonoid oligomers.
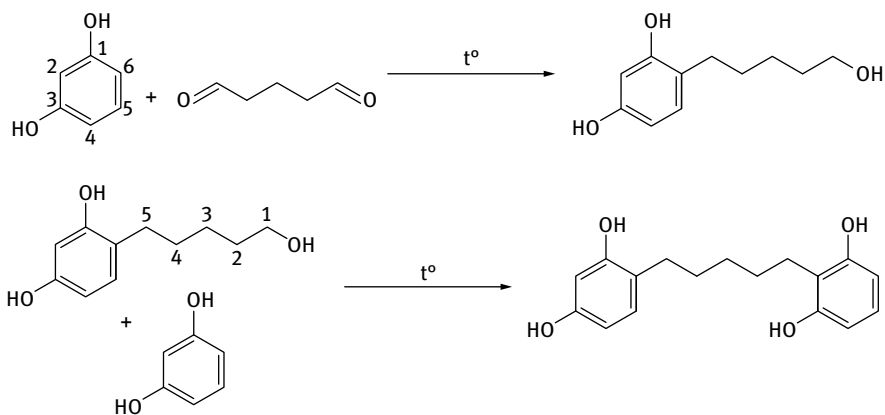
Scheme 3.7: Resorcinol-glutaraldehyde reaction simultaneous to the tannin-resorcinol-glutaraldehyde reaction and leading to resorcinol-glutaraldehyde oligomers in the prepared matrix resin.
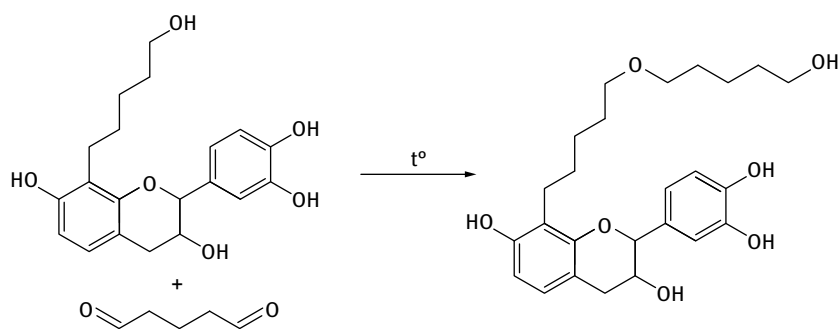
Scheme 3.8: Example of oligomers formed by reaction of glutaraldehyde with itself when linked to a flavonoid unit.
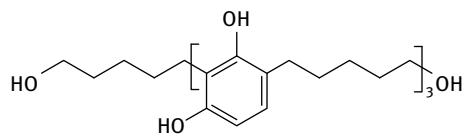
Scheme 3.9: Resorcinol-glutaraldehyde trimer formed by the competitive side reaction of resorcinol and glutaraldehyde.

Resorcinol-glutaraldehyde linear oligomers are also formed and are present in the matrix resin mixture.

Experimental investigations have also been carried out on the potential use of tannin-furfuryl alcohol resins for bio-based composites using vegetal fibers reinforcement. Results showed that a mixture containing 54 % of furfuryl alcohol and 45 % of modified quebracho tannin extract, and 0.9 % paratoluenesulfonic acid as a catalyst yields a resin that can be used with a nonwoven flax fiber mat to manufacture lightweight composites with good mechanical properties and a very short curing time with a regular hot press. The panels made were tested for tensile and flexural modulus and strength, water resistance and thermodegradation.

Under the conditions described [11] the process yielded composites having, in average, a fiber content of 54.6 % of total mass, and a relatively low density of 716 kg/m^3, which is under the theoretical maximum density that could be achieved, lignocellulosic material having an estimated density of around 1500 kg/m^3 and the measured density of the resin being 1360 kg/m^3 [12]. This shows that this material can be quite porous. However, this porosity is a key feature of the fast pressing process being used. Under acid conditions, the furfuryl alcohol reacts with the tannins in a moderate proportion, and reacts strongly with itself by its characteristic self-condensation mechanism [13], leading to the generation of a great amount of water [14]. This water needs to be quickly evacuated through the composite during the pressing, as the steam pressure can lead to a spreading of the reinforcement mat as it has been observed in other composites using resins with water as a solvent [15]. Attempts to get a high density composite using a lower curing temperature to reduce steam formation led to considerably longer pressing times and materials that may be still soft at the press exit. Catalyst proportion cannot be increased further as the mixture will reach the threshold of the exothermal self-sustaining condensation at room temperature. Thus, with 1 % of pTSA catalyst, the pot life of this matrix resin does not exceed 8 min (Fig. 3.1).

Despite its lower density compared to classical composite materials, these tannin-furanic composites showed good mechanical properties and may be suitable for non-structural applications. After pressing, the shape retention is good, and no warping was observed. Mechanical testing showed that the composite modulus of elasticity (MOE) in tension is about 2.2 GPa on average, with a tensile strength of 17.4 MPa. The modulus has been measured at 3.1 GPa in bending, with a bending strength of 32 MPa. The Brinell hardness was measured giving 2.55 HBS 10/100, with an elastic recovery of 25 %, which is comparable to the properties of untreated beech wood [16]. All properties and their standard deviation are summarized in Tab. 3.1.

Thermogravimetric analysis (TGA) of the composite (Fig. 3.2) showed that it could withstand temperatures up to 150 °C in regular use without damages, the mass variation in the 50 to 100 °C being due to sample drying. Here the fiber reinforcement is the first to show a beginning of degradation after 150 °C, and the DTA curve follows the same pattern that was observed for wood pyrolysis [17]. Thus, it presents a shoulder around 250 °C that can be mainly attributed to hemicelluloses and the main peak in

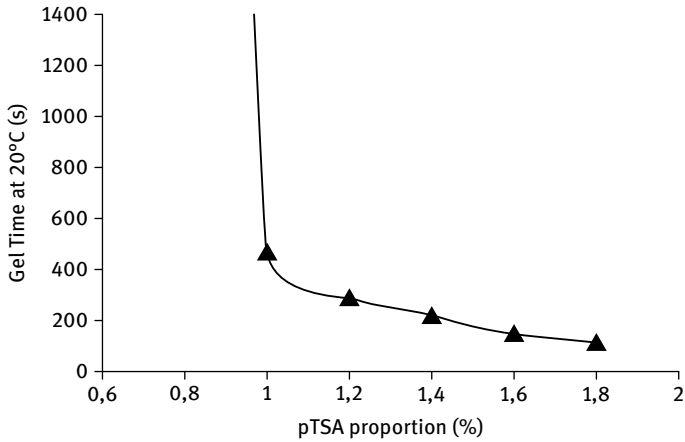**Fig. 3.1:** Gel time of tannin-furfuryl alcohol matrix as a function of the proportion of the with para-Toluen sulphonic acid (pTSA) catalyst used.

Tab. 3.1: Physical and mechanical properties of the composite.

Property		Unit	Average value	Standard deviation
Tensile	MOE	GPa	2.171	0.145
	Strength	MPa	17.4	2.30
Flexural	MOE	GPa	3.132	0.200
	Strength	MPa	32.2	2.91
Density		kg/m^3	716	25.5
Brinell hardness		N/mm^2	25.5	0.26
Elastic recovery		%	25.1	1.35
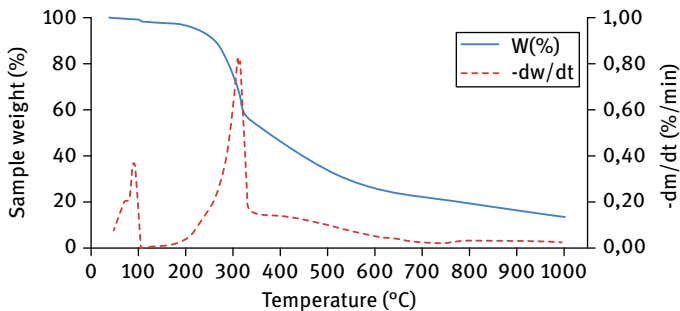
Fig. 3.2: Thermogravimetric analysis (TGA) curve of the composite (thick line) and differential thermal analysis (dotted line).

the 270 to 330 °C that corresponds to the degradation of cellulose [17]. Cellulose represents a large proportion of the flax fiber weight, usually 70 to 75 % [17]. The pyrolysis of the tannin-furanic type matrix occurs in a much broader temperature range, from 200 °C to 600 °C [12]. The position of the main peak depends on the tannin to furfuryl alcohol ratio. While pure polyfurfuryl alcohol exhibits a main peak around 470 °C [19], this moves down to 400 °C with a resin containing 25 % of tannin [12], and in the resins at hand it seems to be more in the 350–370 °C range by looking at the shoulder in the DTA curve.

Swelling in water as well as weight uptake was recorded in cold water for 2 h and 24 h. The composites performed fairly well with an average of only 10. 4 % swelling after 24 h. Despite not meeting the criteria for exterior grade panels, the material maybe suitable for a wide range of uses, including general use in both dry and wet environments, and structural use in dry environment according to the European norm EN 622-3 [4] (Tab. 3.2).

Tab. 3.2: EN 622-3 requirements and composite performances.

		Nonstructural		Structural	Results	Std deviation
		Dry	Wet	Dry		
2 h	Swelling	—	—	—	4.90 %	1.30 %
	Uptake	—	—	—	11.40 %	0.80 %
24 h	Swelling	< 15 %	< 12 %	< 15 %	10.40 %	1.60 %
	Uptake	—	—	—	33 %	1.90 %
Flexural strength		> 15 MPa	> 18 MPa	> 21 MPa	32.2 MPa	2.91 MPa
Flexural MOE		—	—	> 2500 MPa	3132 MPa	200 MPa

Composites prepared by impregnating nonwoven mats of mixed natural fibers, mainly flax, hemp, and a small percentage polylactic acid, with epoxydized soybean oil/maleic anhydride matrices, also yielded composites 85 % natural [20]. The advantage of these composites was their light color in relation to tannin based ones (Fig. 3.3), and they yielded a good modulus of elasticity (MOE) and modulus of rupture (MOR) in bending for composites 65 % matrix resin/35 % natural fibers. Composites 50 % matrix resin/50 % natural fibers gave also good results when tested in tension. The best results appear to be obtained using (i) higher curing temperatures (180 °C) with long postcure times and (ii) medium temperature (150 °C) and longer press times (360 s).

In conclusion natural fiber nonwoven mat composites of good performance can be prepared with a number of biosourced matrix resins, the ones reviewed here being condensed tannin-hexamine, tannin-resorcinol-aldehyde, tannin-furfuryl alcohol, and an epoxidized vegetable oils.

Fig. 3.3: Color difference of a fiber nonwoven mat composite bonded with an epoxidezid vegetable oils matrix, lighter colored, and a fiber nonwoven mat composite bonded with a tannin-hexamine system.

References

[1]   Theis M, Grohe B. Biodegradable lightweight construction boards based on tannin/hexamine bonded hemp shaves. Holz Roh-Werkst. 2002; 60: 291–296.

[2]   Pizzi A, Kueny R, Lecoanet F, Massetau B, Carpentier D, Krebs A, Loiseau F, Molina S, Ragoubi M. High resin content natural matrix-natural fibre biocomposites. Ind Crops Prod. 2009; 30(2): 235–240.

[3]   Nicollin A, Kueny R, Toniazzo L, Pizzi A. High density composites from natural fibers and tannin resin. J Adh Sci Technol. 2012; 26: 1537–1545.

[4]   European Norm EN 622-2 Fiberboards – Specifications – Part 2: Requirements for hardboards; 2003.

[5]   Sauget A, Nicollin A, Pizzi A. Fabrication and mechanical analysis of mimosa tannin and commercial flax fibers biocomposites. J Adhesion Sci Technol. 2013; 27(20): 2204–2218.

[6]   Zhou X, Pizzi A. Tannin–resorcinol–aldehyde cold-set wood adhesives with only formaldehyde as hardener. Eur J Wood Wood Prod. 2013; 71: 537–538.

[7]   Oksman K, Skrifvas M, Selin JF. Natural fibers as reinforcement in polylactic acid composites. Compos Sci Technol. 2003; 63: 1317–1324.

[8]   Bakare IO, Okieimen FE, Pavithran C, Abdul Khalil HPS, Brahmakumar M. Mechanical and thermal properties of sisal fiber-reinforced rubber seed oil-based polyurthane composites. Mater Des. 2010; 31: 4274–4280.

[9]   Sauget A, Zhou X, Pizzi A. Tannin-resorcinol-formaldehyde resin and flax fibers biocomposites. J J Renewable Mat. 2014; 2(3): 173–181.

[10] Sauget A, Zhou X, Pizzi A, MALDI-ToF Analysis of Tannin-Resorcinol Resins by Alternative Aldehydes. J Renewable Mat. 2014; 2(3): 186–200.

[11] Nicollin A, Li X, Girods P, Pizzi A, Rogaume Y. Fast pressing composite using tannin-furfuryl alcohol resin and vegetal fibers reinforcement. J Renewable Mat. 2013; 1(4): 311–316.

[12] Li X, Nicollin A, Pizzi A, Zhou X, Sauget A, Delmotte L. Natural tannin-furanic thermosetting moulding plastics. RSC Advances. 2013; 39(3): 17732–17740.

[13] Foo LY, Hemingway RW. Condensed tannins: reactions of model compounds with furfuryl alcohol and furfuraldehyde. J Wood Chem Tech. 1985; 5(1): 135–158.

[14] Choura M, Belgacem NM, Gandini A. Acid-catalysed polycondensation of furfuryl alcohol: mechanisms of chromophore formation and cross linking. Macromolecules. 1996; 29: 3839–3850.

[15] Nicollin A, Kueny R, Toniazzo L, Pizzi A. High density biocompsite from natural fibers and tannin resin. J Adh Sci Tech. 2012; 26: 1537–1545.

[16] Rautkari L, Properzi M, Pichelin F, Hughes M. An innovative thermo densification method for wooden surfaces. In: Proceedings of the 10th world conference on timber engineering; 2008 Jun 2–5; Miyazaki, Japan. Engineered Wood Products Association Publisher; 2008. p. 177.

[17] Gašparovič L, Koreňová Z, Jelemenský L. Kinetic study of wood chips decomposition by TGA. Chemical Papers. 2010; 64(2): 174–181.

[18] Bledzki AK, Mamun AA, Lucka-Gabor M, Gutowski VS. The effects of acetylation on properties of flax fiber and its polypropylene composites. Express Polym Letters. 2008; 2: 413–422.

[19] Burket CL, Rajagopalan R, Marencic AP, Dronvajjala K, Foley HC. Genesis of porosity in polyfurfuryl alcohol derived nanoporous carbon. Carbon. 2006; 44: 2957–2963.

[20] Sauget A, Pizzi A. Exploratory results for composites of natural fiber mats with a natural matrix of epoxidized vegetable oils, J Adh Sci Technol. 2012; DOI: 10.1080/01694243.2012.701478.

Frank C. Beall and Henrique Reis

4 Ultrasonic press control and evaluation of wood-based composite panel properties

Abstract: Composite press control and the subsequent evaluation of panels produced can be done separately or integrated for closed-loop process control. Ultrasonic press control is based on determining a key minimum point in ultrasonic transmission through one or more boards in the press. The time of press opening can be conservatively determined and/or adjusted to the type of resin or the desired internal bond. After pressing, panels can be evaluated for average elastic or strength properties or variation in properties.

4.1 Introduction

This chapter focuses on wood composites that are formed from particles, chips, or flakes, including medium density fiberboard, particleboard, and oriented strandboard (OSB). Plywood is not included since its characteristics and processing are quite different from the composite panels. One common characteristic of the formation of composite panels is the density gradient produced in the pressing process (Fig. 4.1). Typi-
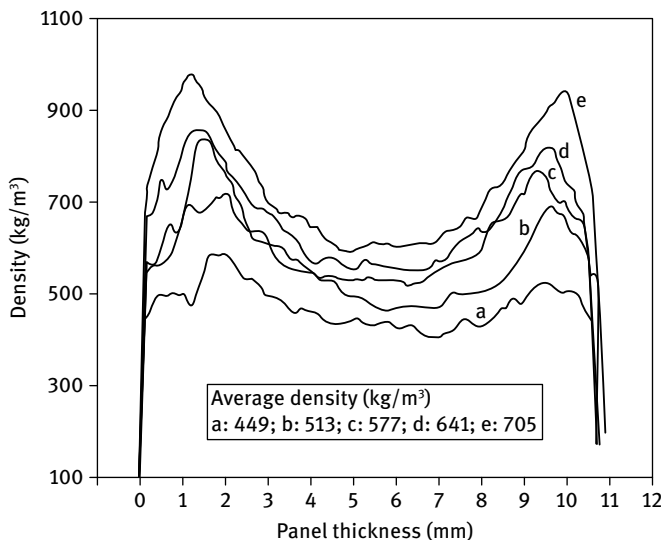
Fig. 4.1: Density gradient of laboratory-fabricated OSB panels with the indicated target average densities [1].

cally, the surface "layers" are each about 30 % of the thickness, and about 50 % greater in density than the core, each of which is dependent on the average density of the board. The denser surface results in a desirable feature of a more uniform and compact surface; however, the strength of the board is largely controlled by the core. The performance of the oriented strandboard with this density profile mimics the performance of a board with sandwich construction, where the outer higher-density layers are located where the maximum bending stresses exist. and the lower density core is located where the maximum shear stresses occur. At the same time, the less dense core contributes to the board bending stiffness by increasing its cross-section bending moment of inertia.

In a typical composites mill, a "mat" is assembled on a "former". and is precompressed before being loaded into the press. Most industrial presses have 20 "openings", or pairs of heated platens. After curing, the boards are removed with an "unloader", and then normally move to an air-cooled board cooler before being subsequently processed. After cooling, the boards are typically evaluated by measuring the internal bond (IB; tension perpendicular). In IB tests, specimens of 50 by 50 mm in area are bonded to like-size metal blocks that can be pulled in tension to determine the load at failure. This is done for only a few selected panels on the basis of economical considerations (often once a shift), and this data is assumed to reflect the condition of other panels in the same production run. Since the IB is dependent on the time in the press, a change in IB properties can be addressed by a change in press time. Therefore, these processes involve a very crude open-loop control system. With any major changes in the raw material and/or adhesive, the IB values are assessed for modifying the press cycle. The length of the press time is critical from both an economical and technical perspective. For example, an overly short press time can lead to "blows" from residual internal board steam pressure that exceeds the strength of the adhesive bonding. Even without a blow, the panel can still have an unacceptably low IB if the press is opened too early. Extending press time is one of possible means of increasing the degree of curing and therefore the IB; however, this can cause overcuring problems and a lower IB, as well as a decrease in production rate.

4.2 Background

4.2.1 Assessment methods

Hot pressing is a very complex process involving mechanical, physical, and chemical changes, with a three-dimensional gradient of temperature, gas pressure, and moisture content changing through the mat with time. Therefore, interactions between the initial mat conditions and the press conditions may significantly affect resin curing and bonding behavior. Many techniques, largely off-line, have been used to evaluate the curing process and bonding behavior. Once the board has been produced, its per-

formance in service is affected by the type and loading of resin, density, and density gradient, and, for OSB, flake orientation.

4.2.1.1 Nonacoustic methods

Several techniques have been used to determine the bonding efficiency of wood-based raw materials [2]. None are candidates for on-line process control, but can be used to understand fundamental interactions.

Surface analysis techniques have been used to investigate the adherend surface to infer its bonding performance. Because of the relatively modest cost of the equipment, contact angle measurements have been used to estimate the wettability or the surface free energy of wood. Other surface analytical instruments, such as x-ray photoelectron spectroscopy and infrared spectroscopy, have been used to measure the chemical composition of the wood surface to estimate the potential bonding ability. However, wood adhesion is not just controlled by chemical properties. Physical properties, such as density and porosity, will also influence resin performance.

Thermal analysis techniques, such as differential scanning calorimetry, dynamic mechanical thermal analysis, and torsional braid analysis, can measure the changes related to either the chemical reaction or the mechanical properties of the curing resin. Although these techniques can provide useful information on the extent of resin cure, samples for wood adhesion measured by these methods are usually in the form of bulk resin, mixtures of resin and wood powders, resin-impregnated glass cloth, or wood wafers. Because of the lack of the true interaction between resin and wood, optimal conditions for resin curing determined by these methods may not be suitable for optimal bonding processes for hot pressing.

Several techniques, such as an optical fiber method and dielectric analysis, have been applied to monitor the curing of bulk polymers or wood-based composites during pressing. Since only the resin information is obtained, these techniques are unlikely to be suitable for monitoring hot-pressed wood composites in which determining resin condition is not sufficient to insure a highly integrated structure. Moreover, these techniques require embedded sensors in the test materials, causing problems of intrusion and nonrepeatability.

There have been models to predict the endpoint in curing or development of bond strength, but the variations in mat formation and compression, moisture content of the furnish (and contributed by the resin) do not permit adequate press control using such models.

4.2.1.2 Ultrasonic methods

Ultrasonic testing (UT) techniques have been used for polymer cure monitoring with a variety of probe arrangements to excite different kinds of waveforms, such as longitudinal, shear, guided waves, and interface waves (another type of guided wave).

Because of the direct connection between the propagating behavior of sound waves and the mechanical properties of the material, information on the extent of resin cure and bonding strength between resin and adherend can be obtained by measuring various ultrasonic parameters. Among all ultrasonic parameters, measurement of velocity is the simplest. Another technique is the acousto-ultrasonics (AU) approach, which combines the advantages of acoustic emission (AE) and conventional UT. Typical uses of AU are with laminated composites and composite-like materials that are highly heterogeneous and anisotropic. Unlike conventional UT that usually measures velocity and attenuation, AU affords more flexibility to assess different properties with diverse parameters.

In AU, as in conventional through-transmission ultrasonics, a pulse or burst is injected into a material and the response is captured at a second point. The received signal characteristics are a result of multiple reflections, wave interactions, and mode changes [3] and can be processed by extracting different types of signal waveform parameters. These characteristics can be described by parameters that are measures of signal attenuation, velocity, shape, and frequency content.

Root mean square (RMS) voltage is often used as a measure of signal energy. The inverse of RMS voltage can be used to approximate signal attenuation. RMS can be calculated from

$$\text{RMS} = \frac{\sqrt{\sum V_i}}{n},$$

where n is a number of measured data points from signal and V_i is the voltage value at point i.

Signal velocity is calculated from transit time t, the time from the transmitter to the receiver, based on the assumption of a direct signal path of distance d:

$$V = d/t.$$

In order to detect the first arrival, the threshold level for the received signal must be placed just above the noise level. In highly attenuating and dispersive materials, such as wood, the leading edge of the waveform may be difficult to detect, decreasing the apparent velocity. It should also be obvious that the assumption of the direct signal path overestimates the actual velocity in perhaps every case.

Signals can also be processed by determining moments from the following expression:

$$M_n = \int y(x) x^n \, \mathrm{d}x,$$

where n is the moment order and x is the particular domain of the signal (for example, time or frequency). The zero-th moment is simply the area of the waveform. By dividing the first moment by the zero-th moment, we obtain a centroid. The time centroid (TC) is sometimes referred to as "mean time", and is therefore related to its shape. When an ultrasonic signal is injected into a flawless medium, most of its energy is typically near the beginning of the waveform. Reflections and mode changes occur from boundries

and material flaws, causing a skewing of the signal in time domain. Power spectrum characteristics can also be expressed by the n-th moment of the waveform, where x is represented by frequency. Spectral moments are combined measures of amplitude and frequency; with a larger n, more weight is placed on frequency. Physically, the frequency centroid indicates the center frequency of the signal relative to the amount of received energy.

Since its initial development to evaluate fiber-reinforced composites [4], most AU studies have concentrated on the post-evaluation of the formation and performance of composites and composite-like materials [5]. It was not until 1987 that the first AU research relating to the cure monitoring of wood adhesion was reported, in which a lap joint of maple was used with a transmitter and receiver mounted on either side to monitor the curing of an epoxy bond line [6] (Fig. 4.2). As the waves propagated through the bond line, they interacted with the curing resin and the response was used to monitor curing development.
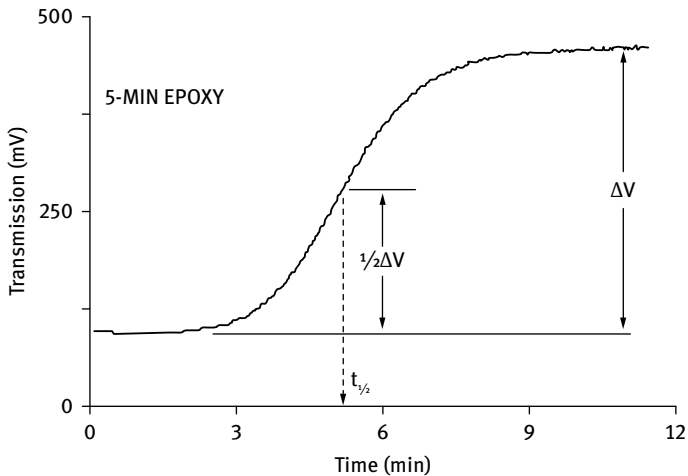
Fig. 4.2: Cure time of epoxy resin as monitored by RMS. The initial transmission, up to about 2 min, represents the coupling effect of the resin before curing started. The halftime to cure served as a useful parameter to compare different resins.

Because of the similarity with fiber-reinforced composites, AU is very appropriate for use with wood and wood-based materials. Since the hot-pressing process is dynamic and its products are highly dependent upon processing factors, the technique required for cure monitoring must not only minimize the interference caused by the press but also provide precise feedback. Because multiple reflections are one of the attributes of AU, well-defined pathways are not critical. Since AU provides various parameters to assess different mechanical properties of interest, it is an excellent candidate to monitor the hot-pressing process.

4.3 Main focus of this chapter

4.3.1 Press control

Studies were performed to develop a technique, using AU, to nonintrusively monitor the bonding development of particleboard during hot pressing using a computer-controlled 610 × 610 mm laboratory press [2, 7, 8].

4.3.1.1 AU equipment

Fig. 4.3 shows a block diagram of the AU system and press. The transmitting equipment included a frequency generator to establish a constant 60 kHz, sweep generator to gate the continuous waveform into tone-burst with a duration of 333 μs and repetition rate of 50 Hz, power amplifier to increase the amplitude of the tone-burst to 300 V peak-to-peak, and transmitter to transform the voltage into ultrasonic waves. Stainless steel waveguides were screwed into threaded wells in the platens to protect transducers from the high temperature of the hot press and to have each platen act as a transmitter or receiver. The receiving equipment included a receiver to convert the ultrasonic waves into voltage, 40 dB preamplifier with 30 kHz to 1 MHz bandpass, 20 dB amplifier, and A/D converter to process the signal. Since RMS voltage had been used
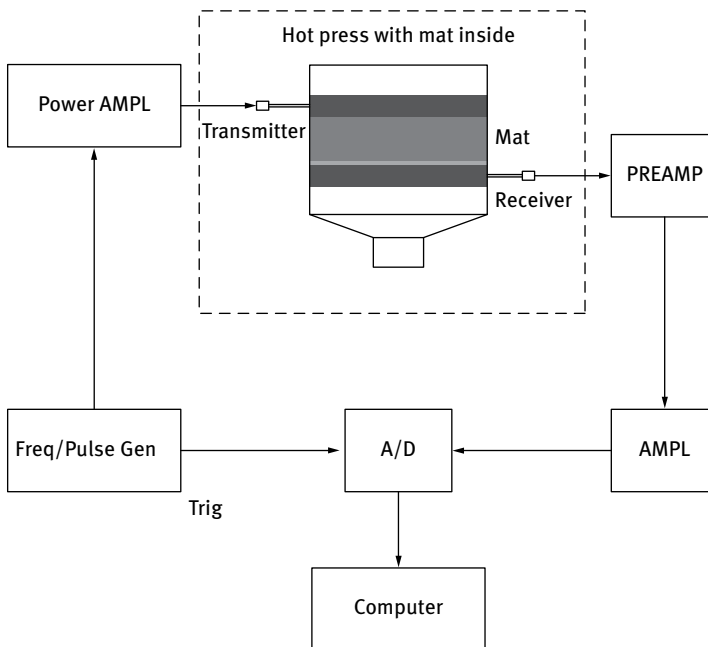
Fig. 4.3: Block diagram of a nominal acousto-ultrasonics system used in the Press Monitor system.

successfully in a series of studies in monitoring curing behavior of wood resins [9], this parameter was used for signal processing. A series of 14 boards, 20 mm thick and with 6 % resin content, were pressed at 160 °C and removed between 240 and 600 s. IB samples were then tested for each board to establish the correlation between AU transmission and strength development of a reference 600 s board (Fig. 4.4). In addition, in order to characterize the effects of interactions between press or mat variables and AU transmission, a series of boards were made using a 600 s press cycle for a range of resin content (2–10 %), temperature (120–200 °C), and thickness (10–30 mm).
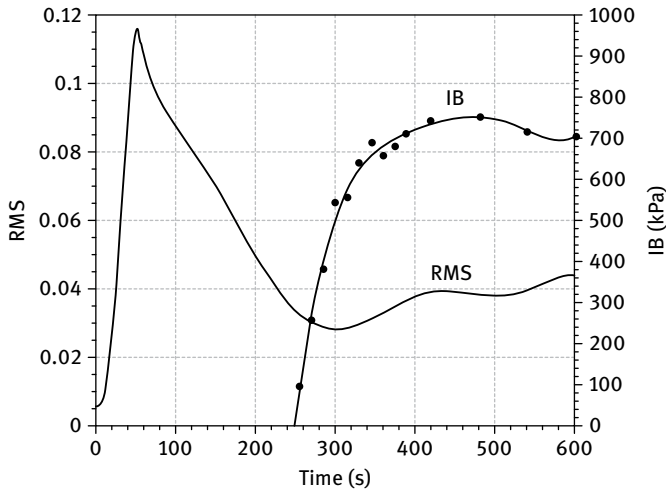
Fig. 4.4: Internal bond and RMS values of composite panels for different pressing times. The initial RMS peak represents the maximum pressure at the mat, after which relaxation occurs to the point of the onset of curing.

4.3.1.2 Ultrasonic output during pressing

The output signal from the transducer is affected by a number of key variables, including the development of strength of the mat (modulus); the attenuation of ultrasound from the presence of moisture and steam, and temperature of the mat; and acoustic coupling between the platens and mat. Some of these effects vary with the depth into the mat (platen to platen), but the level of energy transmission tends to be controlled by the weakest location in the mat (the core). Since transmission is measured through the entire thickness, there is no convenient method to differentiate the layer contributions to variability, and therefore these are lumped effects that change the level of ultrasonic transmission. It is also well known that wood composites in the press cure nonuniformly across the area of the mat. When all of these factors are considered, we can model the ultrasonic output by the following equation:

$$T_i = f(k_i, A_i, M_i),$$

where:

T_i AU transmission at point i over the time of pressing;

k_i coupling coefficient, $k_i = f(p, s)$, where p is the pressure at the surface and s the surface roughness;

A_i attenuation coefficient, $A_i = f(A_m, T, t)$, where A_m is the material coefficient, T the temperature, and t the material thickness;

M_i modulus of rupture, $M_i = f(r_c, r_t, r_b, b)$, where r_c is the resin content, r_t the resin type, r_b the resin bonding, and b the particle layering, geometry, etc.

Values of T can be used to determine the point at which the mat is sufficiently cured for the intended purpose. For example, this point can be a fixed time period after the minimum of the RMS curve, a specific RMS level after the minimum, or when the RMS reaches a plateau of essentially zero slope.

In Fig. 4.4, the RMS curve can be divided into four segments: 0–300, 300–400, 400–500, and 500–600 s to represent different stages of bonding development. In the first segment, RMS depends mainly on the change of press pressure (peaking at 50 s). From 300 to 400 s, the increase of RMS output reacts directly to the increase of IB. As the resin completely curs, RMS reaches a plateau. With extended pressing, RMS beyond 500 s reflects the degraded condition of the board. Using real-time observation of the change of RMS, the in situ strength development of the board during pressing can be monitored. It is also possible for the relative difference between the minimum and subsequent plateau in the RMS output curve to be used to evaluate the bonding quality of the board.

4.3.1.3 Effects of board variables

The variables that can be detected by ultrasound and may be possible to manipulate include resins (adhesives), biobased materials characteristics, and panel properties. Two major types of commercial resins (urea formaldehyde and phenol formaldehyde) have been shown to affect the curing curve in pressing. A differential loading of resin in surface and/or core can also affect the ultrasonic transmission. Other variables such as blending and bonding efficiency have not been previously assessed. The size, shape, and thickness of the biobased materials have unknown effects on ultrasonic transmission. Another variable, particulate orientation (especially for OSB) is expected to be determinable through special ultrasonic techniques. Press control includes variables such as the pressure cycle, temperature, time, and heating method (direct contact or gas-through). In terms of panel properties, only one (internal bond) has been reported, but others such as elastic modulus and density gradient may be measurable. In order to verify that the AU technique was responsive to different pressing conditions, several common variables, such as board thickness, resin content, and press temperature, were investigated for the effects of interactions between press or mat variables

and AU transmission (RMS). All curves of AU transmission (RMS) were smoothed, and the AU-plateau criterion (the beginning of the stage C–D) was used to determine the completion of curing.

– *Thickness*. The effect of board thickness on RMS was studied on boards made at 160 °C and 6 % resin content in five thicknesses. Using the AU-plateau criterion, the optimum time for press opening was 265, 330, 430, and 580 s for 10, 15, 20, and 25 mm boards, respectively. To further investigate the relationship between board thicknesses and curing times, a regression analysis was performed on the data resulting in an r^2 of 0.968, with curing time increasing at 20.5 s/mm.

– *Cure time*. Curing is occasionally determined by measuring the core temperature of boards in the press because bulk urea-formaldehyde resin cures within 30 s after the temperature reaches 100 °C. The time for core temperature to reach 100 °C was 91, 162, 243, and 338 s for 10, 15, 20, and 25 mm boards, respectively. Subtracting these values from the curing times determined by the AU-plateau criterion, the time differences were 174, 168, 187, and 242 s for 10, 15, 20, and 25 mm boards, respectively. These differences indicated that the use of an arbitrary time after the core temperature reaches 100 °C is quite unreliable to determine the cure completion of UF resin blended within the composite material.

– *Resin content*. The effect on curing was studied with resin contents of 2–10 %. However, changing the resin content introduces other mat variables that affect the process. For example, a mat with a lower resin content has a higher amount of furnish and a lower moisture content, causing greater compressive stress development and lower heat transfer. In addition, it requires a higher press pressure to overcome the greater stress, which causes a higher ultrasonic coupling between the mat and platens, resulting in a higher AU transmission. The most interesting observation about the effect of resin was that all RMS output curves reached plateaus at about the same time, indicating that the required curing times were almost identical for all resin contents.

– *Temperature*. Lower press temperature indirectly increases AU transmission because of the greater pressure required for mats to overcome higher built-up stress, and subsequent better coupling. These pressures are reduced more slowly because of the longer time for stress relaxation. In contrast, higher press temperature enhances wood compressibility and accelerates resin curing. Higher temperature pressing also has lower AU transmission because of reduction in strength and stiffness of wood from its softened polymers.

– *Density*. Board density and density profile also affects AU transmission since a lower density core attenuates and disperses a greater amount of AU energy. Higher density boards have a greater ratio of surface to core density that could affect wave transmission because of the layering effect through the thickness. This effect would also be important in on-line measurements of board properties.

4.3.2 On-line measurement of board properties

Press monitoring can provide a guide for optimal press opening based on development of mat strength, and subsequent on-line measurements can independently gather data for variability within and between boards. A press monitoring system is generally limited to a single opening of typical 20-opening presses, and provides essentially a lumped value of output from which to determine press opening. An on-line system could be used to determine the mean and variability of IB for each press opening, and with multiple gauges, both central and edge values. This output can also be used to determine if any openings have heat transfer problems.

The first generation equipment to be used on-line in particleboard mills used wheeled fixtures in direct opposition to transmit a pulse through the board [10] (Fig. 4.5). Since attenuation of ultrasound through the board is temperature sensitive, an infrared gauge was used to provide measurement for compensation. An equation was developed to correlate IB with known board properties

$$IB = a + bV_o + cT + dx + ex^2,$$

where V_o is output voltage, T is temperature, and x is thickness.

Using the above equation in laboratory conditions, with particleboard conditioned to extremes of 40–105 °C and an IB range of 680–840 kPa, the correlation was 85 % (Fig. 4.6). In production runs, the correlation of predicted to actual IB with a much more limited temperature range was 95 % for an IB range of 420–840 kPa [11]. One of the difficulties in the measurement was the need for consistent contact pressure
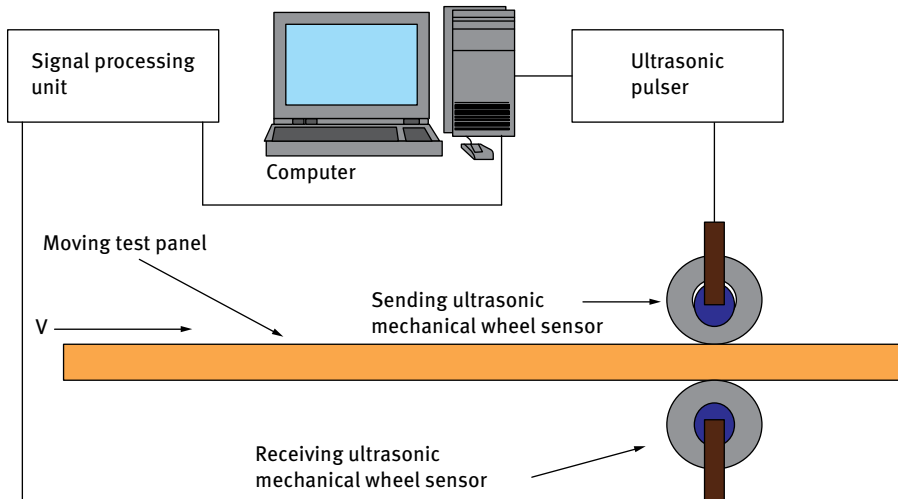
Fig. 4.5: Schematic representation of the commercial contacting wheeled fixture manufactured by Acoustic Emission Technology under contract with Weyerhaeuser.
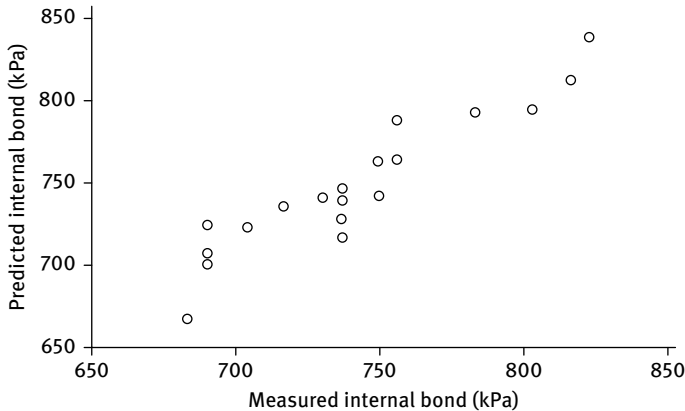
Fig. 4.6: Internal bond predicted from a laboratory acoustic-ultrasonics system vs that measured through testing. The boards were exposed to a wide range of temperature (40–105 °C) to develop an algorithm to compensate for thermal attenuation.

of the wheels on the particleboard. This pressure caused considerable downtime for maintenance. A subsequent patent [12] for air coupling was issued, but this advancement was not commercialized. It would have required a high energy transducer, which was not available at the time.

4.4 Future research directions

4.4.1 Press control

No research has been reported following that conducted on using RMS to determine the critical point of bonding in the press. Only one short trial was conducted by Weyerhaeuser in a production particleboard plant to demonstrate the prototype system on a commercial press. Since many composite panel plants use IB as the key variable for board strength, more research is needed to obtain greater sensitivity of the AU output during pressing. For example, a number of mills operate with an IB target of 350 kPa. In referring to Fig. 4.4, that IB value occurs on a very steep part of the curve. Conversely, the minimum value of RMS occurs closer to 500 kPa. Obviously, if the press control system is to work effectively, the change in the AU parameter must be more sensitive to bond development.

The variation of IB values between OSB mills in the US has been reported to vary from about 250 to 450 kPa [13]. Within the US, there is no standard for minimum IB, and there are no means of relating IB to engineering properties of OSB. In Canada, where most OSB for the US market is produced, the standard is 350 kPa. However, US

mills do use IB as a measure of quality assurance in production. It is a particularly useful measure when changes are made in wood raw material, resin, or additives.

In Fig. 4.4, RMS changes are shown to be sensitive to changes of pressure on the mat. The first portion to the maximum value is essentially the increase of pressure on the mat during press closure. At the peak, the mat has reached the controlled thickness (either by stops or transducers), at which point the pressure decreases as relaxation occurs in the mat. This decrease in pressure is nearly linear until curing begins in the mat, which is indicated by the decrease of the RMS slope.

– *AU parameter analysis.* The change in IB with time (about 250–300 s) at the most critical point is about 10 kPa/s (Fig. 4.4). In this same range of time, the change of RMS is only about 10 % (0.030–0.033). If the minimum value of RMS were used to determine press opening, then the resultant IB value would be more than 50 % greater than the nominal value of 350 kPa. Unfortunately, no studies have been reported on the use of any other AU parameter to track resin curing. Ideally, this would have greater sensitivity approaching the minimum of the RMS curve.

– *Opening monitoring.* Press operators are generally aware of which press opening is the slowest in curing and therefore can manually control press opening. However, changes in the heating of platens are often affected by the removal of condensate, which can change at any opening. With the use of an IB on-line gauge, the lowest IB opening can be identified, and if possible, corrected. However, if the lowest opening cannot be corrected, the press monitor can be attached to that opening to control the opening at an appropriate IB value. This type of monitoring would be very helpful with changes in batches or types of resins and/or during startups. Reliance solely on the on-line IB monitor means that it requires several press loads before IB values can be obtained.

– *Variable analysis.* Changes in raw material, especially resin, can cause substantial changes in IB values. The resin blending process is subject to gradual and abrupt changes in a production setting. In such changes, the press monitor can be used to identify upstream resin blending problems for correction, but also can compensate by modifying the press opening time. Another variable that also is subject to similar changes is moisture content of the furnish. Neither of these two variables have been studied to understand their relative contribution to changes in curing.

4.4.2 On-line air coupling

4.4.2.1 Air-coupled transducers
Ultrasonic inspection techniques have been extended in recent years to noncontact air-coupled ultrasonic generation and detection. This is particularly important for quality assessment of wood and wood products because these products do not lend themselves to immersion inspection techniques, and the use of a liquid couplant would contaminate them.

Most air-coupled ultrasonic methods use conventional piezoelectric elements with carefully impedance matching or capacitance transducers. A large acoustic impedance mismatch exists between the piezoelectric element and surrounding air when PZT-based air-coupled sensors are used. The acoustic impedance in typical PZT ($\approx 30 \times 10^6$ kg/m^2 s) is several orders of magnitude greater than that of air (400 kg/m^2 s). Furthermore, the attenuation of sound traveling through air increases rapidly for frequencies above ≈ 1 MHz. To overcome this mismatching difficulty, several solutions have been tried. Kelly et al. [14] used multilayered silicon rubbers as a half-wavelength matching layer on a piezoelectric transducer. Kraub et al. [15] used a SiO$_2$-aerogel as an impedance matching layer. Reily and Hayward [16] have improved the impedance matching by using piezocomposite active elements of different piezoceramic fractions, shapes, and distributions. Typically, these solutions work for narrow bandwidths and require much tuning effort.

Capacitive transducers have received increased interest because of their higher sensitivity and wide bandwidth, and their applications range from material inspection and materials characterization [17] to ultrasonic imaging [18]. Capacitive ultrasonic transducers consist of a thin polymer membrane (metalized) and a conducting backplate. Because of the very small mechanical impedance of the thin membrane, the capacitance transducer has a much smaller impedance mismatch between the membrane and air, which makes it ideal for coupling into air. The surface of the backplate is patterned into a series of holes by roughening and/or micromachining [13]. The metalized polymer membrane is then placed on the patterned backplate to both the sending and the receiving transducer. Applying a transient voltage between the backplate and the grounded metalized surface of the membrane in the presence of a bias voltage induces vibrations in the membrane, which generates ultrasound in air. Similarly, receiving the vibrating sound signals is achieved using the same transducer as a reciprocal device.

4.4.2.2 Transducer arrangements

A variety of air-coupled arrangements show how they can be used in ultrasonic through-transmission testing, ultrasonic guided-wave testing, and nonlinear noncollinear wave mixing testing. A good review of sensor placement in traditional ultrasonics can be found in [19, 20].

Through-transmission

Fig. 4.7 shows two noncontacting air-coupled sensors in a through-transmission configuration. This system could replace the previously-mentioned ultrasonic rolling sensors. It would have the advantages of the elimination of the mechanics of the rolling contact and the variation that occurs from dry coupling. The major challenge is the need for much greater power of the transmitter.
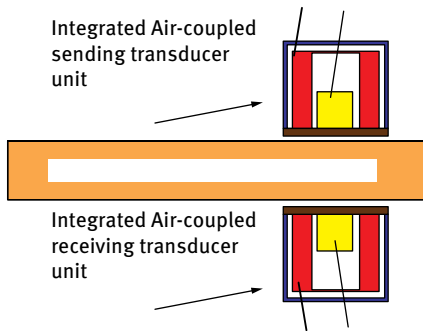
Integrated Air-coupled sending transducer unit

Integrated Air-coupled receiving transducer unit

Fig. 4.7: Conceptual noncontacting air-coupled transducer arrangement for through-transmission.

Guided waves

In an infinite isotropic solid medium only two types of independent wave propagation exist, dilatational and shear waves. Both waves propagate with constant velocities and are nondispersive. When geometry constraints are introduced and the dimensions are close to the acoustic wavelength, the wave becomes dispersive and is called a guided wave. As a result, guided waves exist in plates and plate-like structures such as wood composite panels where the thickness is generally smaller than the acoustic wavelengths. Rose [19] provides an excellent review of both bulk and guided wave propagation including their advantages in materials characterization.

Traditionally, the guided wave approach in plate-like structures assumes that the material properties remain constant through the thickness. For wood composite panels, the material density and moduli vary with depth, and the material may not be isotropic. Elastodynamic wave propagation in graded materials is a rarely treated problem [21–23]. For example, at the boundary of two media, an incident pulse normal to the interface is split into two parts, where the first part continues propagating into the material and the second part is reflected. The amplitude ratio of the reflected and the transmitted parts is governed by the normalized difference in the acoustic impedance of the two media only, provided that the impedance change is a pure step function in space. However, if the acoustic impedance is broadened spatially (i.e. graded), the ratio of the transmitted and reflected parts is frequency dependent. In the case of wood composites, the thickness of the plate-like structure is graded, and because the plate thickness is of the same order of magnitude as the ultrasonic wavelength, the waves are dispersive and guided by the plate geometry. Fig. 4.8 shows the use of four air-coupled ultrasonic sensors in a possible configuration to interrogate wood composite panels. Although the transducers are shown perpendicular to the surface, their optimal performance typically occurs when they are oriented at an angle with respect to the board surface. By proper selection of this angle, different guided wave modes can be generated [19].
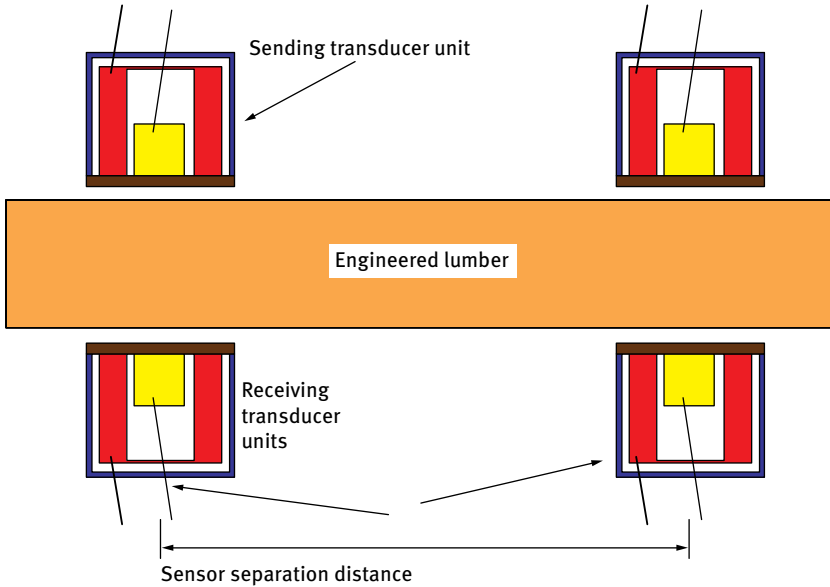
Fig. 4.8: Conceptual guided wave configuration using four sensors.

Noncollinear wave mixing

When two monochromatic waves k_1 and k_2 with frequencies f_1 and f_2, respectively, are propagated in a medium with nonlinear elastic constants, such that they intersect at an angle φ, they can generate a scattered wave k_3, with a sum or difference frequency ($f_3 = f_1 \pm f_2$). The scattered wave propagates in the $k_1 - k_2$ plane and at an angle γ with respect to k_1. This scattered wave arises from the higher-order terms present in the nonlinear acoustic wave equation. The type and polarization of the scattered wave depends on the type and polarization of the two primary waves. Jones and Kobett [24] found that for interaction to be possible, resonance and polarization conditions must be met. Consequently, out of 54 potential interaction cases, there are only nine interaction cases which satisfy both the resonance and polarization conditions, which are case dependent. For example, in the case when two dilatational waves interact to produce a shear wave, the resonance and polarization conditions are met when the following two equations are satisfied:

$$\cos[\varphi] = \left(\frac{c_L}{c_t} \right)^2 \left[1 - \frac{1}{2} \frac{f_1}{f_2} \left(1 - \frac{c_t^2}{c_L^2} \right) \left(\frac{f_2^2}{f_1^2} + 1 \right) \right],$$

$$\tan[\gamma] = \frac{-f_2 \sin[\varphi]}{f_1 - f_2 \cos[\varphi]},$$

where c_L and c_t are the dilatational and shear velocities, respectively. Three parameters, $\frac{f_2}{f_1}$, φ, and γ, are interdependent in the above equations; once one is chosen (e.g. $\frac{f_2}{f_1}$, γ), the other two are fixed (e.g. φ). The frequencies are defined such that $f_2 < f_1$,

and the resultant shear wave, i.e. k_3, has a frequency $f_3 = f_1 - f_2$, and is polarized in the plane parallel to the plane in which the longitudinal waves propagate, i.e. the plane defined by k_1 and k_2. A more detailed discussion of the noncollinear wave-mixing technique can be found in [24–27].

Fig. 4.9 shows the potential use of three sensors (including potential air-coupled sensors) to interrogate the panel using the noncollinear wave mixing approach. In Fig. 4.9, k_1 and k_2 are the primary waves, which can be the longitudinal or the shear waves that result from the refraction of the wave produced by sensors 1 and 2. In this sensor configuration, the plane defined by k_1 and k_2 is perpendicular to the specimen surface, and the resultant wave k_3, travels in the $k_1 - k_2$ plane. Fig. 4.9 (a) represents the case when two refracted dilatation waves of different frequencies f_1 and f_2 intersect, and the k_3 frequency is $f_3 = f_1 - f_2$. Fig. 4.9 (b) represents the case when two refracted shear waves of the same frequencies $f_1 = f_2 = f$ intersect, and the k_3 fre-
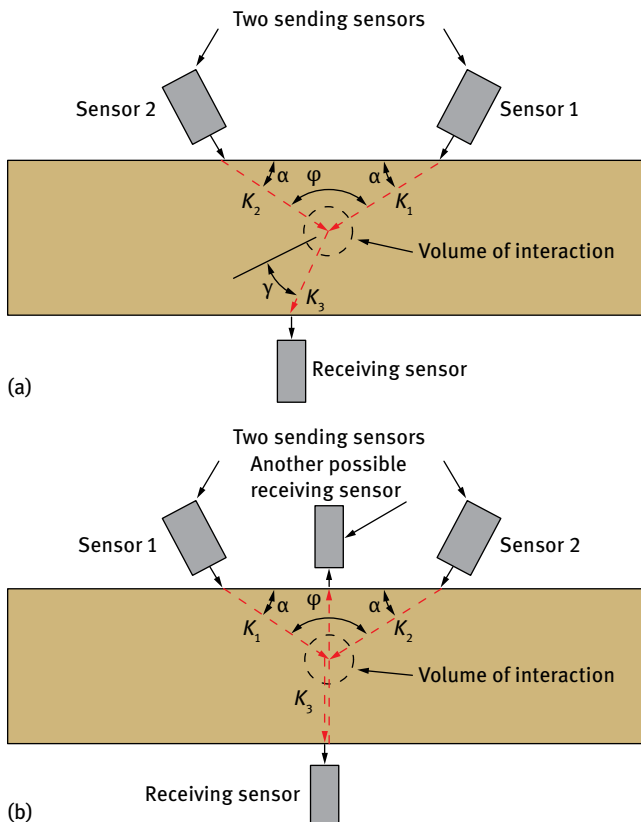
Fig. 4.9: Schematic diagram of possible sensor configuration for noncollinear wave mixing interrogation of material properties of wood panels. The sensors can be either air-coupled or dilatational sensors mounded on variable shear wedges.

quency is $f_3 = f_1 + f_2$. Also, because of symmetry for this sensor arrangement, angle γ of the resultant nonlinear wave is such that k_3 is perpendicular to the surface of board and because of the panel geometry, k_3 can be detected on either side with an acoustic sensor. The use of sensor configurations illustrated in Fig. 4.9 (b) is discussed in detail by Croxford et al. [28]. Another possibility to interrogate the panel is to use critically refracted longitudinal waves (i.e. subsurface longitudinal waves), where k_1 and k_2 travel parallel to the specimen surface and intercept at angle φ. The use of critically refracted subsurface waves in the wave mixing approach is discussed in detail in [25–27].

4.4.3 Preliminary results from single-sided testing

As a first step toward air-coupling, some testing was done with transducers coupled to the same side on laboratory-prepared OSB boards [29]. Nine groups of 10-mm-thick, nonoriented OSB boards (710×710 mm) were produced with three resin contents (1.5, 2.5, and 3.5 % pMDI) and three densities (580, 620, and 660 kg/m^3). For the ultrasonic test, specimens were cut to 300×300 mm to provide three specimens for each resin content, and within each of these groups, three densities. Two dilatational transducers were mounted on one surface of the board with 110 mm spacing (center to center). Three ultrasonic parameters were measured: phase velocity, frequency spectrum ratio, and power spectral density ratio. A square wave pulse with a center frequency of 100 kHz was generated and amplified by a function generator and gated amplifier, and sent to the transmitter. The received signal was passed through a bandpass second order Butterworth filter (2–500 kHz), amplified, and each signal was averaged 50 times to minimize noise. Ten independent measurements were taken for each panel at different locations to obtain average values. The frequency spectrum ratio was determined by

$$\frac{\text{Area}_{\text{low frequency}}}{\text{Area}_{\text{high frequency}}} = \frac{\int_{f_1}^{f_2} X(f)\,\mathrm{d}f}{\int_{f_3}^{f_4} X(f)\,\mathrm{d}f},$$

where $X(f)$ is the signal in the frequency domain as a function of the frequency f, and $f_1 < f_2 \leq f_3 < f_4$. The area under these two peaks can be found using the trapezoidal rule.

This result is shown in Fig. 4.10. Groups 1, 2, and 3 were 1.5, 2.5, and 3.5 % resin content, respectively. The second number within a group relates to density, where 1, 2, and 3 are 620, 580, and 660 kg/m^3, respectively. Because resin content is associated with board strength, this relationship shows promise for interrogating the surface and/or core of boards for mechanical properties.
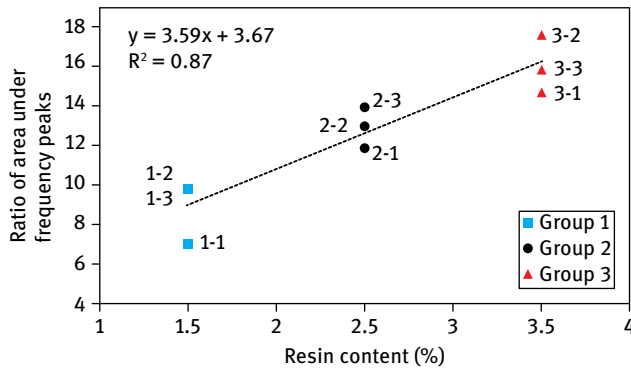
Fig. 4.10: Single-sided ultrasonic parameter vs resin content for laboratory-made oriented strandboards.

4.5 Conclusions

The first two conclusions are related to the current and patented systems for assessing IB in the press and after pressing. The last two conclusions are related to enhancements that could be made to improve the devices.

1. The use of RMS output with a press monitor provides adequate sensitivity to the formation of bonding in the press. However, its sensitivity is not adequate for detection of lower, but acceptable values of IB.
2. The on-line IB gauge has excellent sensitivity to within- and between-board IB even with boards that are not cooled. However, the direct contact with the board greatly reduces its long-term performance. In addition, other board properties are not obtainable.
3. Improvements in a press monitor may be achievable by the use of other AU parameters to provide earlier values of the bonding formation. In addition, the use of air coupling could improve the ease of moving the transducers to monitor other press openings.
4. The on-line IB gauge could be substantially improved through the use of non-contacting transducers. Additionally, it may be possible to obtain other board properties (shear, modulus of elasticity, modulus of rupture) through the use of multiple transducers and/or single-sided interrogation.

References

[1] Chen S, Du C, Wellwood R. Effect of panel density on major properties of oriented strandboard. Wood Fiber Sci. 2010; 42(2): 177–184.
[2] Chen L, Beall FC. Monitoring bond strength development in particleboard during pressing using acousto-ultrasonics. Wood Fiber Sci. 2000; 32(4): 466–477.

[3]   Vary A. The Acousto-Ultrasonic Approach. In: Duke JC Jr, editor. Acousto-Ultrasonics: Theory and Applications. New York: Plenum Press; 1988. pp. 1–21.

[4]   Vary A, Bowles KJ. An ultrasonic-acoustic technique for non-destructive evaluation of fiber composite quality. Polymer Engineering and Science. 1979; 19(5): 373–376.

[5]   Duke JC Jr, editor. Acousto-Ultrasonics–Theory and Application. New York: Plenum Press; 1989.

[6]   Beall FC. Acousto-ultrasonic monitoring of glueline curing. Wood Fiber Sci. 1987; 19(2): 204–214.

[7]   Beall FC, Chen L. Monitoring of resin curing in a laboratory press using acousto-ultrasonics. In: Pellerin RF, McDonald KA, editors. Proceedings, Eleventh Symposium on Nondestructive Testing of Wood. Madison, WI: Forest Products Society; 1999. pp. 9–18.

[8]   Beall FC, Chen L. Ultrasonic monitoring of resin curing in a press for the production of particle board and similar materials. Patent No. 6,029,520; Feb 29, 2000.

[9]   Beall FC. Monitoring of in-situ curing of various wood-bonding adhesives using acousto-ultrasonic transmission. Int J Adhesion and Adhesives. 1989; 9(1): 21–25.

[10] Shearer DM, Beetham RC, Beall FC. Bond strength measurement of composite panel products, Patent No. 4,750,368; 1988.

[11] Green AT. Quantification of particle board on the mill line. In: Reis H, editor. Proceedings, Nondestructive Testing and Evaluation for Manufacturing and Construction. Urbana, IL: Hemisphere Publishing Corporation; 1989: 149–161.

[12] Shearer DM, Beetham RC, Beall FC. Bond strength measurement of composite panel products. Patent No. 4,856,334; 1989.

[13] Wong KA, Panda S, Ladabaum I. Curved micromachined ultrasonic transducers. In: Proceedings, IEEE Ultrasonic Symposium; 2003. pp. 572–576.

[14] Kelly SPG, Hayward G, Gomes TE. An air-coupled ultrasonic matching layer employing half-wavelength cavity resonance. In: Proceedings, IEEE Ultrasonic Symposium; 2001. pp. 965–967.

[15] Kraub O, Gerlach R, Fricke J. Experimental and theoretical investigations of SiO_2-aerogel matched piezo-transducers. Ultrasonics. 1994; 32(3): 217–222.

[16] Reily D, Hayward G. Through air transmission for ultrasonic nondestructive testing. In: Proceedings IEEE Symposium; 1991. pp. 763–766.

[17] Carr H, Wykes C. The performance of capacitive transducers. Ultrasonics. 1993; 31: 13–20.

[18] Gan TH, Hutchins DA, Billson DR, Schindel DW. High resolution air coupled ultrasonic imaging of thin materials. In: Proceedings IEEE Ultrasonics Symposium; 2000. pp. 897–900.

[19] Rose JL. Ultrasonic Waves in Solid Media. Cambridge: Cambridge University Press; 1999.

[20] Bray DE, Stanley RK. Nondestructive Evaluation, revised Edition. Boca Raton: CRC Press, Inc.; 1997.

[21] Chiu T-C, Endogen F. One-dimensional wave propagation in a functionally graded elastic medium. J Sound and Vibration. 1999; 222(3): 453–487.

[22] Vollmann J, Profunser DM, Bryner J, Dual J. Elastodynamic wave propagation in graded materials: simulations, experiments, phenomena, and applications. Ultrasonics. 2006; 44: e1215–e1221.

[23] Aebi LK, Loeffel J, Bryner J, Vollmann J, Dual J. Frequency selective wave propagation in graded materials. IEEE Ultrasonics Symposium; 2007. pp. 1625–1628.

[24] Jones GL, Kobett DR. Interaction of elastic waves in an isotropic solid. J Acoust Soc Am. 1963; 35(1): 5–10.

[25] McGovern ME, Buttlar WG, Reis H. Characterization of oxidative aging in asphalt concrete using a non-collinear ultrasonic wave mixing approach. Insight, Non-Destructive Testing and Condition Monitoring. 2014; 56(7): 367–374.

[26] McGovern ME, Buttlar WG, Reis H. Estimation of oxidative aging in asphalt concrete. Insight, Non-Destructive Testing and Condition Monitoring. 2015; 57(1): 25–34.

[27] McGovern ME, Reis H. Damage characterization in dimension limestone claddings using non-collinear ultrasonic wave mixing. J Optical Engineering. Special issue: Structural Health Monitoring, Guided Waves and Nonlinear Acoustic Techniques. 2015; 55(1): 011012-1/011012-12.
[28] Croxford AJ, Wilcox PD, Drinkwater BW, Nagy PB. The use of non-collinear mixing for nonlinear ultrasonic detection of plasticity and fatigue. J Acoust Soc Am. 2009; 126(5): EL117–EL122.
[29] McGovern ME. Private communication; 2015.

Further reading

Aebi L, Loeffel K, Bryner J, Vollmann J, Dual J. Frequency selective wave propagation in graded materials. In: Ultrasonics Symposium. IEEE; 2007. pp. 1625–1628.
Beall FC. Nondestructive evaluation of adhesion using acousto-ultrasonics. In: Proceedings on Wood Adhesives; 1990. Madison, WI: Forest Products Society; 1991. pp. 97–102.
Beall FC. Wood: Acoustic emission and acousto-ultrasonic characteristics. In: Cahn RW, Lifshin E, editors. Concise Encyclopedia of Materials Characteristics. New York: Pergammon Press; 1993. pp. 551–554.
Beall FC. Overview of acousto-ultrasonics applied to wood and wood-based materials. In: Vary A, editor. Proceedings, Second International Conference on Acousto-Ultrasonics. Atlanta: The American Society for Nondestructive Testing, Inc.; 1993. pp. 153–161.
Biernacki JM, Beall FC. Development of an acousto-ultrasonic scanning system for nondestructive evaluation of wood and wood laminates. Wood and Fiber Sci. 1993; 25(3): 289–297.
Castillo M, Acevedo P, Moreno E. KLM model for lossy piezoelectric transducers. Ultrasonics. 2003; 41(8): 671–679.
Chiu T-C, Endogen F. One-dimensional wave propagation in a functionally graded elastic Medium. J Sound and Vibration. 1999; 222(3): 453–487.
Holland SD, Chimenti DE. Air-coupled acoustic imaging with zero-group-velocity lamb waves. Appl Phys Lett. 2003; 83: 2704.
Holland SD, Telles SV, Chimenti DE. Air-coupled, focused ultrasonic dispersion spectrum reconstruction in plates. J Acoustical Soc Am. 2004; 115: 2886.
Lawry TJ, Roa-Prada KRS, Ashdown JD, Saulnier GJ, Scarton HA, Pinezich JD. Electrical optimization of power delivery through thick steel barriers using piezoelectric transducers. Energy Harvesting and Storage: Materials, Devices, and Applications. Proc SPIE 7683; 2010. 768314. DOI: 10.1117/12.852563.
Lockwood GR, Foster FS. Modeling and optimization of high-frequency ultrasound transducers. IEEE Trans. Ultrason Ferroelect Freq Contr. 1994; 41(2): 225–230.
Reis H, McFarland DM. On the acousto-ultrasonic characterization of wood fiber hardboard. J Acoustic Emission. 1986; 5(2): 67–70.
Svilainis L, Dumbrava, V, Motiejunas G. Optimization of the ultrasonic excitation stage. In: IEEE 30th International Conference on Information Technology Interfaces; Dubrovnik; 2008. pp. 791–796.
Teles SV. Ultrasonic guided waves in composite plates [thesis]. [Ames, IA]: Iowa State University; 2004.
Vollmann J, Profunser DM, Bryner J, Dual J. Elastodynamic wave propagation in graded materials: simulations, experiments, phenomena, and applications. Ultrasonics. 2006; 44: e1215–e1221.
Wu L, Chen Y. PSPICE approach for designing the ultrasonic transducer for medical diagnostic applications. Sensors Actuators A Phys. 1999; 75(2): 186–198.

Xiaozhou Song, Yafang Lei, and Zhangjing Chen

5 Reconstituted composite from crop stalks

Abstract: Crop stalks are a renewable resource. The effective utilization of crop stalks has drawn increased attention worldwide. There is a growing need to effectively use crop stalks [1]. In order to produce high strength and environmental safe reconstituted composites from crop stalks, this chapter discusses the composite manufacturing from cotton stalks, soybean stalks, capsicum pepper stalks, tobacco stalks, and corn stalks.

The raw material characteristics, the manufacturing process, forming mechanisms, and some other variables affect properties of composites and its bonding mechanism [2]. First, the characteristics of five common crop stalks were analyzed using optical microscopy, fiber isolation, and analysis of chemical components. The processing technologies of reconstituted composites are discussed. By means of Fourier transform infrared spectroscopy (FTIR) and scanning electron microscope (SEM), mechanisms of adhesive bonding were analyzed.

5.1 Introduction

Using wheat and rice straw to manufacture the boards can be traced back to the early 20th century [3]. In 1905, the straw and adhesive mixing panels were already manufactured in Germany [4]. In 1930, Swedish scientists invented wheat (rice) straw wallboard [5]. Scientists in Britain in the 1940s patented manufacturing paper panels made of grass straw. The technology has been therefore transferred to more than two dozen countries around the world.

In 1968, straw particleboards were developed [6]. The technical challenge is how to maintain high bond strength and less swelling shrinkage. In the 1980s, in the United States and Canada experimental investigation on producing composites using wheat straw, rice straw, and rice husk began [7]. European companies specialized in wood-based panel equipment have invested in the technology and equipment of straw system panels [8].

Early in the 1960s, the cotton stalk was used to manufacture the composites [9]. Its fiber morphology and structure and other aspects of performance are very similar to the hardwood [10, 11]. In theory, cotton stalk can be used to make panels the same way as hardwood.

Straw plants are mostly an annual herb. It is harvested within a season [12]. The manufacturers may have difficulties in collecting and storing the straw material. It is very different from lumber and usually requires large storage space. Straw raw material is light and has an unusually high initial moisture content (MC). There is the risk of fire and other safety issues involving in the straw storage [13]. Straw contains more

sugar and more easily rots [14]. Thus, the collection, storage and quality assurance of raw material straw are key factors to be considered in the production of straw-based panels.

5.2 Characteristics of crop stalks

Raw material properties largely determine the physical and mechanical properties of the final products. Although the same as a plant fiber, crop stalk fiber is different from wood fibers in its anatomical structure, fiber morphology, and chemical compositions.

5.2.1 Cotton stalk

The cotton plant (*Malvaceae Gossypium*) can reach 2 m in height. The stem diameter of the average cotton plant is 2 cm, and the average density is $0.332 \, g/cm^3$. The cotton stalk consists of 14.52 %, phloem, 81.46 % xylem, and 4.02 % pith components (Fig. 5.1).

The outer part of the cotton stalk consists of the periderm, phloem, and parenchyma. The epidermis is the outermost layer. The periphery of cork cells is parenchyma cells and or irregular shape.

Xylem cells are composed of fiber, vessels, rays, and parenchyma cells. The fiber makes up 62.22 %, vessels 17.18 %, and rays 20 %. The fiber cells are arranged in neat rows, which are larger than in the phloem. There are pits on the fiber cell wall, and they are oval with smaller apertures and less in number. The vessels are scattered among the fiber cells. The pits on the cell wall are spirally arranged in large quantity with oval pits. The radial arrangement of rays is easy to see. Ray cells are arranged in single, double, or triple rows. The fiber morphology of phloem and xylem of cotton stalk is shown in Fig. 5.2. The fiber dimensions of cotton stalk are presented in Tab. 5.1.

Pith is by large thin-walled, loosely arranged cells with the void gaps among the cells. It is polyhedral or oval.

Tab. 5.1: Average fiber dimension of cotton stalks.

	Xylem	Phloem
Fiber length (µm)	1023	1655
Fiber width (µm)	19.75	17.13
Fiber inner diameter (µm)	13.05	8.75
Fiber wall thickness (µm)	3.34	4.32
Aspect ratio length/width ratio	51.85	95.82
Cavity wall than thickness/diameter ratio	0.51	0.99
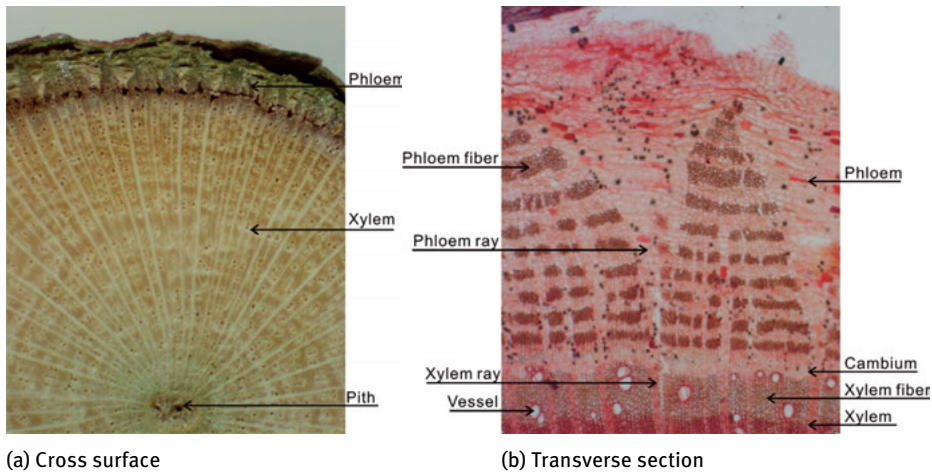
(a) Cross surface

(b) Transverse section
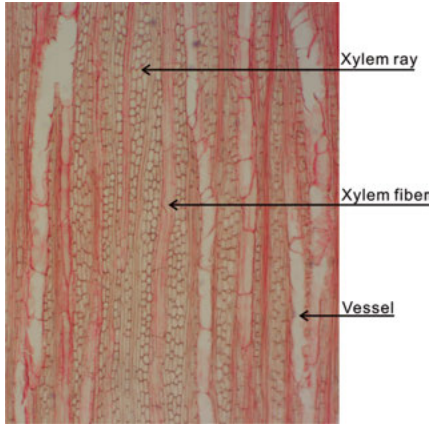
(c) Tangential section

Fig. 5.1: Cross-section photo images of cotton stalk.

In cotton stalks, the cells in the phloem have an average length of up to 1655 μm, average width of 17.13 μm, the average cell wall thickness of 4.32 μm, wall cavity 0.99. The fiber ends acuminate, blunt tip, a smaller cell cavity within the cell by an average of 8.75 μm. The cotton stalk fiber is shorter than cells at the phloem, typically 1023 μm; wood fiber has an average width of 19.75 μm, an average cell wall thickness of 3.34 μm, large cell lumen, the inner diameter of the average cell 13.05 μm, wall cavities the average of 0.51 (Tab. 5.2).

The average length of cotton stalk fibers is greater than that of poplar wood. The cotton stalk fiber has an average thickness 3.83 μm, and an average inner diameter of 10.90 μm. Compared to wood, the cell wall of a cotton stalk is thinner and the cell lumen is larger.

(a) Phloem fiber

(b) Xylem fiber
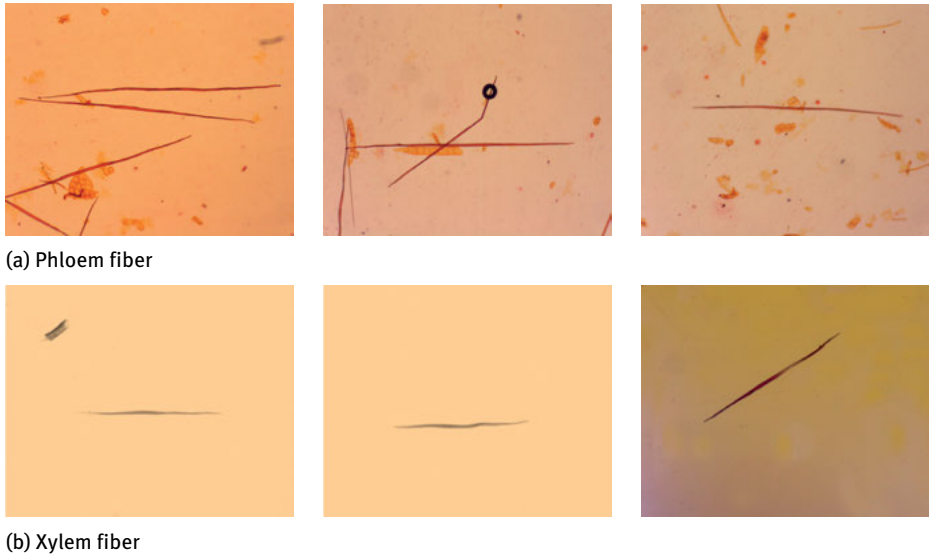
Fig. 5.2: Fiber morphology of phloem and xylem of cotton stalks.

Tab. 5.2: Comparison of average dimension of fiber between cotton stalks and timber.

	Cotton stalk	Poplar	Hardwood	Softwood
Fiber length (µm)	1339	940	1000–2000	3000–5000
Fiber width (µm)	18.44	22.80	10–50	20–50
Fiber inner diameter (µm)	10.90	10.26	—	—
Fiber wall thickness (µm)	3.83	12.20	2.42–5.30	2.20–12.50
Aspect ratio length/width ratio	73.84	41.20	40–100	75–200
Cavity wall thickness/diameter ratio	0.75	0.86	—	—

The chemical composition of raw materials is one of the main characteristics of raw materials. Tab. 5.3 shows the chemical compositions of cotton stalk. Compared with Masson pine and poplar, cotton stalks contain more ash and extractives, but less holocellulose and lignin content. The main component in cotton stalk ash is silica. This ash content can affect the adhesive bonding capability. The extractives are pigment, tannins, resins, etc., which are aqueous materials. These extractives contain a lot of organic substances such that at a certain temperature, moisture conditions are prone to mold and mildew. The pentosane is the main component of hemicellulose and is easily breaks down at high temperatures. The cellulose content is low, which can affect the strength of the product. The lignin is a natural adhesive material and its content will affect the product intact.

Tab. 5.3: Comparison the chemical composition of cotton stalks and wood raw materials (%).

Material	Ash	Extractive			Cellulose	Pentosane	Lignin
		Cold water	Hot water	1 % NaOH			
Cotton stalk	3.09	4.38	7.64	26.85	43.18	19.01	21.05
Mason pine	0.33	2.21	6.77	22.87	51.83	8.54	28.42
Poplar	0.32	1.38	3.46	15.61	43.24	22.61	17.10

5.2.2 Tobacco stalks

Tobacco belongs to Solanaceae genus. It's stem is straight, nearly circular, and hollow. Tobacco stalk stems are about 2 m high with a stem outside diameter of 3 to 5 cm and stalk wall thickness of 0.5–1.5 cm. The density of a tobacco stalk is 0.306 g/cm^3. The microscopic structure of a tobacco stalk cross-section is presented at Fig. 5.3. It mainly consists of the phloem, xylem, and pith.

The tobacco stalk has an epidermis, periderm, and phloem. Epidermal cells are rectangular or square parenchyma cells; pericytes are quite developed and are located in the medial cortex table. The phloem has sieve cells, fiber cells, and axial phloem parenchyma cells. They are irregular, polygonal, with sharp pointed ends. Axial phloem parenchyma cells have an irregular shape. The xylem consists mainly of vessels, fibers, rays, and axial parenchyma cells. The vessels in cross-section are round or oval. Its fibers are arranged radially, polygons in shape and the dimensions are presented in Tab. 5.4. Fine rays are multiple layers of 2–4 cells. The pith is located at the center of tobacco stems and is composed of parenchyma, and has an oval shape.

Epidermis
Phloem
Phloem fiber
Cambium
Vessel
Xylem fiber
Xylem
Xylem ray
Pith
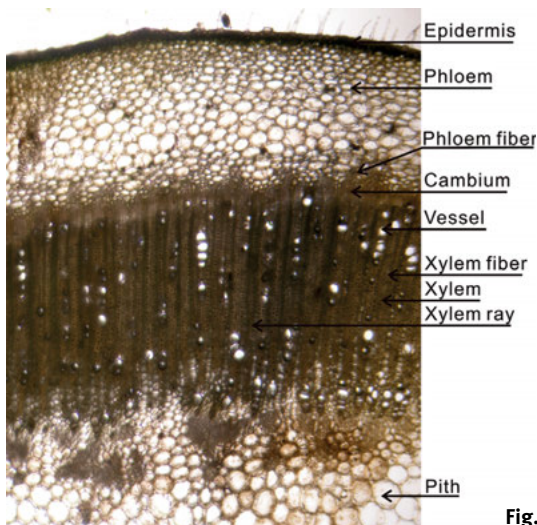
Fig. 5.3: Transverse section of a tobacco stalk.

Tab. 5.4: Fiber dimensions of a tobacco stalk.

	Xylem	Phloem
Fiber length (μm)	1160	5947
Fiber width (μm)	28.93	44.38
Fiber inner diameter (μm)	21.84	24.15
Fiber wall thickness (μm)	3.54	4.14
Aspect ratio length/width ratio	40.20	132.32
Cavity wall thickness/diameter ratio	0.32	0.35

The fiber length of a tobacco stalk is 5947 μm. It has relatively short wood fiber, with an average of 1160 μm. The fibers are flat and wide, with a thin wall. Fibers are softer and flexible and easy to compress (Fig. 5.4). Tobacco stalks and wood have a similar chemical composition, mainly composed of cellulose, hemicellulose and lignin composition, ash, and extractive.

(a) Phloem fiber

(b) Xylem fiber
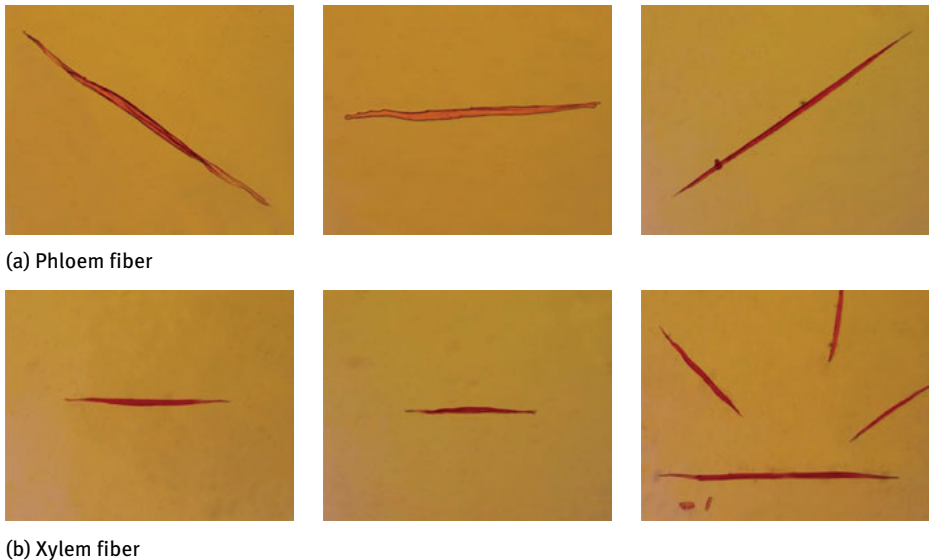
Fig. 5.4: Fiber morphology of the phloem and xylem of tobacco stalks.

5.2.3 Soybean stalks

Soybean (*Glycine max (Linn.) Merr.*) is an annual herb. A soybean stalk is about 40–110 cm high. The mature stalk has a diameter of 0.5–2 cm, and its density is 0.298 g/cm^3. The microscopic structure of a soybean stalk cross-section is presented in Fig. 5.5.
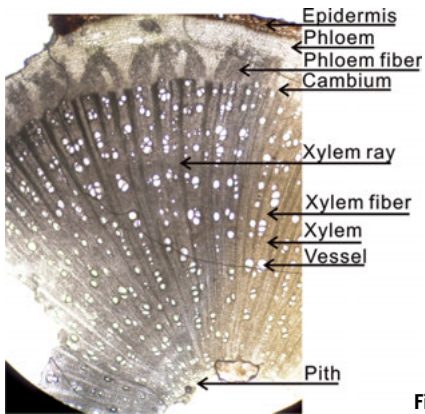
Fig. 5.5: Transverse section of a soybean stalk.

Tab. 5.5: Fiber dimension of soybean stalks.

	Xylem	Phloem
Fiber length (μm)	748	1729
Fiber width (μm)	19.68	20.69
Fiber inner diameter (μm)	12.12	9.94
Fiber wall thickness (μm)	3.78	4.68
Aspect ratio length/width ratio	37.67	83.24
Cavity wall thickness/diameter ratio	0.63	0.98
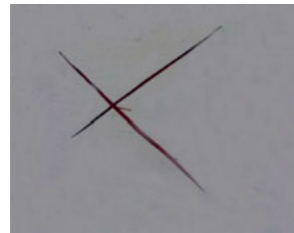
(a) Phloem fiber
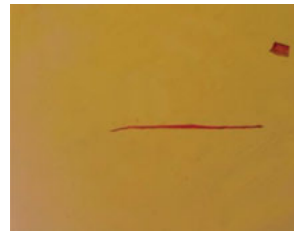
(b) Xylem fiber

Fig. 5.6: Fiber morphology of (a) phloem and (b) xylem of soybean stalks.

The fiber has a length of 1729 μm, with an average fiber thickness of 4.68 μm (Fig. 5.6). The marrow cell wall is thin, of a nearly spherical shape, similar to a sponge. Soybean straw is composed of cellulose, hemicellulose and lignin composition, ash, and extractive.

5.2.4 Corn stalks

Corn stalks (*Zea mays L.*) are about 150 to 300 cm high. The stem diameter of a corn stalk is about 2.0–4.5 cm. The basic density is 0.314 g/cm^3. The microscopic structure of a corn stalk cross-section is presented at Fig. 5.7.
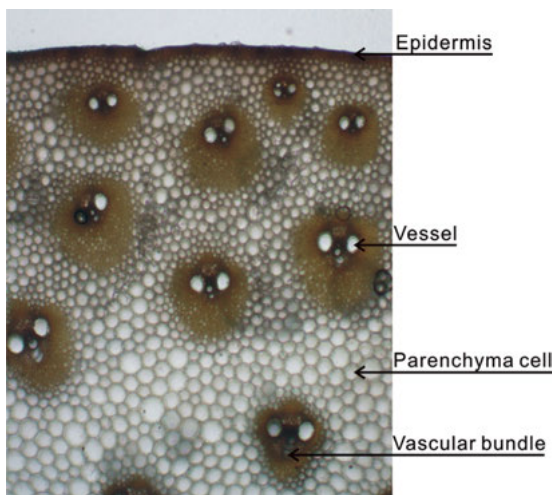
Fig. 5.7: Photo image of the cross-section of a corn stalk.

Corn stalks have an epidermis, parenchyma cells, and microtubule bundles. There are several layers of thick-walled cells tightly packed within the epidermis, which play a protective role for the stem. The stalks contain more silicide and wax, which affects the wetting and bonding of adhesives. The basic organization in the epidermis is parenchyma cells, which function as the storage of nutrients (Fig. 5.8).

The corn stalk has an average fiber length of 1880 μm, an average width of 16.86 μm, an average thickness 4.66 μm, an average fiber inner diameter of 7.55 μm, with a wall cavity ratio of 1.40 (Tab. 5.6).

The main components of corn stalks are cellulose, hemicelluloses, and lignin. Compared with wood, corn stalks have a higher ash, extractive, and pentosan content. Its lignin content is similar to Poplar wood. However, it has a low cellulose content.
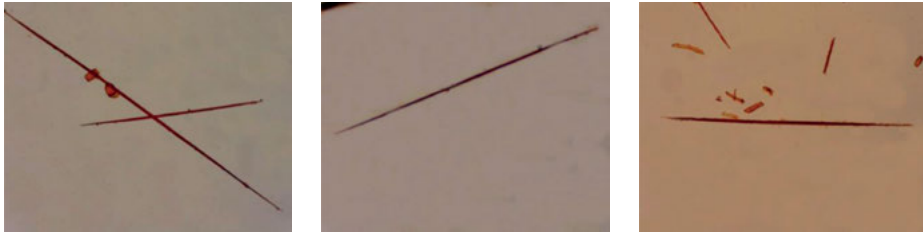
Fig. 5.8: The epidermis fiber morphology of corn stalks.

Tab. 5.6: Fiber dimensions of corn stalks.

	Average
Fiber length (μm)	1880
Fiber width (μm)	16.86
Fiber inner diameter (μm)	7.55
Fiber wall thickness (μm)	4.66
Aspect ratio length/width ratio	111.27
Cavity wall thickness/diameter ratio	1.40

5.2.5 Capsicum pepper stalks

Capsicum peppers (*Capsicum annuum L.*) stalks are relatively small, and are multi-branched. Its leaves are alternate. Pepper straw stems are about 35–60 cm high, with a stem diameter of about 0.5–2.0 cm. Its density is 0.36 g/cm^3. The microscopic structure of a pepper stalk cross-section is presented at Fig. 5.9.
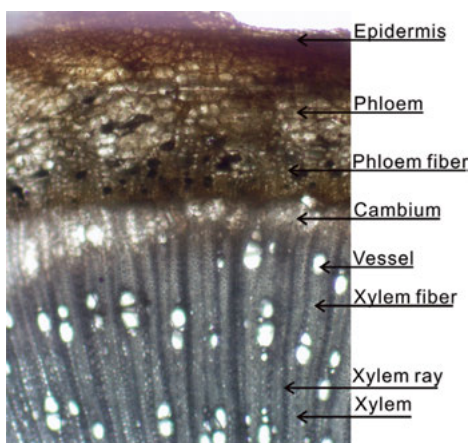
Fig. 5.9: Transverse section of a capsicum stalk.

The stalk has an average fiber wall thickness of 2.96 µm, and an average inner diameter of 15.16 µm; The xylem fiber has an average length of 704 µm and average width of 17.52 µm. The average wall thickness is 2.62 µm (Tab. 5.7).

Tab. 5.7: Fiber dimensions of capsicum stalks.

	Xylem	Phloem
Fiber length (µm)	704	801
Fiber width (µm)	17.52	21.07
Fiber inner diameter (µm)	12.28	15.16
Fiber wall thickness (µm)	2.62	2.96
Aspect ratio length/width ratio	40.19	38.03
Cavity wall thickness/diameter ratio	0.44	0.39

Pepper stalks mainly consist of phloem, xylem, and pith, with a volume ratio or 10.71 %, 81.92 %, and 7.36 %, respectively. The higher lignification pepper stalk has relatively short fibers. Most fibers are irregular, with a spiral form (Fig. 5.10). Pepper stalks have an average length of 801 µm with an average width of 21.07 µm. The chemical composition is listed in Tab. 5.8.

(a) Phloem fiber
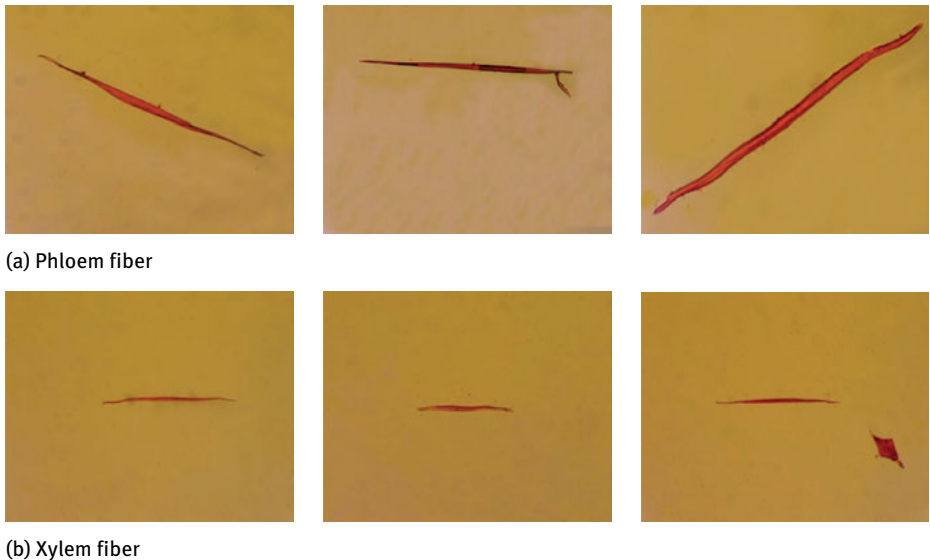
(b) Xylem fiber

Fig. 5.10: Fiber morphology of (a) phloem and (b) xylem of capsicum stalks.

Tab. 5.8: Comparison of the chemical components between several crop stalks and timber (%).

Material	Ash	Extract (hot water)	Cellulose	Pentosane	Lignin
Cotton stalk	3.09	7.64	43.18	19.01	21.05
Tobacco stalk	4.95	14.72	38.96	18.28	19.57
Soybean stalk	2.27	9.43	42.78	23.24	20.06
Corn stalk	4.53	22.15	37.72	24.65	17.47
Capsicum stalk	4.08	8.43	43.21	23.07	19.65
Mason pine	0.33	6.77	51.83	8.54	28.42
Poplar	0.32	3.46	43.24	22.61	17.10

5.3 The manufacturing process

Scrimberring the stalk into composites is a complex physical and chemical process. The properties of raw materials, the combing process, the pressing process, and the adhesive will affect the physical and mechanical properties of the final composites. The compression is an important step in reorganizing stalk materials into the board. The stalk bundles after adhesive spreading is compressed within a certain time into a designed density and thickness of the composites under the temperature and pressure. This process involves a series of complicated physical and chemical changes, such as raw tissue compression, heat and mass transfer, adhesive curing, and water repellent redistribution. The process of manufacturing reconstituted composite from crop stalk can be divided into seven major steps (Fig. 5.11).

Pre-processing of corp stalk
→ Stalk softening and combing
→ Corp stalk drying
→ Sizing corp stalk bundles
→ Paving crop stalk scrimber
→ Hot press
→ Completion
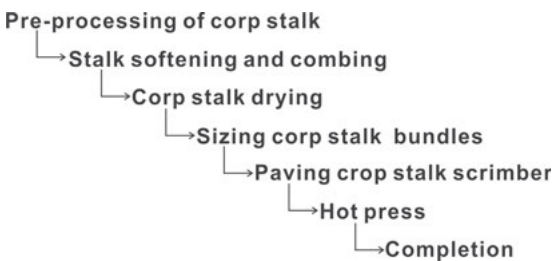
Fig. 5.11: Process of manufacturing reconstituted composite from crop stalks.

The straw scrimber processing floorplan is shown in Fig. 5.12.
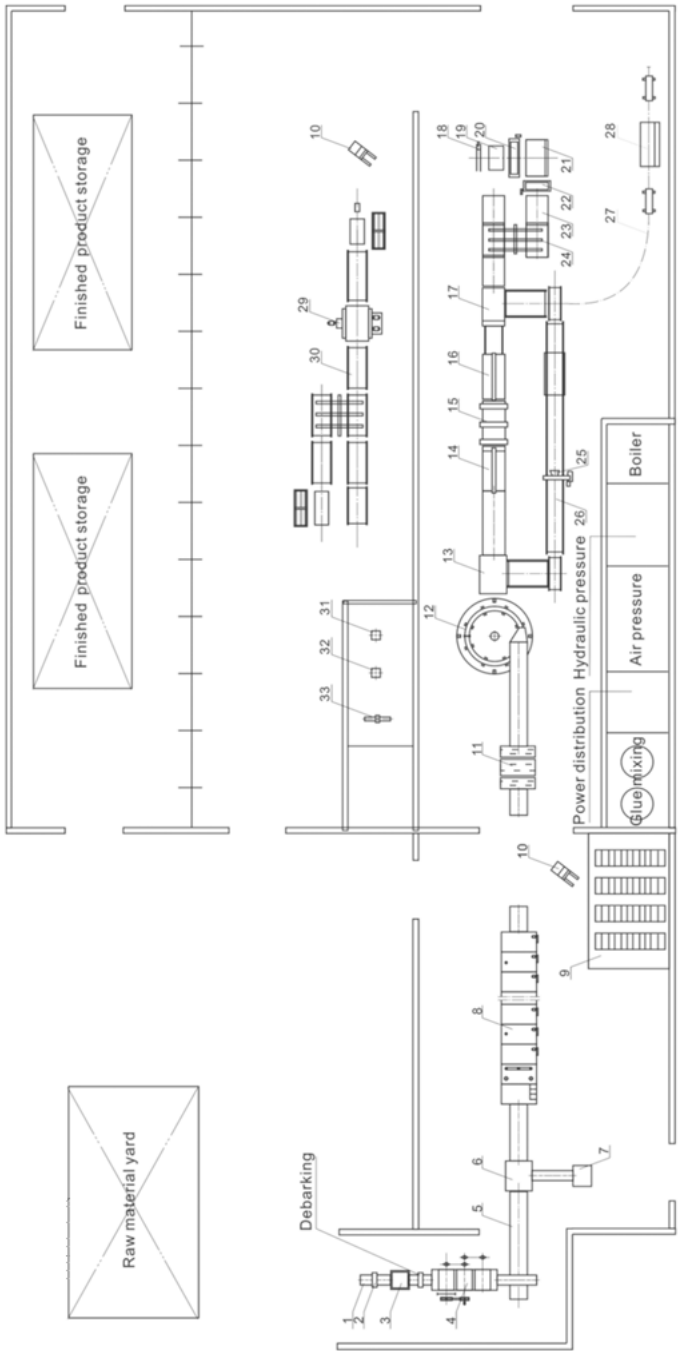
Fig. 5.12: Technological plane layout chart of reconsolidated crop stalks.

5.3.1 Raw material preparation

This step is to remove leaves and impurities from the stalk. The stalks will be softened to reduce the hardness of straw and increase their plasticity. The bark is difficult to form into a good stalk bundle, but also affects the performance of the composites. Therefore, the bark needs to be removed in this step. In addition, during the preparation of straw material storage, it is necessary to prevent the occurrence of rot, mildew, and other deteriorations.

5.3.2 Stalk softening and combing

Stalks are usually cut into 350 mm lengths. Low moisture stalks are hard and brittle and are prone to break. Prior to combing, they are soaked to be softened using cold water (at atmospheric pressure $23 \pm 2\,°C$), hot water cooking ($90 \pm 2\,°C$), or alkali cooking ($90 \pm 2\,°C$). The stalk MC will increase during cooking (Tab. 5.9). After 8 h of cooking, the soybean stalk MC can increase 45 %. As a hollow stalk, it is not recommended to cook tobacco or corn stalk in hot water. They can be soaked in cold water at room temperature 1.2 h prior to combing. After being cooked for 3 h with hot water, the soybean and pepper stalk needs to be cooled to achieve a good combing effect (Fig. 5.13). It is not recommended to cook tobacco and corn stalks longer than 3 h.

Stalk combing is done primarily by rolling on a combing machine. The stalks, softened through the rolling device, are flattened, cracked, and spread out laterally on a sheet.

Tab. 5.9: Relationship between cooking time and MC of the crop stalks with an initial MC of 12.4 %.

Softening time (h)	1	2	3	4	6	8
Soybean stalk MC (%)	103.53	124.42	135.63	138.96	145.94	150.67
Pepper stalk MC (%)	89.43	106.58	116.00	122.99	133.04	137.58
Tobacco stalk MC, solid part (%)	102.64	126.79	137.16	156.04	166.23	171.52
Tobacco stalk MC, hollow part (%)	244.50	304.09	312.25	—	—	—
Corn stalk MC (%)	314.36	346.94	392.61	—	—	—

5.3.3 Crop stalk drying

Crop stalks with high MC need to be dried prior to adhesive spreading. A large amount of energy is needed to evaporate the moisture. At high temperature and pressure, the mat with high moisture is prone to blistering and delamination defects, which directly affects the product quality and performance. The high MC of stalk bundles often causes uneven temperature distribution, which generates internal stress. The final

(a) Tobacco stalk bunch

(b) Soybean stalk bunch

(c) Pepper capsicum stalk bunch

(d) Corn stalk bunch

Fig. 5.13: The combing effect of crop stalks.

products will develop warping and distortion. Therefore, in order to improve product quality, before adhesive spreading, stalks must be dried to s certain MC.

The final MC of the straw bundles needs to be controlled at 6 %. Drying crop stalk is different from drying wood. Crop stalk drying will not develop deformation and checking during drying. Therefore, straw bundles can be dried at high temperature. However, during the drying, it is essential to achieve uniform MC in the stalks.

5.3.4 Crop stalk sizing

The resin is sprayed through the nozzle toward the stalk bundle. The pair of rollers can then squeeze glue evenly in the straw plies. The amount of adhesive is controlled to 6–12 %.

The pressure of the air compressor spray is 0.4–0.6 MPa and the aqueous ammonium chloride solution spray at 0.1–0.2 MPa.

5.3.5 Crop stalk forming

Forming can be done with single-layer structure equipment. Because of the structure of the stalks, forming can be done in a single direction in order to avoid the void space in the mat if using criss-cross forming. If voids exist, even if pressed to the desired thickness, the composite will have space due to the overlap of the stalks. These voids can reduce the interlayer contact area. Thus, reduction in the bond strength between the cotton stalks bundles is expected. It is recommended that the cotton stalk scrimber adapt the single directional pavement structure.

5.3.6 Hot pressing

Hot pressing is to eliminate or reduce the gaps between the stalks, so that stalk bundles can be in close contact with each other to increase adhesive curing, and to achieve a certain density and thickness of final composites. During hot pressing, the moisture in the board, adhesives, and stalk will mingle together, and a series of physical or chemical changes take place. The original loose boards eventually become a solid composite. It has a certain surface quality, and certain physical and mechanical properties. Hot pressing involves several steps with various pressures and temperatures, depending on the raw materials and final products (Fig. 5.14).

Multilayer hot pressing can press the panel in each layer simultaneously with hydraulic systems.
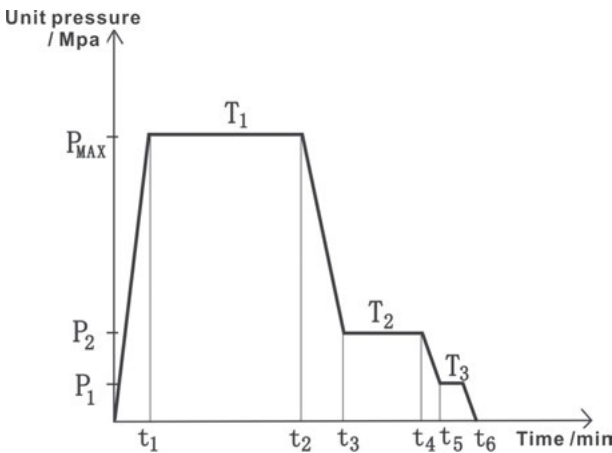
Fig. 5.14: Hot pressing curve of reconsolidated crop stalks. P_{MAX}: maximum pressure, generally 4 MPa about; P_2: equilibrium pressure of 1.0 MPa; P_1: equilibrium pressure of 0.5 MPa; T_1: maximum pressure holding time is determined by the experimental design; T_2: to maintain the equilibrium pressure of time 2 min; T_3: balance pressure holding time of 30 s.

5.3.7 End products

After pressing, the panels were cooled down on a forced-air cooling conveyor. Then, panels are cut using vertical and horizontal trimming saws according to the requirements of the width and length specifications. The panels are stacked up with the stacker, then piled and transported to intermediate storage.

5.3.8 Properties of the composite

The major properties of crop stalk composites are MOR, MOE, internal bond strength (IB), and 2 h thickness swelling (2hTS). The properties of crop stalk composites with a density of $0.7 \, g/cm^3$ are listed in Tab. 5.10 at the technical variables of resin amount of 12 %, pressing temperature of 150 °C, pressing time of 14 min.

Tab. 5.10: Performance of UF and PF stalk composites.

	MOR (MPa)	MOE (MPa)	IB (MPa)	2hTS (%)
UF cotton stalks	57.36	7536.14	0.58	13.52
UF tobacco stalks	30.48	5817.08	0.21	17.06
UF soybean stalks	44.87	6349.03	0.52	13.59
UF capsicum stalks	27.66	6031.92	0.50	8.58
PF cotton stalks	66.93	8192.86	0.81	1.89
PF tobacco stalks	46.05	6126.78	0.42	2.88
PF soybean stalks	53.39	6810.38	0.65	4.91
PF capsicum stalks	35.71	6778.63	0.72	2.74
PF corn stalks	19.67	6216.35	0.13	7.46

Factors affecting MOR of cotton stalk composites
MOR increases with the density of the panel. With the density changed from $0.6 \, g/cm^3$ to $0.8 \, g/cm^3$, MOR increased by 23.15 %. The higher density means more cotton stalk bundles and adhesives.

When the resin amount increases from 9 % to 15 %, MOR increases by 10.54 % (Fig. 5.15). The increase in the amount of glue can increase the contact areas between adhesives and materials. The more glue penetrates deeper, the more the MOR of panels increases. However, the effect of the temperature and pressing duration on the MOE is not significant.
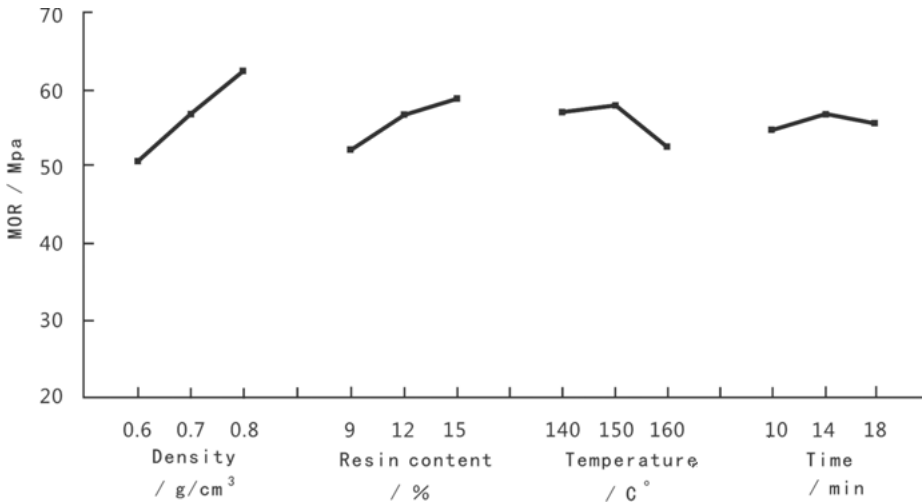
Fig. 5.15: Visual diagram on the influence of technical factors on MOR.

Factors affecting MOE of cotton stalk composites

With the increase of mat density, MOE of cotton stalk composites also increases. When the density increases from 0.6 g/cm^3 to 0.8 g/cm^3, MOE increases 37.97 %. This is because as the density increases, more material is contained per unit volume. The adhesive content increases enhance the strong bond between the cotton stalk bundles. It results in the increase of the rigidity of the panel.
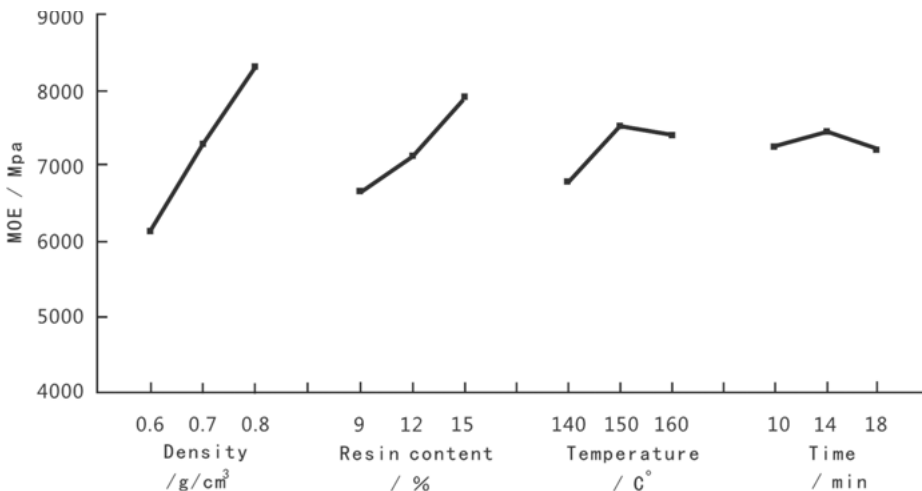
Fig. 5.16: Visual diagram on the influence of technical factors on MOE.

When the adhesive spreading increased from 9 % to 15 %, MOE increased by 17.65 % (Fig. 5.16). Increasing the amount of adhesive makes water content increase accordingly in the mat, and this accelerates the speed of heat transfer to the core. The rigidity and MOE also increase. The effect of temperature and pressing duration on the MOE is not significant.

Factors affecting the bonding strength

When the adhesive spreading increases from 9 % to 12 %, IB increases by 40 % (Fig. 5.17). However, when the resin content increases from 12 % to 15 %, IB declines 9 %.

When the density increases from $0.6 \, g/cm^3$ to $0.8 \, g/cm^3$, IB decreases 18.03 %. The greater density requires more calories to heat the mat. The higher the density, the lower is permeability of the mat, and this causes the lower core temperature and affect adhesives curing. IB will be reduced.

When the pressing time increases from 10 min to 14 min, IB increases by 11.54 %. This is because with the increase of pressing time, the core temperature will increase. This will facilitate the core stalk bundle to reach glass transition point. The adhesive can be fully cured so that the core layer can obtain a decent bonding. But as time continues to extend, IB declined. Because with an increase in the time, the high core temperature will cause stalk fiber through partial gasification, pyrolysis. The fibers are likely to form a brittle layer. The temperature have little effect on IB.
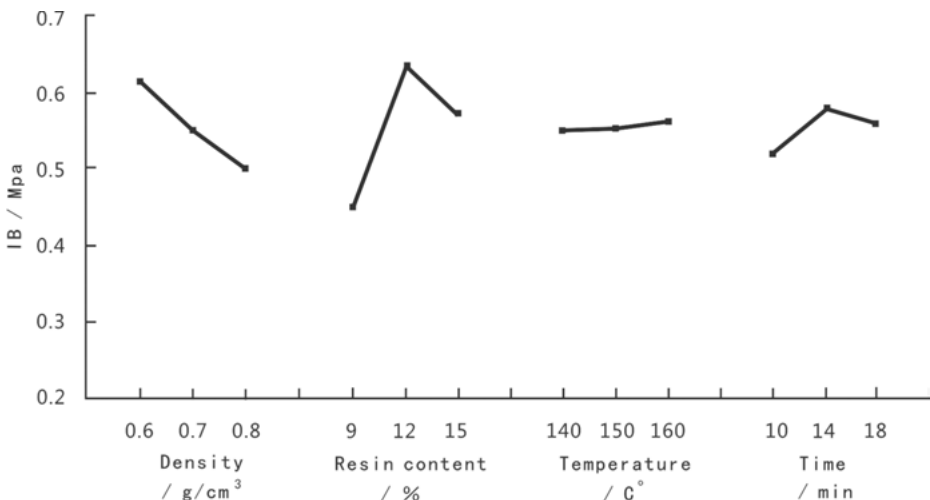
Fig. 5.17: Visual diagram on the influence of technical factors on IB.

Factors affecting thickness swelling of 2 h

When adhesive increased from 9 % to 15 %, 2hTS cotton stalk scrimber reduced by 31.92 % (Fig. 5.18). Due to the increased amount of resin, the stalk bundles have more surface areas covered by the adhesive and prevent the stalk fiber from contact with water molecules, which causes 2hTS to decline.

When the temperature rises from 140 °C to 160 °C, 2hTS falls by 20.50 %. This is because when hot glue inside the slab liquidity strengthened in part adhesives penetrate into the cell lumen cotton stalk fiber within the blocked part of the absorbent cotton stalk fiber channel itself; at the same time, with the hot temperature. The effect of pressing time on 2hTS is not significant.
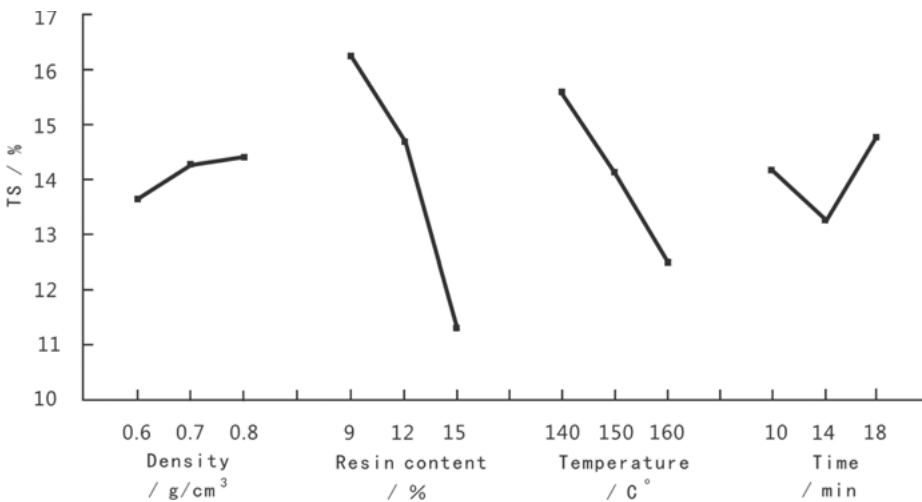
Fig. 5.18: Visual diagram on influence of technical factors on 2hTS.

5.3.9 Stalk composite appearance and other performance

Fig. 5.19 shows several final stalk composites. The stalk composites have a high strength, and good dimensional stability and machining performance. It can be machined by using common wood processing machines and tools on sawing, planing, slotting starting line, nailing, drilling, and mortising.

The straw composites can be painted, stained, and finished in other traditional ways. It has good decorative properties. It can be used for furniture parts and some decorative applications, as well as packaging materials.

(a) UF cotton stalk scrimber

(b) UF tobacco stalk scrimber

(c) UF pepper stalk scrimber

(d) UF soybean stalk scrimber

(e) PF cornstalks scrimber

(f) UF cotton stalk scrimber

Fig. 5.19: Photos of crop stalk reconstituted composites.

5.4 Curing mechanism of urea-formaldehyde resin in stalk composite

5.4.1 Infrared spectroscopy before curing

The infrared spectra of cotton stalks before curing are shown in Fig. 5.20. It can be seen from the figure that the absorption peak of OH stretching vibration happend at 3433.73 cm^{-1}; absorption peak of the saturated alkyl CH stretching vibration at 2929.74 cm^{-1}; absorption peak of hemicellulose acetyl group or a carboxyl group on C=O stretching vibration at 1741.43 cm^{-1}; absorption peak of lignin carbonyl stretching vibration and the benzene ring at 1638.20 cm^{-1}, 1598.59 cm^{-1}, 1508.78 cm^{-1}; at position of 1462–1375 cm^{-1}, it appeared to be the methyl wave number range.

The primarily characteristic peaks are explained in Tab. 5.11.
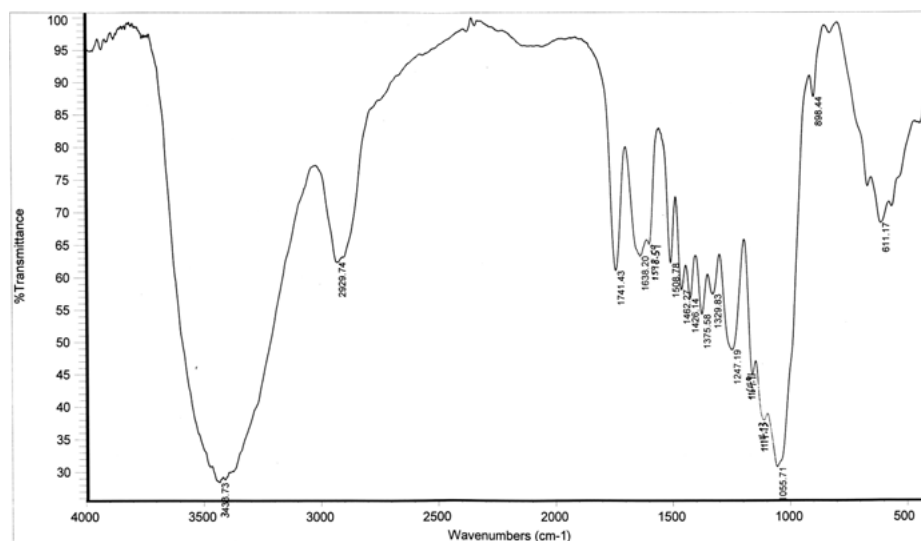
Fig. 5.20: FTIR of cotton stalks before curing.

Tab. 5.11: FTIR spectrum features of cotton stalk bunch.

Wavenumber (cm^{-1})	Light spectrum owned by genus spectrum assignment
3433.73	OH stretching vibration
2929.74	CH stretching vibration
1741.43	An acetyl group or a carboxyl group in C=O stretching vibration (xylem)
1638.20	C=O stretching vibration (lignin conjugated carbonyl)
1598.59	Stretching vibration of the benzene ring skeleton
1508.78	Stretching vibration of the benzene ring skeleton

Tab. 5.11: (continued)

Wavenumber (cm^{-1})	Light spectrum owned by genus spectrum assignment
1462.27	CH bending vibration (lignin, polysaccharides in CH$_2$)
1426.14	CH$_2$ shear vibration (cellulose), CH$_2$ bending vibration (lignin)
1375.58	CH bending vibration (cellulose and hemicellulose)
1329.83	Aromatic CH plane deformation characteristic peaks syringe
1247.19	Guaiac wood lignin CO aryl ring stretching vibration
1164.91	COC stretching vibration (cellulose, hemicellulose)
1114.13	Cellulose, pentosane of OH association with
1055.71	CO stretching vibration (cellulose, hemicellulose), an acetyl group in the alkoxy bond stretching vibration
898.44	CH cellulose and sugars in the ring vibration of deformation
611.17	OH-plane deformation vibrations

5.4.2 Infrared spectroscopy after curing

Fig. 5.21 shows the cured urea-formaldehyde FTIR spectra. It exhibits the absorption peak of NH and OH stretching vibration at 3421.53 cm^{-1}; the absorption peak of CH stretching vibration at 2953.91 cm^{-1}; the absorption peak of ether, hydroxymethyl groups CH stretching vibration at 2917.84 cm^{-1}. This peak value is not so obvious after the urea-formaldehyde resin is set. The amide I absorption peak appeared at 1646 cm^{-1}. After curing, H at amide was replaced. The amide II absorption peak relocated. Specific peaks attributables are explained in Tab. 5.12.

The absorption peak of hydroxyl stretching vibration moved from 3433 cm^{-1} toward lower wave numbers at 3403.55 cm^{-1}. The absorption peak is broadening and this indicates that during hot-pressing process, the hydroxyl groups combined to form hydrogen bonds each other. More hydrogen bonds indicated that less hydroxyl groups remained.

Tab. 5.12: FTIR spectrum features of solidified UF stalk composites.

Wavenumber (cm^{-1})	Light spectrum owned by genus spectrum assignment
3421.53	NH and OH stretching vibration
2953.91	CH stretching vibration
2917.84	Ether, the hydroxymethyl group CH stretching vibration
1646.53	Amide I the C=O stretching vibration
1550.57	Amide II of CN stretching and NH bending vibration within the plane
1382.61	CH deformation vibration
1245.88	Amide I of CN stretching vibration
1164.73	CN stretching vibration
1121.44	The second fatty acid amide ether CO stretching vibration
1032.27	Methylene ether bond COC stretching vibration
774.96	Uron ring skeleton vibration
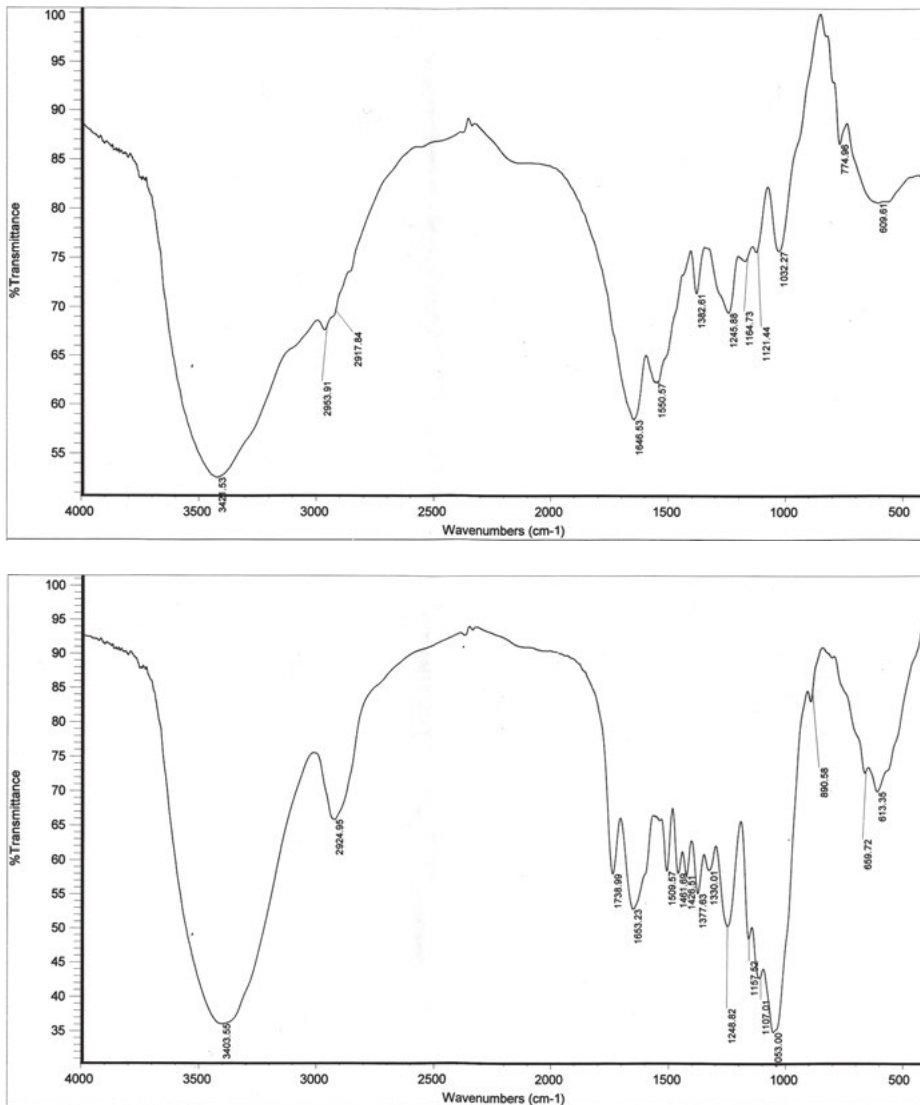
Fig. 5.21: FTIR of cotton stalk after curing.

Absorption peak of carbonyl group appeared at 1741.43 cm^{-1}. Compared to the absorption peak position and shape before curing, this indicates that the chemical reaction occurrs in the hemicellulose and forms relatively stable polymers.

Curing of urea-formaldehyde resin in the composite is usually considered to have generated methylene and dimethylene ether bonds to form a new polymer. Urea-formaldehyde resin before curing is composed of various monomeric methylol urea, methylene bonds, and a small amount of an oligomer consisting of dimethylene link-

age. When the adhesive is set, the hydroxymethyl and amino methylene bond forms, and this results in the three-dimensional structure of the ternary.

The mechanism of urea-formaldehyde bonding in a crop stalk
(1) Mechanical bonding

Mechanical bonding theory is attributed to mechanical adhesion. As can be seen from the scanning electron micrograph (Fig. 5.22), the liquid adhesive filled in crevices in the cotton stalk and some can penetrate into the cotton stalk after curing. This produces engaging connections in the interface areas with the anchoring effect.
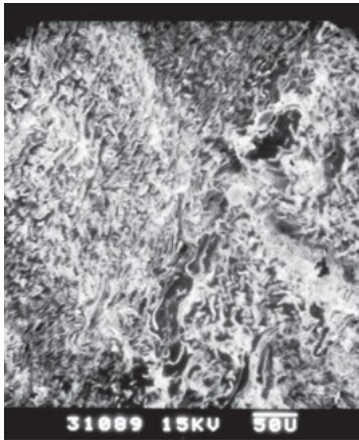
(a) Horizontal plane I
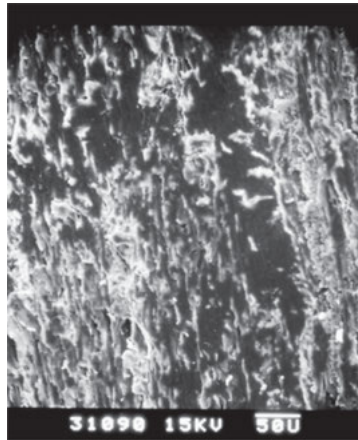
(b) Vertical plane I
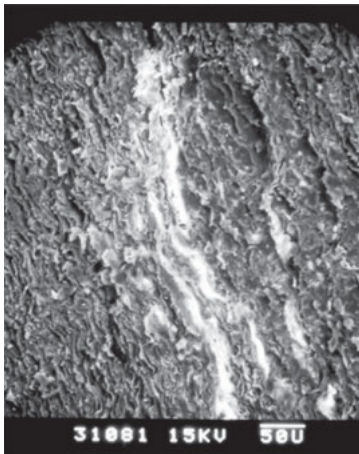
(c) Horizontal plane II
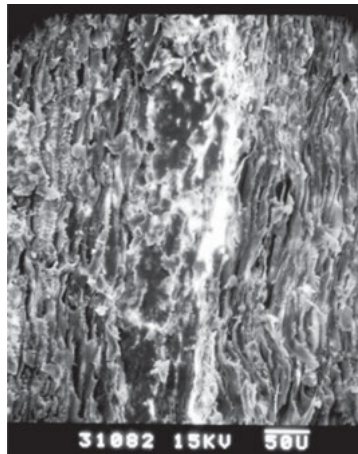
(d) Vertical plane II

Fig. 5.22: Electronic scanning microscopic photo images of UF cotton stalk glue line.

While under pressure, the glue is extruded into the surroundings. This shows that recombination between the substrates is partially due to "glue nail" bonding.

(2) Adsorption bonding

Adsorption theory insists that adhesive bonding is the result of physical adsorption and chemical sorption. The physical adsorption and chemisorption occurs between urea-formaldehyde resin and a cotton stalk. The physical adsorption force is the result of the van der Waals forces, i.e. urea-formaldehyde resin molecules by Brownian motion, the movement of cotton stalk surface diffusion. When the polar groups or molecular chains of the two elements move close to each other. less than 1 nm, they produce the intermolecular attraction. The cotton stalk has the functional groups of $-OH$ to form hydrogen bonds with adhesive molecule $-NH_2$ and $-OH$ by sharing the hydrogen atom. Meanwhile, under high temperature, the cotton stalk cellulose, hemi-celluloses, and lignin on $-OH$ also connects by hydrogen bonds between molecules. Generally, the chemical adsorption force is generally larger than the physical adsorption. The physical adsorption and chemisorption coexist during the bonding process.

(3) Chemical bonding

Chemical bonding theory says that bonding is the result of a chemical reaction [15]. The chemical reactions occur at the adhesive and stalk molecules to obtain high intensity of primary valence bonds. These bonds include the ionic bond, covalent bond, and metal bond. The bond strength is much greater than the intermolecular attraction.

In the bonding process, hydroxyl in the cotton stalk will react with hydroxymethyl to form a covalent bond. In addition, the dehydration among hydroxyl groups generates the ether bond.

(4) Weak boundary layer theory

Weak boundary layers are caused by different materials of the substrate and bonding materials, due to the structural inhomogeneity that can hinder bonding interface layer called a weak boundary layer. The uneven spreading of adhesive can create the void space. The air in the space creates the weak area. This weak interface layer does not mean the inevitable damage of the composite.

(5) Theoretical rheology

The surface of cotton stalk is rough, and the stalk is porous. After adhesive spreading, the liquid adhesive flows into the stalk and attaches to its surface. Under the hot press, adhesive will be squeezed and spread further. The spread and penetration occurs in the cotton stalk. The smaller the liquid viscosity is, the faster the adhesive penetrates. The formation of "gel nails" occurs. However, if the viscosity is too low, the adhesive penetrates too fast. This will lead to starvation of the adhesive in the composite.

The stalk cellulose has a relatively low degree of polymerization compared with wood. The stalk cellulose also has more noncrystalline regions. The hemicellulose and lignin are all noncrystalline substances. The crop stalks also exhibit the glass transition phenomena. It also plays a certain role in the adhesive spreading. The pressing temperature is usually at 140–160 °C. The scrimbers with more moisture have a lower glass transition temperature. Therefore, under pressure, materials is at the glass transition state. When materials are at glass transition state, the stalk bundle softens. It is easily compressed.

Meanwhile, the resin molecules vibrate faster and internal spreading speeds up. The stalk glass transition significantly improved the bond strength of composites.

References

[1]   Haq Z, Easterly JL. Agricultural residue availability in the United States. Applied Biochemistry and Biotechnology. 2006; 129: 15–21.

[2]   Jin W. Comparison and analysis of the main technological factors of influencing mechanical properties of scrimber and PSL. J Forestry Research. 2001; 12(4): 266–268.

[3]   Bowyer J, Stockman L. Agricultural residues-an exciting bio-based raw material for the global panels industry. Forest prod J. 2001; 51(1): 10–21.

[4]   Chung YH, Todd FS. Utilization of agriculture waste for composite panels. The 6th Pacific Rim Bio-based composite symposium, Portland; 2002. pp. 164–168.

[5]   Sauter SL. Developing composites from wheat straw. Proceedings of the 30th international particleboard/composite materials symposium, W.S.U.; 1996. pp. 197–214.

[6]   Boquillon N. Properties of wheat straw particleboards bonded with different types of resin. J Wood Sci. 2004; 3(50): 230–235.

[7]   Wasylciw W, Wang S. Straw-based composite panels: Attributes, issues and UF bonding technology. SUAF Processings; 2001. pp. 24–33.

[8]   Tomoyuki H. Recent development on the processing technology for wood-based materials in Japan. Forestry Agency Ministry of Agriculture, Forestry and Fisheries, Japan; 2000.

[9]   Mously EL, Megahed M. Investigation of the possibility of use of cotton stalks in particleboard production. The 33rd International Particleboard/Composite Materials Symposium, WSU; 1999. pp. 12–15.

[10]   Guler C. Research on the production possibilities of the particleboard from cotton stalks. Turkey: Karaelmas University; 2001.

[11]   Guler C, Ozen R. Some properties of particleboard made from cotton stalk. Holz als Roh- und Werkstoff. 2004; 62: 40–43.

[12]   Han G, Kawai U. Development of high-performance UF-bonded reed and wheat straw medium-density fiberboard. J Wood Sci. 2001; 47(5): 52–59.

[13]   Han G, Zhang C, Zhang D. Upgrading of urea formaldehyde-bonded reed and wheat straw particleboards using silane coupling agents. Jap Wood Res Soc. 1998; 44: 282–286.

[14]   Pandeya KK, Pitmanb AJ. FTIR studies of the changes in wood chemistry following decay by brown-rot and white-rot fungi. International Biodeterioration Biodegradation. 2003; 52: 151–160.

[15]   Johns WE. The chemical bonding of wood: Wood Adhesives and Technology. New York: Marcel Dekker Inc.; 1983.

A. Pizzi

6 Wood welding without adhesives

Abstract: Wood welding is a technique that has been used for bonding wood to wood without an adhesive. Bonding is fast, a matte of second, with good mechanical performance of the joint. The chapter illustrates advantages, limits and characteristics of the use of this technique.

Assembly techniques with mechanical connectors or with adhesives are common in joining solid wood in the furniture, civil engineering, and wood joinery industries. Both kinds of connections show several problems. With mechanical metal connectors, rust stains may appear on the connectors, and corrosion of the connectors can and does occur. With adhesively-bonded joints working with liquid adhesives, the costs are higher than for the use of mechanical connectors as regards manufacturing equipment maintenance. With adhesives the process is relatively longer, unless high investments in adhesive materials and machinery (high-frequency or microwave systems) are made in order to speed up the hardening phase. Thermoplastic welding techniques, which are widely used in the the plastic and car industries, have recently also been applied to joining wood, by melting a thermoplastic polymer between the two wood surfaces to be joined. A variety of techniques such as ultrasound, mechanical friction, and others have been used to melt the thermoplastic polymer in situ. In friction welding techniques the heat needed to melt the material is generated by pressing one of the samples to be joined against the other and to generate friction, and hence heat, which increases the temperature of the weldline rapidly and considerably.

The same mechanically-induced friction welding techniques which are widely used in the the plastic and car industries have also recently been applied to joining wood without the use of any adhesive [1–7]. This works by melting some wood components and, at the interface between the two wood surfaces to be joined, forming a composite of entangled wood fibers drowned into a matrix of melted wood intercellular material, such as lignin and hemicelluloses [1–7]. Linear mechanical friction vibration has been used to yield wood joints satisfying the relevant requirements for structural applications by welding at a very rapid rate [1, 3, 4]. Cross-linking chemical reactions also have shown to occur by CP-MAS ^{13}C NMR. These reactions, however, are lesser contributors during the very short welding period proper [8, 9]. They gain more, but still very limited, importance during the subsequent brief pressure holding period [1, 8, 9].

Also, high-speed rotation-induced wood dowel welding without any adhesive has recently been shown to rapidly yield wood joints of considerable strength [1, 6, 7]. The mechanism of mechanically-induced high speed rotation wood welding is due to

the temperature-induced softening and flowing of the intercellular material, mainly amorphous polymer material bonding the wood cells to each other in the structure of wood. This material is mainly composed of lignin and hemicelluloses. This flow of material induces high densification of the bonded interface [1, 6, 7]. Wood species, relative diameter differences between the dowel and the receiving hole, and press time were shown to be parameters yielding significant strength differences [1, 6, 7]. Other parameters were shown to have a much lesser influence.

The insertion of dowels into solid wood for joinery and furniture without any wood-to-wood welding has been used for centuries. This simple technology has also been applied to join particleboard [10]. However, nowhere in the relevant literature has wood-to-wood welding ever been achieved or even mentioned. Only fusion welding interposed thermoplastic materials has been mentioned in previous literature.

The relative difference in diameter between the dowel and substrate was the most important parameter determining joint strength performance [1, 6, 7]. The real determining parameter, however, is how fast the lignin/hemicelluloses melting temperature is reached. The greater the relative difference between the diameters of the dowel and of the substrate hole, the greater is the friction, hence the lignin melting temperature is reached more rapidly, and a better welding is achieved.

6.1 Systems of frictional wood welding

Two wood welding systems exist today which give strength results of the joint higher than what is required by the relevant standards [1, 2]. A third one, also thoroughly tested [11], instead gives poorer results. These systems are not as limiting as other welding systems such as ultrasound, microwave, and/or radiofrequency heating, and high rotation or high vibration spindle welding, laser welding, and others are all likely to afford some level of wood welding. Some experiments with some of them have been done as well, and will be discussed briefly later. The material flow and melting induced by the elevated temperatures reached leads to high densification of the interface between the two profiles and interfacial loss of the cellular wood structure in the joint, hence increasing the strength of the interface [1–3].

6.1.1 Linear vibration welding

The wood samples to be joined together are first brought into contact with a pressure between 1.3 and 2 MPa, to enable the joint areas to be rubbed together with a linear reciprocating motion (Fig. 6.1). The samples are vibrated with a displacement amplitude of about 3 mm and a vibration frequency of 100 Hz in the plane of the joint. The specimens welded up to now are of a length of up to 1.0–1.8 m [12], as the capacity of the existing machines is not greater than this. The time of welding is roughly 1.5–5 s [1, 4, 5]

and the holding time, still under pressure, after vibration has stopped is 5 s [1, 4, 5]. The obtained results satisfy the strength requirements for structural application. It must be pointed out, however, that the parameters used for wood-to-wood welding give widely different results as regards water resistance, according to the technology used. Older linear welding technologies yield joints which are not water resistant to any great extent, and which can then be used only for strictly interior applications [1]. Newer linear welding technologies instead give joints of much greater resistance to water [4, 5, 9], while the geometry of the joint itself in rotational dowel welding yields joints of almost exterior grade level [13–15].
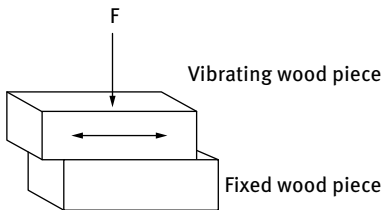
Fig. 6.1: Schematic example of frictional movement used in linear vibration wood welding.

Wood grain orientation differences in the two surfaces to be bonded yields bondlines of different strength in nonadhesives wood-to-wood welding. Longitudinal wood grain bonding of tangential and radial wood sections yield approximately 10 % difference in strength of the joint. Cross-grain (±90°) bonding yields instead much lower strength results, roughly half than what observed for pieces bonded with the grain parallel to each other, although these results still satisfy the relevant wood-joining standards [13–15].
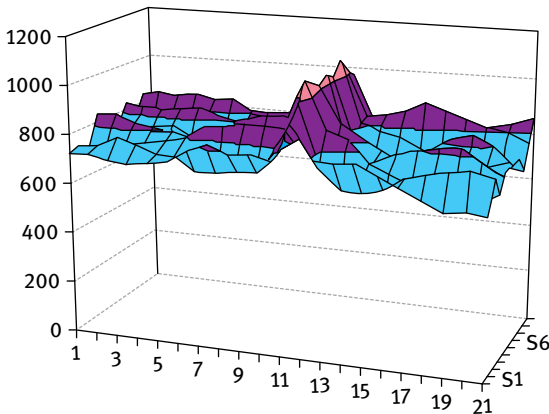
Fig. 6.2: Density map pof linearly friction welded beech indicating the increase in density in the welded interface in relation to the surrounding wood.

Fig. 6.3: Welded bondline. Note the entangled wood cells (fibers) immersed in a mass of molten material. The whole is superposed on a background of elongated, undamaged wood cells.
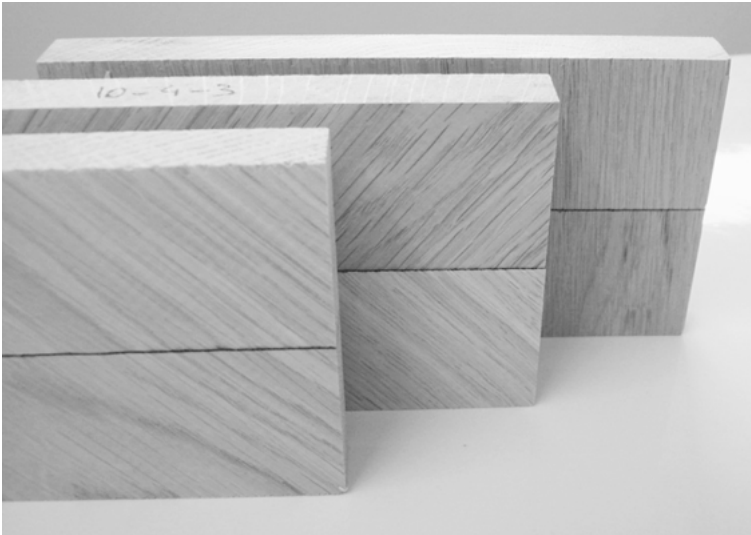
Fig. 6.4: Examples of different butt joints obtained by end-grain welding of oak wood [16].

Of particular interest are studies on wood cross-grain welding [13–16], where the principles of the anisotropy of composites rule the type of strength results that can be obtained in welding. Of particular interest is the case of wood end grain welding [16] where the formation of very strong butt joints by this technique does open the possibility of eliminating wood adhesive bonded fingerjoints. An example of this is shown in Fig. 6.4 for end-grain-welded oak wood joints.

End-grain-to-end-grain welding gave also butt joints of good strength with three high density Australian eucalyptus woods, namely Sidney blue gum (*Eucalyptus saligna*), spotted gum (*Eucalyptus maculata*, *Corymbia maculata spp.*) and black butt (*Eucalyptus pilularis*). The absence or limited tendency to defibration in end-grain-to-end-grain welding for wood densities as high as these, around 800–900 kg/m^3, indicates that end-grain-to-end-grain welding is possible and yields good joint strengths,

but with a different appearance of the welded interphase. At anatomical level three features were noticeable.

(i) The paintbrush-like appearance of the cell tips bent so by the frictional movement during welding. This leaves this cell tips free to intertwine with the same from the surface of the opposite wood piece.
(ii) The absence of any great amount of molten material between the straight shafts of the parallel bundles of cells, showing that the greater part of the intercellular material has molten and flowed away from the cells toward the interphase.
(iii) The amount of molten intercellular material found on the upper surface of the cell tips, giving to the joint, the appearance of an anatomical fingerjoint [17].

6.1.2 High speed rotation dowel welding

Traditionally, wooden dowels of a given diameter (most commonly 10 mm) are forced into a predrilled hole with a smaller diameter by applying pressure. Alternatively, similar dowels can be inserted into holes of the same diameter after application of an adhesive, in general PVAc. In high speed rotation welding fluted rib beech dowels (or even smooth dowels of other woods) are inserted at high rotation speed and insertion rate within a predrilled hole of smaller diameter [2] (Fig. 6.5).
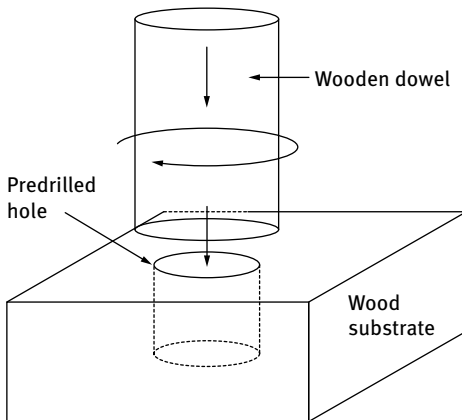
Fig. 6.5: Schematic example of frictional movement used in high-speed rotational dowel welding.

In dowel welding, generally, cylindrical beech fluted dowels of 10 mm in diameter are used. They are placed into a drill, in the place of the drill bit, and inserted within pieces of wood having predrilled holes of 8 mm. For best results the drill rotation rate must be higher than 1200 revolution per minute (rpm), and possibly equal to 1500–1600 rpm. When fusion and bonding are achieved, generally between 1 and 3 s, the rotation of the dowel is stopped, and the pressure may be briefly maintained [2, 6, 7].

Dowel welding by high speed rotation has been used to join two and even three wood blocks. This is the ultimate aim of dowel welding. Strong joints were obtained [7, 18]. An extremely important finding in dowel welding is that its water resistance is far superior to that obtained in linear welding [18]. This is due mainly to the geometry of the joint that allows conservation of approximately 80–90 % of the dry strength once it is wet, the cold water soaked up, and up to 15 % of the original dry strength once redried after 24 hours of cold water soakings [18].

Fig. 6.6: Well-welded dowel where the two pieces to be joined were maintained tightly together by clamping during dowel insertion.
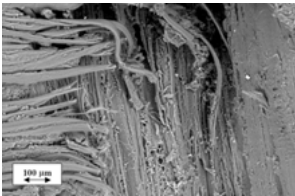
Fig. 6.7: Scanning electron microscope image of the interface of a dowel welded to the substrate. Note the fibres of the dowel and of the substrate at 90° to each other bonded by the melted and resolidified amorphous intercellular material.

High-speed dowel rotation welding has been shown to be capable of holding together structures such as a suspended wood floor of size 4 m × 4 m × 0.2 m without using any adhesive, any nails or any other binding system other than welded dowels [19–21]. When this technique applies to solid wood, several physical, chemical, and mechanical processes occur. The rheological behavior of wood that is compressed and heated simultaneously while a rapid vibrating shift is applied changes, the moisture content at the interface is reduced, and chemical modifications of the wood structure occur during heating and the solidification of the melted joint interface.

The welding or bonding that occur at the interface is probably mainly explained by the melting and solidification of the hemicelluloses, mainly xylans [14, 18], and intercellular middle lamella's lignin and protolignin [1, 14, 18] and partly by the physical entanglement of the fibers interconnected between them as a results of the friction. The direct welding of the cells is explained by the known properties of wood intercellular material: markedly thermoplastic, rigid, and concentrated in the compound middle lamella of the wooden cells. Chemical phenomena also occur [1, 8, 9, 14], mainly in the brief pressure-holding phase immediately after welding, the main one of which is the formation and selfcondensation of furfural [1, 8]. The reactions involved are both of ionic type [1] as well as radical reactions [22].

Analysis of volatile compounds and of gasses emitted as smoke by the welding interface during rotational wood dowel welding of a hardwood (beech) and of a softwood (Norway spruce) has shown that the compounds in the smoke are water vapor, CO_2, degradation compounds from wood polymeric carbohydrates and from amorphous lignin, as well as some volatile terpenes, these latter ones only for the softwood used, namely Norway spruce [23, 24]. The main carbohydrates contributing to the volatile compounds are xylans for beech and glucomannans for spruce. Numerous compounds, in very small proportions derived from the degradation and rearrangement reactions of lignin, have also been identified. The proportion of CO_2 emitted is very low, and neither CO nor methane are emitted, due to the relatively low temperature of dowel welding. Experiments at temperatures slightly higher than that of dowel welding but prolonged in time have shown that the main component of the smoke produced during welding appear to be water vapor.

6.1.3 Bamboo welding

Linear vibration-friction welding, which has several advantages over traditional mechanical fasteners or gluing, was to investigate the possibility to apply for a joining procedure of wood-bamboo sandwich-laminated composite. Being similar to the welded wood and wood, an entanglement network composite of wood and bamboo cells having a molten lignin polymer matrix is formed. The resulting strength indicates that linear vibration welding can be suitable for wood and bamboo species with average tensile strength values suited to the furniture industry, and even wood construction. X-ray microdensitometry analyses show an increase in density for the interfacial material between the wood and bamboo substrates, of which the peak profile between the outer and inner bamboo varies. The most likely one of these identified by FT-IR appears to be a depolymerization and recondensation reaction of lignin and carbohydrate-derived xylans. The micrographs confirm the different extents of bamboo-to-wood welding by scanning electron and optical microscope. The key contribution of this paper, therefore, is that sandwich wood-bamboo welding lumber can be efficiently fabricated by linear vibration welding without any adhesive [25].

Moso bamboo (*Phyllostachys pubescens*) welding (outer-outer, inner-inner and outer-inner) were also studied. The maximum average tensile-shear strength of outer-outer, inner-inner and outer-inner welding were 5.91 MPa, 7.15 MPa, and 6.24 MPa, respectively. The thickness of outer-outer welding layer is the greatest, and the inner-inner welding is the smallest. However, the maximum density reached in the inner-inner welding sample is bigger than in the outer-outer welding [26].

End grain butt joints obtained by friction welding with moso bamboo showed relatively good experimental results compared to beech, oak, and spruce. The average compression shear strength of the welded joints can reach 5.81 MPa, and the departure of bamboo fibers cannot be observed during the welding process. The study of

the microstructure of the welded surface has revealed the reasons for this. During the welding process, the hard vascular bundles become prominent on the welded surface and work as the brush enduring the lateral friction protecting the bamboo from cracking. End-grain-to-end-grain welded joints of moso bamboo have some appearance similarity with fingerjoints, thus ensuring the final satisfactory shear strength in compression [26].

Totally different species can also be welded. Thus, The palmyra palm, a very valuable commercial crop in coastal areas of India, northern Sri Lanka, and mainland southeastern Asia has also been welded. The friction welding has several advantages compared to the traditional mechanical fasteners or gluing. The study on this applied the mechanically induced linear vibration friction welding to the palmyra palm. The high levels of carbohydrates and lignin contributes strongly to the bonding, but a lack of entangled and mixed fiber make the bonding strength not that high [27].

6.2 Applications of wood welding

Several applications of wood welding, both interior and exterior, have been developed. First, both standard linear wood welding and dowel welding cannot be used for exterior applications, but rather only for interior applications. This characteristic is due to the structural type of welded interphase formed in which no chemical cross-links occurs but only physical entanglement cross-linking similar to what happens for example with PVAc glue lines.

6.3 Exterior and semiexterior applications

An improvement in water resistance can be obtained by just varying welding parameters. A change in linear welding conditions, namely higher vibration frequency (150 Hz) and lower displacement (2 mm) during welding, produced a quicker rise in the temperature of the weldline. This allowed a much shorter welding time (1.5 s). X-ray microdensitometry mapping showed a progressive increase in broadening and average density of the weldline as the welding time lengthens. As the welding time lengthens, the maximum temperature reached at the end of welding is progressively higher. This causes increasingly greater degradation. This effect was also confirmed by CP-MAS ^{13}C NMR, and it was found that the lower the degree of deterioration of the weldline of the wood joint, the shorter the welding time is. Monitoring of the temperature of the weldline showed that the temperature reached in wood joints during welding was inversely correlated to its water resistance. Furthermore, the increase in weldline temperature is markedly quicker at a vibration frequency of 150 Hz than at 100 Hz. Thus, the shorter the welding time, the lower the degree of deterioration of the weldline of the wood joint is. This appears to be due to welding occurring when

water vapor is still present in the joint, hence providing a less damaging welding environment [28, 29].

This approach, however, is not sufficient to give exterior or semiexterior wood joints. Thus, a considerable amount of research work has been devoted to rendering the welded interphase waterproof, to be able to apply both linear and rotational welding to exterior and semiexterior applications. Four approaches have been found to successfully to a different extent render welded joints suitable for exterior or semiexterior applications. These were as follows.

(1) Application of rosin, a wood derived, nontoxic, natural, inexpensive, and easily and abundantly available natural material, to the wood faces to be joined by either linear vibration welding or rotational dowel welding has shown to greatly enhance the water resistance of welded wood joints. The method of application has been shown to have a marked effect on the results, with the application and drying of a diluted ethanolic rosin solution to the wood surfaces before welding yielding the best results. The considerable improvement in water resistance does not still allow classification of the joints as a fully exterior grade. However, dowel welding can now be used for protected exterior joints due to a combination of rosin waterproofing and joint geometry. Welded dowel joints holding together for longer than 455 days immersion in water indicate this to be the case. Rosin-treated linear vibration joints held together well in excess of 30 days, but retained a measurable strength, in the best case, only up to 18 days water immersion. The wood anatomy and chemical reasons for the effect of rosin were determined by x-ray microdensitometry and CP-MAS ^{13}C NMR analysis. This is probably the most successful method to waterproof the weldline, but leads to joints that are somewhat more brittle than for untreated welding [30, 31]
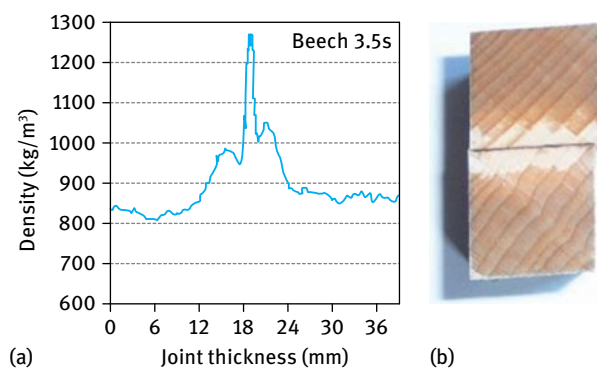
Fig. 6.8: Welded beech joint in presence of rosin: (a) x-ray density distribution around the central peak of the welded interphase composite; the two broad peaks around the thin central peak indicate where the rosin has migrated during welding; (b) welded beech joint after 24 h immersion in cold water showing the weldline kept dry.

In Fig. 6.8 it can be seen why rosin is able to waterproof the welded joint. The thin rosin film deposited by an ethanolic solution on the surfaces to be welded melts during the temperature increase characteristic of mechanical friction welding. It tends then to migrate partially away from the weldline, as shown by the two peaks of density surrounding and superposed to the peak of density of the weldline (Fig. 6.8 (a)). Once the joint is immersed in water the layers of water-insoluble rosin surrounding the weld line clearly prevent the water approaching the weldline, as shown in Fig. 6.8 (b).

(2) Low molecular mass acetylated organosolv lignin from wheat straw and from depolymerized low sulfur organosolv wood lignin have been shown to markedly improve both the water resistance and the mechanical performance of welded dowel wood joints. The acetylated oligomers distribution and extent of acetylation of the two lignins were determined by matrix assisted laser desorption ionization-time of flight (MALDI-TOF) mass spectrometry. Extensive acetylation was confirmed by CP-MAS ^{13}C NMR spectrometry. Force-displacement measurements on welded dowel joints to which acetylated wood lignins were added showed a ductile behavior. This is due to the interpenetration of the elastic acetylated lignin network into the more rigid composite network of the welded interphase [32].

(3) The use of a naturally water repellent wood due to the presence of extractives or other causes, for example Paduk (*Pterocarpus soyauxii*) wood, alone or in combination with a nonwater repellent wood [33]. Linear vibration welding of extractive rich Paduk wood from central Africa containing a high proportion of a native mixture of insoluble extractives has been shown to yield joints of much upgraded water resistance. This has been shown to be due to the protecting influence the extractives from the wood itself has on the welded interphase, due to their inherent water repellency. Joints of unusually high percentage wood failure but modest strength were obtained, Paduk wood brittleness apparently yielding weldline strengths always higher than that of the surrounding wood itself. This indicated that Paduk wood welded joints present enhanced weather exposure durability in relation to welded joints using other species of wood, such as beech for example, as shown in Fig. 6.9.

(a)   (b)
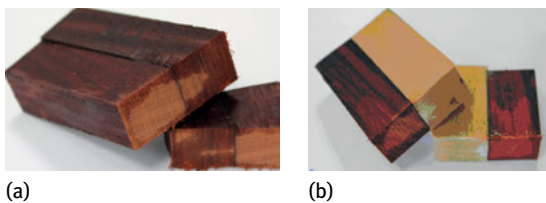
Fig. 6.9: Example of welded water repellent wood species (Paduk) effect after 24 h immersion in cold water: (a) dry surroundings of the weldline for Paduk-Paduk joints, and (b) dry surroundings of the weldline for Paduk-beech joints, indicating the effect of a water-repellent species on nonwater repellent ones once coupled in wood welding.

(4) The use of hydrocarbons and tar residues issued from the distillation of wood, commonly known in France as "goudron de Norvege". These have a clear waterproofing action when applied to the wood surface in a diluted alcoholic solution before welding [34]. Their problem is their apparent unpleasant smell and suspected toxicity.

6.4 Interior applications

Their are a considerable number of interior applications for which wood welding has been demonstrated as being useful.

(1) In furniture, for example, the minimalist Z-chair of Rietveld (Netherlands architect, 1936) and design variations on the same theme were prepared as originally conceived by its designer, without any support angular, by just inserting two ranks of dowel each rank welded a different angle (Fig. 6.10) [35]. Equally, different types of furniture joints [36–38], of table surfaces [39, 40], and even wardrobes [41] can be manufactured with welded dowels (Fig. 6.11).

Fig. 6.10: Rietveld minimalist Z-chair built by rotational dowel welding according to the original model.

Fig. 6.11: Furniture piece built without any nails, screws or gluing but exclusively by rotational dowel welding.

(2) In structural applications a life-size suspended floor was built and tested just by using welded dowels. It passed all the requirements of the relevant European norms for this type of construction [42] (Fig. 6.12) as well as housing walls using the same construction principles [43]. With same approach, welded dowels, different kind of welded lam-beams [44, 45] (Fig. 6.13) and I-beams [45] (Fig. 6.14) were prepared and tested, yielding results acceptable or well superior to the relevant international standards requirements.

Fig. 6.12: Suspended floor of dimensions 4 m × 4 m × 0.22 m built exclusively by rotational dowel welding.

Fig. 6.13: Laminated beam built by insertion of long dowels through 4 wood layers using a sunflower oil welding retardation system.

Fig. 6.14: I-beam built by exclusively using welded dowels at the intersection joints.

References

[1]   Gfeller B, Zanetti M, Properzi M, Pizzi A, Pichelin F, Lehmann M, Delmotte L. Wood bonding by vibrational welding. J Adhesion Sci Techn. 2003; 17(11): 1573–1589.

[2]   Pizzi A, Leban J-M, Kanazawa F, Properzi M, Pichelin F. Wood dowel bonding by high-speed rotation welding. J Adhesion Sci Technol. 2004; 18(11): 1263–1278.

[3]   Leban J-M, Pizzi A, Wieland S, Zanetti M, Properzi M, Pichelin F. X-ray microdensitometry analysis of vibration-welded wood. J Adhesion Sci Technol. 2004; 18(6): 673–685.

[4]   Mansouri HR, Omrani P, Pizzi A. Improving the water resistance of linear vibration-welded wood joints. J Adhesion Sci Technol. 2009; 23(1): 63–70.

[5]   Omrani P, Pizzi A, Mansouri H, Leban J-M, Delmotte L. Physico-chemical causes of the extent of water resistance of linearly welded wood joints. J Adhesion Sci Technol. 2009; 23(6): 827–837.

[6]   Kanazawa F, Pizzi A, Properzi M, Delmotte L, Pichelin F. Parameters influencing wood-dowel welding by high-speed rotation. J Adhesion Sci Technol. 2005; 19(12): 1025–1038.

[7]   Ganne-Chedeville C, Pizzi A, Thomas A, Leban J-M, Bocquet J-F, Despres A, Mansouri HR. Parameter interactions in two-block welding and the wood nail concept in wood dowels welding. J Adhesion Sci Technol. 2005; 19(13/14): 1157–1174.

[8]   Delmotte L, Ganne-Chedeville C, Leban J-M, Pizzi A, Pichelin F. CP-MAS, ^{13}C NMR and FTIR in-
      vestigation of the degradation reactions of polymer constituents in wood welding. Polymer
      Degrad & Stabil. 2008; 93; 406–412.

[9]   Delmotte, Mansouri HR, Omrani P, Pizzi A. Influence of wood welding frequency on wood con-
      stituents chemical modifications. J Adhesion Sci Technol. 2009; 23(9): 1271–1279.

[10] Resch L, Despres A, Pizzi A, Bocquet J-F, Leban J-M. Welding-through doweling of wood panels.
      Holz Roh Werkstoff. 2006; 64(5): 423–425.

[11] Stamm B, Windeisen E, Natterer J, Wegener G. Chemical investigations on the thermal be-
      haviour of wood during friction welding. Wood Science and Technology. 2006; 40(7): 615–627.

[12] Stamm B, Natterer J, Navi P. Joining wood by friction welding. Holz Roh Werkstoff. 2005; 63(5):
      313–320.

[13] Golé J, Resines Reinforcees. In: GFP, Groupe francais d'Etudes et d'Applications des Polymeres,
      editor. Proprietes Physiques des Polymeres: Mise en Œuvre; 1979. Chap. 7, pp. 255–305.

[14] Properzi M, Leban J-M, Pizzi A, Wieland S, Pichelin F, Lehmann M. Influence of grain direction
      in vibrational wood welding. Holzforschung. 2005; 59(1): 23–27.

[15] Omrani P, Mansouri HR, Pizzi A, Masson E. Influence of grain direction and preheating on linear
      wood welding. Eur J Wood Wood Prod. 2010; 68 (1): 113–114.

[16] Omrani P, Mansouri HR, Pizzi A. Wood end grain linear welding: influence of wood grain direc-
      tion on linear welding. J Adhesion Sci Technol. 2009; 23(16): 2047–2055.

[17] Mansouri M, Leban J-M, Pizzi A. End-grain butt joints obtained by friction welding of high den-
      sity eucalyptus wood. Wood Sci Technol. 2010; 44(3): 399–406.

[18] Pizzi A, Despres A, Mansouri HR, Leban J-M, Rigolet S. Wood joints by through-dowel rotation
      welding: microstructure, ^{13}C NMR and water resistance. J Adhesion Sci Technol. 2006; 20(5):
      427–436.

[19] Bocquet J-F, Pizzi A, Despres A, Mansouri HR, Resch L. Wood joints and laminated wood beams
      assembled by mechanically welded wood dowels. J Adhesion Sci Technol. 2007; 21(3/4):
      301–317.

[20] Oudjene M, Khalifa M, Segovia C, Pizzi A. Application of numerical modelling to dowel-welded
      wood joints. J Adhesion Sci Technol. 2010; 24(2): 359–370.

[21] Bocquet J-F, Pizzi A, Resch L. Full-scale (industrial) wood floor using welded through dowels.
      J Adhesion Sci Technol. 2006; 20(15): 1727–1739.

[22] Wieland S, Bozhang S. Pizzi A, Properzi M, Stampanoni M, Abela R, Lu X, Pichelin F. Vibration
      welding of wood: X-ray tomography, additives, radical concentration. Forest Products J. 2005;
      55(1): 84–87.

[23] Omrani P, Masson E, Pizzi A, Mansouru HR. Emission gasses and degradation volatiles from
      polymeric wood constituents in wood dowels friction welding. Polymer Degrad & Stabil. 2009;
      93: 794–799.

[24] Omrani P, Masson E, Pizzi A, Mansouri HR. Emission gases in linear vibration welding of wood.
      J Adhesion Sci Technol. 2009; 23(1): 85–94.

[25] Hu J, Pizzi A. Wood–bamboo–wood laminated composite lumber jointed by linear vibra-
      tion–friction welding. Eur J Wood & Wood Prod. 2013; 71(5): 683–686.

[26] Zhang H, Pizzi A, Lu X, Zhou X. Optimization of tensile shear strength of linear mechanically
      welded outer-to-inner flattened moso bamboo (*Phyllostachys pubescens*). Bio Resources.
      2014; 9(2): 2500–2508.

[27] Zhang H. Bamboo end grain welding. Unpublished results; 2014.

[28] Mansouri HR, Omrani P, Pizzi A. Improving the water resistance of linear vibration-welded
      wood joints. J Adhesion Sci Technol. 2009; 23(1): 63–70.

[29] Omrani P, Pizzi A, Mansouri H, Leban J-M, Delmotte L. Physico-chemical causes of the extent of
      water resistance of linearly welded wood joints. J Adhesion Sci Technol. 2009; 23(6): 827–837.

[30] Mansouri HR, Pizzi A, Leban JM, Delmotte L, Lindgren O, Vaziri M. Causes for the improved water resistance in pine wood linear welded joints. J Adhesion Sci Technol. 2011; 25(16): 1987–1995.

[31] Pizzi A, Mansouri HR, Leban JM, Delmotte L, Omrani P, Pichelin F. Enhancing the exterior performance of wood linear and rotational welding. J Adhesion Sci Technol. 2011; 25(19): 2717–2730.

[32] Pizzi A, Zhou X, Navarrete P, Segovia C, Mansouri HR, Placentia-Pena MI, Pichelin F. Enhancing water resistance of welded dowel wood joints by acetylated lignin. J Adhesion Sci Technol. 2013; 27(3): 252–262.

[33] Ganier T, Hu J, Pizzi A. Causes of the water resistance of welded joints of Paduk wood (Pterocarpus soyauxii Taub.). J Renewable Resources. 2013; 1(1): 79–82.

[34] Vaziri M. unpublished work; 2014.

[35] Renaud A. Minimalist Z chair by rotational dowel welding. Eur J Wood Prod. 2009; 67(1): 111–112.

[36] Segovia C, Pizzi A. Performance of dowel-welded wood furniture linear joints. J Adhesion Sci Technol. 2009; 23(9): 1293–1301.

[37] Segovia C, Pizzi A. Performance of dowel-welded T-joints for wood furniture. J Adhesion Sci Technol. 2009; 23(16): 2073–2084.

[38] Segovia C, Renaud A, Pizzi A. Performance of dowel-welded L-joints for wood furniture. J Adhesion Sci Technol. 2011; 25(15): 1829–1837.

[39] Segovia C, Zhou X, Pizzi A. Wood blockboards for construction by wood welding with pre-oiled dowels. J Adhesion Sci Technol. 2013; 27(5/6): 577–585.

[40] Belleville B, Stevanovic T, Cloutier A, Pizzi A, Salenikovich A, Blanchet P. Production and properties of wood-welded panels from two Canadian hardwoods. Wood Sci Technol. 2013; 47(5): 1005–1018.

[41] Segovia C. University Henri Poincaré-Nancy 1 [PhD thesis]. Epinal, France; 2010.

[42] Bocquet J-F, Pizzi A, Resch L. Full-scale (industrial) wood floor assembly and structures by welded-through dowels. Holz Roh Werkstoff. 2007; 65(2): 149–155.

[43] Resch L. University Henri Poincaré-Nancy 1 [PhD thesis]. Epinal, France; 2011.

[44] O'Loising C, Oudjene M, Shotton E, Pizzi A, Fanning P. Mechanical behaviour and 3D stress analysis of multilayered wooden beams made with welded-through wood dowels. Composite Structures. 2012; 94(2): 313–321.

[45] O'Loising C, Oudjene M, Ait-Adler H, Fanning P, Pizzi A, Shotton E, Meghlat E-M. Experimental study of timber-to-timber composite beam using welded-through wood dowels. Construct Build Mat. 2012; 36: 245–250.

José Reinaldo Moreira da Silva, Anna Carolina de Almeida Andrade, and Jordão Cabral Moulin

7 Surface quality of mechanically processed wood

Abstract: To add value to wood products and their composites manufactured by mechanical processing, it is necessary to know the characteristics of these materials to achieve the best quality possible, once the parts with better quality are destined for more noble uses. The main characteristics analyzed to evaluate the quality of wood pieces and its composites are their surfaces, which makes it important to study methodologies to characterize the surfaces. The aim of this study was to describe methodologies to characterize the surfaces of wood and its composites. The methodologies used were feed per tooth (f_z), visual analysis, roughness and the sunset laser. Each methodology applied presented peculiar advantages and disadvantages; this observed, the choice of methodology must consider the requirements of the final product quality, depending on its use.

The knowledge about the characteristics of any material provides advantages, such as its correct use, production optimization and, consequently, a better quality product. Thus, the study of wood and wood composite characteristics is important and necessary to achieve these benefits, especially when these materials are mechanically processed.

7.1 General considerations on wood formation

Wood is an organic, renewable material, with ranging characteristics from species to species, within the same species and within the tree. All existing variations are mainly attributed to genetic and environmental factors; therefore, they make wood a heterogeneous material and can cause variations in anatomical, chemical, physical and mechanical properties of wood [1].

In general, woods are chemically made of 49 % carbon, 44 % oxygen, 6 % hydrogen, 0.1–1 % nitrogen, and 0.1 % mineral compounds [2]. By the combination of these elements, a highly organized and complex chemical structure is formed. It is mainly represented by cellulose, lignin and hemicelluloses. However, there are the extractives and, in addition, the presence of mineral components is still observed in wood.

Chemical composition ranges among wood species. According to Haygreen and Bowyer [2], hardwoods have, on average, 40−44 % cellulose, 15−35 % hemicelluloses, and 18−25 % lignin. On the other hand, coniferous woods have an average percentage composition of 40−44 % cellulose, 20−32 % hemicelluloses, and 25−35 % lignin. These chemical constituents are responsible for the establishment of wood cells, which will range in type and number of cells.

The chemical composition of the wood allows that composites be produced by applying appropriate technologies and adhesives; the particulate and laminated panels such as wood composites are cited for this. For the production of wood composites there is also need for adequate anatomical and physical characteristics of wood.

According to Browning [3], wood is formed by different types of cells and, when living, they perform the basic functions of conduction of water and minerals, material storage and mechanical support. The types of cells may range in shape, size and arrangement [4].

According to Esau [5], wood cells are generated by the meristematic tissue, through cell divisions of the cambial and apical meristem. In the initial stage, cell elongation occurs and, subsequently, an increase in the number of these cells prevails. The function of the meristematic tissue is influenced by the tree hormone rate, which is associated with environmental conditions and genetic factors.

According to Esau [5], in spring and summer the induction of meristem cells occurs, causing rapid cell divisions as a result of the increase in hormone rate. This effect results in thinner cell walls and greater lumen diameter. The wood generated under this condition is called earlywood. In contrast, in fall and winter the cells are characterized by thick walls and smaller lumen diameter. These characteristics are due to their slower formation. The wood formed under these conditions is characterized as latewood; early and late wood can be seen in Fig. 7.1.
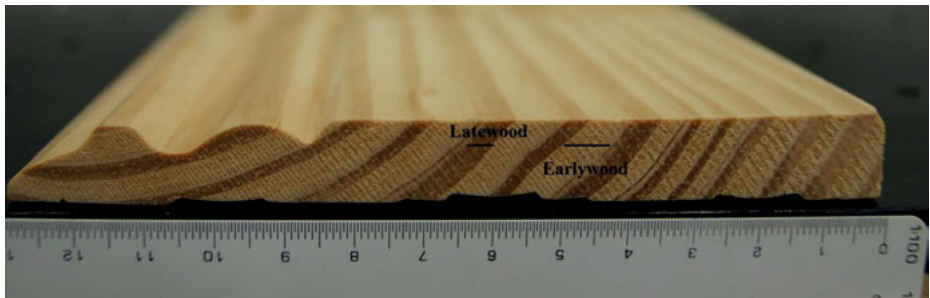
Fig. 7.1: Early and late wood.

The variation in type, amount, and arrangement of the anatomical elements formed by wood can be observed in the axial (bottom-top) and radial (pith-bark) direction. According to Downes et al. (1997), the variation in the axial direction is observed in intensities lower than those found in the radial direction.

Wood anatomy plays an important role; Downes et al. [6] mention that the physical and mechanical properties of wood can be affected by the size and amount of fibers, vessels, and also by the amount of parenchymal tissue. In this context, the increase in the number and size of vessels may cause a decrease in wood density (specific gravity). It is associated with fact that vessels have more voids, which could be

occupied by fibers. Panshin and De Zeeuw [4] warn about the presence of inlays and content such as bud resins, crystals, silica, etc., which, when in large amounts, can also increase wood mass and, consequently, its density.

Another important physical property of wood is the contractions, which can range in relation to tree position. In general, the axial contraction is greater in juvenile wood, that is, closer to the pith, rapidly decreasing from the pith towards the bark. This change in magnitude is associated with the rapid reduction in the cell wall microfibril angle, with an increase in cell length and in the content of cellulose [4].

Wood is a material characterized as anisotropic, since its properties behave differently in different axes. Fig. 7.2 illustrates the variation in the appearance of the faces of *Eucalyptus grandis* wood after the straight cut by a chisel [7]. The variation that exists in different planes and/or directions may be associated with different types, amounts and arrangements of the anatomical elements of wood [4].
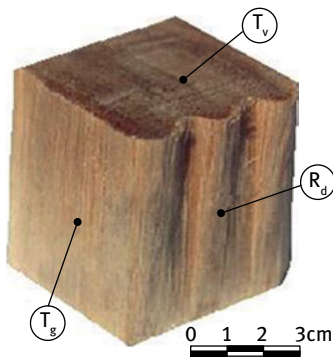
Fig. 7.2: Different aspects in the three planes of Eucalyptus grandis wood after the straight cut by a chisel, where: T_v = transverse plane; R_d = radial longitudinal plane, and T_g = tangential longitudinal plane. Source: [4].

The variation in the anatomical characteristics of wood in different planes is directly reflected in the quality of machined wood.

A study conducted by Burdulu et al. [8] to evaluate surface roughness of radial and tangential wood boards of *Populus nigra L.* and *Pinus nigra A.*, showed a better-quality machined surface in tangential boards, with lower roughness values. In the study by Kilic et al. [9] with *Fagus orientalis* and *Populus tremula*, there was no difference in roughness between the two boards. The same result was found by Martins et al. [10] for *Eucalyptus benthamii*.

Based on wood planes and direction of the cutting tool edge, families of orthogonal cutting are formed. These families are defined by two numbers representing angles. The first angle is formed between the tool cutting edge and the axial length of wood fibers. The second angle is formed between the cutting direction and the axis of wood fibers. Thus, it is possible to find families with cuts of 0°–90°, 90°–0° end 90°–90° [11].

Silva et al. [12] associated families of orthogonal cuttings for classical peripheral cuttings, which are performed in mechanical wood processing units, such as furniture

factories. According to these authors, the cutting family 0°–90° can be represented by cross section processes of boards with circular saw blades (Fig. 7.3) and/or handsaws. The family 90°–0° can be associated with planing processes, longitudinal cutting in circular saws or axial peripheral milling (Fig. 7.4). Finally, it is possible to associate the family 90°–90° with peripheral face milling performed on top of the boards in the cross direction (Fig. 7.5).
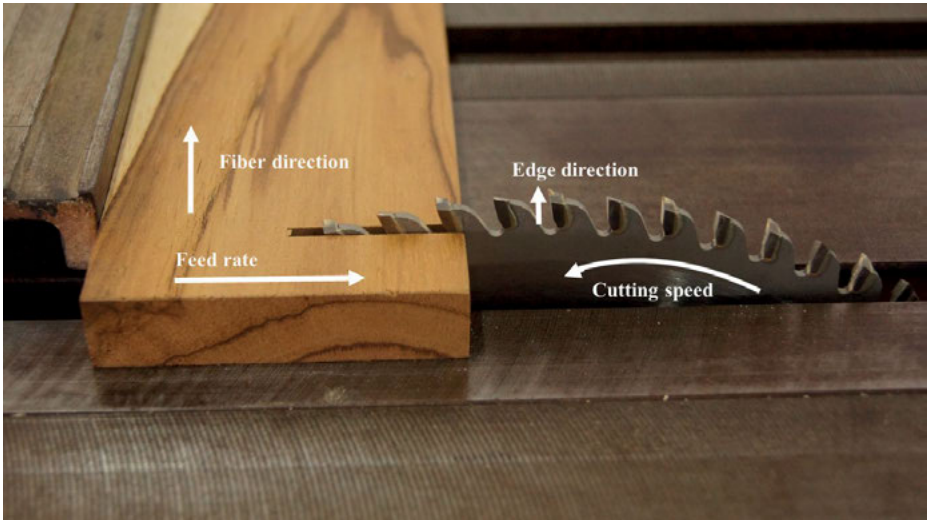
Fig. 7.3: Cutting family 0°–90°.
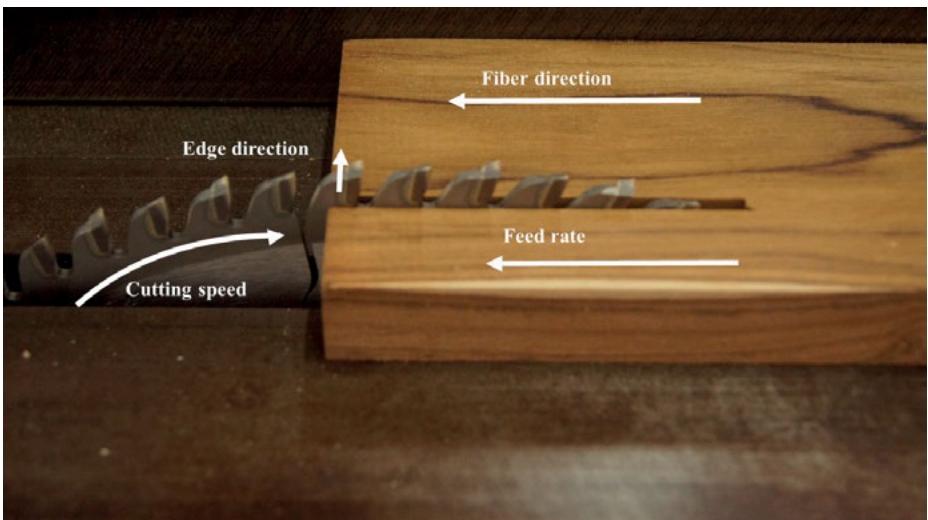
Fig. 7.4: Cutting family 90°–0°.
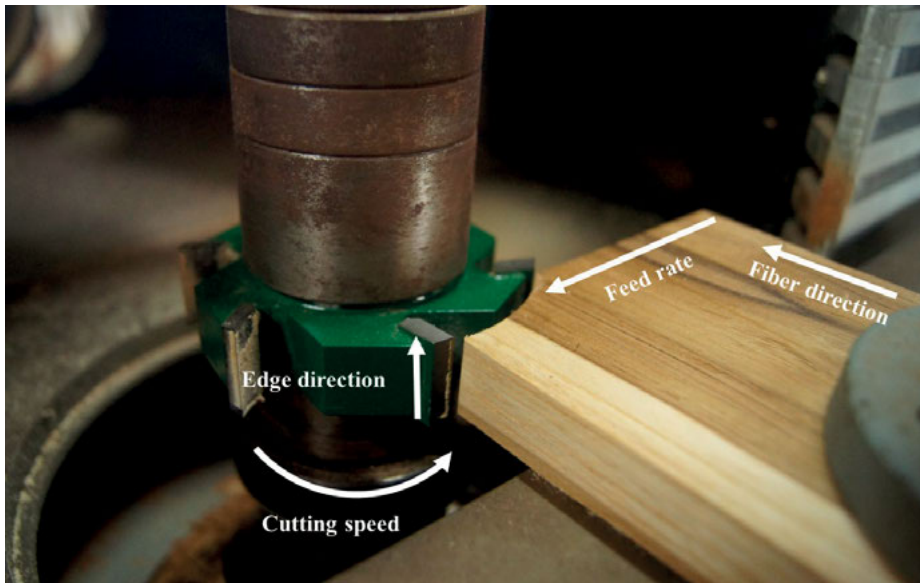
Fig. 7.5: Cutting family 90°–90°.

The physical property of the most commonly used wood in different wood segments is wood density. According to Stewart and Polak [13], the apparent density is one of the properties that provides more information on wood characteristics. In general, the larger the magnitude, the greater the shrinkage and the more difficult the work, and, in most cases, it increases the difficulty in drying.

Wood density is often directly associated with wood mechanical strength. It can also be associated with mechanical wood processing, and should lead to the maturity of its strength forces, that is, forces that exceed the internal mechanical strength of the material should be applied when cutting wood. Based on this principle, wood density becomes an important parameter for the choice of the cutting tool. Thus, characteristics such as tooth pitch, angles, and cutting tool material can range, according to wood density. Tab. 7.1 shows indications of angle of attack, according to density and moisture content of the wood to be processed.

The knowledge of the characteristic angles of cutting tools provides help to predict portions of the quality of the machined surface [16]. In Fig. 7.6, the basic angles of a circular saw teeth are outlined. It is important to emphasize that the nomenclature of the teeth angles of the tools ranges between several researchers. Therefore, knowing the definitions given to each angle is more important than knowing the nomenclature.

The free angle, or clearance (α), is a measure of the projections of the back of the tooth and the tangent on the tooth. On the other hand, the wedge (or tooth) angle (β) is a measure of the projections of the back and chest of the tooth. The angle of attack (γ) is the measure formed by the tool radius and the edge of the chest.

Tab. 7.1: Recommendations of exit angles as a function of cutting type and wood.

Cutting type	Wood type	Angle of attack
Longitudinal	Green wood with low basic density	20° to 25°
	Dry wood, medium and high specific mass	15° to 20°
Cross section	Green wood with low specific mass	15°
	Dry wood, medium and high specific mass	10°
	Pendulous cutting	5° to −5°

Adapted from [14].

Geometric center ⊗
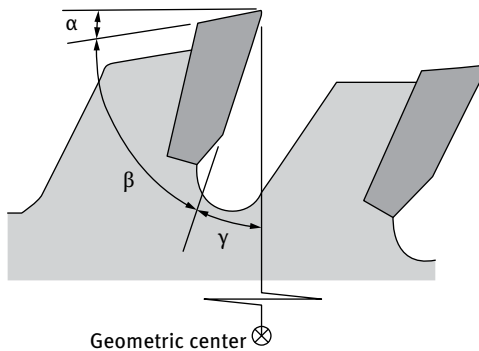
Fig. 7.6: Illustrative aspects of the basic angles of the teeth of a circular saw, where α = free angle, β = wedge angle, and γ = angle of attack. Source: [15], adapted by [7].

If the angle of attack (γ) ranges from −2° to 2°, a strong fiber compression occurs, requiring high machining efforts. The obtained surface is considered of low quality. The clearance (or free) angle (α) is necessary to reduce the friction between the back of the teeth and the newly processed surface. If friction has a strong magnitude, it may increase the cutting force required for processing wood, besides hampering chip output and even causing a reduction in surface quality. For most circular saw manufacturers, the ideal value for the clearance angle is close to 10° ($5° \leq \alpha \leq 15°$). The change in wedge angle (β) predicts tooth resistance against the attack on wood and is dependent on the type of material and methodology used in its manufacture. The lower the value of the wedge angle is, the lower is the effort needed to process wood. However, lower values tend to lead to wood precleavage and twisting, or tooth breakage. For most circular saw manufacturers, the minimum β value is 45°, based on the strength of the material used in its manufacture. In Brazil, almost all the material used in tooth manufacturing for circular saws used in the wood industry is the hard metal (HM), commonly called Widia.

7.2 Surface evaluation

When it comes to wood and wood composites machining, product qualification occurs by surface analysis and elements of quality definition. Silva, Braga, and Martins [17] showed that there are two research strands which conceptualize the quality of a machined surface:

(i)   The first group of researchers conceptualized the quality of processed wood only by normative values. Thus, this group uses mathematical parameters, such as the feed per tooth (f_z), or the depth of the cycloid arc (t). These elements can be expressed in marks per linear inch or millimeters. It is known that the higher the feed per tooth or the depth of the cycloid arc, the worse the quality of the processed surface.

(ii) Not only does the second group consider the parameters listed above, but also the presence of flaws on the wood surface. These flaws are usually generated in function of the wood structure by the presence of different types of cells and their different sizes and orientations.

In order to qualify the surface of the processed wood and wood composites, the methods used are described, emphasizing the peculiar characteristics of each one, stating the positive and negative aspects of their use.

7.2.1 Quality assessment by feed per tooth (f_z)

The feed per tooth (f_z) is represented by the distance between the depressions produced during the mechanical wood and wood composites processing (Fig. 7.7). It is observed that its formation is due to the circular movement of the tool (cutting speed),
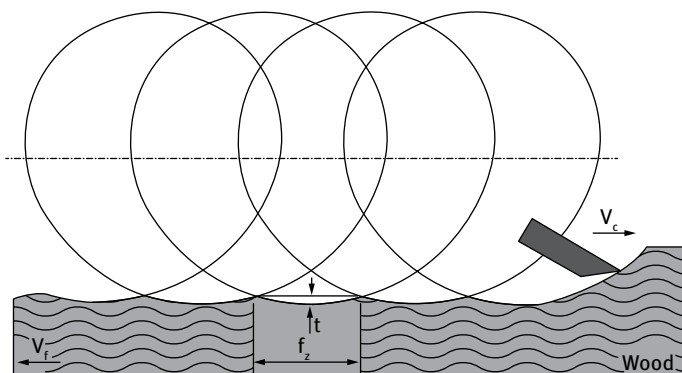
Fig. 7.7: Normative planing values, where f_z = feed per tooth, t = depth of the cycloid arc, V_c = cutting speed and V_f = feed rate. Source: [18], adapted by [7].

associated with the linear movement of the piece of wood or wood composites (feed rate). It is observed that the lower the magnitude is, the better is the quality of workmanship, a fact that is based on the need to rework after processing; that is, if there are high and distant ridges, sanding will be necessary, so that the surface is appropriate to receive finished products.

The feed per tooth can be obtained in two different forms. The first form is the calculated feed per tooth (calculated f_z), and the second, the measured feed per tooth (measured f_z). Equation (7.1) shows the form to determine the calculated feed per tooth:

$$f_{z,\text{ calculated}} = \frac{V_f}{n\,z},\qquad\qquad (7.1)$$

where:

$f_{z,\text{ calculated}}$	calculated feed per tooth, in mm;
V_f	piece feed rate, in mm min^{-1};
n	rotation of the tool holder axis, in min^{-1};
z	number of active teeth in the tool (dimensionless).

It is observed from equation (7.1) that all the elements that make up the calculated feed per tooth may be obtained during the mechanical processing, directly in the machine. Subsequently, with the aid of Tab. 7.2, we have the quality rating of the surfaces from different processings [19].

Tab. 7.2: Quality rating of workmanship for milling cutters, straightening and thicknessing, as a function of feed per tooth values (f_z).

Feed per tooth f_z (mm)	Surface quality
0.3 to 0.8	Fine
0.8 to 2.5	Medium
2.5 to 5.0	Coarse

Source: [19].

According to [20], it is possible to assign qualities to wood and wood composites, as a function of feed per tooth values, and assign different pieces obtained for different forms of use. Therefore, after processing, if the feed per tooth value is up to 1 mm, the pieces can be generally used in furniture manufacture. On the other hand, if the feed per tooth is higher than 1 mm and lower than 2.5 mm, the piece is indicated for use in floors and apparent structures. Pieces with feed per tooth values higher than 2.5 mm are suitable nonapparent structures and gates.

The advantage of using the calculated feed per tooth for classifying the surfaces of processed woods and wood composites is the ease in data acquisition, which is directly in the machine, and also its application in the equation. However, the drawback

has been the fact of not considering intrinsic wood variations affecting the elements of the equation and, consequently, the final calculated amount.

The measured feed per tooth is a variation in the calculated feed per tooth, since it is observed that it is not possible to control all the elements of equation (7.1), due to the electrical characteristics of the machine engine, by the manual action of the operator and especially the definition of the number of active teeth of the tool. Under these setting conditions, not all teeth leave their mark on the surface.

In order to obtain the measured feed per tooth, the distance between the marks left by the teeth should be measured directly in the processed wood piece or wood composites (Fig. 7.8). Another way for its determination is to launch a known distance $(1'' = 25.40\,\text{mm})$ from a brand and then count the number of marks until the end of this distance. With these values, it is possible to determine the average value of the distances between the marks.
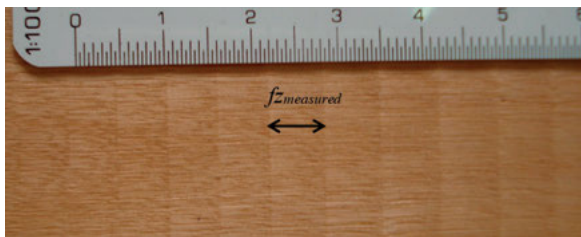
Fig. 7.8: Image of the feed per tooth measuring method $f_{z,\,measured}$.

However, the feed per tooth does not have the same size throughout the length of the processed surface. In Fig. 7.9, it is possible to observe the presence of defects in the wood, such as the presence of knots, which reduces, on average, 28 % the size of the measured feed per tooth. Performing the mean variation analysis, it is observed that, before the knot, f_z has a normal size while, in the knot, it decreases due to knot strength and, soon after, the knot increases due to the inertia of a force greater than the necessary to cut normal wood, and only then, does the feed per tooth stabilize again, at normal size. It is observed that at the edge of the knot there is a reduction of 0.36 mm to 0.26 mm in the feed per tooth value.

The feed per tooth is not visible at the top milling both wood as wood composite, as evidenced in Fig. 7.10.

The advantage of using the measured feed per tooth to characterize processed wood and wood composites surfaces is the ease in the actual acquisition of values only by images and simple measuring equipment. This process allows the inclusion of variations intrinsic to wood, since it is the surface as it presents itself, besides allowing us to know the variation of individual advances. In this case, it can function as a quality control of the work of different operators. However, the visualization of the

Fig. 7.9: Variation in the size of the feed per tooth measured due to the presence of a wood knot.

(a)   (b)
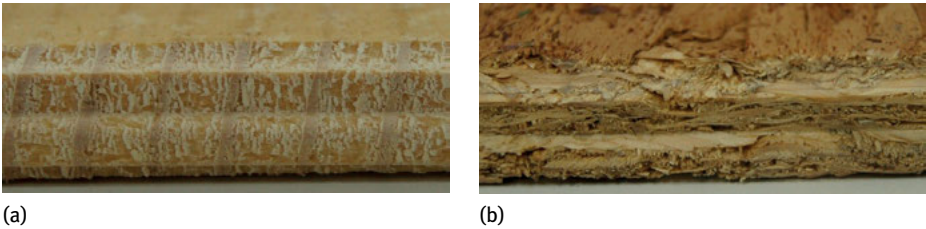
Fig. 7.10: Top milling in wood (a) and wood composites (b).

ridges with marks for setting the feed per tooth is difficult in most cases, damaging its measurement. In such cases, it is possible to use techniques such as the use of chalk or varnishes to enhance the ridges.

7.2.2 Quality assessment by the depth of the cycloid arc (*t*)

It is known that the depth of the cycloid arc (Fig. 7.9) is the mark left by the teeth of the tool. This parameter can be calculated according to equation (7.2):

$$t = \frac{f_z^2}{4D},$$
(7.2)

where:
t depth of the cycloid arc, in mm;
f_z feed per tooth, in mm;
D diameter of the cutting tool, in mm.

The advantage and disadvantage of using the depth of the cycloid arc, similar to the use of the calculated feed per tooth, are the ease of data acquisition and of not considering wood variations, respectively.

7.2.3 Quality assessment by visual analysis

The standard ASTM D 1666-11 [21] predicts a qualification methodology of machined surfaces in wood and wood composites whose principle is to consider the existing defects on the surfaces as generated by the attack of the cutting tool. Scores are assigned to these defects, due to the need of rework to obtain defect-free pieces (Tab. 7.3). Score 1 corresponds to the best surface quality; it has no defect. On the other hand, score 5 corresponds to the lowest quality, with a higher degree of defects. In order to facilitate qualifying agents, ASTM D 1666-87 [21] presents several photos exemplifying the qualities, according to the scores to be assigned.

Tab. 7.3: Scores assigned to each quality of the machined wood surface.

Scores	Quality of the machined wood surface	Classification of the flat surface
1	Surface free of any defects	Excellent
2	Presence of light to medium raised grain	Good
3	Presence of strong raised grain and light pullout	Regular
4	Presence of strong raised grain and light to medium pullout	Bad
5	Presence of strong pullout, independent of the presence of raised grain	Very bad

Source: [21].

Silva [7], working with the procedure of ASTM D-1666-87 [22], adapted the presented methodology. The author used three evaluators to conduct the evaluation of the processed surfaces. First, the scores were assigned by each evaluator alone. Subsequently, the evaluation was performed by two evaluators together and, finally, by the three evaluators together. The proposal is to seek a consensus in the evaluation of qualities. However, if a consensus were not reached, the calculation of the mean of the seven evaluations would be performed, with three isolated evaluations, three evaluations with two evaluators, and an evaluation with the three evaluators. This procedure, according to [7], allowed a reduction in the subjectivity of the evaluation of the processed surfaces.

On top milling it is possible to qualify the surface wood and wood composites when these are processed into high and low speeds as shown in Fig. 7.11.

The advantage in the qualification of processed surfaces by visual analysis is the speed of the method, besides allowing the evaluation to be performed across the processed surface, and not only in some sampling points. However, it is necessary to know defect patterns by the evaluators. Thus, this methodology requires constant training of evaluators, in order to reduce subjectivity and/or interference of the evaluator in surface quality.

(a)

(b)

(c)

(d)
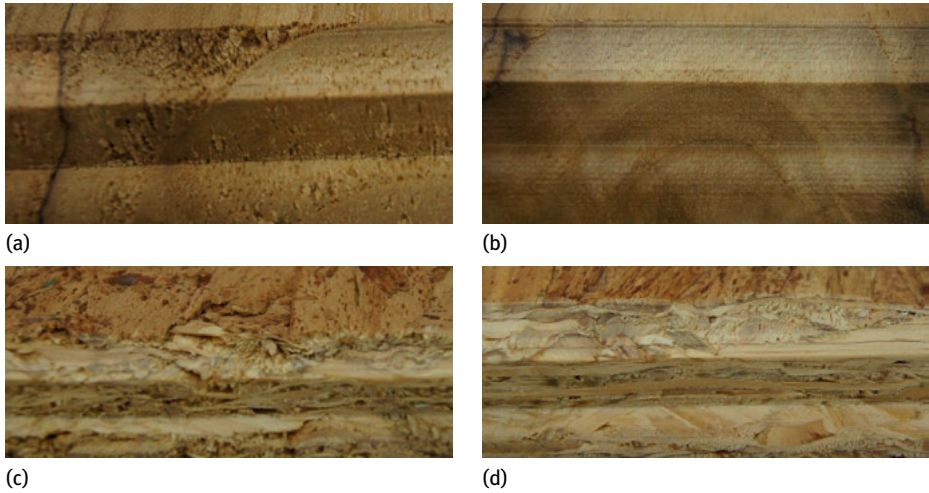
Fig. 7.11: Milling top wood with high (a) and low feed rate (b) and wood composites with high (c) and low feed rate (d).

7.2.4 Quality assessment by surface roughness

The rugosimeter is a device used to determine linear profiles. It measures vertical variations (topography) as a function of horizontal displacement in material surfaces. These devices were developed for evaluations in metal products. However, results observed by Silva et al. [23] showed (Fig. 7.12) that the rugosimeter can be used for scanning processed wood and wood composites surfaces.

Roughness parameters represent the shape of the mathematical expression between the vertical surface variation, expressed by peaks and valleys, and the horizontal displacement of the sensor (needle).

Fig. 7.12: Methodology for roughness measurement on wood surfaces.

The rugosimeter provides parameters such as "Ra", "Rt", "Rq", "Rz", "Ry", and "Sm". Silva et al. [17] analyzing *Eucalyptus grandis* wood, concluded that the roughness parameters "Ra" and "Rq" tend to increase as the feed rate increases. The minimum, medium and maximum values, as well as the standard deviation of the roughness parameters "Ra", "Rq", "Rz", "Ry", and "Sm" obtained by the above authors, are in Tab. 7.4. These authors found differences in the surface profiles of *Eucalyptus spp.* wood (Fig. 7.13).

Tab. 7.4: Minimum, medium, and maximum values, and standard deviation of different roughness parameters, for *Eucalyptus spp.* wood.

Values	Roughness parameters (µm)					
	Ra	Rq	Rz	Rt	Ry	Sm
Minimum	3.32	4.17	15.35	21.33	17.70	251.00
Medium	5.05	6.44	22.25	30.16	27.77	484.23
Maximum	8.39	11.40	33.65	51.55	47.72	1309.22
Standard deviation	1.27	1.73	4.47	6.64	6.31	213.01
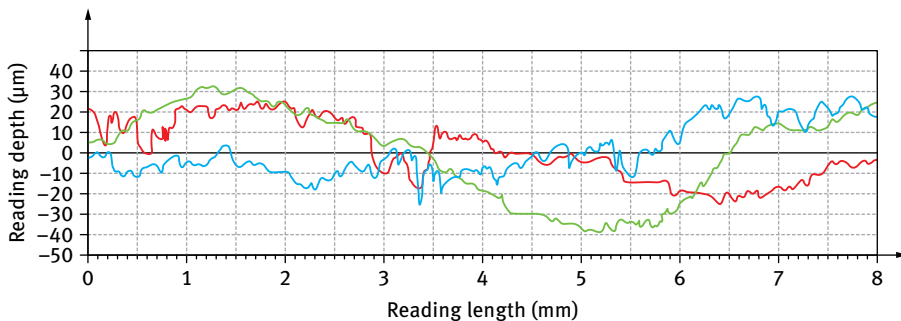
Fig. 7.13: Average roughness profiles of milled *Eucalyptus spp.* wood, with six teeth. The red curve represents a forward speed of 15 m min^{-1}, 10 000 rpm, $\alpha = 5°$, $\beta = 60°$, and $\gamma = 25°$. The blue curve represents a forward speed of 30 m min^{-1}, 6000 rpm, $\alpha = 5°$, $\beta = 60°$, and $\gamma = 25°$. The green curve represents a forward speed of 15 m min^{-1}, 10 000 rpm, $\alpha = 5°$, $\beta = 65°$, and $\gamma = 20°$.

The advantage in the qualification of processed surfaces by roughness is in the level of detail that is given to the surface, where variations in the micrometer range are evaluated and can lead to changes in quality. However, the slowness of the process with an emphasis on the small sample region is one of the setbacks of this methodology. It is observed that a specimen requires multiple readings that are carried out at small lengths (typically 0.8 mm). Another limiting factor is the presence of large depressions that go beyond the established "cut-off" and saturates the reading.

7.2.5 Quality assessment by sunset laser

According to Rabelo [24], when using laser light as a light source more information about the material under study can be obtained. Among all the characteristics of the laser, the one which allows its use in the sunset laser technique is the light ability to be addressable and concentrated [25], which enables its use in the qualification of biological materials. According to Soragi [26], laser has been gaining ground as a methodology for the qualification of surfaces of biological materials, since it is a non-destructive technique.

Silva et al. [28] used laser as a tool to identify and classify the texture of the surface of three native wood species, and observed that laser is efficient in separating two texture extremes: coarse and fine texture, represented, respectively, by *Bowdichia virgilioides* ("sucupira") and *Balfouro dendronriedelianum* ("pau-marfim"). For the average texture, the proposed sorting process was not able to differentiate medium texture from coarse texture.

The use of laser light for the determination of grain orientation in wood has been observed in several studies [28–31].

Souza et al. [32] used the sunset laser technique in the evaluation of the rupture zone in flexural tests and found that, when applied to laser light, the rupture generated in the specimen was better visualized.

Silva et al. [23] evaluated the capture technique of *Eucalyptus sp.* wood surface images by low laser light intensities applied in different angles. The images were processed, based on the interference patterns formed on the surface of the material, using the shadows formed by wood lighting. The results were compared from different angles and the spectral analysis was conducted to characterize the frequencies in each profile. The authors concluded that lighting approximately parallel to the wood surface presented the most well-defined images, enabling the visualization of the ridges, and relating them to the different feed per tooth (f_z) values. Therefore, the potential of this technique was proven to be viable, requiring development of its improvement and robustness, as well as image treatments for its measurement. The periodic irregularities of the illuminated surface result in shadow patterns that were treated by processing techniques and image and numerical analyses, compared with the desired parameters.

Andrade [33] suggested that the sunset laser technique could be used to qualify flat surfaces, as an alternative to methodologies using visual evaluation and feed per tooth. In this study, the author found a high ratio between the established qualification methodologies and the sunset laser technique.
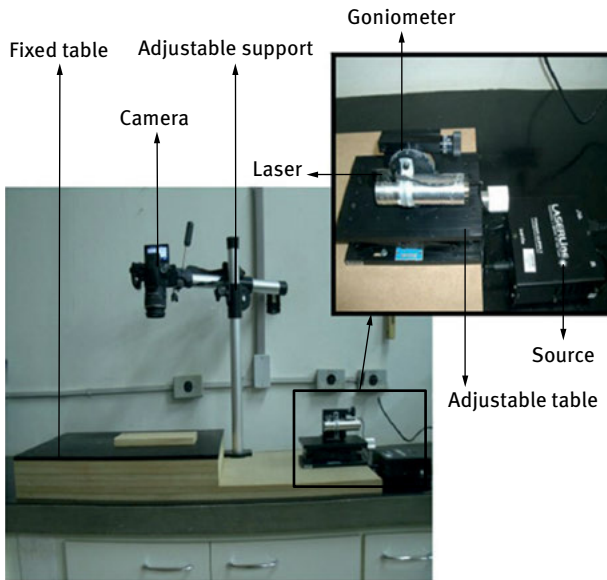
Fig. 7.14: Setup for the acquisition of images by the sunset laser technique. Source: [33].

The sunset laser technique consists in lighting with the aid of a low energy laser light source on the flat surface. The laser light is positioned on the surface with a 3° inclination in a totally dark environment, where images are made using a high-resolution camera (Fig. 7.14).

After obtaining the images, they are processed in free software (e.g. ImageJ). Image processing is done primarily transforming the RGB color images into 8 bit images. Subsequently, binarization is performed for pixel amplitudes that range between 0 and 40 (Fig. 7.15).

Three 450×450 pixel polygons are launched on the processed images, and the defect area within these polygons is calculated. Two polygons are positioned in the image distant in 150 pixels of each end. The last polygon is launched in the center of the image (Fig. 7.16).

As advantages of the use of the sunset laser technique, it is possible to mention the low investment for the acquisition of equipment and supplies, besides the possibility to use free software for image analysis. However, like any new analysis technique, it requires calibration with other techniques already conceptualized, such as vusual analysis [21]. There is also a great expenditure of time necessary for the acquisition and processing of images.
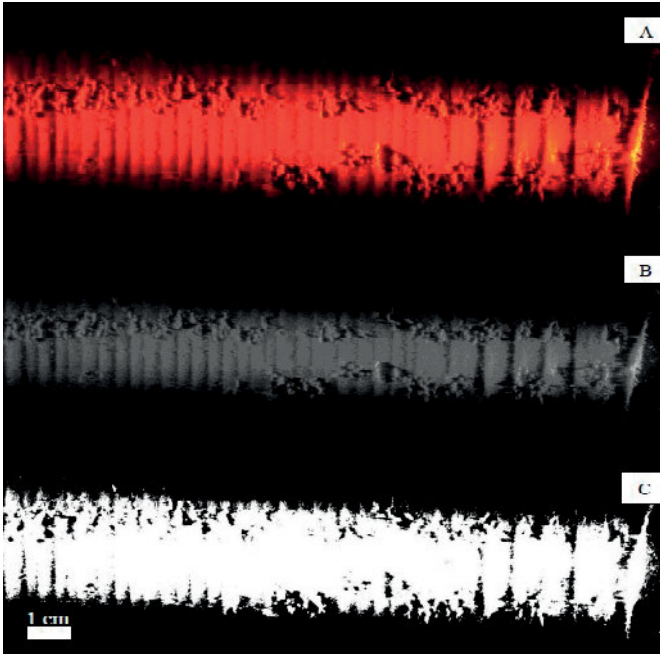
Fig. 7.15: Images of surfaces illuminated with sunset laser; (A) original image, RGB color format, (B) image in grayscale (8 bit), and (C) binarized image. Source: [33].
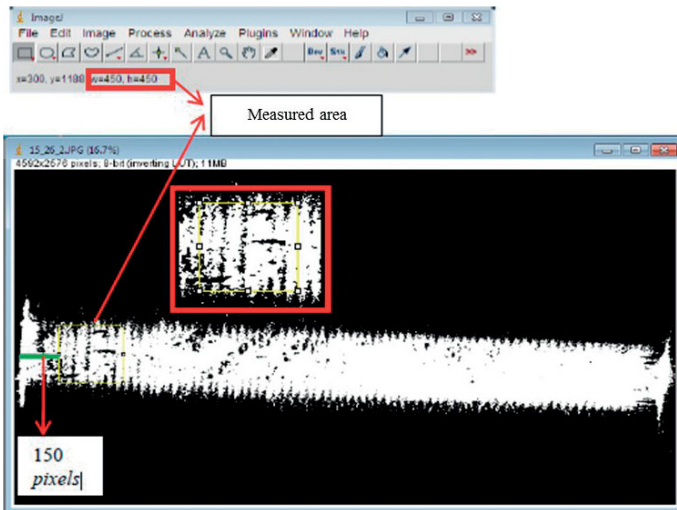
Fig. 7.16: Demonstration of the area to be analyzed. Source: [33].

References

[1]   Tsoumis G. Science and technology of wood: structure, properties, utilization. New York, VN: Reinold; 1991.

[2]   Haygreen JG, Bowyer JL. Forest products and wood science. 2nd edition. Ames: Iowa State University; 1989.

[3]   Browning BL. The chemistry of wood. New York: Interscience Publishers; 1963. 689 p., volumes I and II.

[4]   Panshin AJ, De Zeeuw C. Textbook of wood technology. 4th edition. New York: McGraw-Hill; 1980. 722 p.

[5]   Esau K. Anatomia das plantas com sementes. São Paulo: Edgard Blucher; 1993.

[6]   Downes GM, Hudson IL, Raymond CA, Dean GH, Michell AJ, Schimleck LR, Evans R, Muneri A. Sampling plantation eucalyptus for wood and fibre properties. Collingwood: CSIRO; 1997.

[7]   Silva JRM. Relações da usinabilidade e aderência do verniz com as propriedades fundamentais do Eucalyptus Grandis Hill Ex. Maiden [Tese (Doutorado em Engenharia Florestal)]. Curitiba: Universidade Federal do Paraná; 2002. 179 p.

[8]   Burdurlu E, Usta U, Ulupinar M, Aksu B, Erarslan T. The Effect of the Number of Blades and the Grain Size of Abrasives in Planing and Sanding on the Surface Roughness of European Black Pine and Lombardy Poplar. Turk J Agric For. 2005; 29: 315–321.

[9]   Kilic M, Hiziroglu S, Burdurlu E. Effect of machining on surface roughness of wood. Building and Environment. 2006; 1: 1074–1078.

[10] Martins SA, Ferraz AM, Santos CMT, Del Menezzi CHS, Souza MR. Efeito da usinagem na rugosidade da superfície da madeira de Eucalyptus benthamii. Floresta e Ambiente. 2011; 18(2): 135–143.

[11] McKenzie WM. Fundamental aspects of the wood cutting process. Forest Products J Madison: 1960; 10(9): 447–456.

[12] Silva JC, Matoa JLM, Oliveira JTS, Evangelista WV. Influência da idade e da posição radial na flexão estática da madeira de Eucalyptus grandis Hill ex. Maiden. Revista Árvore. 2005; 29(5): 795–799.

[13] Stewart HA, Polak DJ. Relating specifc gravity and mechanical properties of hardwoods to maching defects. Forest Products J Medison. 1974; 35(10): 69–72.

[14] Gonçalves MTT. Processamento da madeira. Bauru: SP; 2000.

[15] Freud. Freud Catalogo generale. 18th ed. Tavagnacco (Udine) Italia; Pozzo s.p.a.; 1998. 207 p.

[16] Bonduelle A. Usinagem, qualidade e custo. Revista da Madeira Curitiba. 2001; 61: 82–86.

[17] Silva, JRM, Braga PPC, Martins M. Identificação de parâmetros de rugosidade para qualificação de pisos de Eucalyptus grandis. Revista da Madeira Curitiba. 2008 [cited 2014 Nov 10]; 65. Available from: http://remade.com.br/br/artigos_tecnicos.php?sub=63&categoria=Esp% E9cies&subcategoria=Eucalipto.

[18] Weissenstein C. Usinagem, condições da ferramenta decide bom acabamento. Revista da Madeira Curitiba. 2000; 57: 30–32.

[19] Serviço Nacional de Aprendizagem Industrial. Acabador de móveis. Ubá: CFP/JAGS; 1995.

[20] Leitz. Das leitz lexikon. 3rd edition. Unterschneidheim; 2001.

[21] American Society for Testing and Materials. ASTM D 1666-11: standard method for conducting machining tests of wood and wood base materials. Philaldelphia; 2011. 20 p.

[22] American Society for Testing and Materials. ASTM D1666-11 standard method for conducting machining tests of wood and wood base materials (reapproved 1994). Philaldelphia; 1995. pp. 226–245.

[23] Silva JRM, et al. A utilização de rugosímetro na qualificação de superfícies usinadas em madeiras de Eucalyptus sp. In: Encontro Brasileiro em Madeiras e em Estruturas de Madeira 10. São Pedro: Anais, EBRAMEN; 2006. 1 CD-ROM.

[24] Rabelo GF. Avaliação da aplicação do "speckle" dinâmico no monitoramento da qualidade da laranja [Tese (Doutorado em Engenharia Agrícola)]. Campinas: Universidade Estadual de Campinas; 2000. 149 p.

[25] Hecht E. Optics 4. New York, PA: Wesley; 2001.

[26] Soragi LC. Qualidade de superfícies usinadas em madeira de Toona ciliata M. Roem. Lavras, UFLA; 2009.

[27] Faria RO, et al. Reliability of wood grain orientation measurements using laser illumination. Biosys Eng Lon. 2008; 100(4): 479–483.

[28] Silva MR, et al. Interação da luz laser para a avaliação da textura de madeiras nativas e de Eucalyptusgrandis W. Hill exMaiden laser light interaction for texture evaluation of native woods and Eucalyptus grandis W. Hill exMaiden. Ciência Florestal Santa Maria. 2005; 15(2): 167–175.

[29] Hu C, Tanaka C, Ohtani T. Online determination of the grain angle using ellipse analysis of the laser light scattering pattern image. J Wood Science London. 2004; 50(4): 321–326.

[30] Lowery DP. A spiral grain classification system and its application. Forest Products J Madison. 1966; 16(1): 47–50.

[31] Noskowiak AF. Spiral grain in treesda review. Forest Products J Madison. 1963; 13: 266–275.

[32] Souza TM, et al. Non-destructive technology associating PIV and Sunset laser to create wood deformation maps and predict failure. Biosys Eng Lon. 2014; 126: 109–116.

[33] Andrade ACA. Sunset laser na análise de deifeitos em madeiras usinadas [Dissertação (Mestrado em Ciência e Tecnologia da Madeira)]. Lavras: Universidade Federal de Lavras; 2015.

Further reading

Harrington JJ. Hierarchical modelling of softwood hygro-elastic properties. Christchurch, 2002. 296 f. Tese (Doctor of Philosophy) University of Canterbury, Christchurch; 2002.

Hoadley, RB. Understanding Wood. Newtown, CT: Taunton Press; 1980.

Weing A. Oberflächenqualität. Werkzeug: Präsentation Hydrotechnik; 2000. 1 CD-ROM.

Jorge Manuel Martins, Cristina Coelho, João Pereira,
João Macias Ferra, and Luísa Carvalho

8 Strategies to reduce formaldehyde emissions from wood-based panels: Impact on physico-mechanical properties and machinability

Abstract: Formaldehyde is a common organic compound used as raw-material in several industrial applications, namely in urea-formaldehyde (UF), melamine-urea-formaldehyde (MUF) and phenol-formaldehyde resin (PF) production. These resins have been used in the manufacture of wood-based panels for decades, playing a central role within their production and properties. Since the reclassification of formaldehyde as "carcinogenic to humans" by the International Agency for Research on Cancer (IARC) in 2004, several efforts have been made by industry to reduce formaldehyde in wood-based panels. New product classes based on formaldehyde emission emerged and different world regions have established their own classifications, reference methods, and standards, for example CARB in California, F**** in Japan, and E1Plus in Europe.

Reduction in the F/U molar ratio has been a strategy adopted in the last decades to decrease formaldehyde emission. However, this reduction decreases the reactivity of UF resins. Another strategy is the use of scavengers. Natural or bio-based substances such as pozzolan, tannins, charcoal, starch, chitosan, and chemical compounds such as as primary and secondary amines, sodium sulfites, borax, and ammonium phosphates have been tested. Commercial formaldehyde scavengers are available on the market, usually based on amino compounds, polyalcohols, and other compounds. However, in certain cases they penalize physico-mechanical properties and have adverse effects such as discoloration of wood and formaldehyde reemission. Furthermore, the abrasive characteristics of formaldehyde scavengers could affect the machinability of wood-based panels. It is known that substances such as starch, added as fillers to the resin in plywood production, increase tool wear.

In this chapter, a review of several formaldehyde test methods and release classes, as well as a comparison of results obtained at our laboratory (chamber, gas analysis, desiccators, and perforator methods) for particleboard produced with low formaldehyde emission (UF and MUF) resins are presented. An overview of the use of formaldehyde scavengers in wood-based panels is presented, as well as the latest development achieved by our team. The performance of several scavengers, namely sodium metabisulfite, ammonium bisulfite, and urea, is assessed through the resulting physico-mechanical properties and formaldehyde emission (perforator, desiccators, and gas analysis). The tested scavengers showed distinct performances under different emission testing conditions, which were interpreted in terms of the sta-

bility of the formed chemical compounds. The impact of the addition of formaldehyde scavengers on machinability is also addressed in a few case studies.

Keywords: formaldehyde emission, machinability, formaldehyde scavenger

8.1 Strategies to reduce formaldehyde emissions from wood-based panels

8.1.1 The concern about formaldehyde and current status

Formaldehyde is a ubiquitous compound in the environment [1]. Being a simple, one-carbon molecule that is rapidly metabolized, it is endogenously produced, and is also formed through the metabolism of many xenobiotic agents [2]. It occurs in most life forms, including humans, and has been detected in indoor and outdoor air; in treated drinking water, bottled drinking water, surface water, and groundwater; on land and in the soil; and in food [3].

In outdoor air, formaldehyde is present as a result of its formation from the combustion of organic materials (e.g. in automobiles, forest fires, and power plants), its formation from the breakdown of hydrocarbons in the air, and releases from industrial facilities. Sources of formaldehyde in the home include building materials, smoking, household products, and the use of unvented fuel-burning appliances like gas stoves or kerosene space heaters. Formaldehyde, by itself or in combination with other chemicals, serves a number of purposes in manufactured products. Formaldehyde is produced worldwide on a large scale, and it is used as a chemical feedstock in several industrial applications, namely for the production of formaldehyde-based adhesives for wood and wood composites, as UF, melamine-formaldehyde (MF), phenol-formaldehyde (PF), phenol-resorcinol-formaldehyde (PRF). It is also used to add permanent-press qualities to clothing and draperies, as a component of glues and adhesives, and as a preservative in some paints and coating products.

In homes, the most significant sources of formaldehyde are likely to be pressed wood products made using adhesives that contain urea-formaldehyde (UF) resins. Pressed wood products made for indoor use include: particleboard (used as subflooring and shelving and in cabinetry and furniture); hardwood plywood paneling (used for decorative wall covering and used in cabinets and furniture); and medium density fiberboard (used for drawer fronts, cabinets, and furniture tops). Medium density fiberboard contains a higher resin-to-wood ratio than any other UF pressed wood product and is generally recognized as being the highest formaldehyde-emitting pressed wood product.

Formaldehyde is toxic by inhalation, ingestion, and skin absorption causing nasal and eye irritation at higher concentrations. The first considerations about indoor air quality and formaldehyde emissions happened in the end of 1970s, during the en-

ergy crisis due to building insulation. The encouragement of the insulation of houses to avoid additional energy consumption has reduced the air exchange with outside, reducing the ventilation rates, and consequently entrapping the gaseous pollutants inside homes. This situation led to an increase of some health problems related to the exposure to formaldehyde by inhalation. "Sick building dyndrome" (SBS) and "building related illness" (BRI) are terminologies which have become widespread since then.

Since 2006 formaldehyde is classified as "carcinogen to humans (Group 1)" by the IARC (International Agency for Research on Cancer). On December 20, 2013 the EU REACH Committee adopted a decision to reclassify formaldehyde as a category 1B carcinogen "presumed to have carcinogenic potential for humans, classification is largely based on animal evidence". The current EPA classification is B1: "probable human carcinogen, based on limited evidence in humans, and sufficient evidence in animals". On July 7, 2010, President Obama signed the Formaldehyde Standards for Composite Wood Products Act CARB formaldehyde emission limits Phase II for composite wood products, which are in force since January 2013.

Formaldehyde emissions have become an important issue in public opinion. Tab. 8.1 presents the occupational exposure limits (OELs) in several countries.

Since 1965, the wood panel industry has reduced consecutively formaldehyde emission from its products (Fig. 8.1).

In Fig. 8.2, the values of European formaldehyde classes E3, E2, and E1 before and after 1992 are presented.

After 1992 formaldehyde emission has been decreased and attained almost the values of natural wood.

8.1.2 Current test methods for determining formaldehyde emissions

8.1.2.1 Introduction

For the determination of formaldehyde emission in wood-based products, several methods and standards have emerged in Europe, the United States, and Japan. Each method measures a slightly different emission characteristic and frequently produces results in different and noninterchangeable units [4]. This proliferation of test methods and incomparable results often creates confusion among government regulators, consumers, and industry personnel [4]. Furthermore, the formaldehyde emission values in the 1970s and 1980s were substantially higher, and therefore the test methods developed need to be adapted and improved to the current emission ranges. New test methods have been proposed in order to comply with the new requirements of higher accuracy, lower detection limits, speed, and reliability.

The release of formaldehyde depends on internal and external factors. The internal factors include the type of wood and resin employed, parameters and operating conditions in panel production, and panel age. External factors are temperature, air

Tab. 8.1: Occupational exposure limits (OELs) for formaldehyde [2].

	TWA (8 h)		STEL (5 min)		References
	(ppm)	(mg/m^3)	(ppm)	(mg/m^3)	
EU countries					
Austria	0.5	0.6	0.5	0.6	GVK (2011)
Belgium			0.3	0.38	Belgium (2014)
Denmark	0.3	0.4	0.3	0.4	BEK (2011)
Finland	0.3	0.37	1	1.2	Finland (2012)
France	0.5		1		INRS (2012)
Germany (AGS)	0.3	0.37	0.6	0.74	BAUA (2006)
Germany (DFG)	0.3	0.37	0.6	0.74	DFG(2015)
Hungary		0.6		0.6	Hungary(2000)
Ireland	2	2.5	2	2.5	HSA (2011)
Latvia		0.5			n.a.
Norway	0.5	0.6	1	1.2	Norway (2011)
Poland		0.5		1	Poland(2002)
Spain			0.3	0.37	INSHT (2010)
Sweden	0.3	0.37	0.6	0.74	SWEA (2011)
The Netherlands		0.15		0.5	NED (2007)
United Kingdom	2	2.5	2	2.5	HSE (2011)
Non EU countries					
Australia	1	1.2	2	2.5	Safe Work Australia (2011)
Canada (Ontario)			1		Ontario Ministry of Labour (2013)
Canada (Québec)			2	3	IRSST(2010)
China			0.5		n.a.
Japan	0.1	0.12			JSOH (2015)
New Zealand	0.5		1		HS(2013)
Singapore			0.3	0.37	n.a.
South Korea	0.5	0.75	1	1.5	n.a.
Switzerland	0.3	0.37	0.6	0.74	SUVA (2015)
USA (NIOSH)	0.016		0.1		NIOSH (2007)
USA (OSHA)	0.75		2		OSHA (2006)

exchange rate, and the total panel area in relation to the total volume of the space in which the panels are placed [4].

Test methods for the determination of formaldehyde emission should take into account the factors listed above, in order to be reliable and reproducible.

The existing methods can be divided by two main principles: measurable emission (the really emitted amount of formaldehyde under the test conditions) and the emittable potential of formaldehyde in the panel (the emitted (free) formaldehyde is determined without considering if that quantity may be released or not, and in how much time) [5].

Tab. 8.2 summarizes the most important test methods and related standards for the determination of formaldehyde from wood-based panels.
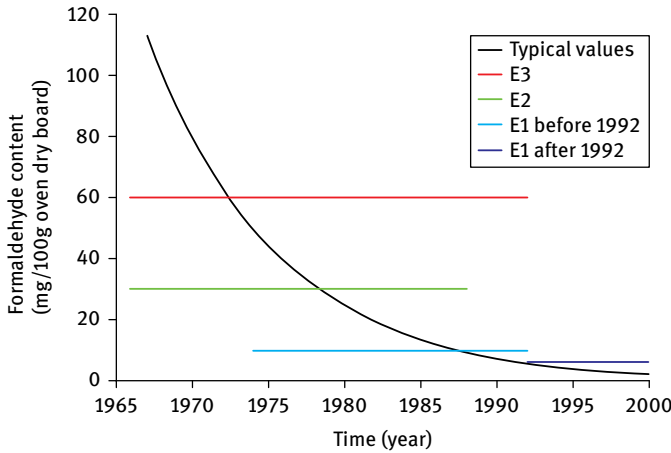
Fig. 8.1: Evolution of formaldehyde emission in wood-based panels.
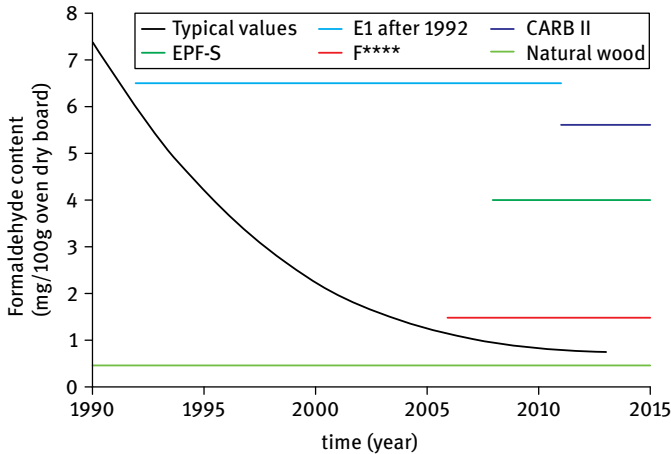
Fig. 8.2: European formaldehyde classes E3, E2, E1 before and after 1992.

Tab. 8.2: Standards and test methods for the determination of formaldehyde
from wood-based panels [6, 7].

Test method	Standard, standard draft, or method name
Chamber	ASTM E 1333, ASTM D 6007, EN 717-1, JIS A 1901 and 1911, ISO 12460-1 and 2
Gas analysis	EN 717-2, recently superseded by ISO 12460-3
Flask method	EN 717-3, method AWPA
Desiccator	ASTM D 5582, ISO 12460-4, JIS A 1460, JAS MAFF 235, JAS 233, AS/NZS 4266.16
Perforator	EN 120, recently superseded by ISO 12460-5
Other	Field and Laboratory Emission Cell "FLEC", Dynamic Microchamber "DMC"

8.1.2.2 Perforator method

The perforator method, according to EN 120 (recently superseded by EN ISO 12460-5) [8] (Fig. 8.3) measures the formaldehyde content of wood-based panels. This test is the most popular in Europe for measuring formaldehyde content in particleboard and MDF. The standard EN 13986 indicates this method for unfaced particleboard, OSB, MDF, and flaxboards. This method is quick and expeditious, being more indicated to daily factory production control. The formaldehyde is extracted from test pieces (110 g of 25×25 mm specimens) by means of boiling toluene for 2 h and then transferring it into distilled or demineralized water. The formaldehyde content of this aqueous solution is determined photometrically by the acetylacetone method. This method is based in the Handtzsch reaction, which envolves the cyclization of 2,4-pentadione, ammonium acetate, and formaldehyde to form DDL (dihydropyridine 3,5 diacetyl-1,4-dihydrolutidine), which presents a maximum absorbance at 412 nm.

The disadvantage of this method is the environmental impact of the toluene emission and residues. The results are expressed in mg/100 g oven dry board. The perforator values for particleboards, OSB, and MDF are applied to wood-based panels

Fig. 8.3: Perforator method (EN 120).

conditioned to reference moisture content (6.5%). For different moisture contents, correction factors, calculated by an equation stated in the specifications standards for each type of wood-based panel, are used. This correction factor is questionable, as it depends upon other factors other than the moisture content of boards [9]. The accuracy of this method for values below 4 mg/100 g oven dry board has been very discussed. A similar method was established by ISO 12460-5.

8.1.2.3 Chamber method

This method evaluates the real emission of formaldehyde from a product under typical indoor conditions in real life and over a defined time scale in a climate-controlled chamber. The formaldehyde concentration in the air inside the chamber is measured.

The European standard EN 717-1, chamber method [10] presents three volume options: $> 12\,m^3$, $1\,m^3$, and 225 l (Fig. 8.4: $1\,m^3$). The operating conditions are: temperature of $(23 \pm 0.5)\,°C$ and relative humidity of $(45 \pm 3)\,\%$. The air exchange rate is 1/h. In a

Fig. 8.4: Chamber method (EN 717-1: $1\,m^3$).

chamber of $1\,m^3$ (Fig. 8.4) two test pieces of $500 \times 500 \times$ board thickness (mm) were placed. Formaldehyde emitted from the test pieces mixes with the air in the chamber, which is sampled at least twice a day. The formaldehyde concentration is determined by drawing air from the outlet of chamber through two gas washing bottles containing water, which absorbs the formaldehyde. The concentration of formaldehyde in the chamber atmosphere is calculated from the concentration in the water in the gas washing bottles and the volume of the sampled air. It is expressed in mg/m^3. Sampling is periodically continued until the formaldehyde concentration in the chamber reaches the steady-state, which requires at least 11 days (EN 717-1). Each of the standards specifies a different method for determining when a steady-state condition is achieved. All, however, accept a change in formaldehyde emission of less than 5 % over a given period as representing a quasi-steady-state condition. In addition, all the standards propose that the test is stopped after 28 days, even if the steady-state condition is not reached [11].

The American standard ASTM E 1333 presents a large test chamber that aims to imitate the conditions of a livingroom of $22\,m^2$. The conditions are slightly different from the European standard: temperature of $(25 \pm 1)\,°C$, $(50 \pm 4)\,\%$ of relative humidity and air exchange of 0.5/h. A smaller chamber $(0.02\,a\,1\,m^3)$ is presented in the standard ASTM D 6007. The CARB (Californian Air Resources Boards) recently approved regulations that require the use of these chambers for the qualifying tests. The International Organization for Standardization (ISO) presents as a reference method the standard ISO/FDIS 12460-1 $(1\,m^3)$ and a derived method (ISO/DIS 12460-2).

8.1.2.4 Gas analysis

The gas analysis (EN 717-2, recently superseded by EN ISO 12460-3) [12] determines formaldehyde release at accelerated conditions: temperature of 60 °C and within a period of 4 hours. In this method, a test piece with dimensions of $400 \times 50 \times$ board thickness (mm) and edges sealed is placed in a closed chamber at $(60 \pm 0.5)\,°C$ with a relative humidity lower than 3 %, an airflow of $(60 \pm 3)\,l/h$, and under an overpressure of 1000–1200 Pa. Formaldehyde released from test piece is continually drawn from the chamber and passes though gas wash bottles containing water that absorbs formaldehyde (EN 717-2) (Fig. 8.5). The formaldehyde is determined at hourly intervals of up to 4 h. Every hour, the air is automatically led into one of a series of pairs of wash bottles. At the end of test, the formaldehyde release is calculated from the formaldehyde concentration, the sampling time, and exposed area of the test piece expressed in $mg\,m^2\,h$. The standard EN 13986 indicates this method for faced and coated overlaid or veneered wood-based panels.

In this method, as well as the other European methods, the concentration of formaldehyde is determined photometrically (UV/Vis spectrometer) using the acetylacetone method.

Fig. 8.5: Gas analysis method (EN 717-2).

8.1.2.5 Desiccator method

The desiccator method, defined in the Japanese standard JIS A 1460 [13] is one of the most economical methods, but it has a drawback. The test pieces are conditioned under standard conditions at a temperature of (20 ± 2) °C and a relative humidity of (65 ± 5) % until they have reached constant mass, which can take one week. Test pieces are cut into rectangles of 150×50 mm. A number of test pieces, corresponding as close as possible to 1800 cm^2 total surface area (ends, sides, and faces), are attached to a supporting metal and placed on a stainless steel wire net above a crystallizing dish containing water inside the desiccator with a nominal dimension of 240 mm (Fig. 8.6). The lid is placed on the desiccators, and the samples are sealed inside for 24 h at

Fig. 8.6: Desiccator method (Japanese standard JIS A 1460).

$(20 \pm 1)\,°C$. The emitted formaldehyde is absorbed by the water in the crystallizing dish. The concentration of formaldehyde in the water is determined by a photometric method, using the acetylacetone method, but the reaction conditions and reagents quantities are different from the European standards EN 120, EN 717-1, and EN 717-2. The emission of formaldehyde is expressed in [mg/l].

ASTM D 5582 presents a desiccator method with some differences: the desiccator diameter (250 mm) and the procedure duration (2 h). Other standards that are based on the same principle are JAS 233 and JAS 235. A recent harmonized standard was adopted by the International Standardization Organization, as ISO/CD 12460-4.

8.1.2.6 Flask method

The flask method as described in EN 717-3 [14] is a modified version of the flask method developed at the Fraunhofer Institute for Wood Research WKI by Roffael in 1975. A slight modified version of this method was published as EN 717-3. It is a quick method suitable for internal quality control in production lines of wood-based panels. This method consists in suspending test pieces with a total mass of 20 g in a closed container (flask), containing water (50 ml) and maintained at a $(40 \pm 1)\,°C$ during 3 h. The formaldehyde content in water is determined photometrically by the acetylacetone method and expressed in mg/kg dry board. The AWPA (American Wood Protection Association) presents a similar method, with the same principle but with different dimensions of the flask. This method does not have great acceptance by the market, nor is it significantly used at the industrial or academic level. However, a similar method is used in the automotive industry.

8.1.2.7 Other methods

There are other methods, but they are used mostly in academic or testing laboratories. One of the examples is the DMC (dynamic microchamber) used in the United States in factory control quality, but it has not yet been accepted as standard. This method utilizes a combination of a small chamber and electrochemical sensors. It has the advantage of a short test duration and preconditioning. Another example is the FLEC (field and laboratory emission cell) first implemented in Scandinavia. In this device, a controlled purified air flow enters the cell and passes through the testing material. The outlet air passes through adsorption tubes, which are connected to a thermal desorption and analysed in GC/MS or GC/FID system. The great advantage is that it it is a transportable emission cell for mobile application [15].

8.1.3 Formaldehyde emission classes

In recent years, national regulations for formaldehyde were established and/or refor-mulated in some countries limiting the formaldehyde emission from wood-based pan-els. The classification of wood-based panels according to formaldehyde emission is established in the specification standards of each product. The harmonized European standard EN 13986 (wood-based panels for use in construction) classifies formalde-hyde emission into two classes: E1 or E2 (Tab. 8.3). Internal discussions within the Eu-ropean wood-based panel associations led EPF (European Panel Federation) to launch its own formaldehyde standard EPF-S, which corresponds to a perforator value below 4 mg/100 g oven dry wood for PB and 5 mg/100 g oven dry wood for MDF (thickness > 8 mm). Driven by IKEA (IOSMAT 0003), an equivalent class with half E1 formalde-hyde emission limits was also introduced: the so-called E0 (or E0.5). Although this class was not yet officially recognized by CEN, a new class "E1Plus" was launched in the revised version of EN 13986, Annex B; Tab. B.3. This class can be achieved for un-faced, coated, overlaid, or veneered wood-based panels. This class indicates the limit value of $0.08 \, \text{mg/m}^3$ (corresponding to 0.065 ppm). The group EDGS (Expert Group on Dangerous Substances) from the European Commission proposed a harmonized classification that combines the French and German systems from the AgBB (Commit-tee for Health-related Evaluation of Building Products). In case of formaldehyde, six classes (f1–f6) with threshold limits of < 10, < 60, < 80, < 100, < 120, and > 120 μg/m^3 were defined in a way as not to violate the established rules as classes E1 (emission $< 0.124 \, \text{mg/m}^3$ air, defined in EN 13986), the new class E1Plus, whose limit is 80 μg/m^3, and the Royal Decree from Belgium and AgBB that establishes a limit of 100 μg/m^3. The European Panel Federation (EPF) announced a new pan-European Project called "Compulsory E1", which seeks to ensure common legislation throughout Europe for the production, import, and marketing of wood-based panels and of products made from them at the E1 level (or below). Since 2007, all EPF members have agreed to pro-duce particleboard [16].

In Japan, more strict limits are defined in standards JIS A 5908 and 5905 as, by descending order F**, F*** and F****. The F** is more or less equivalent to the Euro-pean E1 class, while F*** and F**** are much lower. The emission of F**** is close to the emission of solid untreated wood, between 0.5 and 2 mg/100 g [4].

In the United States, ANSI A208.1 and 2 refer to the limits for formaldehyde emission presented in Tab. 8.3. More recently, CARB (California Air Resources Board) established more stringent formaldehyde limits for wood-based panels, being nowa-days the reference for the wood-based panels market. Phase 1 limits are roughly equivalent to the E1 (and F**) class, while phase 2 limits are similar to F***. These regulations state that, beyond the compliance of those emission limits, wood-based panels and finishing goods for sale or used in California must also be certified by a CARB-approved third party certification laboratory, unless they are approved ultra low emission formaldehyde (ULEF) or no added formaldehyde (NAF) products. NAF

and ULEF products must demonstrate a 90 % or better compliance with a 0.04 ppm (ASTM E1333) limit. Formaldehyde emissions are also taken into account in the classification of green buildings, as the Building Research Establishment Environmental Assessment Method (BREEAM), the Green Star from Australia, the Comprehensive Assessment System for Building Environmental Efficiency (CASBEE) from Japan, the Building and Environmental Performance Assessment Criteria (BEPAC) from Canada, and the legislation LEED Leadership in Energy and Environmental Design (LEED).

Tab. 8.3: Overview on actual upper limits of formaldehyde emission.

Region	Standard	Test method	Board class	Board type	Limit value
Europe	EN 13986	EN 717-1	E2	PB, OSB and MDF (unfaced)	> 0.124 mg/m^3 air
		EN 120			8 < mg/100 g oven dry board ≤ 30
		EN 717-1		PW, SWP and LVL (unfaced), PW, PB, OSB, MDF, LVL (and others) overlaid	> 0.124 mg/m^3 air
		EN 717-2			3.5 < mg/m^2 h ≤ 8
		EN 717-1	E1	PB, OSB and MDF (unfaced)	≤ 0.124 mg/m^3 air
		EN 120			≤ 8 mg/100 g oven dry board
		EN 717-1		PW, SWP and LVL (unfaced), PW, PB, OSB, MDF, LVL (and others) overlaid	≤ 0.124 mg/m^3 air
		EN 717-2			≤ 3.5 mg/m^2 h
Japan	JIS A 5908 & 5905	JIS A 1460	F**		≤ 1.5 mg/l
			F***		≤ 0.5 mg/l
			F****		≤ 0.3 mg/l
USA	ANSI A208.1 & 2	ASTM E1333 (large chamber)		PB, MDF	≤ 0.3 ppm
				PW	≤ 0.2 ppm
	CARB	ASTM E1333	Phase 1	PB	0.18 ppm
				MDF	0.21 ppm
			Phase 2	PB	0.09 ppm
				MDF	0.11 ppm

PB: particleboard, MDF: medium density fiberboard, PW: plywood, OSB: oriented strand board, LVL: laminated veneer lumber

8.1.4 Strategies to reduce formaldehyde emissions from wood-based panels

8.1.4.1 Formaldehyde emission from wood-based panels

Although wood itself emits formaldehyde, the main source of formaldehyde emission in wood-based panels is the formaldehyde-based resins used in their production. Formaldehyde released from wood-based panels in service is caused, not only by residual formaldehyde trapped as gas in the structure of the board, but essentially due to hydrolysis (reversibility of reactions) of weaker formaldehyde bonds, namely methylol groups, acetals, and hemiacetals, as well as methylene ether bridges [17].

Formaldehyde release is affected by internal and external factors. Internal factors include the type of wood and resin employed, operating conditions, and parameters during pressing, as well as panel age. External factors are related to the place in which panels are located, such as temperature, air humidity, and air exchange rate, as well as the total panel area in relation to the total volume of the room.

8.1.4.2 Strategies to reduce formaldehyde emissions

There are several strategies to reduce formaldehyde emissions. Acting on resin, the strategies include the optimisation of adhesive synthesis. Although significant reductions in formaldehyde emissions were achieved, it is still not sufficient. Another way is the reduction of formaldehyde to urea (or amine groups $(NH_2)_2$) molar ratio. However, the minimum limit has already been attained, since further lowering the molar ratio impairs resin cure due to the excessively low free formaldehyde content. On the other hand, the conventional catalysts (also called latent catalysts) consume formaldehyde to create an acid environment, essential for the cure reaction. The reinforcement of the polymeric structure with resin additives is another possibility. Costa et al. [18] tested the incorporation of sucrose and obtained good results. They postulated that if the sucrose is added under strongly acid environment promotes sucrose dissociation into monosaccharides and favors their reaction with urea. These compounds continue to polymerize, becoming part of the UF polymer. The resin development originates particleboard with improved mechanical properties. Use of formaldehyde free adhesives: alternatives have a higher price and a lower reactivity.

Acting at board level, the strategies include the application of coatings, laminates, polymer (PVC), and metal films as diffusional barriers. The use of formaldehyde scavengers is also a possibility; the scavengers can be blended with resin or wood in powder or solutions form, and the scavengers can also be use as a posttreatment of boards, for instance being sprayed on the board surface. Posttreatment of boards after pressing to reduce formaldehyde emissions is also a strategy. Currently used methods include panel impregnation with formaldehyde scavenging species, such as aqueous solutions of ammonia, ammonium salts, or urea [19, 20]. The use of ammonia, however, tends to be used less and less, due to toxicity concerns.

Another strategy is the creation of diffusional barriers in the panel surfaces that keep formaldehyde confined. The application of a laminate, overlay, or coating to obtain a final decorative appearance could also prevent formaldehyde emission. This includes the use of paints, varnishes, veneers, laminates, or resin-impregnated papers. A few works in the literature compare the effectiveness of different barrier materials on formaldehyde reduction [21–24]. Epoxy powder coatings and laminate finishes usually imply the highest reduction levels, e.g. above 90 %. Combination of liquid coatings with formaldehyde scavenging additives can significantly improve FE reduction. It must be noted that emissions of other volatile organics (VOCs), in addition to formaldehyde, must also be considered when using coatings.

Tab. 8.4: Strategies to reduce formaldehyde emission.

Strategies to reduce formaldehyde emission	Drawbacks
Avoid formaldehyde based resins	Alternatives have a higher price and lower reactivity.
Adopt other formaldehyde based resins	MF and PF resins have a higher price and lower reactivity.
Substite conventional catalysts	Alternative catalysts do not provide total cure extension at reasonable pressing times.
Optimize UF resins synthesis	We have achieved significant, but not sufficient, reductions in formaldehyde emissions
Use formaldehyde scavenger	Allow the formaldehyde emission at solid wood level, but can compromise physical-mechanical properties and machinability.

8.1.4.3 Formaldehyde scavengers

Formaldehyde scavengers, capable of capturing formaldehyde either physically or chemically and forming stable products, are added to formaldehyde-based resins or to wood particles before pressing. These additives should provide long-term formaldehyde emission reduction, in principle along the panel's service life without reemission [25].

The problem with formaldehyde scavengers is the fact that these compounds react with formaldehyde during pressing, and not only after panel manufacture, which will have a negative effect on bonding strength and other properties, since less formaldehyde will be available for the cure reaction.

There are a couple of requirements which formaldehyde scavengers should satisfy:
– the scavengers should also maintain resin reactivity or cure rate in order to keep productivity levels;
– no discoloration of wood material;

- no significant changes of plant operating conditions;
- not adversely affect the quality of surface in the subsequent operations as the application of both coatings and laminates and machining.

There are different types of scavengers. They can be used as resin additives, i.e. chemical compounds that reinforce polymeric matrix, reducing hydrolysis of cured adhesive. Bioadditives, such as tannins, lignin, starch, wheat flour, and rice husk flour, are also used as formaldehyde scavengers. 'The addition of tannin solution of UF resin lead to significant formaldehyde emission decrease, due to the reactivity of the hydroxyl groups towards formaldehyde, but caused some reduction in internal bond strength and increased water absorption [26]. Basta et al. [27] obtained good results using different starch derivatives as scavengers. Proteins present in pulp and paper sludge were associated to formaldehyde reduction, but wood-based panel performance was lessened [28]. Zhang et al. [29] used nanocrystalline cellulose previously aminofunctionalized with an alkoxysilane, and significant improvements in bond strength and formaldehyde emission in panels were observed. There are also nonreactive additives: porous materials that scavenge formaldehyde by adsorption without chemical reaction (i.e. charcoal, pozzolan, zeolites, nanomesoporous Diatomaceous earth) have also been tested [30–32].

The reactive additives are chemical compounds that react with formaldehyde and form stable compounds. They are added to resin or directly to wood particles or fibres. Examples of these products are ammonia or ammonium compounds (ammonium acetate, carbonate, chloride, persulphate, carbamate, di-hydrogenophosphate), alkali salts of oxigenated sulfur compounds (sodium sulphite and metabisulphite), organic −NH compounds such as amides and amines (urea, alkyl amines, acetoacetamide, dihydrazide), borax and functionalized paraffin waxes (nitroparaffins). Other types of scavenger include scavenging resins: UF resin with formaldehyde to urea molar ratio well below 1.0 or UF pre-polymers.

The most common commercial scavengers are: urea (solid or solution), sodium metabisulphite and ammonium bisulphite, ethylene urea, encapsulated sodium metabisulphite, nitroparaffins. Sodium metabisulfite is an inorganic compound with molecular formula of $Na_2S_2O_5$, forming, in water, sodium bisulfite:

$$Na_2S_2O_5 + H_2O \rightarrow 2NaHSO_3.$$
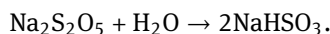
The reaction of aldehydes with sodium bisulfite produces a sodium salt of the bisulfite adduct [33]. This is a stable compound, with potential use as formaldehyde scavenger in wood based panels. The addition of sodium metabisulfite to an UF resin will form sodium bisulfite that will reacts with free formaldehyde present:

$$NaHSO_3 + CH_2O \rightarrow NaHOCH_2SO_3.$$
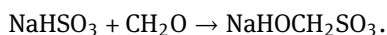
In Tab. 8.5, an overview of the main scavengers is presented, as well as their advantages and drawbacks.

Tab. 8.5: Advantages and drawbacks of common scavengers.

Scavenger	Advantages	Drawbacks
Solid Urea [34]	Low cost; nontoxic; normally used in the core layer	Formaldehyde is reemitted by hydrolysis with heat; penalty of physico-mechanical properties; hygroscopicity; decreased resin stability, reduction of cure speed, and reduction of "tack" of the mat
Urea in solution [35]	Low cost; nontoxic; normally used in surface layer	Low internal bond and high thickness swelling (UF pre-polymer is more effective than urea solution); can cause blistering during the press and overlaying with laminates
Sulphur compounds as sodium metabisulphite [18, 34]	Strong decrease of formaldehyde emission; long term effects	Release sulphur dioxide at high temperature which is toxic; release of particles in air causes respiratory tract irritation; direct mixing with resin affect pH causing resin pre-cure; can cause wood discoloration namely in MDF process.
Primary and secondary amines [26, 34]	Propylamine, methylamine, ethylamine, cyclopenthylamine present good scavenging ability	Alkyl amines react with methylol groups disturbing resin cross-linking; in MDF slight increase of thickness swelling but internal bond is not affected
Ammonium compounds [37]	Reemission of formaldehyde suppressed in contrast of ammonia gas	Do not always provide sufficient formaldehyde scavenging performance, unless combined with urea; ammonia gas (post treatment) was abandoned – toxicity by inhalation
Starch UF precondensate [38, 39]	Low cost, biodegradability, and renewability; low toxicity	Decrease the physico-mechanical properties; efficiency depends on the starch origin and the synthesis stage addition; availability for mass production
Tannin powder or solution [31, 40]	Good reactivity of OH groups; bio-based compound; low toxicity	Penalty of physico-mechanical properties; availability for mass production; dark color

8.2 Impact of formaldehyde-reducing strategies on formaldehyde emission and physico-mechanical properties

8.2.1 Physico-mechanical properties of wood-based panels

Wood-based panels, and more specifically particleboards and MDF, can be characterized by several tests and methods. Boards are usually assessed according to methods defined by recognized international organizations such as the European Committee for Standardization, also known as the Comité Européen de Normalization (CEN), American Society for Testing and Materials (ASTM), Japanese Industrial Standards (JIS), and other regional standard organizations. Each organization defines some differing tests or experimental conditions for evaluating similar properties. In the case studies presented, all physico-mechanical properties were evaluated according to the European standards (EN), except for formaldehyde emission, where Japanese standards were used. For particleboard and MDF, the common tests and corresponding standards to evaluate particleboards properties are: density (EN 323) [41], internal bond (EN 319) [42], moisture content (EN 322) [43], and thickness swelling (EN 317) [44]. Modulus of elasticity in bending, also called modulus of elasticity (E_m), and bending strength are determined according to EN 310 [45]. Modulus of elasticity is calculated from the slope of the linear region of the load-deflection curve. Bending strength is calculated from the ratio of the bending moment and the maximum load (F_{max}) to the moment of its full cross section, as stated in EN 310. The test piece is supported by two roller-bearing parallels and then a load is applied to the test piece by an equidistant and parallel cylindrical load head capable of measuring the deflection and the load applied (Fig. 8.7). Tensile strength perpendicular to the plane of the board is also commonly called an "internal bond" and is determined according to EN 319. Fig. 8.7 shows the apparatus of an internal bond test. Swelling in thickness after immersion in water, "thickness swelling", is determined by measuring the increase in thickness of a test piece after complete immersion in water for 24 h. Fig. 8.8 shows a running test apparatus according to the EN 317. The moisture content of boards is determined by the loss of mass of a test piece dried in an oven at $103 \pm 2\,°C$, and density is determined from the ratio between the mass of a test piece and its volume. The apparatus of these tests are also shown in Fig. 8.8.

In the EN 312 standard, particleboards can be classified according to different grades, from P1 to P7, where the minimal requirements are defined according to the final application of the product. For each grade general requirements are defined, such as the range of moisture content or specific requirements. For example, a P1 grade refers to "general purpose", and a P2 is for "Interior fitments – dry conditions" while P7 is for "heavy-duty load bearing – humid conditions".
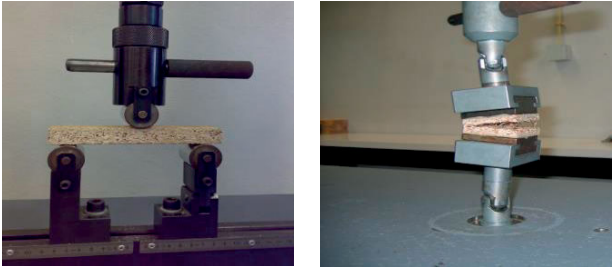
Fig. 8.7: Example of the determination of a bending (left) and internal bond test (right).

Fig. 8.8: Example of density determination (left), moisture content (center), and thickness swelling (right).

8.2.2 Case studies

Case study 1

Several panels produced in our laboratory, bonded with different resins (UF and MUF) and doped with different formaldehyde scavengers, were tested using three different methods: the perforator method (EN 120), the gas analysis method (EN 717-2), and the desiccator method (JIS A1460). Due to the reduced size of the samples, the chamber method could not be used. A commercial particleboard was also tested using the former three methods, and also using the chamber method (EN 717-1).

Due to the different behavior of the bonding systems, mainly bonding strength and mechanical spring-back, only panels having a thickness of 17 ± 0.2 mm, a density of 650 ± 20 kg/m^3, and an internal bond higher than 0.40 MPa (EN 319) were evaluated for formaldehyde emissions/content.

Fig. 8.9 shows the results for the panels, which were evaluated both with EN 120 and JIS A1460. It can be observed that there is a very weak correlation for the values of the two methods. They can easily have differences of 40 % for values around 1 mg/l (JIS A1460). The results for very low formaldehyde emissions and very low formaldehyde content seems to be completely independent. These results can be easily justified by the presence of scavengers, which produce a very different behavior during both tests, mainly due to the temperature and environmental humidity: the JIS A1460 test is car-
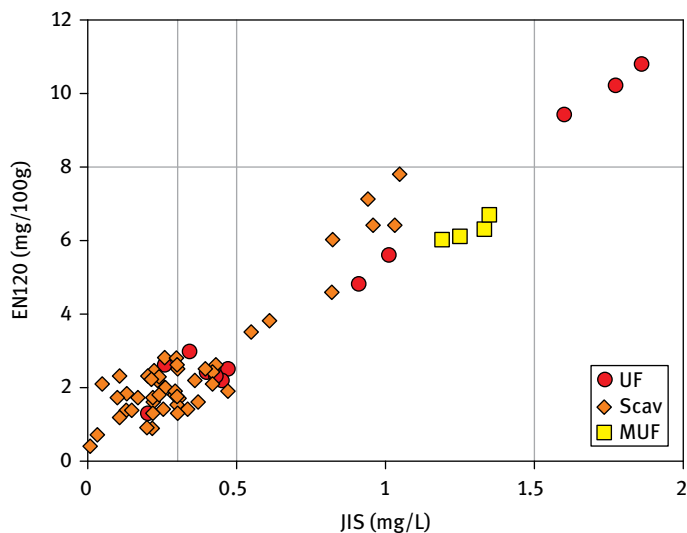
Fig. 8.9: Formaldehyde content (EN 120) and formaldehyde emission (JIS A1460) for the same samples.

ried out at near ambient temperature and relative humidity, while the EN 120 is carried out at a much higher temperature (over 110 °C) and in the presence of toluene.

In Fig. 8.10, the results for the panels, which were evaluated both with EN 120 and EN 717-2, are presented. As expected, the results are globally very similar of those presented in Fig. 8.1. In this case, we also have a formaldehyde content test and a formaldehyde emission test. As both methods are used for the same classification standard, the fact that some of the samples have different classification (E1 or E2) is a very important finding.

These results cannot be as easily justified as before due to the presence of scavengers, which still have very different behavior during both tests, mainly due to the air temperature and humidity. The EN 717-2 test is performed at a temperature of 60 °C and in the presence of dry air, while EN 120 is carried out at a much higher temperature (over 110 °C) and in the presence of toluene. The different permeability of the panels and the fact that EN 120 is supported on a phase-equilibrium (toluene-water), while EN 717-2 is a dynamic "desorption" test, could possibly explain these results.

Fig. 8.11 shows the results for panels, which were evaluated both with EN 717-2 and JIS A1460. As expected, these results gave better correlations than the ones of both Fig. 8.10 and Fig. 8.11, since we are in the presence of two emission evaluation tests. Nevertheless, there are still some major differences that can also be justified by the dynamic nature of both methods. In fact, JIS A1450 is supported on a phase-equilibrium (air-water), while EN 717-2 is a dynamic "desorption" test.
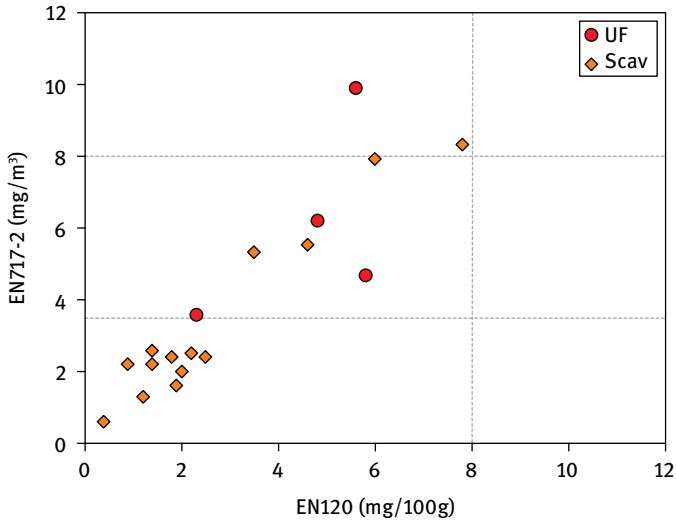
Fig. 8.10: Formaldehyde content (EN120) and formaldehyde emission (EN717-2) for the same samples.
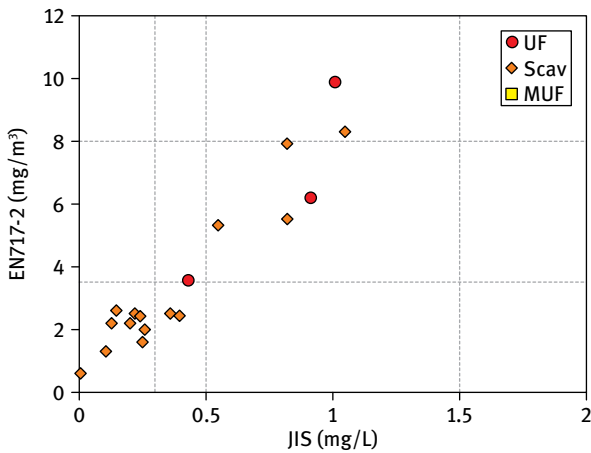
Fig. 8.11: Formaldehyde emission values (JIS A1460 and EN717-2) for the same samples.

Tab. 8.6: Results for the four tests performed on a commercial panel.

Method	Value	Japan	Europe
EN 120 (mg/100 g oven dry board)	5.3		E1
EN 717-1 (mg/m^3 air)	0.166		E2
EN 717-2 (mg/m^3 air h)	5.6		E2
JIS A1460 (mg/l)	1.60	F*	

Tab. 8.6 presents the results for both the formaldehyde emissions/contents values and the products classification for a commercial panel, which were evaluated with the EN 717-1, EN 717-2, and JIS A1460 methods. These results show that this board can be classified either as E1 or E2, according to the method that was selected.

These results were expected and could be justified by the conditions of the tests, as mentioned before (JIS A1460 and EN 717-1 tests are carried out at near ambient temperature and humidity; the perforator method is conducted in the presence of boiling toluene at around 110 °C, and the gas analysis test is conducted at a temperature of 60 °C, in the presence of dry air).

Case study 2

Formaldehyde scavengers can be added in powder or solution form, and the incorporation can be done in different ways, in the core layer, in the face layer, or in both, directly to the resin or mixed with particles or fibres. In general, it was noticed that the physico-mechanical properties are affected. Our team carried out several studies of formaldehyde scavengers, changing the amount, the effect of the addition at core layer or face layer. After a preliminary study, the following scavengers were the most promising ones: urea (solid or solution form), sodium metabisulphite, and starch. An encapsulated scavenger based on sodium metabisulphite was also tested. In the first stage different quantities of scavengers were tested, and it was concluded that an excess of scavenger may prejudice physical-mechanical properties of particleboards, even while decreasing the formaldehyde emission values. For liquid urea it was verified that the one with better results (formaldehyde emission/internal bond), was obtained for (0.5/0.5). These results may indicate that an excess of scavenger may prejudice physical-mechanical properties of particleboards, even though decreasing the formaldehyde emission values. The solid urea (0/0.5) test provided the best values of internal bonds, while its formaldehyde emission was higher than the low limit imposed. In the case of starch, for the optimized quantity, acceptable internal bond strength was obtained costing a small penalization in formaldehyde emission [46].

The main conclusions of this work were as follows.
– Some scavengers may work as catalysts, increasing the extension of the cure reaction.
– The structure of the starches used was different because of their origins, triggering distinct performances as formaldehyde scavengers.
– The scavengers approved led to a decrease of formaldehyde emission. However they also lead to a decrease in physical-mechanical properties, mainly of the internal bond.
– Some scavengers, the urea solution and the starch, present the most promising results, since they seem to be the most effective scavengers.
– Both encapsulated scavenger and sodium metabisulphite show good performance.

Fx (SL/CL)　　　　–　　　　(0/0.5)　　　(0.5/0.5)　　　(0.5/0)　　　(0.8/0.4)
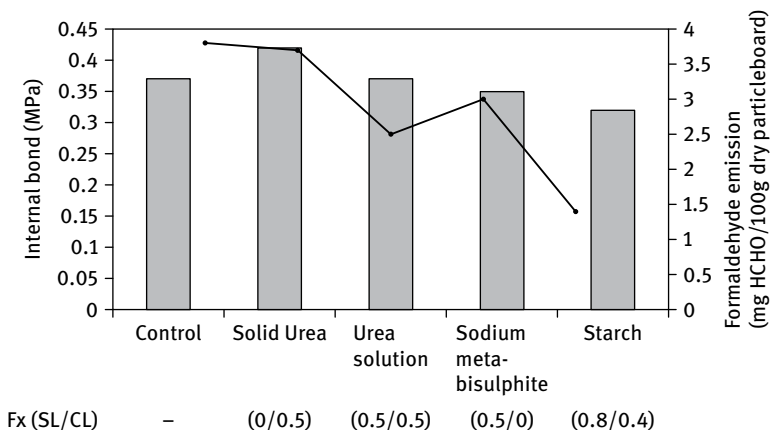
Fig. 8.12: Values of internal bond and formaldehyde emission for several scavengers;
SL: surface layer, CL: core layer.

Giving the promising results obtained with sodium methabisulphite, the effect of this scavenger was tested [47]. Two addition processes were tested: mixing resin to scavenger prior to blending, or blending scavenger with glued particles. The amount of scavenger added was 10 wt% relative to solid resin. The adhesive system was a UF resin (7 wt% based in mass of oven dry wood), 2% of paraffin, and 3% of catalyst.

Fig. 8.13 shows a comparison of formaldehyde content of particleboards produced without scavenger, with scavenger added to the resin, and with scavenger added to glued wood particles. Three resins with different formaldehyde to urea molar ratio were tested. It was concluded that formaldehyde content is not affected by the addi-
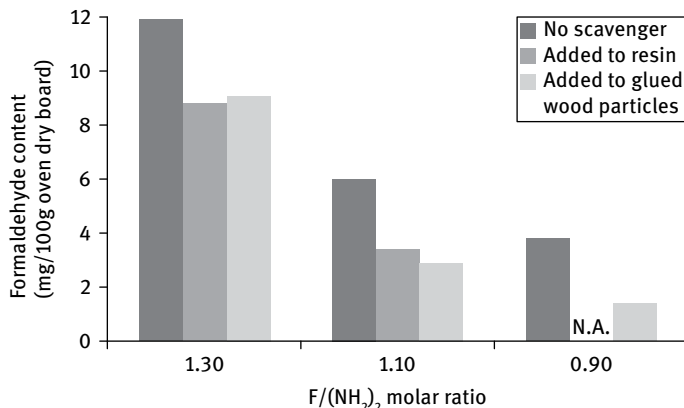
Fig. 8.13: Formaldehyde content of particleboards produced without scavenger, with scavenger added to the resin, and with scavenger added to glued wood particles (N.A.: not available).

tion procedure. However, internal bonds are substantially impaired when scavenger is added directly to resin.

The scavenging performaned of sodium metabisulfite in solid form, ammonium bisulfite in liquid solution, and urea were evaluated using three different formaldehyde evaluation standard methods: perforator, desiccators, and gas analysis [48]. Urea was applied in solution (30 wt%) in the face layer to avoid the "blistering effect" noted when a decorative paper is pressed over a urea prill. In the core layer, urea was applied in solid form (prills) to avoid an increase in internal moisture content that inhibits heat transfer.

A control series was produced with the same resin and operating conditions, but without adding scavenger.

(a)

(b)
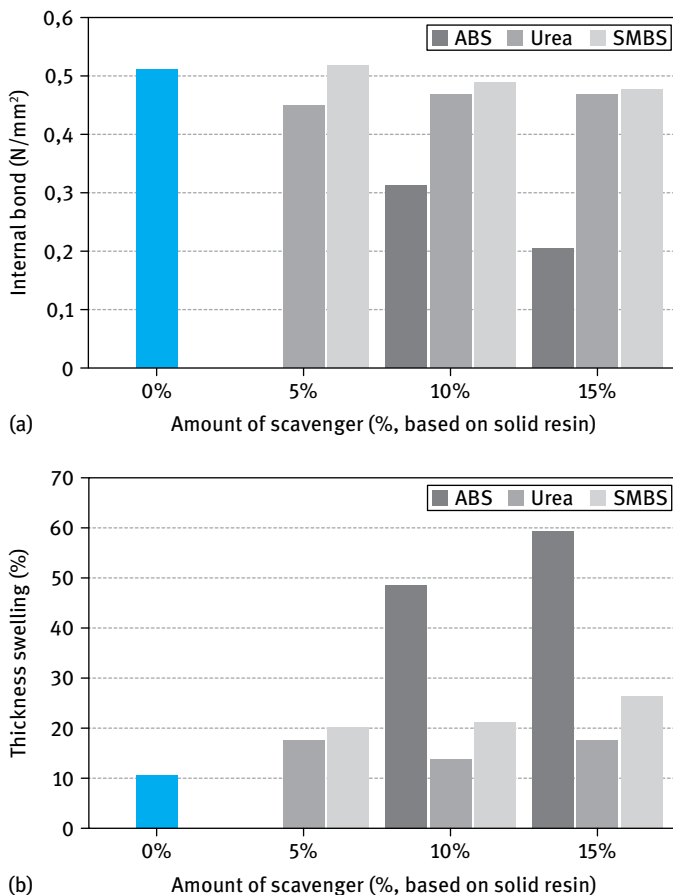
Fig. 8.14: Comparison between internal bond and thickness swelling with different amounts of formaldehyde scavengers (SMBS: sodium metabisulphite; ABS: ammonium bisulphite).

(a)

(b)
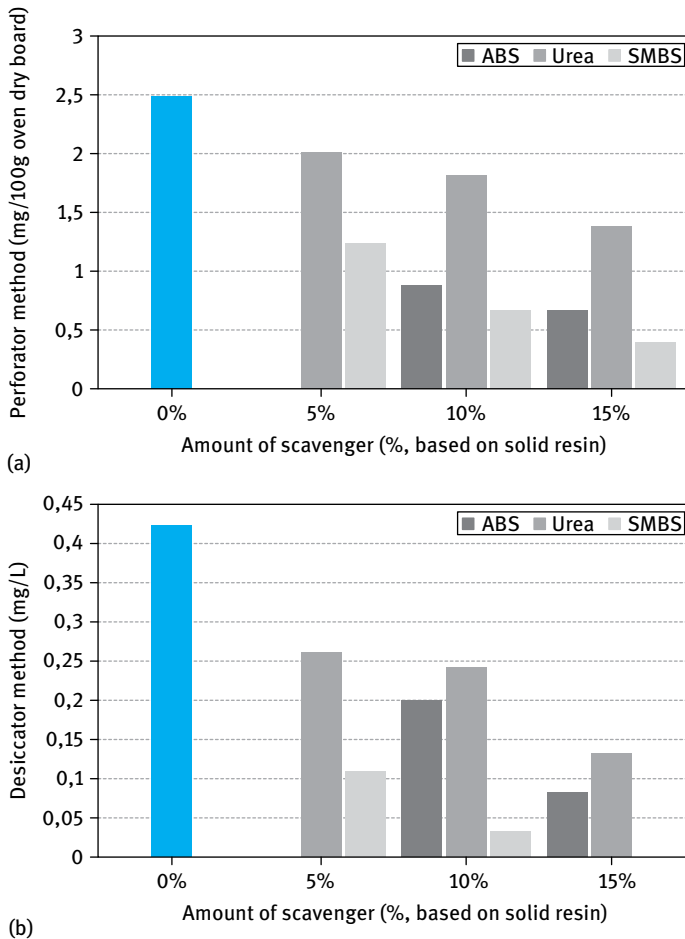
Fig. 8.15: Formaldehyde content by perforator method (EN 120) and formaldehyde emission by desic-cator method (JIS A1460) of particleboards produced with different formaldehyde scavengers.

Fig. 8.14 shows the internal bond and thickness swelling of the particleboards pro-duced. It can be observed that particleboards produced with sodium metabisulphite do not present a significant reduction in internal bond, nor is there substantial nega-tive change in thickness swelling. Urea behaves similarly, and Ammonium bisulphite presents the higher penalty in internal bond and thickness swelling.

In Fig. 8.15 the formaldehyde scavenging ability of the three scavengers is com-pared with the perforator and desiccator method.

In the case of the perforator method, urea presents the lowest ability for scav-enging formaldehyde, which supports the idea that urea is no longer a preferred formaldehyde scavenger to produce ultra-low emission wood-based panels. Sodium metabisulfite and ammonium bisulfite present similar results. In the case of the des-

iccator method, sodium metabisulfite presents zero formaldehyde emission when incorporated at 15 wt%, while ammonium bisulfite and urea present a significant reduction in formaldehyde emission. Probably the better performance of sodium metabisulfite in the desiccator method might be related to higher hydrolysis resistance of the adduct formed in the reaction with formaldehyde. The addition reaction between formaldehyde and urea used as scavenger forms methylolureas, which tends to undergo hydrolysis in the presence of moisture, releasing formaldehyde. This explains the poor performance of urea addition in the desiccator method, since test objects are subjected to a high relative humidity. Ammonium bisulfite shows a similar behavior, indicating that the compound formed by reaction with formaldehyde also has low moisture resistance. Under the gas analysis method, urea does not show any scavenging ability, which might be related to the low thermal stability of the oligomeric species formed by reaction of urea scavenger with formaldehyde even at a relatively low temperature of 60 °C. Ammonium bisulfite has a behavior similiar urea, which might indicate that compounds formed between ammonium bisulfite and formaldehyde do not present the same stability as those formed with sodium metabisulfite.

Costa et al. [49] conducted a study of the performance of scavengers on volatile organic compound (VOC) emissions from wood-based composites produced with poplar and maritime pine (*Pinus pinaster Ait.*) and European poplar (*Populus spp.*). In this work, it was concluded that urea has no effect on VOC reduction of particleboards made from *Pinus pinaster* and *Populus spp*. Sodium metabisulphite presented strong reduction on aldehyde emission of particleboards made from *Pinus pinaster*. Particleboards made from poplar presented a residual emission of aldehydes, and sodium metabisulphite has no effect on TVOC reduction.

8.3 Impact of formaldehyde-reducing strategies on machinability

8.3.1 Introduction

During the cutting of wood-based products, several wear mechanisms may simultaneously contribute to the general wear of the cutting tool. Among these wear mechanisms are gross fracture or chipping, abrasion, erosion, microfracture, chemical and electrochemical corrosion, and oxidation [50]. The abrasive characteristics of formaldehyde scavengers could affect the machinability of particleboard. It is known that substances such as starch, added as fillers to the resin in plywood production increase tool wear. As far as we know, there is no published literature about the influence of formaldehyde scavengers on the machinability of wood-based panels.

Particleboard machinability has been studied by several researchers. Several studies have been focused on board cutting characteristics and on properties that influence the cutting process: board structure [51], tools geometry [52], and chip size

[53]. McKenzie was the pioneer in establishing models for the wood-cutting process. He also developed models for routing particleboard, relating the cutting force with density, chip thickness, rake angle, fiber angle, and dullness [54].

Another important issue is the surface quality of a particleboard. Several works have shown that in the case of particleboards the main quality criterion is established by edge evaluation, which has to be free of any disruptions after milling or sawing [55]. The edge quality of wood-based panels has been the object of several research projects [56]. However, the establishment of a method to assess edge quality needs to be pursued further. A novel method for evaluating the influence of the operating parameters of wood machining (planning and sanding) on the quality of the finished surface was established by Coelho et al. [57]. This method, based on an artificial vision system, was later applied with some modifications to the analysis and characterization of the edge quality of particleboards, which permitted establishment of some quality criteria [58].

8.3.2 Case studies

Case study 1

The impact of formaldehyde scavengers on machinability and edge quality of particleboard was studied. Three-layer boards were manufactured with different formaldehyde scavengers. The effect of these additives was studied regarding the machining conditions (power consumption, cutting force) and particleboard edge quality, assessed by means of an artificial vision system.

In particleboard production, wood furnish was provided by a particleboard manufacturer (Sonae Indústria, Oliveira do Hospital) and a standard mix was used for the core layer and face layer. A commercial UF resin (supplied by Euroresinas, Sonae Indústria) for the production of class E1 particleboard was used. Wood particles were then blended with the resin and paraffin in a laboratory glue blender and several scavengers: solid urea and urea in solution (provided Euroresinas, Sonae Indústria), sodium metabisulphite (Panreac), and a UF pre condensate with starch (provided Euroresinas, Sonae Indústria). In the case of urea, two different fractions of particle sizes were studied, one of them referred to as "coarse", provided by the industrial producer of UF resins. and the other labeled "fine", obtained from the "coarse" urea after screening with the screen of 0.25 mm. All scavengers, both in solid or liquid form, were added to wood particles before the addition of glue. The same glue formulation was used for all tested scavengers. Three-layer particleboard was hand formed in a metallic container with $220 \times 220 \times 80$ mm. The pressing cycle (stage duration, press closing time, platen temperature) was scheduled in order to simulate a typical particleboard continuous pressing operation. The values of the process parameters are presented in Tab. 8.7.

After pressing, the boards were conditioned at 20 °C and 65 % of relative humidity and then machined. The sawing operation was performed on a semiautomatic five

Tab. 8.7: Process parameters for particleboard preparation.

Parameter	Value
Board size (mm)	220 × 220 × 16
Target board density (kg/m^3)	630 ± 20
Particle moisture content (%)	FL-3.5; CL-4
Resin content wt% (resin solids/oven dry weight of particles)	FL-6.3; CL-6.9
Hardener content wt% (solids/oven dry weight of resin)	FL-1; CL-3
Paraffin content wt% (solids/oven dry weight of particles)	0.15
Scavenger content wt% (active compound/oven dry weight of particles)	Different contents (FL, CL)

FL: face layer,   CL: core layer

Tab. 8.8: Levels of machining (expected).

Feed rate (m/min)	Feed per tooth (µm)	
	30 Hz	50 Hz
9.0	97	59
17.0	184	111

head multifunctional machine. The sawing element was equipped with a 300 mm diameter steel blade (3.2 mm in thickness) composed of 48 cutting elements, and rotating with a nominal speed of 3200 rpm. Two feed rates (FR) and two rotation speed (RS) levels were fixed in order to attain different levels of machining (Tab. 8.8).

In order to permit the on-line manipulation and measure of several operating conditions, the machine was instrumented with a high performance vector AC drive, a current transducer, and a pair of low-cost Murata piezoelectric sensors. The tool is directly driven by an electrical motor with 3 hp of nominal power. The machining conditions and the vibrational sensors signals were recorded for analysis. For acquisition and control of signals, an application in LabView® 7.1 was developed, including a Matlab® module enabling the calculation of the effective feed per tooth using FFT (fast Fourier transform) filtering of the vibrational signals.

For the characterization of the particleboard edge, an artificial vision method was used. This method consists of illuminating the surface with two light sources (laser and lamp) and recording the image (Fig. 8.16). The apparatus is composed of a CCD BW video camera (model Sony XC-ST30), a modified video zoom lens (VZM300), a diode microlaser (VLM 10° line), and a single-channel monochrome image acquisition board (NI1407). The equipment is connected to a PC computer running an image acquisition and processing software developed in Labview®. The numerical treatment was performed with an external application developed in Matlab®.

In order to obtain the images needed for evaluating the edge quality, each sample was photographed using the apparatus. One sample camera angle ($\beta = 15°$) was used
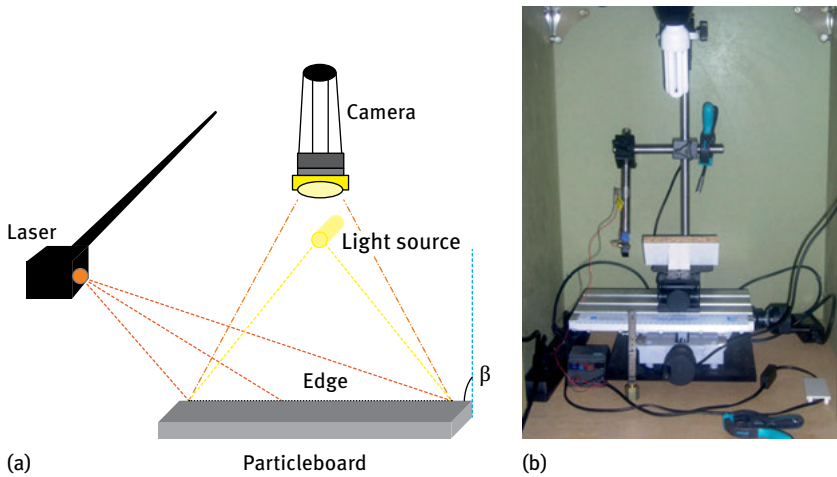
Fig. 8.16: Edge evaluation apparatus: (a) scheme; (b) photo.

with a focalized laser beam light source, and a total of nine photos per sample were taken: two light sources, laser (L) and lamp (S), and three sample positions, left (L), right (R), and center (C). For each image, a virtual profile was extracted. From this virtual profile, an edge quality evaluation criterion was obtained applying a filtering method based on fast Fourier transforms (FFT).

Several trials were performed in order to assess the effect of several formaldehyde scavengers on the machinability and edge quality of particleboards manufactured with these products. Fig. 8.17 shows the relative energy consumption in a function of feed per tooth for several formaldehyde scavengers. It is possible to observe that the incorporation of scavengers has a much lower influence on energy consumption during the cutting operation than the machining conditions, in particular the feed per tooth. The weak bond between the scavengers and both the resin and wood should lead to a greater detaching of small particles, causing different wear behavior. In this work it was not possible to observe this effect. However in Fig. 8.18 we can notice a reduced energy consumption when using starch that can be justified by a wear reduction.

Although the machining conditions are an important factor, the energy consumption also depends on the material characteristics, namely density and mechanical properties. Density was more or less controlled during the formation and hot-pressing of particleboards, although all boards had practically the same density. However, the mechanical properties, as internal bond, are very much affected by formaldehyde scavengers. Fig. 8.18 presents the relationship between energy consumption and internal bond. It can be observed that the values of power consumption are different among the several scavengers for the same internal bond, meaning that the incorporation of formaldehyde scavengers has in fact a more important influence on energy consumption than the internal bond.
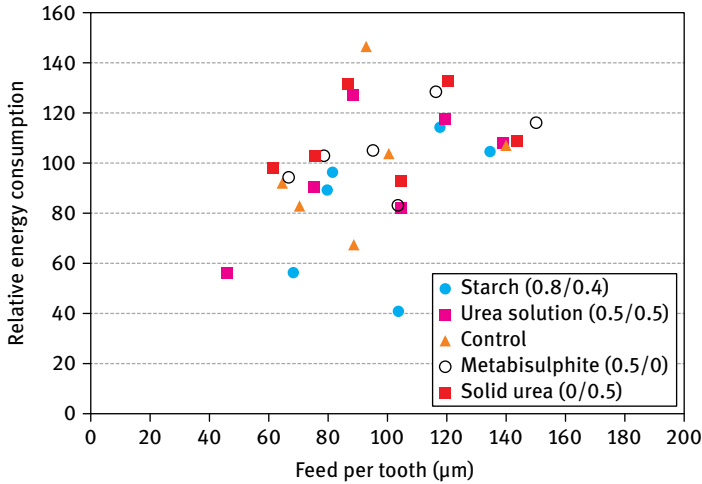
Fig. 8.17: Relative energy consumption in function of feed per tooth for several formaldehyde scavengers.
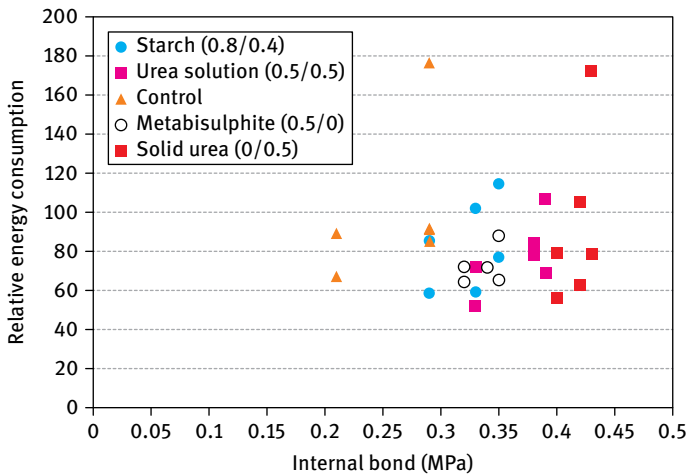
Fig. 8.18: Relative energy consumption in of internal bond for several formaldehyde scavengers.

The comparison between the several scavengers presented in Fig. 8.19 permit us to conclude that the different strategies used to decrease formaldehyde content have a great influence on energy consumption, but especially on edge quality. All scavengers tested have lead to a significant reduction of edge quality. The product with the best performance seems to be the solid urea, because there is only a slight decrease on power consumption and edge quality. One of the reasons could be the fact that solid urea is only applied onto the core layer. The scavenger with the worst performance is
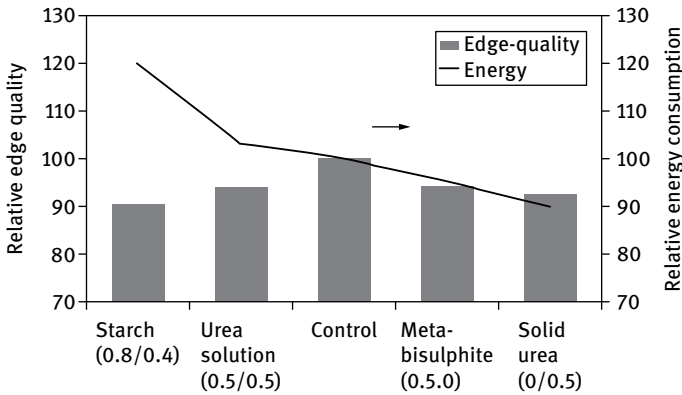
Fig. 8.19: Relative edge quality and relative energy consumption for several formaldehyde scavengers.
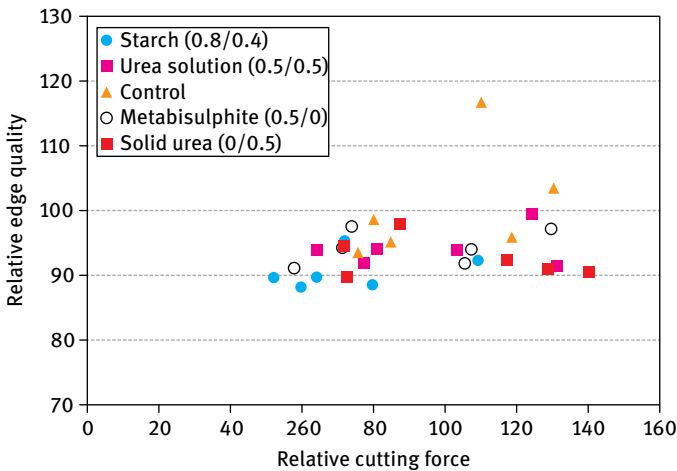
Fig. 8.20: Relative edge quality in function of relative cutting force for several formaldehyde scavengers.

starch. These conclusions are confirmed in Fig. 8.20, where the influence of the relative cutting force on the relative edge quality is presented.

Since urea presented the best results as formaldehyde scavenger, we tested the effect of particle granulometry. Fig. 8.21 shows both the relative edge quality and relative energy consumption for coarse and fine urea. The granulometry of urea particles has a strong influence on the edge quality, although the utilization of particles of a smaller size (< 0.25 mm) seems to not affect machining. This conclusion can be confirmed in Fig. 8.22, which presents the cutting force in function of feed per tooth. These results indicate that urea granulometry has to be carefully selected.
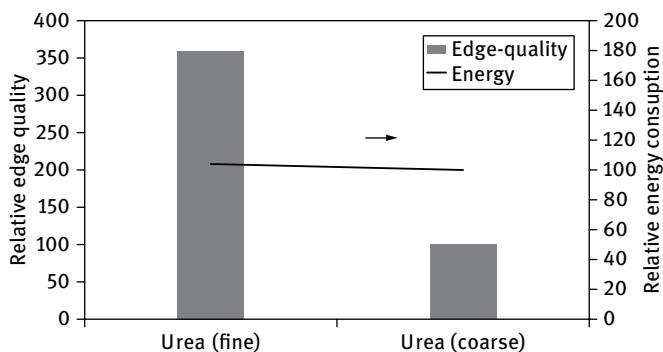
Fig. 8.21: Relative edge quality in function of relative energy consumption for urea with two particle sizes, fine and course.
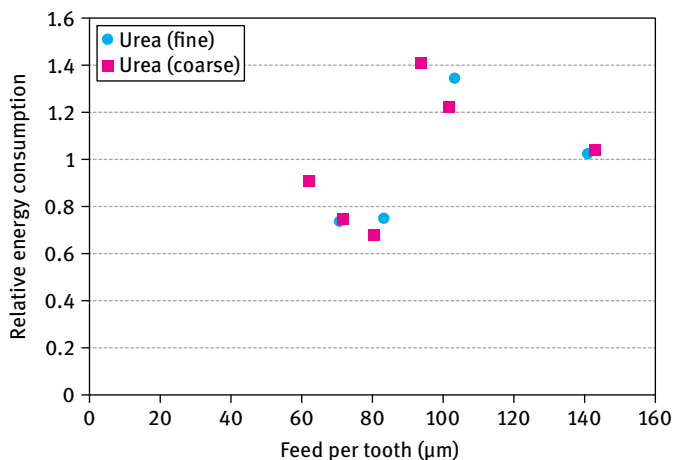
Fig. 8.22: Relative energy consumption in function of feed per tooth for urea with two particle sizes, fine and course.

The main conclusions of this study are:
– The incorporation of scavengers has a much lower influence on energy consumption during the cutting operation than the machining conditions, in particular the feed per tooth.
– The different strategies used to decrease formaldehyde content have a great influence on energy consumption, but especially on edge quality. All scavengers tested had lead to a significant reduction on edge quality.
– The product with the best performance seems to be the solid urea, because it causes only a slight decrease on edge quality but a small reduction in power consumption.

– The scavenger with the worse performance is starch.
– The granulometry of urea particles has a strong influence on edge quality, but not on energy consumption. Urea with fine particles has much better performance than urea with coarse particles.

Case study 2

A new approach to evaluate the quality of low-formaldehyde wood-based panels surfaced with laminates.

In recent years, new market requirements and the availability of raw materials drove to improvements of wood-based panel (WBP) properties and the optimization of their manufacturing process by changes on the basic raw material (different wood species and recycled wood), new adhesive systems (different resins, new catalysts), inclusion of additives (formaldehyde scavengers, fire retardants, moisture repellents, etc.), and even by modification of their basic physical and mechanical properties (density, internal bond, stiffness, etc.).

The surface appearance of wood-based panels (WBP) has always been an important requirement, and therefore WBP are usually overlaid with a decorative laminate such as a low-pressure laminate (single melamine-formaldehyde impregnated sheet of paper).

WBPs are largely applied in furniture, cabinet manufacture, and building construction. For both furniture and cabinet manufacture, the esthetic appearance and processing costs are the most important requirements and are closely linked to machinability (sawing, routing, drilling, etc.) and processing conditions (geometry and size of cutting elements, feed speed, etc.), and they are usually assessed according to surface quality, power consumption, and tool wear. However, the machining operation often endangers the prestige of these products, causing the edges to crumble and therefore resulting in a poor finish quality.

A new methodology, based on the use of two different systems (artificial vision system for edge quality evaluation and a process monitoring system) is proposed, and the results of a preliminary performance study (WBP overlaid with different kind of laminates) are presented.

Several WBPs (Tab. 8.9) were overlaid in a lab scale hot-press, 30 cm wide, with a decorative laminate and sawed using a semiautomatic five-head multifunction machine, the Weinig Profimat N22. The moulder fifth element, the sawing element, was equipped with a 300 mm diameter steel blade (3.2 mm in thickness) composed of 48 cutting elements, and rotating at a nominal speed of 3200 rpm. Two feed rates (FR) and two rotation speed (RS) levels were fixed in order to attain different levels of machining (Tab. 8.10). Several operation conditions were controlled using a high performance vector AC drive and the operation data collected with an application developed in LabView® 7.1 from the signal of current transducers and from the signal of a pair of low-cost Murata piezoelectric.

Tab. 8.9: Description of WBP samples.

Producer	Producer	Grade
PB-I	A	Standard PB
PB-II	B	Standard PB
PB-I-hq	A	High quality standard PB
PB-H	A	Moisture resistant PB
PB w/MDF faces	B	PB with MDF faces
PB-E1-I	A	PB – low formaldehyde emission < E1
PB-E1-II	B	PB – low formaldehyde emission < E1

Tab. 8.10: Levels of machining (expected).

Feed rate (m/min)	Feed per tooth (µm)	
	30 Hz	50 Hz
9.0	97	59
17.0	184	111

For the evaluation of particleboard edge quality, an artificial vision method was used. This method consists of illuminating the surface with two light sources (laser and lamp) and recording the image (Fig. 8.24). The apparatus is composed of a CCD BW video camera (Sony XC-ST30), a modified video zoom lens (VZM300), a diode micro laser (VLM 10° line), and a single channel monochrome image acquisition board (NI1407).

There are several type of WBPs on the market; seven of those were select for this study: two standard particle boards (PB-I and PB-II) from two different Portuguese manufactures, one particleboard producing better machinability (PB-I-hq), one particleboard presenting moisture resistant characteristics (PB-H), one particleboard produced with MDF faces (PB w/MDF faces), and two low-formaldehyde particleboards (PB-E1-I and PB-E1-II) from two different Portuguese manufacturers. The different WBPs were selected because there were simple and clear differences between them. The PB-I and PB-II were standard particleboard produced with two different UF resins, but with the same density and similar wood mix, there may be slight differences in the amount of resin; the PB-I-hq is an improved PB-I with higher amount of resin and small size particles, the PB-H is a particleboard produced from the same wood mix as PB-I but using a different resin (MUF resin); PB w/MDF faces is a composed board manufactured with a standard core layer, but with the face layers consisting of fibers, just as on MDF. PB-I and PB-E1-I, have the same wood mix, as well as PB-II and PB-E1-II , but the resins are different. PB-I and PB-II have a standard UF resin, but PB-E1-I and PB-E1-II have a UF resin with low formaldehyde emission with addition of formaldehyde scavengers.
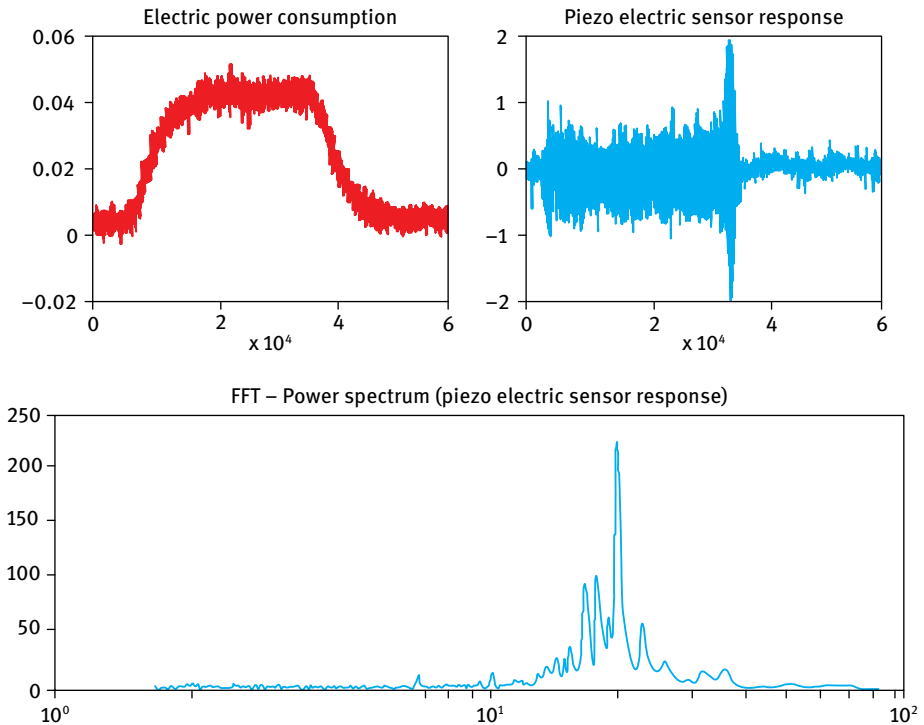
Fig. 8.23: Raw data from the operation of the computer controlled modified industrial moulder.

During the sawing operation the electric power consumption and the piezo electric sensor response (Fig. 8.23) were recorded and several criteria where calculated: total energy, total wear. and vibration; the samples edge quality was then evaluated (Fig. 8.25), and the remains criteria were established: edge quality and edge noise.

The data collected from the sawing operations and from the edge quality evaluation procedure were processed in order to establish several quality criteria. The impact of core material on those criteria is presented in Fig. 8.26.

From the analysis of those results it is clear that edge quality, tool wear, vibration, and total energy are highly dependent on the core material, and that the two products with a much better the edge quality are PB-H and PB w/MDF faces, the products with the lower performance in terms of vibration and tool wear, higher values, are PB-E1-I and PB-E1-II, and the total energy involved in sawing PB w/MDF faces and PB-I-hq are the higher.

On the other hand, edge noise and specific gravity (introduced for internal control) seem to be independent of the core properties. The independence of the first of the criteria, edge noise, may be justified by its dependence on the laminate characteristics, which was maintained constant, given that the same laminate was used all over the

Fig. 8.24: Artificial vision edge quality evaluation system.
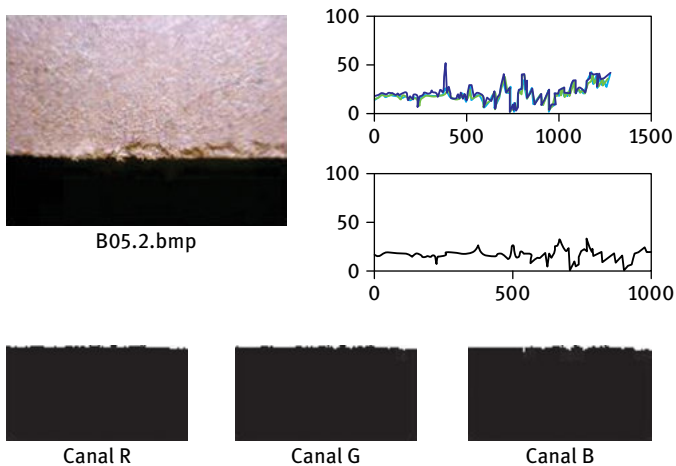
Fig. 8.25: Data from the artificial vision edge quality evaluation system.

study. The second has to be clearly independent because the boards were all selected to have a target density, and it is introduced in this study for internal control purpose.

Because the different criteria where established separately, it is important to analyse their independence before making further conclusions. In Fig. 8.27, 8.28, and 8.29 the relationship between edge quality and tool wear, tool wear and total energy, and edge quality and total energy are presented.

From the analysis of Fig. 8.27, we can observe that there are two clearly different relations, one for the standard PB, including the PB-I-hq, and the other for the prod-
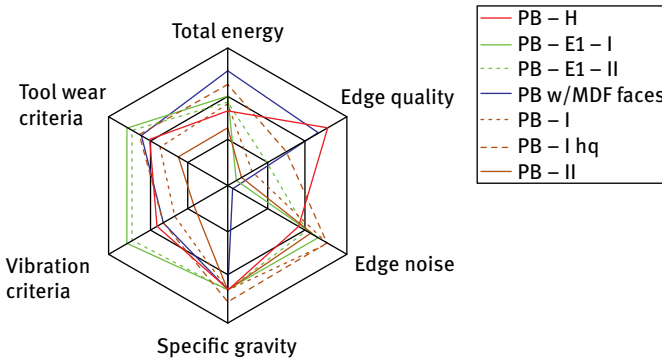
Fig. 8.26: Impact of the product type on the quality criteria.
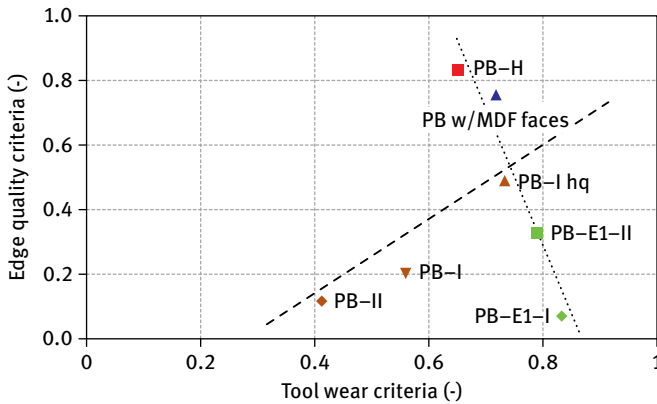
Fig. 8.27: Edge quality as function of tool wear.

ucts manufactured with different resins, different resin content, and core structure. The edge quality increases with the tool wear for the standard PB, which can be justified by the increase on resin content. The edge quality decreases with tool wear for the special products, including the low formaldehyde ones, which might be justified by the reduction of the product cohesion and homogeneity. The PB-H are produced using a MUF resin with higher crosslink ability and therefore are more brittle. The PB w/MDF faces have fibres on its external layers and therefore have a more abrupt density profile. The low formaldehyde products have lower crosslinking ability due to the presence of less free formaldehyde and thought the particles are more loose. The inclusion of additives, such as urea, increases the tool wear.

The same behavior can be globally observed in Fig. 8.28 and 8.29. In both of the figures the relationship for PB w/MDF faces does not follow the same rule as in Fig. 8.27, perhaps because this is a clearly a complete different product, for which the density profile has a strong impact on both the total energy and edge quality.
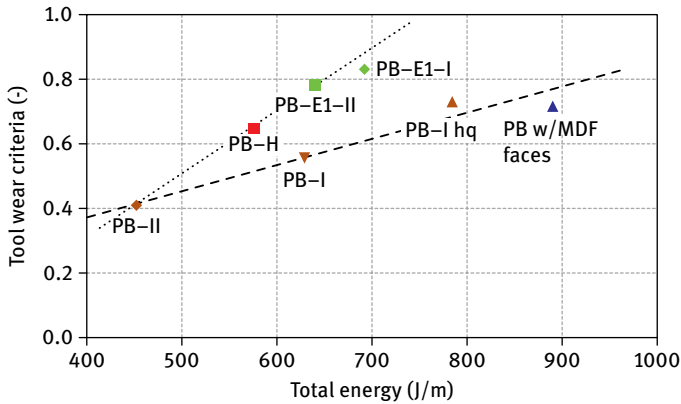
Fig. 8.28: Tool wear as function of total energy.
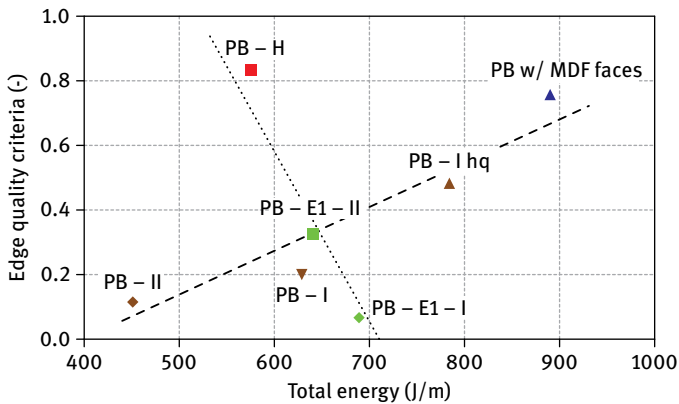
Fig. 8.29: Edge quality as a function of total energy.

In conclusion, the present methodology seems to be a promising tool for evaluating the impact of core properties on the quality of overlaid WBPs, as it clearly allows the quantification of those impacts.

As expected, the use of different resins and different amounts of resin, either in order to increase quality (PB-i-hq), to increase moisture resistance (PB-I-H), or to reduce formaldehyde emissions (PB-E1-I, PB-E1-II), and the use of fibers (PB w/MDF faces) has an important impact on the edge quality and tool wear.

The use of specially designed resins to reduce formaldehyde emissions, in conjunction with the use of formaldehyde scavengers, seems to greatly increase the tool wear and to reduce the edge quality.

8.4 Future perspectives

The issue of formaldehyde emissions has only recently stirred the WBP industry, in view of the mandatory VOC emission labeling system imposed by French regulations in 2012. This affects all construction products, flooring and wall surfaces, and indoor paints and lacquers. Formaldehyde emissions are seriously restricted: upgrading the rating from C (lowest) to A+ (highest) implies reducing formaldehyde emission from $120\,\mu g/m^3$ (or greater) to $10\,\mu g/m^3$ (or lower), measured in a ventilated test chamber after 28 days of storage. The measurement procedure is based on the ISO 16000 testing method. In the short term, this will imply definition of a new class for formaldehyde emission levels for WBPs within Europe, corresponding to emission levels very similar to the ones already established in Japan and USA, namely classes F**** and Carb II, respectively. One other class must be clearly defined, corresponding to emission levels within the range of natural wood [59, 60]. This must take into account that the wood species, and the amount and type of recycled wood, used in panel production can affect "natural" formaldehyde emission significantly [61].

Also recently, the California Environmental Protection Agency adopted two new classifications for WBPs produced with two particular kinds of adhesives: no-added formaldehyde resins (NAF), and ultra-low-emitting formaldehyde resins (ULEF). Additionally, the U.S. Green Building Council has defined the Leadership in Energy and Environmental (LEED) rating system for green building construction, which specifies that wood composite materials must contain no added urea-formaldehyde resins.

In this context of more stringent regulations, classes E1 and E2, which are currently still allowed in Europe, China, Australia, and Africa, will be reviewed and probably abolished in 2020. It will also be necessary to clarify the relation between

Tab. 8.11: Possible future WBP classes concerning formaldehyde emission levels [25].

WBP classes	Formaldehyde emission level	Complying adhesive systems
E0/Carb II/EPF-S	4–5 mg/100 g oven dry board	UF resin modified with 1–5 % melamine; molar ratio $F/(NH_2)_2$ between 1.00 and 0.90
F**** ULEF (Ultra Low Emitting Formaldehyde Resins)	0.3 mg/ml	MUF resin with 5–10 % melamine; molar ratio $F/(NH_2)_2$ between 0.90 and 0.80
Natural wood	0.007–0.0125 ppm	MUF resin with 10–16 % melamine; molar ratio $F/(NH_2)_2$ between 0.85 and 0.70
LEED (Leadership in Energy and Environmental Design)	Not specified	MF and PF resins (composite materials must contain no added urea-formaldehyde resins)
NAF (No Added Formaldehyde Resins)	Not specified	p-MDI; soy-based adhesive technology; bioadhesives; acrylic resins

the different methods for emission measurement, in order to standardize the existing classification systems throughout the world (Japan, Europe, USA, and China, among others).

Tab. 8.11 presents the WBP classes, concerning formaldehyde emission that will probably prevail in the near future, as well as the complying adhesives.

References

[1]   IARC (International Agency for Research on Cancer). Formaldehyde. In: Monographs on the Evaluation of the Carcinogenic Risk of Chemicals to Humans. Lyon: IARC; 2012. pp. 401–435.

[2]   SCOEL/REC/125. Formaldehyde, Recommendation from the Scientific Committee on Occupational Exposure Limits Draft document for public consultation; 2015.

[3]   NTP (National Toxicology Program). Final report on carcinogens background document for formaldehyde. Rep Carcinog Backgr Doc: i-512; 2010. Available from: https://ntp.niehs.nih.gov/ntp/roc/twelfth/2009/november/formaldehyde_bd_final.pdf.

[4]   Athanassiadou E, Ohlmeyer M. Emissions of Formaldehyde and VOC from Wood-based Panels. In: Fan M, Ohlmeyer M, Irle M, editors. COST Action WG3 (E49) Performance in use and new products of wood based composites. London: Brunel University Press; 2009. pp. 219–240.

[5]   Dunky M. Challenges with formaldehyde based adhesives. In: Properzi M, Pichelin F, Lehmann M, editors. Proceedings of the COST E34 Conference, Innovations in Wood Adhesives. Bern, University of Applied Sciences. Biel, Switzerland: HSB; 2004. pp. 91–106.

[6]   Athanassiadou E. Formaldehyde free aminoplastic bonded composites. In: Proceedings of the 5th International Conference on Environmental Pollution. Thessaloniki, Greece: Aristotelian University; 2000. p. 170.

[7]   Maruztky R. Global formaldehyde regulations and requirements: Current situation and developments. In: 6th European Wood-based Panel Symposium. Hannover; 2008, Oct 10.

[8]   EN 120. Wood-based panels – Determination of formaldehyde content – Extraction method called the perforator method.

[9]   Roffael E, Johnsson B. The perforator value in balance. Proceedings of the International Panel Products Symposium, Llandudno, Wales, UK; 2011.

[10]   EN 717-1. Wood-based panels – Determination of formaldehyde release – Part 1: Formaldehyde emission by the chamber method.

[11]   Irle, M., Analysing formaldehyde and how it can be done. Wood-based panels International; 2011 May.

[12]   EN 717-2, Wood-based panels – Determination of formaldehyde release – Part 2: Formaldehyde release by the gas analysis method.

[13]   Japanese Industrial Standard (JIS A 1460 (2001)) – Building boards Determination of formaldehyde emission: Desiccator method.

[14]   EN 717-3:1996 Wood-based panels – Determination of formaldehyde release – Part 3: Formaldehyde release by the flask method.

[15]   Salthammer T, Mentese S, Marutzky R. Formaldehyde in the Indoor Environment. Chem Rev. 2010; 110: 2536–2572.

[16]   Wood based Panels International; 2015, Dec, 2016 Jan.

[17]   Dunky M. Urea-formaldehyde (UF) adhesive resins for wood. Int J Adhes Adhesives. 1998; 18: 95–107.

[18] Costa N, Pereira J, Ferra Cruz P, Agostinho Moreira J, Martins J, Magalhães F, Mendes A, Carvalho L. The role of sucrose in amino polymers synthetized by the strongly acid process. J Adhesion Sci Tech. 2013; 27(7): 763–774.

[19] Sene M-L. Research of alternative solutions able to limit the formaldehyde release in panels (manufacturing & use). Pessac, France: Rescoll Centre Technologique; 2009.

[20] Dunky M, Grunwald D, Haelvoet W. Emissions. In: Johansson CJ, Pizzi T, Leemput MV, editors. Wood Adhesion and Glued Products. WG2: Glued Wood Products, State of the art Report of COST Action E13; 2001.

[21] Lee, J-h, Kim J, Kim S. Formaldehyde emission and burning behaviours from wood- based panels according to various surface finishing methods. Proceedings of 5th International Symposium on Sustainable Healthy Buildings. Seoul, Korea; 2011, 10 Feb. pp. 327–334.

[22] Barry A, Corneau D. Effectiveness of barriers to minimize VOC emissions including formaldehyde. Forest Prod J. 2006; 56: 38–42.

[23] Composite Panel Association, Technical Bulletin – VOC Emission Barrier Effects of Laminates, Overlays and Coatings for Particleboard, Medium Density Fiberboard (MDF) and Hardboard; 2003.

[24] Myers GE. Effects of post-manufacture board treatments on formaldehyde emission: a literature review (1960–1984). Forest Prod J. 1986; 36: 41–51.

[25] Carvalho L, Magalhães F, Ferra J. Formaldehyde Emissions from Wood-Based Panels – Testing Methods and Industrial Perspectives. In: Cheng CB, Ln FH, editors. Formaldehyde: Chemistry, Applications and Role in Polymerization. Hauppauge, NY: Nova Science Publishers. Inc.; 2012. pp. 73–107.

[26] Boran S, Usta M, Gümüşkaya E. Decreasing formaldehyde emission from medium density fiberboard panels produced by adding different amine compounds to urea formaldehyde resin. Int J Adhes Adhes. 2011; 31: 674–678.

[27] Basta AH, El-saied H, Gobran RH. Enhancing environmental performance of formaldehyde-based adhesives in lignocellulosic composites, part III: evaluation of some starch derivatives. Des Monomers Polym. 2006; 9: 325–347.

[28] Migneault S, Koubaa A, Riedl B, Nadji H, Deng J, Zhang T. Potential of pulp and paper sludge as a formaldehyde scavenger agent in MDF resins. Holzforschung. 2011; 65: 403–409.

[29] Zhang H, Zhang J, Song S, Wu G, Pu J. Modified nanocrystalline cellulose from two kinds of modifiers used for improving formaldehyde emission and bonding strength of urea-formaldehyde resin adhesive. BioResources. 2011; 6: 4430–4438.

[30] Kim S. The reduction of indoor air pollutant from wood-based composite by adding pozzolan for building materials. Constr Build Mater. 2009; 23: 2319–2323.

[31] Kim S, Kim HJ, Kim HS, Lee HH. Effect of bio-scavengers on the curing behavior and bonding properties of melamine-formaldehyde resins. Macromol Mater Eng. 2006; 291(9): 1027–1034.

[32] Funk M, Wimmer R, Adamopoulos S. Diatomaceous earth as an inorganic additive to reduce formaldehyde emissions from particleboards. Wood Mat Sci Engineering. 2015; DOI: 10.1080/17480272.2015.1040066.

[33] Caron S. Practical synthetic organic chemistry: reactions, principles, and techniques. Hoboken NJ: John Wiley & Sons Inc.; 2011.

[34] Tomita B. Overview and topics on reduction of formaldehyde from wood-based materials in Japan. In: Irle M, editor. Proceedings of the Final Conference of COST Action E49, Nantes; 2009, Sept 14–15. pp. 13-26.

[35] Park BD, Kang EC, Park JY. Thermal curing behaviour of modified urea-formaldehyde resin adhesives with two formaldehyde scavengers and their influence on adhesion performance. J Appl Polym Sci. 2008; 110(3): 1573–1580.

[36] Gao W, Du G, Kamdem P. Influence of Ammonium Pentaborate (APB) on the Performance of Urea Formaldehyde (UF) Adhesives for Plywood. J Adhesion. 2015; 91: 186–196.

[37] Fujji I, Murata Y, Euda S, Negishi S, Taguchi T. Formaldehyde scavenger and wood material using same. Patent 8389125 B2; 2013.

[38] Zhu X, Xu E, Lin R, Wang X, Gao Z. Decreasing the Formaldehyde Emission in Urea-Formaldehyde Using Modified Starch by Strongly Acid Process. J Appl Polym Sci. 2014; 131(9): 1–6.

[39] Lehmann W. Method and composition for reduction of formaldehyde emission in wood composite panels. Patent 4397756; 1983.

[40] Boran S, Usta M, Ondaral S, Gumuskaya E. The efficiency of tannin as a formaldehyde scavenger chemical in medium density fiberboard. Composites Part B: Engineering; 2012. DOI: 10.1016/j.compositesb

[41] EN 323. Wood-based panels – Determination of density.

[42] EN 319. Particleboards and fibreboards – Determination of tensile strength perpendicular to the plane of the board.

[43] EN 322. Wood-based panels – Determination of moisture content.

[44] EN 317. Particleboards and fibreboards – Determination of swelling in thickness after immersion in water.

[45] EN 310. Wood-based panels – Determination of modulus of elasticity in bending and of bending strength.

[46] Silva F, Pereira J, Ferra J, Mena P, Liberal JP, Magalhães F, Mendes A, Martins J, Carvalho L. Development of a System for the Production of Low Formaldehyde Emission Particleboards. In: Spear M, editor. Proceedings of the International Panel Products Symposium. University of Wales Bangor School of Education publisher; 2009. pp. 49–60.

[47] Costa N, Pereira J, Ferra J, Cruz P, Martins J, Magalhães F, Mendes A, Carvalho L. Sodium metabisulphite as a scavenger of air pollutants for wood-based building materials, Int Wood Prod J. 2013; 4(4): 242–247.

[48] Costa N, Pereira J, Ferra J, Cruz P, Martins J, Magalhães F, Mendes A, Carvalho L. Scavengers for achieving zero formaldehyde emission of wood-based panels. Wood Sci Technol. 2013; 47(6): 1261–1272.

[49] Costa N, Ohlmeyer M, Ferra J, Magalhães FD, Mendes A, Carvalho L. The performance of scavengers on VOC emission in particleboards made from pine and poplar. Eur J Wood Prod. 2014; 72: 117–121.

[50] Sheikh-Ahmad JY, Bailey JA. High-temperature wear of cemented tungsten carbide tools while machining particleboard and fibreboard. J Wood Sci. 1999; 45: 445–455.

[51] Beer P, Sinn G, Kowaluk G, Lacki W, Dziurka D. Mechanical properties of particleboards induces work to cut. In: Lachenmayr G, Scholz F, editors. Proceedings of the 17th International Wood Machining Seminar. Rosenheim, Germany: Fachhochschule Rosenheim publisher; 2005. pp. 319–323.

[52] Furukawa H, Tsutsumoto T, Banshoya K. Cutting performance of edge-sharpened diamond-coated milling tools. Proc. of the 16th International Wood Machining Seminar; Matsue, Japan. Matsue: IWMS-16 Organizing Committee; 2003, pp. 57–64.

[53] Wong DC, Schajer GS. Particleboard Machining Quality Improvement by Control of Particle Geometry. In: Lachenmayr G, Scholz F, editors. Proceedings of the 17th International Wood Machining Seminar. Rosenheim, Germany: Fachhochschule Rosenheim publisher; 2005. pp. 141–151.

[54] McKenzie W. Power Demand in rooting wood and wood composites. In: Taylor J and Wong D, editors. Proc. of the 18th International Wood Machining Seminar: FP Innovations; Forintek-Vancouver, Canada. Vancouver: IWMS-18 Organizing Committee; 2007. pp. 207–214.

[55] Hoffmeister H, Grübler T, Loohß T. Image Processing as a Tool for Process-Integrated Quality Assessment. In: Lachenmayr G, Scholz F, editors. Proceedings of the 17th International Wood Machining Seminar. Rosenheim, Germany: Fachhochschule Rosenheim publisher; 2005. pp. 468–478.

[56] Porankiewicz B, Tanaka C. Workpiece edge quality after milling melamine-coated particleboard. Mem Fac Sci Eng Shimane Univ Series A. 2001; 35: 139–147.

[57] Coelho C, Martins J, Meausoone PJ, Masson D, Carvalho L, Costa C. Method for evaluating the influence of wood machining conditions on the objective characteristics and subjective perception of a finished surface. Wood Sci Technol. 2008; 42: 181–195.

[58] Garrido N, Martins J, Carvalho LH, Mendes JG, Costa C. Influence of sawing conditions on the quality of particleboard edges. In: Taylor J and Wong D, editors. Proc. of the 18th International Wood Machining Seminar: FP Innovations; Forintek-Vancouver, Canada. Vancouver: IWMS-18 Organizing Committee; 2007. pp. 247–255.

[59] Schafer M, Roffael E. On the formaldehyde release of wood. Holz Roh Werkst. 2000; 58: 259–264.

[60] Martins J, Pereira J, Pinto B, Coelho C, Carvalho LH. Effect of recycled wood on formaldehyde release of particleboard. In: COST Action E49 Conference Measurement and Control of VOC Emissions from Wood-Based Panels, Fraunhofer WKI, Braunschweig, Germany; 2007, Nov 28–29. Published in CD.

[61] Durkic C, Bueso J, Fliedner E. Dynea AsWood™ – Technologies for Composite Boards with formaldehyde emissions as defined by nature. In: Frihart C and Hunt C, editors. International Conference on Wood Adhesives; Lake Tahoe, Nevada, USA. Madison: Forest Products Society; 2009. pp. 57–64.

Index